University of Cincinnati

Date: 4/19/2019

I, Elizabeth N Orr, hereby submit this original work as part of the requirements for the degree of Doctor of Philosophy in Geology.

It is entitled:

"Deciphering tectonic and climatic controls on erosion and sediment transfer in the NW Himalaya"

Student's name: **Elizabeth N Orr**

This work and its defense approved by:

Committee chair: Lewis Owen, Ph.D.

Committee member: Richard Beck, Ph.D.

Committee member: Craig Dietsch, Ph.D.

Committee member: Dylan Ward, Ph.D.

33115

Deciphering tectonic and climatic controls on erosion and sediment transfer in the NW Himalaya

A dissertation submitted to the
Graduate School
of the University of Cincinnati
in partial fulfillment of the
requirements for the degree of

DOCTOR OF PHILOSOPHY

in the Department of Geology
of the McMicken College of Arts and Sciences

by

Elizabeth N. Orr
MSc., Royal Holloway, University of London
BSc., University of Glasgow

19th of April 2019

Dissertation Committee

Dr. Lewis A. Owen
Dr. Dylan Ward
Dr. Craig Dietsch
Dr. Richard Beck

Abstract

Central to examining orogenic belt formation and evolution are efforts to define the relative roles of tectonics and climate in landscape denudation, and the complex feedbacks that exist between them. Studies in high altitude, high relief mountain settings such as the Himalayan-Tibetan orogen show that these relationships are not completely straightforward and that denudation can scale with tectonics, precipitation and/or topography. Steep north-south trending gradients in elevation, relief, rock uplift and precipitation make the NW Himalaya an excellent location to examine these controls of landscape denudation.

As a first step to help elucidate the erosional processes involved in sediment mobilization from primary sources at catchment headwaters, rates of lateral rockwall slope erosion are defined for a suite of 12 catchments between the Baltistan region of Pakistan and Garhwal, northern India. These rates are derived from ^{10}Be cosmogenic nuclide concentrations in medial moraine sediment, and affirm that between ~0.02 and 7 m of lateral slope erosion through periglacial processes can be achieved across a single millennium in this setting, and >2 km when extrapolated for the whole Quaternary. This erosion is sufficient to influence topographic change at the catchment head, and emphasizes the importance of localized erosion when evaluating broader landscape change. Statistically significant relationships are apparent between slope erosion and apatite fission track cooling ages and inferred rates of exhumation. The distribution and magnitude of these latter records of denudation are argued to be the result of the Indo-Eurasian convergence and the geometry and shortening of the Main Himalayan Thrust. Rockwall slope erosion in the NW Himalaya is therefore found to be primarily governed by tectonically driven rock uplift, with precipitation as a secondary control.

To examine the nature and timing of sediment transfer from primary sources to transient sinks, such as landforms and sediment deposits, 18 new and 29 recalculated ^{10}Be fan surface exposure ages define the timing of surface abandonment for a suite of 10 fans across the Greater Himalaya ranges in Ladakh, Lahul, Kullu and Garhwal in northern India. The fans are found to evolve during interglacials and periods of deglaciation, which are associated with a higher intensity monsoon. As glacial conditions or periods of relative cooling and increasing aridity become reestablished, aggradation ceases or becomes more restricted and the fan surfaces stabilize and/or are abandoned. A regional temporal framework of landform abandonment/aggradation cessation and incision events for the monsoon-influenced western Himalaya ranges (MWHR) and the semi-arid western Himalaya ranges (SWHR) are defined for the NW Himalaya. The timing of regional landform abandonment events for the MWHR and SWHR is consistent with the fan record, occuring during periods of relative cooling and increasing aridity. Regional incision events are less straightforward as they are recognized across various climatic conditions, likely due to the ubiquitous nature of erosion in these active alpine settings. A preservation bias in favor of Holocene geomorphic evidence in the MWHR is due to elevated rates of erosion in this region, which rapidly rework and overprint landforms and sediment deposits. Lower rates of erosion in the SWHR, assist in the preservation of geomorphic evidence throughout the last glacial. Climate and climate-driven processes largely moderate sediment transfer in the NW Himalaya; however, the distribution of precipitation and temperature are themselves influenced by the structural evolution of the orogen.

Although the primary controls of erosion and sediment transfer in this study are shown to be rock uplift and climate respectively, this research overall argues that the various components of Himalayan mountain range evolution cannot each be governed by one mechanism alone. Instead, the coupling between tectonics and climate is central to examining processes of erosion and sediment transfer in this setting and in evaluating broad trends in landscape change. The specific

nature and rates of landscape change on the catchment scale are shown to be influenced by longstanding catchment-specific feedbacks between topography, geology, surface processes, climate and tectonics, in addition to regional forcings on the mountain range and/or orogen scale. Catchment-wide landscape change can be viewed as a continuum of sediment transfer cycles, which trace sediment from a source to its eventual evacuation from the catchment. Each step within a transfer cycle is moderated by a set of preconditioning factors, and one or more forcing factor. This approach emphasizes the important contribution of preexisting landscape dynamics and variability in external forcings over space and time, in the landscape development of high altitude, high relief mountains ranges of the Himalayan-Tibetan orogen.

‘When we try to pick out anything by itself,
we find it hitched to everything else in the universe’

– *John Muir* (1838−1914)

Acknowledgments

My PhD program, research projects and associated field campaigns have been funded by the Department of Geology at the University of Cincinnati, PRIME Laboratories at Purdue University, National Geographic, the Geological Society of America and the UC Graduate Student Governance Association.

I would like to extend my sincere thanks to my primary advisor Professor Lewis Owen for his invaluable instruction and continued support throughout this process. I would like to acknowledge my committee members, Dr. Dylan Ward, Dr. Craig Dietsch and Dr. Richard Beck who have generously shared their time and expertise with me over the past four years. Heart felt thanks are extended to Sourav Saha for his support, experience and humor in the field and out, and to Sarah Hammer for her instruction and friendship in the Geochronology Laboratories. I would also like to acknowledge Dr. Jeff Havig, Dr. Tom Lowell, Dr. Aaron Diefendorf and Jason Cesta for constructive conversations about research projects and career. Thanks are also extended to Dr. Marc Caffee for comments on iterations of manuscripts. Many thanks to Discover Ladakh Adventure Tours and Travel for providing vital logistical support across three field campaigns.

In my four years at the University of Cincinnati, my path has crossed countless people who have contributed to my research, and professional and personal development (sadly, too many people to mention individually). I would therefore just like to thank the students, postdocs, staff and faculty of the Department of Geology, past and present, for making this process as enjoyable and rewarding as it has been.

Finally, none of this would have been possible without the unwavering support, generosity and patience of my friends and family on either side of the Atlantic Ocean, and my partner. Thank you for putting up with me.

I would like to dedicate this dissertation research to my grandmother – for had she lived in a different time and under different circumstances, she would have done this and more.

Table of Contents

page

Abstract……ii

Acknowledgments…… vii

1. Introduction……1

2. Regional setting……...4

3. Methodology……6

3.1 Remote sensing and terrain analyses……6

3.2 Sedimentological analyses……6

3.3 Cosmogenic nuclide analyses……7

3.4 Statistical analyses……8

4. Foci summaries……9

4.1. *Focus 1*. 'Rates of periglacial rockwall slope erosion in the upper Bhagirathi catchment, Garhwal, northern India'……9

4.2. *Focus 2*. 'Rockwall slope erosion in the NW Himalaya'……11

4.3. *Focus 3*. 'Climate driven late Quaternary fan surface abandonment in the NW Himalaya'……....13

4.4. *Focus 4*. 'Defining controls of regional geomorphic change in the NW Himalaya'……...14

5. Discussion ……..15

5.1. Controls of landscape change……15

5.2. Cycles of Himalayan catchment sediment transfer……17

6. Future directions……...18

7. References……..23

8. Manuscript 1……..30

9. Manuscript 2……..90

10. Manuscript 3……..142

11. Supplementary items……182

11.1 Supplementary geomorphic maps……182

11.2. Supplementary items 1 (Manuscript 1)……...184

11.3. Supplementary items 2 (Manuscript 2)……...198

11.4. Supplementary items 3 (Manuscript 3)……...202

1. Introduction

Much attention has been paid to understanding the large-scale coupling between tectonic and climatic processes in the geology and dynamics of orogenic belts and the particular processes that govern smaller-scale landscape development. Central to this field of research are the efforts to evaluate the relative roles of these forcings in landscape denudation, and the feedbacks between them (Willett, 1999; Godard et al., 2006; Whipple and Meade, 2006; Whipple, 2009; Roe and Brandon, 2011). From single grain to orogen scale, landscape denudation has been investigated using techniques of geomorphology, sedimentology, geochemistry, numerical dating and physical and numerical modeling (e.g. DeCelles et al., 2001; Bookhagen et al., 2005; Hobley et al., 2010; Anoop et al., 2012; Egholm et al., 2012; Scherler et al., 2015). Studies have been far from unanimous; denudation in high altitude, high relief settings such as the Himalayan-Tibetan orogen has been shown to scale with tectonics (Burbank et al., 2003; Godard et al, 2014; Scherler et al., 2014), precipitation (Thiede et al., 2004; Grujic et al., 2006; Clift et al., 2008; Gabet et al., 2004; Wulf et al., 2010; Deeken et al., 2011) and/or topography (Vance et al., 2003; Scherler et al., 2011, 2014).

Over recent years, the onset and acceleration of late Cenozoic glaciation in the Himalayan belt is argued to have enhanced landscape denudation through intensified rates of sedimentation and localized incision (Zeitler et al., 2001; Korup and Montgomery, 2008; Owen and Dortch, 2014). However, there is a growing volume of literature that argues that Himalayan landscape change, specifically erosion and sediment transfer is instead governed by tectonically driven rock uplift, and that climate and climate-driven surface processes play an important yet secondary role (Burbank et al., 2003; Thiede and Ehlers, 2013; Scherler et al., 2014).

Steep north-south trending gradients in elevation, relief, rock uplift and precipitation make the NW Himalaya an excellent location to examine the strength of coupling between climate and tectonics, for a particular aspect of landscape change (Bookhagen and Burbank 2006, 2010; Scherler et al., 2011). The aim of this dissertation is to pursue two main lines of enquiry; the first is to improve our understanding of the erosional processes involved in the mobilization of sediment from primary sources at the headwaters of glaciated catchments in the NW Himalaya. The second aim is to investigate the nature and timing of sediment transfer from these primary sources to transient sinks, and discuss the insights that these sinks provide in deciphering the controls of landscape change. The rationale for these studies is to examine some of the insights that catchment scale erosion and sediment transfer processes offer for understanding the broader scale evolution and mass flux of mountain belts such as the Himalayan-Tibetan orogen. The objectives of each study are detailed below:

Focus 1 looks to constrain rates of rockwall slope erosion in the upper Bhagirathi catchment of Garhwal, northern India (Fig. 1). This catchment has a well-defined glacial chronostratigraphy and comprehensive records of past and modern glacier behavior. Rockwall slope erosion is calculated by measuring ^{10}Be cosmogenic nuclide concentrations in medial moraine sediment of Gangotri glacier. An important aim of this focus is to test the feasibility of applying this method in a monsoon-influenced catchment with high background denudation rates, and to develop an appropriate sampling strategy for *Focus 2*. The slope erosion dataset is compared to records of catchment-wide erosion and exhumation to evaluate the extent to which slope erosion may differ to other records of landscape change, which have been averaged across various spatial and temporal scales. Slope erosion rates from this study in upper Bhagirathi, and then published rates from Chhota Shigri in the Lahul Himalaya, northern India (Scherler and Egholm, 2017) and Baltoro in the Central Karakoram, Pakistan (Seong et al., 2009) are compared to catchment

parameters and regional climate records to examine the possible controls of slope erosion in the NW Himalaya.

In *Focus 2*, the aim is to define the distribution and magnitude of rockwall slope erosion in the NW Himalaya, by building upon the work of *Focus 1*. Beryllium-10 concentrations are measured in medial moraine sediment to quantify slope erosion rates for a suite of 12 catchments (Fig. 1). To resolve the primary controls of rockwall slope erosion in the NW Himalaya, the patterns of slope erosion are compared to those in geology, tectonics, climate and topography.

Alluvial/debris-flow fans serve as temporary stores of poorly sorted deposits, which include debris-flow, glaciofluvial, fluvial, lacustrine and aeolian sediment (Ballantyne, 2002a,b; Barnard et al., 2006). Much of this sediment originates from the periglacial realms of the catchments and is therefore moderated by the slopes of the source catchments (Barnard et al., 2004a,b; Nicholas and Quine, 2007). Our understanding of the evolution of these landforms with respect to the wider catchment, and the influence of climate and/or tectonism within these sedimentary systems is incomplete. Well-preserved fans in the NW Himalaya provide an excellent opportunity to assess the controls of fan formation in high-relief mountain settings, as well as evaluate how these controls may vary between areas of contrasting climatic regime. In *Focus 3,* 18 new and 29 recalculated ^{10}Be fan surface exposure ages define the timing of surface abandonment for a suite of 10 fans across the Greater Himalaya ranges between Ladakh and Garhwal in northern India (Fig. 1). These fan surface ages are compared to local and regional climate and glacial records to evaluate the contributions of climate and climate-driven surface processes in the timing of fan aggradation and stabilization in the NW Himalaya, throughout the late Quaternary.

Focus 3 demonstrates that climate-driven processes and glaciation play a significant role in fan development. The aim of *Focus 4* is to determine whether this relationship extends to other

geomorphic records of the NW Himalaya. Existing geomorphic records are compiled to construct a regional temporal framework of landform abandonment/aggradation cessation and incision events for the monsoon-influenced western Himalaya ranges (MWHR) and the semi-arid western Himalaya ranges (SWHR) of the NW Himalaya. A further aim of this focus is to determine whether cycles of these regional geomorphic events are recognized in the western end of the orogen.

2. Regional setting

The Himalayan-Tibetan orogen has formed as the result of continued continental collision and partial subduction between the Indian and Eurasian lithospheric plates, which commenced at ~55 Ma (Searle et al., 1997). In the NW Himalaya, the Indus-Tsangpo Suture Zone marks the collision zone between these continental plates and the northern boundary of the Tethyan Himalaya (Fig.1). Deformation-driven crustal shortening from the early Miocene to the Pleistocene initiated the development of a series of foreland propagating thrust systems that divide the Himalayan lithotectonic units south of the Tethyan Himalaya into the Greater Himalaya crystalline sequence, the Lesser Himalaya sequence, sub-Himalaya and foreland basin (Searle, 1986; Steck et al., 1998; Schlup et al., 2003; Vannay et al., 2004; Thakur et al., 2014). The Greater Himalaya is further divided into two sub-units: the southern Greater Himalaya sequence (GHS-S) and the northern Greater Himalaya sequence (GHS-N; DeCelles et al., 2001; Thiede and Ehlers 2013). Continued crustal shortening and thrust and strike-slip faulting throughout the orogen means that the NW Himalaya remains tectonically active in the present (Hodges et al., 2004; Vannay et al., 2004; Bojar et al., 2005).

Northwest Himalayan climate is primarily governed by two atmospheric systems: the Indian summer monsoon advects moisture from the Indian ocean between late May and September and

the northern hemispheric westerlies, which bring moisture from the Mediterranean, Black and Caspian seas between December and March (Gadgil 2003; Lang and Barros 2004; Wulf et al., 2010; Mölg et al., 2013). The imposing orographic barrier of the Himalaya creates a steep precipitation gradient perpendicular (S−N) to the strike of the mountain belt, which became established during the late Miocene (~8 Ma; Qiang et al., 2001; Liu and Dong, 2013). The northward decline in annual precipitation today falls from ~1500−3000 mm in the Lesser and Greater Himalaya ranges, to <150 mm in the interior of the Tibetan Plateau (TRMM 1998−2005, Bookhagen and Burbank, 2006). Most Greater Himalaya glaciers are large, temperate and melt-dominated, and are fed by monsoonal precipitation (Benn and Owen, 2002; Su and Shi, 2002). Glaciers in the semi-arid Greater and Tethyan Himalaya are usually small (1–10 km^2) cold-based sub-polar types: precipitation-sensitive and sublimation-dominated (Benn and Owen, 2002).

The study area for this dissertation extends from the Balistan region in the semi-arid Karakoram of Pakistan to Uttarkhand in the Garhwal Himalaya of northern India (Fig 1). This area encompasses sites from the Ladakh and Zanskar Ranges of Jammu and Kashmir and the Lahul-Spiti and Kullu districts in Himachal Pradesh. The investigated catchments present a broad range of morphologies, ranging from steep relief catchments with narrow floors and fluvial gorges, to broad, gently sloping catchments with wide and cultivated floors. The catchments are predominantly glaciated and preserve glacial, fluvial, paraglacial and periglacial landforms and deposits, which include moraines, mass movements, debris-flow/alluvial fans and cones, fill and strath terraces, and outwash and till deposits (Sharma et al., 2016; Orr et al., 2017, 2018; Saha et al., 2018).

3. Methodology

3.1. Remote sensing and terrain analyses

Geomorphic maps were prepared in the field across three field campaigns and then refined using Advanced Spaceborne Thermal Emission and Reflection Radiometer (ASTER) global digital elevation models (GDEMs; 30-m-resolution), Landsat Enhanced Thematic Mapper Plus (ETM+; 15 m resolution) imagery, Google Earth imagery and published geomorphic and geologic maps. Geomorphic and sedimentological techniques described by Benn and Owen (2002) and Benn and Evans (2010) were employed to identify and differentiate between landforms and sediment deposits. Terrain and hydrological data for the investigated catchments were acquired using Spatial Analyst and 3D Analyst toolboxes in ArcGIS. Equilibrium line altitudes for past and contemporary glaciers were also calculated using these tools, following methods of Osmaston (2005) and Benn et al., (2005). Climatic data (e.g. CRU CL 2.0, TRMM 2B31) was extracted and interpolated for each study area using GIS. Catchment surface temperatures were projected from local weather station data and an adiabatic environmental lapse rate of 7°C/km (Derbyshire et al., 1991; De Scally, 1997; Thayyen et al., 2005; Siddiqui and Maruthi, 2007; Bashir and Rasul, 2010; Pratap et al., 2013; Kattel et al., 2013).

3.2. Sedimentological analyses

Detailed sediment and geomorphic descriptions were made of the landforms and deposits examined in the field. Further sedimentological analysis was conducted at the University of Cincinnati in the Sedimentology and X-Ray Laboratories in the Department of Geology and the Advanced Material Characterization Center (AMCC), in order to elucidate the characteristics and transport histories of sediment from various landforms. These analyses included clast size

(Wentworth, 1922; Allen 1981), shape (Hambrey and Glasser, 2003; Hambrey et al., 2008; Lukas et al., 2013), roundness (Sneed and Folk, 1958; Ballantyne and Benn, 1994), surface weathering (Sheridan and Marshall, 1987; Owen et al., 2003) and sample clay mineralogy (Chenn 1977; Moore and Reynolds, 1997).

3.3. Cosmogenic nuclide analyses

Following the initial interaction of primary cosmic rays with the Earth's atmosphere, a secondary cascade of nuclear particles bombard atomic nuclei in target minerals of rock, regolith and sediment, and cause the accumulation of cosmogenic nuclides (Lal, 1991; Gosse and Philips, 2001; Bierman et al., 2002). This study focuses on the accumulation of ^{10}Be in quartz. Nuclide production in quartz is moderated by latitude, atmospheric pressure and elevation, density of material, depth of sample from the surface, surface erosion, shielding, and temporal changes in geomagnetic strength and solar modulation (Lal, 1991 Uppala et al., 2005; Lifton et al., 2005, 2008; Balco et al., 2008; Martin et al., 2016; Marrero et al., 2016; Lifton, 2016). The ^{10}Be concentrations measured in bedrock or surface boulders provide an inferred age of exposure to cosmic rays (e.g. *Focus 3, 4*). Beryllium-10 concentrations in detrital samples from fluvial catchments can be used to infer time-averaged catchment-wide erosion rates. If there is no inherited ^{10}Be, the concentrations are considered to reflect the mean surface concentrations of the source area and are inversely proportional to the derived erosion rates. In *Focus 1* and *2* rockwall slope erosion is quantified by applying this method to medial moraine sediment.

The extraction of quartz and ^{10}Be sample preparation was conducted at the Geochronology Laboratories at the University of Cincinnati, applying the community standards and chemical procedures of Kohl and Nishiizumi (1992). The ^{10}Be/^{9}Be of the samples was measured using accelerator mass spectrometry at the Purdue Rare Isotope Measurement (PRIME) Laboratory at

Purdue University (Sharma et al., 2000). Upon the recommendations of Portenga et al. (2015), native ^{9}Be was measured in each sample and subtracted from the initial ratios. The ^{10}Be production rates for each catchment were calculated with a revised sea-level high-latitude spallogenic production rate of 4.08±0.23 Be atoms/g/a (Martin et al., 2017; http://calibration.ice-d.org/), ^{10}Be half-life of 1.36 Ma (Nishiizumi et al., 2007) and a 30-m-resolution GDEM in MATLAB R2017.a, using methods described in Dortch et al. (2011). The accumulation of ^{10}Be during burial, englacial transport and exhumation of sediment to the glacier surface between rockwall and medial moraine was calculated using the Ward and Anderson (2011) analytical model, and then subtracted from the final ^{10}Be concentrations.

Rockwall slope erosion rates for *Focus 1* and *2* were calculated from the total ^{10}Be concentrations and catchment production rates using methods described in detail by Lal (1991), Granger et al. (1996), Balco et al. (2008), and Dortch (2011). The ^{10}Be boulder exposure ages for *Focus 3* were calculated using the Cosmic Ray Exposure program calculator (CREp) of Martin et al. (2017), using the LSD scaling model (Lifton et al., 2014) with the ERA40 atmospheric model (Uppala et al., 2005) and Lifton VDM 2016 geomagnetic database. Published ^{10}Be ages quoted in *Focus 3* and *4* were recalculated using this calculation scheme.

3.4. Statistical analyses

Statistically significant relationships between ^{10}Be concentrations and catchment matrices were identified using Pearson Moment Correlation Coefficient values. A p-value of <0.01 (at >99% confidence level) was applied. Principle Component Analysis was then used to identify and discuss the primary controls of slope erosion using the R statistical package (The R Core Team, 2018).

To constrain regional events of landform abandonment/aggradation cessation and incision for the MWHR and SWHR, we constructed cumulative probability density functions using the 'ksdensity' kernel in MATLAB R2017.a. The timing of the regional geomorphic events is reported using the gaussian peak (≥3 ages) and the uncertainty by gaussian standard deviation values. Landform abandonment events refer to times of restricted sedimentation where landforms stabilize.

4. Foci summaries

4.1. *Focus 1*: 'Rates of periglacial rockwall slope erosion in the upper Bhagirathi catchment, Garhwal, northern India.'

Methodology: Section 3.1−3.3

Publication status: *in revision.* Submitted to *Earth Surface Processes and Landforms* special issue *'Geomorphic diversity of the Indian sub- continent: Progress and Updates'*

Periglacial rockwall slope erosion is defined for the upper Bhagirathi catchment using cosmogenic ^{10}Be concentrations in sediment from ablation-dominated medial moraines on Gangotri glacier. Medial moraine sediment characteristics for the lower ~3km of the ablation zone are broadly similar, despite the discrete origins of each landform. Geomorphic and sedimentological analyses confirm that the moraines are predominately composed of rockfall and avalanche debris mobilized from steep relief bedrock slopes via periglacial weathering processes.

Beryllium-10 concentrations range from 1.1±0.2 to 2.7±0.3x10^4 at/g SiO_2, yielding rockwall slope erosion rates from 2.1±0.4 to 5.3±1.2 mm/a. The ^{10}Be concentrations vary between samples of each moraine and between individual landforms; no relationship is evident between nuclide concentration and proximity of sample location to either a glacier margin or snout. Samples from the stable, centermost moraine of Ganogtri glacier have ^{10}Be concentrations that fall within error

of each other and show no evidence of sediment input from discrete sources, and are therefore considered to best reflect rates of slope erosion in upper Bhagirathi. The rates of rockwall slope erosion are sufficient to moderate slope sediment flux, glacier dynamics and the topographic configuration of catchment headwaters. Slope erosion rates in upper Bhagirathi are likely to have varied over space and time, and encompassed shifts in climate, glacier mass balance and seismicity, which each operate across various timescales (10^6–10^1 years).

Slope erosion rates exceed the averaged catchment-wide and exhumation rates of Bhagirathi and the Garhwal region, which supports the view that erosion at the headwaters can outpace the wider catchment (Sorkhabi et al., 1996; Searle et al., 1999; Vance et al., 2003; Thiede et al., 2009; Lupker et al., 2012; Thiede and Ehlers 2013; Scherler et al., 2014). The difference in erosion rates is likely because these records refer to landscape change across different temporal and spatial scales; slope erosion is sensitive to short-term local change such as stochastic mass wasting events, which on the catchment scale is not recognized (Yanites et al., 2009; Ward and Anderson, 2011; Willenbring et al., 2013; Sadler and Jerolmack, 2014).

The ^{10}Be concentrations in medial moraine sediment for the upper Bhagirathi catchment and the catchments of Chhota Shigri in Lahul, northern India (Scherler and Egholm, 2017) and Baltoro glacier in Central Karakoram, Pakistan (Seong et al., 2009) show no statistically significant relationship with topography (e.g. catchment area, mean elevation, mean slope, relative relief) or projected catchment temperatures. A tentative relationship lies between annual rainfall and ^{10}Be concentration, where higher rainfall coincides with lower concentrations and therefore higher inferred slope erosion rates. This supports the extensive work on the coupling between precipitation and erosion, where enhanced moisture in the monsoon-influenced Lesser and Greater Himalaya drives more rapid landscape change, compared to the semi-arid interior of the orogen (Thiede et al., 2004; Grujic et al., 2006; Clift et al., 2008; Gabet et al., 2004; Wulf et al.,

2010; Deeken et al., 2011). This relationship is not completely straightforward, as similar ^{10}Be concentrations are shared by samples from semi-arid and monsoon catchments.

Rockwall slope erosion in the three study areas, and more broadly across the NW Himalaya is thought to be governed by individual catchment dynamics that vary across space and time. Developing this dataset further, by including more sites throughout the NW Himalaya will help to decipher the local and regional forcings which contribute to landscape change.

4.2. *Focus 2*: 'Rockwall slope erosion in the NW Himalaya'

Methodology: Section 3.1, 3.3, 3.4

Publication status: Ready to submit to *Earth Surface Processes and Landforms* (awaiting publishing of *Focus 1*).

The distribution and magnitude of periglacial rockwall slope erosion is defined for 12 catchments in northern India using methods consistent with *Focus 1*. Beryllium-10 concentrations range from $5.3\pm0.8\text{x}10^4$ to $260.0\pm12.5\text{x}10^4$ at/g SiO_2, which yield erosion rates between 0.02 and 7.2±1.1 mm/a. Consistent with the findings of *Focus 1*, no relationship is apparent between nuclide concentration and proximity of sample location to either a glacier margin or snout. Any internal variability in concentrations within the catchments is likely because the medial moraine sediment is poorly mixed and/or has a non-proportional sediment supply that is dominated by stochastic rockfall events (Small et al., 1997; Muzikar, 2008; Ward and Anderson, 2011). Between ~0.02 and ~7 m of lateral erosion can be achieved in this setting across a single millennia, and >2 km when extrapolated for the whole Quaternary. The magnitude of erosion, particularly in the GHS-S is sufficient to affect the strength of hillslope-glacier coupling, catchment sediment flux, glacier dynamics, and help to set the pace of topographic change at the catchment head.

The rockwall slope erosion records from Garhwal, Kullu, Lahul, Ladakh and Baltistan are combined to create a regional erosion dataset (Seong et al., 2009; Scherler and Egholm 2017; *Focus 1*). Rockwall slope erosion largely outpaces the local catchment-wide erosion rates and exhumation in the NW Himalaya (Dortch et al., 2011; Thiede and Ehlers 2013; Scherler et al., 2014; Dietsch et al., 2015). This demonstrates the importance of accounting for localized erosion ($<10^1$ km^2) and its effects on down-catchment reaches in studies of wider landscape change.

Rockwall slope erosion rates become progressively less rapid with distance north from the Main Central Thrust, into the interior of the orogen. The distribution and magnitude of this erosion is most closely associated with patterns in apatite fission track (AFT) cooling ages, inferred rates of Quaternary exhumation and records of Himalayan denudation and rock uplift (Sorkhabi et al., 1996; Searle et al., 1999; Jain et al., 2000; Schlup et al., 2003, 2011; Thiede et al., 2004, 2005, 2006, 2009; Kristein et al., 2006, 2009; Walia et al., 2008). This suggests that tectonically driven uplift, rather than climate, provides a first order control on patterns of slope erosion. Rockwall slope erosion is therefore argued to be part of the erosional response to uplift, which has resulted from the Indo-Eurasian convergence and the geometry and shortening of the Main Himalayan Thrust. Precipitation is likely to play a secondary role in defining the spatial distribution of erosion. Of the catchment parameters that can be defined in the NW Himalaya with some precision, mean rockwall slope, mean catchment and snowline elevation and mean annual temperature also have statistically significant relationships with the ^{10}Be concentrations. Other attributes which likely influence slope erosion, yet cannot be accounted for in this study include rockwall lithology and rock strength, seismicity and glacial erosion.

The specific rates of rockwall slope erosion for each catchment are therefore likely to be dictated by longstanding feedbacks between topography, geology, surface processes, climate and tectonics. The relative roles of these parameters in driving erosion are likely to vary across space

and time. This study demonstrates the importance of periglacial slope erosion and localized erosion in understanding wider landscape change of high altitude, high relief mountain ranges.

4.3. *Focus 3*: 'Climate driven late Quaternary fan surface abandonment in the NW Himalaya'

Methodology: Section 3.1−3.3

Publication status: *In press*. GSA Special Paper *'Ice-Age glaciers, water, and wind — Interdisciplinary Quaternary science round the world'* in memory of Stephen C. Porter.

The timing of surface abandonment for ten alluvial/debris-flow fans across contrasting climatic settings in the NW Himalaya of northern India are defined using cosmogenic ^{10}Be surface exposure dating. Debris-flow fans in the Garhwal, Kullu and Lahul regions of the monsoon-influenced Greater Himalaya were largely abandoned during the Mid−Late Holocene. Large alluvial fans and smaller debris-flow fans in the semi-arid Ladakh region of the Greater and Tethyan Himalaya have surface ages which extend throughout the last glacial. A preservation bias favors Holocene ages for fan surfaces in the monsoon- influenced ranges, because elevated rates of erosion in this region rapidly rework and overprint landforms and sediment deposits over timescales of 10^4−10^1 years (Gabet et al., 2004; Wulf et al., 2010). The lower rates of landscape change in the semi-arid interior ranges help to preserve a longer fan record (Dietsch et al. 2015; Jonell et al., 2018).

The type, size and morphology of the fans are shown to be influenced by the topography and fluvial channel behaviors of the source catchments and trunk valleys. With the exception of the Karzok fans in the Ladakh region, the timing of fan abandonment throughout the NW Himalaya coincides with periods of relative cooling and increasing aridity (Fleitmann et al., 2003, 2007; Wang et al., 2005; Herzschuh et al., 2006; Leipe et al., 2004; Rawat et al., 2015). During warm, wet conditions, fans aggrade and evolve as sediment is released and then transferred throughout the catchments. As the climate then transitions to cooler and drier conditions, aggradation ceases

or becomes more restricted, and the fan surface stabilizes. The exposure ages for each fan also coincide with one or more local glacial stages and between one and five regional glacial stages (Dortch et al., 2013; Murari et al., 2014; Owen and Dortch, 2014; Saha et al., 2018). This study proposes that fans evolve during interglacial periods or phases of deglaciation during a higher intensity monsoon, and then as glacial conditions become reestablished, the fans stabilize.

The interaction between climate and internal catchment dynamics such as geology, topography and sediment supply is shown to dictate the nature and timing of fan evolution and abandonment in the NW Himalaya. Climate-driven processes and glaciation are considered to be important factors in fan sedimentation, catchment sediment flux and the topographic evolution of the NW Himalaya during the late Quaternary.

4.4. *Focus 4*: 'Defining controls of regional geomorphic change in the NW Himalaya'

Methodology: Section 3.3, 3.4

Publication status: *In press*. GSA Special Paper *'Ice-Age glaciers, water, and wind — Interdisciplinary Quaternary science round the world'* in memory of Stephen C. Porter.

Regional landform abandonment/aggradation cessation and incision events for the MWHR (monsoon western Himalayan ranges) and SWHR (semi-arid western Himalayan ranges) are defined by a compilation of 206 recalculated ^{10}Be surface exposure ages from fan, and fill and strath terrace surfaces. Records of landform abandonment are recognized in the MWHR region throughout the past ~50 ka with regional events at 1.4±0.5 and 0.6±0.2 ka. Records of incision extend from ~70 to 0.6 ka, with regional incision events at 6.9±3.7, 3.6±1.0, 1.8±0.6 and 1.0±0.1 ka. In the SWHR region records of landform abandonment extend over the past 56 ka and >110 ka. Regional events occur at 31.5±5.1 and 20.0±5.3 ka. Records of incision are recognized throughout the past ~120 ka, with events at 35.9±5.8, 13.7±3.9 and 2.2±1.7 ka. This record

demonstrates a similar preservation bias to *Focus 3*, where records of geomorphic change in landscapes with rapid background denudation rates are restricted to the Holocene.

Regional landform abandonment events largely occur during periods of weakening monsoon strength and cooling, and local and regional glacier advances. Regional incision events from the MWHR and SWHR regions are recognized across various climatic conditions due to the ubiquitous nature of erosion in mountain settings. The most significant regional incision event for both the MWHR and SWHR regions occur at the time of extensive glaciation at the onset of the Holocene. This incision event likely reflects enhanced glacial and fluvial erosion during this glaciation and its associated phase of deglaciation. More broadly, these regional records of geomorphic change illustrate the importance of climate and climate-driven surface processes in landscape change throughout the NW Himalaya.

5. Discussion

5.1. Controls of landscape change

The aim of this dissertation has been to take steps to decipher the primary controls of select processes of erosion and sediment transfer operating at the catchment scale in the Himalayan-Tibetan orogen, with the view to contributing to the longstanding debate over the role of climate versus tectonics in driving short and long term landscape change. Several approaches have been employed in order to address this question. The first phase of investigation involved the quantification and discussion of the rates and nature of periglacial rockwall slope erosion throughout the NW Himalaya. In *Focus 1* and *2*, slope erosion rates range between 0.02 and 7.2±1.1 mm/a. This magnitude of lateral erosion is argued to be sufficient to influence topographic change at the catchment head across geomorphic timescales (10^5–10^2 years), and

emphasizes the importance of localized, periglacial erosion when evaluating broader landscape evolution. Collectively, these studies suggest that the distribution and magnitude of rockwall slope erosion is primarily the result of tectonically driven rock uplift throughout the orogen. Precipitation has a secondary role in influencing rates of slope erosion.

The aim of *Focus 3* and *4* was to further our understanding of the development and abandonment of transient sediment sinks in high altitude, high relief settings, and explore the implications that this has for wider landscape change. These studies suggest that fans and other depositional landforms such as fill terraces evolve during interglacials and periods of deglaciation, which are associated with a higher intensity monsoon. As glacial conditions or periods of relative cooling and increasing aridity become reestablished, these landforms stabilize. Regional incision events in the NW Himalaya are less straightforward as they are recognized across various climatic conditions, likely due to the ubiquitous nature of erosion in these active alpine settings. That said, *Focus 3* and *4* suggest that climate and climate-driven processes largely moderate sediment transfer in the NW Himalaya. A preservation bias in favor of young Holocene records in the monsoon-influenced Himalaya is argued to be the result of rapid background denudation rates. This relationship tentatively extends to the slope and catchment-wide erosion record, where more rapid erosion is focused in regions with shorter records of geomorphic change.

Many studies argue that sediment flux and erosion in Himalayan catchments is primarily a function of orographically focused monsoon rainfall (Bookhagen et al., 2005; Bookhagen and Burbank, 2006; Gabet et al., 2006; Wulf et al., 2010). This dissertation, in part, aligns itself with this argument. *Focus 3* and *4* outline the importance of climate, specifically precipitation in landscape change, yet acknowledge that patterns in precipitation and temperature, and therefore climate driven surface processes, are influenced by the structural evolution of the orogen. *Focus 1* and *2* take this a step further and show that the distribution and magnitude of periglacial slope

erosion is strongly moderated by tectonically driven uplift, yet is unable to discount the influence of precipitation. These opposing conclusions show that neither climate nor tectonics can or should be ignored when investigating processes of erosion and sediment transfer in this mountain setting. It is therefore better to argue that the sedimentary systems of mountain ranges in the NW Himalaya are instead affected by the feedbacks between climate and tectonics, rather than one mechanism in isolation. Crucially these conclusions apply to the regional and/or mountain range scale. On a more local scale, catchments that share similar characteristics and are in close proximity to one another, can record slope and catchment-wide erosion rates that differ by an order of magnitude and/or have asynchronous aggradation and incision events. Each focus of this dissertation therefore concludes that although the patterns of periglacial slope erosion and the development of landforms throughout the NW Himalaya can be explained by a combination of broad scale climate and tectonic processes, the specific nature and rate of geomorphic change in each catchment is likely dictated by longstanding catchment specific feedbacks between topography, geology, surfaces processes, climate and tectonics. The relative roles of these different parameters and the nature and rates of landscape change are therefore likely to vary across space and time. Studies that discuss similar themes must therefore consider the importance of catchment specific dynamics, while also recognizing that inconclusive or variable records of geomorphic change does not mean that orogen-scale interactions are not at play.

5.2. Cycles of Himalayan catchment sediment transfer

Several theoretical models use sediment availability, sediment transfer or geomorphic event frequency as indexes for landscape change (Ryder 1971; Church and Ryder 1972; Ballantyne et al., 2002b; McColl, 2012). The majority of these models propose that dynamical change is first initiated by the onset of deglaciation, and concludes before the onset of the following glacial. It is unclear whether the stabilization of deglaciated terrain or a ‘steady-state’ landscape can be

achieved across short interglacial periods in the Himalayan-Tibetan orogen. Catchment-wide landscape change can instead be viewed as a continuum of sediment transfer cycles. This approach has been devised from the findings of this study in combination with the wider geomorphological and glaciological literature of the NW Himalaya.

A set of preconditioning factors (Table 1) and one or more forcing factors trigger a shift in erosion or sediment flux (i.e. step through model; Fig. 2), the effects of which are then carried forward. These cycles can occur in isolation, alongside others, or feed into multiple cycles. For example, a seismic event (i.e. forcing factor, Table 1) triggers the mobilization and transfer of sediment from a rockwall (i.e. source; Fig. 2) to a series of debris cones at the base of the slope (i.e. transient sediment sink; Fig. 2). These debris cones are then part of the revised landscape settings, of which subsequent geomorphic change is conditioned by. Theoretically, this sediment is evacuated from the catchment or mountain range following one or more of these cycles, which can extend across 10^5–10^1 years. This approach acknowledges the important contribution of preexisting landscape dynamics and variability in external forcings for landscape development, and offers a useful framework for interpreting the evolution of Himalayan catchments.

6. Future directions

This study has exercised two main approaches to further our understanding of Himalayan landscape change using cosmogenic nuclides: the first to quantify rates of inter-catchment erosion, and the second to constrain the timing and nature of landform development. New research questions and additional research objectives that build upon the progress made in this dissertation have been identified, and are summarized below.

A continued effort to constrain the rates of periglacial rockwall slope erosion in the NW Himalaya would be beneficial. *Focus 1* and *2* highlight concerns over whether one to three medial moraine samples are sufficient to provide ^{10}Be concentrations that are representative of the source area. Sampling systematically up the length of the medial moraine and across different grainsizes would help to address these concerns and assess the variability in nuclide concentrations in the supraglacial realm of glaciers. Moreover, constraining bedrock erosion rates of the rockwalls using cosmogenic nuclides would compliment the detrital erosion record of this dissertation, as well as provide new insights into erosion at the catchment head. Past studies have quantified headwall retreat and slope erosion by dating and estimating volumes of slope deposits such as talus (Andre, 1997; Curry and Morris, 2004; Hinchecliff and Ballantyne, 2008) and modeling supraglacial debris flux using remote sensing techniques (Heimsath and McGlynn, 2008; Gibson et al., 2017). Comparing the results of these methods to nuclide derived erosion rates would offer a novel insight into the complexities of landscape change in the periglacial realms of the investigated catchments. Investigating the rock fracturing and other rock properties of the source rockwalls would also help to elucidate some of the controls of the frequency and magnitude of rockfall events in the NW Himalaya.

Secondly, a continued effort to improve the size and resolution of the chronological datasets that define fan development and surface abandonment is a necessary next step. This would involve broadening the variety of investigated fans in terms of type, morphology, size and age. Defining the timing of sedimentary unit deposition for each fan from *Focus 3* using optically stimulated luminescence dating would help to substantiate the timing and drivers of fan aggradation.

This study alongside others, has demonstrated that erosion can vary significantly in both mechanism and magnitude throughout a drainage basin (Wittmann et al., 2009; Scherler et al., 2014; Portenga et al., 2015). These latter studies have used cosmogenic nuclide concentrations in

sediment derived from tributaries, trunk streams and terraces to quantify this variability. A similar project has been developed by the author for the monsoon- influenced Kullu river basin in Himachal Pradesh, with the specific aim of discussing the role of transient sediment sinks in erosion rates inferred using nuclide concentrations. Samples for this project were retrieved in a 2017 field campaign. This project will refer to the Beas Kund slope erosion dataset (*Focus 2*), fan surface ages (*Focus 3*) and regional phases of incision (*Focus 4*) from Kullu to trace sediment transfer throughout a catchment with rapid background denudation rates.

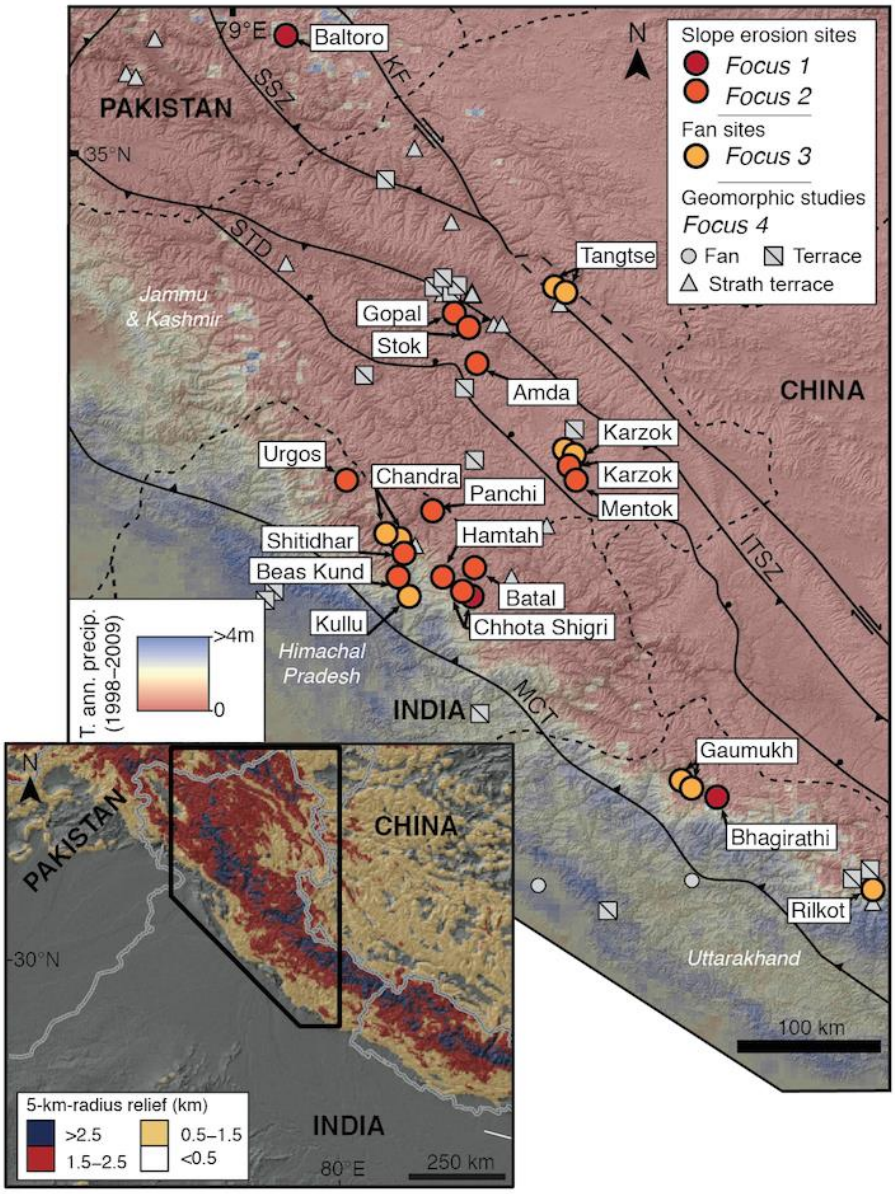

Fig. 1. Overview of the study area in the NW Himalaya. Hillshade map is overlain by total annual precipitation (TRMM 2B31; Bookhagen and Burbank, 2006). Major faults from Hodges (2000) and Schlup et al. (2003). Inset map illustrates the location (black polygon) of the study areas (relief map with swath polygons modified from Bookhagen and Burbank 2006).

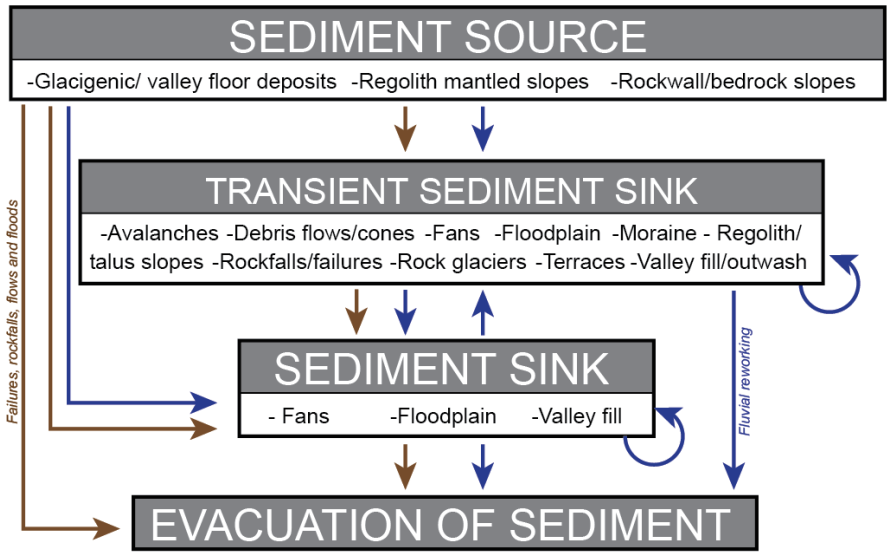

Fig. 2. Sediment transfer and erosion processes within a Himalayan alpine catchment showing the sources, sinks (including examples) and mechanisms for sediment transport (blue arrows: fluvial reworking; brown arrows: failures, rockfalls, flows and floods). The nature and rates of each sediment transfer episode involves the geomorphic sequence of landscape modification (Table 1).

Table 1. Geomorphic sequence of landscape modification.

1. PRECONDITIONING			2. FORCING		3. RESULT
Pre-existing geologic settings	Geomorphic regime/history	- Glacial, fluvial, periglacial, hillslope - Regolith characteristics and distribution, stochastic events	Climate	- Moisture (permafrost, frost action/sorting, vegetation change) - Temperature (permafrost, frost action/sorting, vegetation change)	Adjustment to sediment supply, transfer and storage
	Lithology	- Rock strength, rock mass quality, jointing and structure	Erosion	- Glacial, fluvial, periglacial, wind	
	Tectonic history	- Structural evolution/events, rock uplift	Glaciation	- Glacial processes (destructive and formative)	
	Topography	- Slope, relief, hypsometry	Human activity	- Land use change/pressure	
			Tectonics	- Rock uplift, seismicity	
			Weathering	- Physical, chemical, biological	

7. References

Allen, T., 1981. Particle size, shape and distribution. In Particle size measurement. p. 103−164. Springer, Boston, MA.

André, M.F., 1997. Holocene rockwall retreat in Svalbard: a triple- rate evolution. Earth Surface Processes and Landforms: The Journal of the British Geomorphological Group, 22(5), p.423−440.

Anoop, A., Prasad, S., Basavaiah, N., Brauer, A., Shahzad, F., Deenadayalan, K., 2012. Tectonic versus climate influence on landscape evolution: a case study from the upper Spiti valley, NW Himalaya. Geomorphology, 145, p.32−44.

Balco, G., Stone, J., Lifton, N., Dunai, T., 2008. A complete and easily accessible means of calculating surface exposure ages or erosion rates from ^{10}Be and ^{26}Al measurements. Quaternary Geochronology, 3, p.174−195.

Ballantyne, C.K., 2002a. Paraglacial geomorphology. Quaternary Science Reviews, 21(18−19), p.1935−2017.

Ballantyne, C.K., 2002b. A general model of paraglacial landscape response. The Holocene, 12(3), p.371−376.

Ballantyne, C.K., Benn, D.I., 1994. Paraglacial Slope Adjustment and Resedimentation following Recent Glacier Retreat, Fåbergstølsdalen, Norway. Arctic and Alpine Research, 26(3), p.255−269.

Barnard, P., Owen, L., Finkel, R., 2004a. Style and timing of glacial and paraglacial sedimentation in a monsoon−influenced high Himalayan environment, the upper Bhagirathi Valley, Garhwal Himalaya. Sedimentary Geology, 165, p.199−221.

Barnard, P.L., Owen, L.A., Sharma, M.C., Finkel, R.C., 2004b. Late quaternary (Holocene) landscape evolution of a monsoon−influenced high Himalayan valley, Gori Ganga, Nanda Devi, NE Garhwal, Geomorphology, 61(1−2), p.91−110.

Barnard, P.L., Owen, L.A., Finkel, R.C., 2006. Quaternary fans and terraces in the Khumbu Himal south of Mount Everest: their characteristics, age and formation. Journal of the Geological Society, 163(2), p.383−399.

Bashir, F., Rasul, G., 2010. Estimation of water discharge from Gilgit Basin using remote sensing, GIS and runoff modeling. Pakistan Journal of Meteorology, 6(12).

Benn, D.I., Evans, D.J.A., 2010. Glaciers and Glaciation. Hodder Education. London, UK, p.802.

Benn, D.I., Owen, L.A., 2002. Himalayan glacial sedimentary environments: a framework for reconstructing and dating former glacial extents in high mountain regions. Quaternary International, 97−98, p.3−26.

Bierman, P.R., Caffee, M.W., Davis, P.T., Marsella, K., Pavich, M., Colgan, P., Mickelson, D., Larsen, J., 2002. Rates and timing of earth surface processes from in situ−produced cosmogenic Be−10. Reviews in mineralogy and geochemistry, 50(1), p.147−205.

Bojar, A.V., Fritz, H., Nicolescu, S., Bregar, M., Gupta, R.P., 2005. Timing and mechanisms of Central Himalayan exhumation: discriminating between tectonic and erosion processes. Terra Nova, 17, 5, p.427−433.

Bookhagen, B., Burbank, D., 2006. Topography, relief and TRMM−derived rainfall variations along the Himalaya. Geophysical Research Letters, 33, 105.

Bookhagen, B., Burbank, D., 2010. Toward a complete Himalayan hydrological budget: Spatiotemporal distribution of snowmelt and rainfall and their impact on river discharge. Journal of Geophysical Research 115, F3, p.1−25.

Bookhagen, B., Thiede, R., Strecker, M., 2005. Late Quaternary intensified monsoon phases control landscape evolution in the northwest Himalaya. Geology 33, 1, p.149−152.

Burbank, D., Blythe, A., Putkonen, J., Pratt−Sitaula, B., Gabet, E., Oskin, M., Barros, A., Ojha, T., 2003. Decoupling of erosion and precipitation in the Himalayas. Nature 426, p.652−655.

Chen, P.Y., 1977. Table of key lines in X−ray powder diffraction patterns of minerals in clays and associated rocks. Indiana Geological Survey Occasional Paper 21, p.1–67.

Church, M., Ryder, J.M., 1972. Paraglacial sedimentation: a consideration of fluvial processes conditioned by glaciation. Geological Society of America Bulletin, 83(10), p.3059−3072.

Clift, P., Giosan, L., Blusztajn, J., Campbell, I., Allen, C., Pringle, M., Tebrez, A., Danish, M., Rabbani, M., Alizai, A., Carter, A., Luckge, A., 2008. Holocene erosion of the Lesser Himalaya triggered by intensified summer monsoon. Geology 36, p.79−82.

Curry, A.M., Morris, C.J., 2004. Lateglacial and Holocene talus slope development and rockwall retreat on Mynydd Du, UK. Geomorphology, 58(1−4), p.85−106.

DeCelles, P.G., Robinson, D.M., Quade, J., Ojha, T.P., Garzione, C.N., Copeland, P., Upreti, B.N., 2001. Stratigraphy, structure, and tectonic evolution of the Himalayan fold- thrust belt in western Nepal. Tectonics, 20(4), p.487−509.

Deeken, A., Thiede, R.C., Sobel, E.R., Hourigan, J.K., Strecker, M.R., 2011. Exhumational variability within the Himalaya of northwest India. Earth and Planetary Science Letters, 305(1−2), p.103−114.

Derbyshire, E., Shi, Y., Li, J., Zheng, B., Li, S., Wang, J., 1991. Quaternary glaciation of Tibet: the geological evidence. Quaternary Science Reviews. 10, 485−510.

de Scally, F.A., 1997. Deriving lapse rates of slope air temperature for meltwater runoff modeling in subtropical mountains: An example from the Punjab Himalaya, Pakistan. Mountain Research and Development, p.353−362.

Dortch, J., Owen, L., Schoenbohm, L., Caffee, M., 2011. Asymmetrical erosion and morphological development of the central Ladakh Range, northern India. Geomorphology 135, p.167−180.

Dortch, J., Owen, L., Caffee, M., 2013. Timing and climatic drivers for glaciation across semi-arid western Himalayan-Tibetan orogen. Quaternary Science Reviews 78, p.188-208.

Egholm, D.L., Pedersen, V.K., Knudsen, M.F., Larsen, N.K., 2012. Coupling the flow of ice, water, and sediment in a glacial landscape evolution model. Geomorphology, 141, p.47−66.

Fleitmann, D., Burns, S.J., Mangini, A., Mudelsee, M., Kramers, J., Villa, I., Neff, U., Al-Subbary, A.A., Buettner, A., Hippler, D., Matter, A., 2007. Holocene ITCZ and Indian monsoon dynamics recorded in stalagmites from Oman and Yemen (Socotra). Quaternary Science Reviews 26, 170–188.

Fleitmann, D., Burns, S.J., Mudelsee, M., Neff, U., Kramers, J., Mangini, A., Matter, A., 2003. Holocene forcing of the Indian monsoon recorded in a stalagmite from southern Oman. Science 300, p.1737–1739.

Gabet, E.J., Burbank, D.W., Putkonen, J.K., Pratt−Sitaula, B.A., Ojha, T., 2004. Rainfall thresholds for landsliding in the Himalayas of Nepal. Geomorphology, 63(3−4), p.131−143.

Gadgil, S., 2003. The Indian monsoon and its variability. Annual Review of Earth and Planetary Sciences, 31(1), p.429−467.

GeoMappApp (2014), Marine Geoscience Data System, Available from: http://www.geomappap.org (last accessed: 21/08.2014).

Gibson, M.J., Glasser, N.F., Quincey, D.J., Mayer, C., Rowan, A.V., Irvine−Fynn, T.D., 2017. Temporal variations in supraglacial debris distribution on Baltoro Glacier, Karakoram between 2001 and 2012. Geomorphology, 295, p.572−585.

Godard, V., Lavé, J., Cattin, R., 2006. Numerical modelling of erosion processes in the Himalayas of Nepal: Effects of spatial variations of rock strength and precipitation. Geological Society, London, Special Publications, 253(1), p.341−358.

Godard, V., Bourlès, D.L., Spinabella, F., Burbank, D.W., Bookhagen, B., Fisher, G.B., Moulin, A., Léanni, L., 2014. Dominance of tectonics over climate in Himalayan denudation. Geology, 42(3), p.243−246.

Gosse, J.C., Phillips, F.M., 2001. Terrestrial in situ cosmogenic nuclides: theory and application. Quaternary Science Reviews, 20(14), p.1475−1560.

Granger, D.E., Kirchner, J.W., Finkel, R., 1996. Spatially averaged long−term erosion rates measured from in situ−produced cosmogenic nuclides in alluvial sediment. The Journal of Geology, 104(3), p.249−257.

Grujic, D., Coutand, I., Bookhagen, B., Bonnet, S., Blythe, A., Duncan, C., 2006. Climatic forcing of erosion, landscape, and tectonics in the Bhutan Himalayas. Geology, 34(10), p.801−804.

Hambrey, M.J., Glasser, N.F., 2003. The role of folding and foliation development in the genesis of medial moraines: examples from Svalbard glaciers. The Journal of Geology, 111(4), p.471−485.

Hambrey, M.J., Quincey, D.J., Glasser, N.F., Reynolds, J.M., Richardson, S.J., Clemmens, S., 2008. Sedimentological, geomorphological and dynamic context of debris−mantled glaciers, Mount Everest (Sagarmatha) region, Nepal. Quaternary Science Reviews, 27(25−26), p.2361−2389.

Heimsath, A.M., McGlynn, R., 2008. Quantifying periglacial erosion in the Nepal high Himalaya. Geomorphology, 97(1−2), p.5−23.

Herzschuh, U., 2006. Palaeo-moisture evolution in monsoonal Central Asia during the last 50,000 years. Quaternary Science Reviews, 25(1-2), p.163-178.

Hinchliffe, S., Ballantyne, C.K., 1999. Talus accumulation and rockwall retreat, Trotternish, Isle of Skye, Scotland. Scottish Geographical Journal, 115(1), p.53−70.

Hobley, D., Sinclair, H., Cowie, P., 2010. Processes, rates, and timescales of fluvial response in an ancient postglacial landscape of the northwest Indian Himalaya. Geological Society of America Bulletin, 122, p.1569–1584.

Hodges, K.V., 2000. Tectonics of the Himalaya and southern Tibet from two perspectives. Geological Society of America Bulletin 112, 3, p.324−350.

Hodges, K.V., Wobus, C., Ruhl, K., Schildgen, T., Whipple, K., 2004. Quaternary deformation, river steepening, and heavy precipitation at the front of the Higher Himalayan ranges. Earth and Planetary Science Letters, 220, 3−4, p.379−389.

Jain, A.K., Kumar, D., Singh, S., Kumar, A., Lal, N., 2000. Timing, quantification and tectonic modelling of Pliocene–Quaternary movements in the NW Himalaya: evidence from fission track dating. Earth and Planetary Science Letters, 179(3-4), p.437-451

Kattel, D.B., Yao, T., Yang, K., Tian, L., Yang, G., Joswiak, D., 2013. Temperature lapse rate in complex mountain terrain on the southern slope of the central Himalayas. Theoretical and applied climatology, 113(3−4), p.671−682.

Kohl, C.P., Nishiizumi, K., 1992. Chemical isolation of quartz for measurement of in situ produced cosmogenic nuclides. Geochimica. Cosmochimica. Acta 56, p.3583–3587.

Korup, O., Montgomery, D.R., 2008. Tibetan plateau river incision inhibited by glacial stabilization of the Tsangpo gorge. Nature, 455(7214), p.786.

Kirstein, L.A., Sinclair, H., Stuart, F.M., Dobson, K., 2006. Rapid early Miocene exhumation of the Ladakh batholith, western Himalaya. Geology, 34(12), p.1049-1052.

Kirstein, L.A., Foeken, J.P.T., Van Der Beek, P., Stuart, F.M., Phillips, R.J., 2009. Cenozoic unroofing history of the Ladakh Batholith, western Himalaya, constrained by thermochronology and numerical modelling. Journal of the Geological Society, 166(4), p.667-678.

Lal, D., 1991. Cosmic ray labelling of erosion surfaces: in situ nuclide production rates and erosion models. Earth and Planetary Science Letters,104, p.429−439.

Lang, T.J., Barros, A.P., 2004. Winter storms in the central Himalayas. Journal of the Meteorological Society of Japan. Ser. II, 82(3), p.829−844.

Leipe, C., Demske, D., Tarasov, P.E., 2014. A Holocene pollen record from the northwestern Himalayan lake Tso Moriri: implications for palaeoclimatic and archaeological research. Quaternary International, 348, p.93-112.

Lifton, N.A., Bieber, J.W., Clem, J.M., Duldig, M.L., Evenson, P., Humble, J.E., Pyle, R., 2005. Addressing solar modulation and long−term uncertainties in scaling secondary cosmic rays for in situ cosmogenic nuclide applications. Earth and Planetary Science Letters, 239, p.140–161.

Lifton, N., Smart, D.F., Shea, M.A., 2008. Scaling time−integrated in situ cosmogenic nuclide production rates using a continuous geomagnetic model. Earth and Planetary Science Letters, 268(1−2), p.190−201.

Lifton, N., Sato, T., Dunai, T., 2014. Scaling in situ cosmogenic nuclide production rates using analytical approximations to atmospheric cosmic−ray fluxes. Earth and Planetary Science Letters, 386, p.149−160.

Liu, X., Dong, B., 2013. Influence of the Tibetan Plateau uplift on the Asian monsoon−arid environment evolution. Chinese Science Bulletin, 58(34), p.4277−4291.

Lukas, S., Benn D.I., Boston, C.M., Brook, M., Coray, S., Evans, D.J., Graf, A., Kellerer−Pirklbauer, A., Kirkbride, M.P., Krabbendam, M., Lovell, H,. 2013. Clast shape analysis and clast transport paths in glacial environments: A critical review of methods and the role of lithology. Earth−Science Reviews, 121, p.96−116.

Lupker M, Blard P.H, Lave J, France-Lanord C, Leanni L, Puchol N, Charreau J, Bourlès D. 2012. ^{10}Be-derived Himalayan denudation rates and sediment budgets in the Ganga basin. Earth and Planetary Science Letters 333. p. 146-156.

Marrero, S., Philips, F., Borchers, B., Lifton, N., 2016. Cosmogenic Nuclide Systematics and the CRONUScale Program. Quaternary Geochronology, 31, p.1−72.

Martin, L., Blard, P., Balco, G., Laurent, V., 2017. The CREp program and the ICE−D production rate calibration database: A fully parameterizable and updated online tool to compute cosmic−ray exposure ages. Quaternary Geochronology, 38, p.25−49.

McColl, S.T., 2012. Paraglacial rock−slope stability. Geomorphology, 153, p.1−16.

Mölg, T., Maussion, F. and Scherer, D., 2014. Mid−latitude westerlies as a driver of glacier variability in monsoonal High Asia. Nature Climate Change, 4(1), p.68.

Moore, D.M., Reynolds, Jr.R.C., 1997. X−ray Diffraction and the Identification and Analysis of Clay Minerals.

Murari, M.K., Owen, L.A., Dortch, J.M., Caffee, M.W., Dietsch, C., Fuchs, M., Haneberg, W.C., Sharma, M.C., Townsend-Small, A., 2014. Timing and climatic drivers for glaciation across monsoon-influenced regions of the Himalayan–Tibetan orogen. Quaternary Science Reviews, 88, p.159-182.

Nicholas, A.P., Quine, T.A., 2007. Modeling alluvial landform change in the absence of external environmental forcing. Geology, 35(6), p.527−530.

Nishiizumi, K., Imamura, M., Caffee, M.W., Southon, J.R., Finkel, R.C., McAninch, J., 2007. Absolute calibration of ^{10}Be AMS standards. Nuclear Instruments and Methods in Physics Research Section B: Beam Interactions with Materials and Atoms, 258(2), p.403−413.

Orr, E., Owen, L., Murari, M., Saha, S., Caffee, M., 2017. The timing and extent of Quaternary glaciation of Stok, northern Zanskar Range, Transhimalaya, of northern India. Geomorphology 284, p.142−155.

Orr, E.N., Owen, L.A., Saha, S., Caffee, M.W. and Murari, M.K., 2018. Quaternary glaciation of the Lato Massif, Zanskar Range of the NW Himalaya. Quaternary Science Reviews, 183, p.140−156.

Osmaston. H., 2005. Estimates of glacier equilibrium line altitudes by the Area× Altitude, the Area× Altitude Balance Ratio and the Area× Altitude Balance Index methods and their validation. Quaternary International, 138, p.22−31.

Owen, L., Dortch, J., 2014. Nature and timing of Quaternary glaciation in the Himalayan−Tibetan orogen. Quaternary Science Reviews 88, p.14−54.

Owen, L.A., Derbyshire, E., Scott, C.H., 2003. Contemporary sediment production and transfer in high−altitude glaciers. Sedimentary Geology, 155(1−2), p.13−36.

Portenga, E.W., Bierman, P.R., Duncan, C., Corbett, L.B., Kehrwald, N.M., Rood, D.H., 2015. Erosion rates of the Bhutanese Himalaya determined using in situ−produced ^{10}Be. Geomorphology, 233, p.112−126.

Pratap, B., Dobhal, D.P., Bhambri, R. and Mehta, M., 2013. Near−surface temperature lapse rate in Dokriani Glacier catchment, Garhwal Himalaya, India. Himalayan Geology, 34, p.183−186.

Qiang, X.K., Li, Z.X., Powell, C.M., Zheng, H.B., 2001. Magnetostratigraphic record of the Late Miocene onset of the East Asian monsoon, and Pliocene uplift of northern Tibet. Earth and Planetary Science Letters,187, 1−2, p.83−93.

Rawat, S., Gupta, A.K., Srivastava, P., Sangode, S.J., Nainwal, H.C., 2015. A 13,000 year record of environmental magnetic variations in the lake and peat deposits from the Chandra valley, Lahaul: Implications to Holocene monsoonal variability in the NW Himalaya. Palaeogeography, Palaeoclimatology, Palaeoecology 440, 116–127.

Roe, G.H., Brandon, M.T., 2011. Critical form and feedbacks in mountain- belt dynamics: Role of rheology as a tectonic governor. Journal of Geophysical Research: Solid Earth, 116(B2).

Ryder, J.M., 1971. The stratigraphy and morphology of para−glacial alluvial fans in south−central British Columbia. Canadian Journal of Earth Sciences, 8(2), p.279−298.

Sadler P.M, Jerolmack, D.J. 2014. Scaling laws for aggradation, denudation and progradation rates: the case for time-scale invariance at sediment sources and sinks. Geological Society, London, Special Publications 404: SP404-7.

Saha, S., Owen, L.A., Orr, E.N., Caffee, M.W., 2018. Timing and nature of Holocene glacier advances at the northwestern end of the Himalayan−Tibetan orogen. Quaternary Science Reviews, 187, p.177−202.

Scherler, D., Egholm, D., 2017. Debris supply to mountain glaciers and how it effects their sensitivity to climate change–A case study from the Chhota Shigri Glacier, India (Invited)(206444). In 2017 Fall Meeting.

Scherler, D., Bookhagen, B., Strecker, M.R., 2011. Hillslope- glacier coupling: The interplay of topography and glacial dynamics in High Asia. Journal of Geophysical Research: Earth Surface: 116(F2).

Scherler, D., Bookhagen, B. and Strecker, M.R., 2014. Tectonic control on ^{10}Be- derived erosion rates in the Garhwal Himalaya, India. Journal of Geophysical Research: Earth Surface, 119(2), p.83−105.

Scherler, D., Bookhagen, B., Wulf, H., Preusser, F. and Strecker, M.R., 2015. Increased late Pleistocene erosion rates during fluvial aggradation in the Garhwal Himalaya, northern India. Earth and Planetary Science Letters, 428, p.255−266.

Schlup, M., Carter, A., Cosca, M., Steck, A., 2003. Exhumation history of eastern Ladakh revealed by 40Ar/39Ar and fission−track ages: the Indus River− Tso Morari transect, NW Himalayas. Journal of the Geological Society, 160, p.385−399.

Schlup, M., Steck, A., Carter, A., Cosca, M., Epard, J.L., Hunziker, J., 2011. Exhumation history of the NW Indian Himalaya revealed by fission track and 40Ar/39Ar ages. Journal of Asian Earth Sciences, 40(1), p.334-350.

Searle, M., 1986. Structural evolution and sequence of thrusting in the High Himalayan, Tibetan−Tethys and Indus suture zones of Zanskar and Ladakh, Western Himalaya. Journal of Structural Geology, 8,8, p.923−936.

Searle, M., Parrish, R., Hodges, K., Hurford, A., Ayres, M., Whitehouse, M., 1997. Shisha Pangma Leucogranite, South Tibetan Himalaya: Field Relations, Geochemistry, Age, Origin, and Emplacement. Journal of Geology, 150, p.295−317.

Searle M.P, Noble S.R, Hurford A.J, Rex, D.C. 1999. Age of crustal melting, emplacement and exhumation history of the Shivling leucogranite, Garhwal Himalaya. Geological Magazine 136(5): 513-525.

Seong, Y.B., Owen, L.A., Caffee, M.W., Kamp, U., Bishop, M.P., Bush, A., Copland, L., Shroder,, J.F., 2009. Rates of basin−wide rockwall retreat in the K2 region of the Central Karakoram defined by terrestrial cosmogenic nuclide ^{10}Be. Geomorphology 107(3−4): 254−262.

Sharma, P., Bourgeois, M., Elmore, D., Granger, D., Lipschutz, M.E., Ma, X., Miller, T., Mueller, K., Rickey, F., Simms, P. and Vogt, S., 2000. PRIME lab AMS performance, upgrades and research applications. Nuclear Instruments and Methods in Physics Research, B 172, p.112−123.

Sharma, S., Chand, P., Bisht, P., Shukla, A.D., Bartarya, S.K., Sundriyal, Y.P., Juyal, N., 2016. Factors responsible for driving the glaciation in the Sarchu plain, eastern zanskar Himalaya, during the late quaternary. Journal of Quaternary Science, 31, 495−511.

Sheridan, M.F., Marshall, J.R., 1987. Comparative charts for quantitative analysis of grain textural elements on pyroclastics. In: Marshall, J.R. (Ed.), Clastic Particles. Van Nostrand−Reinhold, New York, p. 98 – 121.

Siddiqui, M.A., Maruthi, K.V., 2007. Detailed glaciological studies on Hamtah Glacier. Lahaul and Spiti District, HP Geological Survey of India, 140, p.92−93.

Sneed, E.D., Folk, R.L., 1958. Pebbles in the lower Colorado River, Texas a study in particle morphogenesis. The Journal of Geology, 66(2), p.114−150.

Sorkhabi, R.B., Stump, E., Foland, K.A., Jain, A.K., 1996. Fission-track and 40Ar39Ar evidence for episodic denudation of the Gangotri granites in the Garhwal Higher Himalaya, India. Tectonophysics, 260(1-3), p.187-199.

Steck, A., Epard, J., Vannay, J., Hunziker, J., Girard, M., Morard, A., Robyr, M., 1998. Geological transect across the Tso Morari and Spiti areas− the nappe structures of the Tethys Himalayas. Eclogae Geologicae Helvetiae 91, p.103−121.

Su, Z., Shi, Y., 2002. Response of monsoonal temperate glaciers to global warming since the Little Ice Age. Quaternary International, 97, p.123−131.

Thakur, V., Joshi, M., Sahoo, D., Suresh, N., Jayangondapermal, R., Singh, A., 2014. Partitioning of convergence in Northwest Sub−Himalaya: estimation of late Quaternary uplift and convergence rates across the Kangra reentrant, North India. International Journal of Earth Science. 103, p.1037−1056.

Thayyen, R.J., Gergan, J.T. and Dobhal, D.P., 2005. Slope lapse rates of temperature in Din Gad (Dokriani glacier) catchment, Garhwal Himalaya, India. Bulletin of glaciological research, 22, p.31−37.

Thiede, R.C., Ehlers, T.A., 2013. Large spatial and temporal variations in Himalayan denudation. Earth and Planetary Science Letters, 371, p.278−293.

Thiede, R.C., Bookhagen, B., Arrowsmith, J.R., Sobel, E.R., Strecker, M.R., 2004. Climatic control on rapid exhumation along the Southern Himalayan Front. Earth and Planetary Science Letters, 222(3−4), p.791−806.

Thiede, R.C., Arrowsmith, J.R., Bookhagen, B., McWilliams, M.O., Sobel, E.R., Strecker, M.R., 2005. From tectonically to erosionally controlled development of the Himalayan orogen. Geology, 33(8), p.689-692.

Thiede, R.C., Arrowsmith, J.R., Bookhagen, B., McWilliams, M., Sobel, E.R., Strecker, M.R., 2006. Dome formation and extension in the Tethyan Himalaya, Leo Pargil, northwest India. Geological Society of America Bulletin, 118(5-6), p.635-650.

Thiede, R.C., Ehlers, T.A., Bookhagen, B., Strecker, M.R., 2009. Erosional variability along the northwest Himalaya. Journal of Geophysical Research: Earth Surface, 114(F1).

Uppala, S.M., Kållberg, P.W., Simmons, A.J., Andrae, U., Bechtold, V.D., Fiorino, M., Gibson, J.K., Haseler, J., Hernandez, A., Kelly, G.A., Li, X., 2005. The ERA- 40 re-analysis. Quarterly Journal of the royal meteorological society, 131(612), p.2961−3012.

Vance, D., Bickle, M., Ivy−Ochs, S., Kubik, P.W., 2003. Erosion and exhumation in the Himalaya from cosmogenic isotope inventories of river sediments. Earth and Planetary Science Letters, 206(3−4), 273−288.

Vannay, C., Grasemann, B., Rahn, M., Frank, W., Carter, A., Baudraz, V., Cosca, M., 2004. Miocene to Holocene exhumation of metamorphic crustal wedges in the NW Himalaya: Evidence for tectonic extrusion coupled to fluvial erosion. Tectonics, 23, p.1−24.

Walia, M., Yang, T.F., Liu, T.K., Kumar, R., Chung, L., 2008. Fission track dates of Mandi granite and adjacent tectonic units in Kulu–Beas valley, NW Himalaya, India. Radiation Measurements, 43, p. S343-S347/

Wang, Y., Cheng, H., Edwards, R.L., He, Y., Kong, X., An, Z., Wu, J., Kelly, M.J., Dykoski, C.A., Li, X., 2005. The Holocene Asian Monsoon : Links to Solar Changes and North Atlantic Climate 854–858.

Ward, D.J., Anderson, R.S., 2011. The use of ablation- dominated medial moraines as samplers for ^{10}Be- derived erosion rates of glacier valley walls, Kichatna Mountains, AK. Earth Surface Processes and Landforms 36(4): p.495−512.

Wentworth, C.K., 1922. A scale of grade and class terms for clastic sediments. The journal of geology, 30(5), p.377−392.

Whipple, K.X., Meade, B.J., 2006. Orogen response to changes in climatic and tectonic forcing. Earth and Planetary Science Letters, 243(1−2), p.218−228.

Whipple, K.X., 2009. The influence of climate on the tectonic evolution of mountain belts. Nature geoscience, 2(2), p.97.

Willenbring, J.K., Gasparini, N.M., Crosby, B.T., Brocard, G., 2013. What does a mean mean? The temporal evolution of detrital cosmogenic denudation rates in a transient landscape. Geology, 41(12), p.1215-1218.

Willett, S. D., 1999. Orogeny and orography: The effects of erosion on the structure of mountain belts: Journal of Geophysical Research, v. 104, p. 28,957−28, 981.

Wittmann, H., Von Blanckenburg, F., Guyot, J.L., Maurice, L., Kubik, P.W., 2009. From source to sink: Preserving the cosmogenic 10Be-derived denudation rate signal of the Bolivian Andes in sediment of the Beni and Mamoré foreland basins. Earth and Planetary Science Letters, 288(3-4), p.463-474.

Wulf, H., Bookhagen, B., Scherler, D., 2010. Seasonal precipitation gradients and their impact on fluvial sediment flux in the Northwest Himalaya. Geomorphology, 118, 1−2, p.13−21.

Yanites, B.J., Tucker, G.E., Anderson, R.S., 2009. Numerical and analytical models of cosmogenic radionuclide dynamics in landslide-dominated drainage basins. Journal of Geophysical Research: Earth Surface, 114(F1).

Zeitler, P.K., Koons, P.O., Bishop, M.P., Chamberlain, C.P., Craw, D., Edwards, M.A., Hamidullah, S., Jan, M.Q., Khan, M.A., Khattak, M., Kidd, W.S., 2001. Crustal reworking at Nanga Parbat, Pakistan: Metamorphic consequences of thermal-mechanical coupling facilitated by erosion. Tectonics, 20(5), p.712−72

8. Rates of rockwall slope erosion in the upper Bhagirathi catchment, Garhwal, northern India

Elizabeth N. Orr[a*], Lewis A. Owen[a], Sourav Saha[a], Marc W. Caffee[b,c]
[a] *Department of Geology, University of Cincinnati, Cincinnati, OH 45221, USA*
[b] *Department of Physics, Purdue University, West Lafayette, IN 47907, USA*
[c] *Department of Earth, Atmospheric and Planetary Sciences, Purdue University, West Lafayette, IN 47907, USA*

ABSTRACT

Rockwall slope erosion is defined for the upper Bhagirathi catchment using cosmogenic ^{10}Be concentrations in sediment from ablation-dominated medial moraines on Gangotri glacier. Beryllium-10 concentrations range from 1.1±0.2 to 2.7±0.3x10^4 at/g SiO_2, yielding rockwall slope erosion rates from 2.1±0.4 to 5.3±1.2 mm/a. Slope erosion rates are likely to have varied over space and time and responded to shifts in climate, geomorphic and/or tectonic regime throughout the late Quaternary. Geomorphic and sedimentological analyses confirm that the moraines are predominately composed of rockfall and avalanche debris mobilized from steep relief rockwall slopes via periglacial weathering processes. Slope erosion affects sediment flux and storage of snow and ice at the catchment head on diurnal to millennial timescales, and more broadly influences catchment configuration and relief, glacier dynamics and microclimates. The slope erosion rates exceed the averaged catchment-wide and exhumation rates of Bhagirathi and the Garhwal region on geomorphic timescales (10^5−10^0 years), supporting the view that erosion at the headwaters can outpace the wider catchment. The ^{10}Be concentrations of medial moraine sediment for the upper Bhagirathi catchment and the catchments of Chhota Shigri in Lahul, northern India and Baltoro glacier in Central Karakoram, Pakistan show a tentative relationship between ^{10}Be concentration and rainfall. As such there is more rapid slope erosion in the monsoon-influenced Lesser and Greater Himalaya compared to the orogen's semi-arid interior.

*Corresponding author. E. N. Orr: orreh@mail.uc.edu
L.A. Owen: owenls@ucmail.uc.edu, S. Saha: sahasv@mail.uc.edu, M. W. Caffee: mcaffee@purdue.edu

We conclude that rockwall slope erosion in the three study areas, and more broadly across the NW Himalaya is likely governed by individual catchment dynamics that vary across space and time.

Keywords: supraglacial processes; sediment flux; glacier; climate; cosmogenic isotopes

INTRODUCTION

Glaciation and glacial erosion are central to the topographic evolution of high altitude mountain belts such as the Himalayan-Tibetan orogen, by influencing rates of sedimentation and localized incision, limiting relief production and elevation, and offsetting tectonic uplift (Brozović et al., 1997; Whipple et al., 1999; Mitchell and Montgomery, 2006; Wulf et al., 2010, 2011; Scherler et al., 2014). The contributions of periglacial erosion at the valley head to the denudation budgets of Himalayan glacierized catchments have been largely overlooked, with the exception of an eloquent study by Heimsath and McGlynn (2008) in the Nepal High Himalaya. This is surprising given that lateral erosion of rockwall slopes via periglacial processes are shown to exceed rates of vertical glacial incision in other alpine settings (Brocklehurst and Whipple, 2006; Foster et al., 2008).

Periglacial weathering processes including freeze-thaw, frost cracking and ice wedging deliver large volumes of rockfall and avalanche debris to the mountain glacier sedimentary system from the valley slopes (Schroder et al., 2000; Matsuoka, 2001; Owen et al., 2003; Hales and Roering, 2005; Sanders et al., 2012; Gibson et al., 2017). The strength of coupling between slope and glacier affect glacier dynamics, catchment sediment flux and can dictate the relief and topographic configuration of catchment divides over time (Thiede et al., 2005; Moore et al., 2009; Montgomery, 2002). Erosion of rockwall slopes in the Himalayan-Tibetan orogen therefore has

broad implications for the distribution of precipitation and the morphological development of its mountain ranges (Burbank et al., 2003; Gabet et al., 2004; Anders et al., 2006; Bookhagen and Burbank, 2006).

The distribution and rates of erosion for the Himalayan-Tibetan orogen scale with tectonics (Burbank et al., 2003; Thiede et al., 2005; Schlerler et al., 2014), topography (Vance et al., 2003) and rainfall (Deeken et al., 2001; Thiede et al., 2004; Grujic et al., 2006; Biswas et al., 2007; Craddock et al., 2007; Gabet et al., 2008; Wulf et al., 2010; Portenga et al., 2015). Erosion at the valley head can outpace catchment and regional landscape denudation rates, and exhibit greater or different sensitivities to local and/or regional external forcing such as shifts in geomorphic, climatic or tectonic regime (Heimsath and McGlynn, 2008; Scherler et al., 2011). We aim to assess the importance of periglacial processes in the Himalayan-Tibetan orogen; an essential first step is the quantification of rockwall slope erosion rates. We chose the upper Bhagirathi catchment of Garhwal, northern India, for this initial investigation. This region is the source area for the Ganges and it contains some of the largest glaciers in the monsoon-influenced Himalaya, including Gangotri glacier. This catchment has a well-defined glacial chronostratigraphy, comprehensive records of past and modern glacier behavior and is easily accessible. We apply geomorphic and sedimentological methods and measure cosmogenic ^{10}Be concentrations in medial moraine sediment to calculate rockwall slope erosion rates. We compare our erosion rates to local catchment-wide erosion and exhumation records to assess the difference between slope erosion and regional landscape denudation in Garhwal. We compare slope erosion rates for upper Bhagirathi, Chhota Shigri in the Lahul Himalaya, northern India and Baltoro in the Central Karakoram of Pakistan with catchment parameters and regional climate records to help identify the factors that may be affecting slope erosion in the NW Himalaya.

REGIONAL SETTING

The Bhagirathi catchment is located in the Uttarkashi district of Uttarakhand, in the Garhwal Himalaya, northern India (Fig. 1). Three major lithotectonic units characterize the geology of the Garhwal Himalaya: 1) Tethyan Himalaya sedimentary series; 2) the High Himalaya crystalline sequence; and 3) the Lesser Himalaya sequence (Searle et al., 1997, 1999; Vannay et al., 2004). Despite the absence of a clear shear zone, Garhwal is bounded in the north by the Tethyan Himalaya low-grade metasedimentary rocks and the South Tibetan Detachment zone (STD; Kumar et al., 2009; Srivastava, 2012). The Main Central Thrust zone defines the southern margin of the region; the boundary between high-grade gneiss, migmatite and granite of the HHS and low-grade metasedimentary rocks of the LHS. The Jhala normal fault trends through central Garhwal and the Bhagirathi catchment, separating quartzo-feldpathic sillimanite gneiss from Harsil metasedimentary rocks (Searle et al., 1999). Maximum regional uplift rates range between 4 and 5.7 mm a^{-1} (Barnard et al., 2004; Scherler et al., 2014). Neotectonics, which include persistent microseismicity and stochastic earthquakes, greatly influence the geomorphic evolution of the region (Searle et al., 1987; Validya 1991; Rajendran et al., 2000; Barnard et al., 2001; Bali et al., 2003). Detailed summaries of the geologic setting and histories of transient erosion, unroofing and exhumation for Garhwal are provided by Scaillet et al. (1995), Searle et al. (1993, 1999), Sorkhabi et al. (1996) and Scherler et al. (2014; Fig. 1).

The climate of the western Himalaya is influenced by two major climatic systems, the southwest Indian monsoon and the northern hemispheric mid-latitude westerlies (Finkel et al., 2003; Bookhagen et al., 2005; Owen, 2009). The majority of annual precipitation (1000−2500 mm a^{-1}) in Garhwal occurs from July to September; during this time the humid air masses of the Indian monsoon penetrate the high-altitude ranges of the Greater Himalaya (Burbank et al., 2004; Scherler et al., 2010; Thayyen and Gergan, 2010; Wulf et al., 2010). Rainfall magnitudes vary

significantly both seasonally and across short distances (10^1–10^2 km) throughout the region, creating localized microclimates that are affected by the variability in terrain and geomorphic regimes (Sharma and Owen, 1996; Barros et al., 2006; Singh et al., 2007; Srivastava, 2012). Most of the annual snowfall above ~1000 m asl occur between December and March (Dobhal et al. 2008; Wulf et al., 2010; Bhambri et al., 2011; Scherler et al., 2014). Glaciers in Garhwal are predominantly fed by winter accumulation, and in turn 97% of river discharge is governed by seasonal snow and glacier melt throughout the region (Singh et al., 2008, Bhambri et al., 2011; Bhattacharya et al., 2016).

Due to the restricted number of meteorological stations located above ~5000 m asl in the Himalaya (Benn et al., 2012; Srivastava, 2012), climate and weather records for the upper Bhagirathi catchment are based on data from only one weather station (Mukhim, 30.6°N, 78.3°E, ~1900 m asl). Mukhim station records mean annual precipitation of 1648 mm and temperature of 15.5°C from 1971 to 2000. An additional weather station has been established at Bhojbasa (~3780 m asl, 30.9°N, 79.0°E), ~4 km from the snout of Gangotri glacier. This station has documented annual temperature ranges between -2.3 and 11°C (2001–09), and a mean winter snowfall of ~546 mm/a (Bhambri et al., 2011).

Montane forests transform to alpine tundra vegetation between ~1000 and 3000 m asl within the upper Bhagirathi catchment. At higher elevations, alpine shrubs and grasses with some sandy-gravel soil development are sparsely distributed or absent (Schweinfurth, 1968; Srivastava, 2012).

The upper Bhagirathi catchment (3400–7200 m asl) covers an area of ~550 km^2, of which ~50% is glaciated (Tangri et al., 2004; Haritashya et al., 2006; Singh et al., 2006). This transverse catchment is delineated by steep relief peaks (>45°) that exceed 6000 m asl, including Shivling (6543 m asl), Meru (6660 m asl) and the Chaukhamba Massif (7138 m asl; Bhambri et al., 2011;

Satyabala, 2016). Below Gaumukh (~4000 m asl, 30.9 °N, 79.1°E) the catchment is unglaciated and becomes wider and deeper as a result of the calving of a steep gorge by the Bhagirathi River. River terraces are present along the valley floors, most of which are cultivated.

At ~30 km long, Gangotri glacier is the largest glacier in the drainage basin. This temperate glacier is fed by a series of smaller tributary glaciers including Chaturangi and Kirti between elevations of 4005 and 5950 m asl (Dutta et al., 2004; Srivastava, 2012, Haritshya et al., 2010). Gangotri glacier has an estimated volume of ~20–30 km^3 (Frey et al., 2014; Bhattacharya et al., 2016), with a thickness ranging from 350 to 450 m in the accumulation zone, and 40 to 65 m at its snout (Srivastava, 2012; Gantayat et al., 2014; Singh et al., 2017). The mean glacier surface velocity is ~48±4.8 m a^{-1} (Bhattacharya et al., 2016), and the contemporary equilibrium-line altitude (ELA) lies between 4510 and 5160 m asl (Owen and Sharma, 1998; Naithanu et al., 2001; Ahmad and Hasnain, 2004, Burbank et al., 2004; Srivastava, 2012; Singh et al., 2017). Medial moraines of variable thickness are present below the ELA, partially mantling the ~26-km-long ablation zone (Haritashya et al., 2010; Scherler et al., 2011; Satyabala, 2012; Srivastava, 2012). Gangotri glacier has an undulating surface characterized by steep relief ridges and depressions, meltwater channels, drainage ponds and ice collapse features. Large lateral moraines trend parallel to the glacier along the lower ~10 km of the ablation zone, helping to form a series of discontinuous ablation valleys that are in-filled by hillslope and avalanche debris. Lacustrine deposits are present at Tapovan (4330 m asl, 30.9°N, 79.1°E; Sharma and Owen 1996; Ranhotra and Bhattacharya, 2004; Haritashya et al., 2010)

The upper Bhagirathi catchment preserves an abundance of moraines, debris flow/alluvial fans and cones, strath/river terraces and landslides (Owen and Sharma, 1998; Burbank et al., 2004; Singh et al., 2017). Mass movements are particularly prevalent throughout the region as a

consequence of glacial and fluvial erosion, heavy monsoon rains, localized storms and earthquakes, which each enhance slope instability (Owen et al., 1996; Barnard et al., 2001, 2004).

Five glacial stages have been defined within the upper Bhagirathi catchment and include the: Bhagirathi (60–23 ka), Sudarshan (21–16 ka), Shivling (~5.2 ka), Gangotri (~2.4–1.9 ka), Bhujbasa (~1.7–0.5 ka), Meru (~0.3±0.1 ka) and Gaumukh (~0.3–0.2 ka; Sharma and Owen, 1996; Barnard et al., 2004; Puri et al., 2004; Srivastava, 2012; Singh et al., 2017; Saha et al., *submitted*). The low erosion rates measured within the drainage basin (<1 mm a^{-1}; Vance et al., 2003) and wider region (0.15–5.4 mm a^{-1}; Haritashya et al., 2006; Scherler et al., 2014) aid in the preservation of glacial landforms across several glacial cycles. The moraine of the Bhagirathi stage (60–23 ka) is located ~30 km downstream from the present glacier snout and records the oldest and most extensive glaciation of the drainage basin. Gangotri glacier has retreated between 6 and 27 m/a over the past 50 years, but since 2007 has ceased retreat. Tangri (2002), Tangri et al. (2004), Bhambri et al. (2012), Srivastava (2012) and Bhattacharya et al. (2016) provide detailed summaries of the glacier stages and retreat.

METHODOLOGY

Background

Past studies have quantified slope erosion by dating and estimating the volume of slope deposits such as talus (Andre, 1997; Curry and Morris, 2004; Hinchecliff and Ballatyne, 2008; Siewert et al., 2012), and modeling supraglacial debris flux (Heimsath and McGlynn, 2008; Gibson et al., 2017). Over recent years slope erosion has been successfully measured using cosmogenic ^{10}Be concentrations in medial moraine sediment (Heimsath and McGlynn, 2008; Seong et al., 2009; Ward and Anderson, 2011; Scherler and Egholm, 2017). Medial moraines form when rockfall and avalanche debris mobilized from the valley slopes is exhumed to the ablation zone surface after

being buried and transported englacially through the accumulation zone (Matsuoka and Sakai, 1999; Goodsell et al., 2005; MacGregor et al., 2009; Mitchell and Montgomery, 2006; Dunning et al., 2014, 2015). The ^{10}Be concentrations of medial moraine sediment are thought to reflect the mean surface concentrations of the source area (Ward and Anderson, 2011). For a given medial moraine sediment package, the shorter the duration of exposure to cosmic rays on the valley head slope, the lower the accumulation of ^{10}Be, and the faster the inferred slope erosion rate. On sub-millennial timescales the ^{10}Be concentrations are likely to reflect slope erosion via periglacial weathering processes, whereas over geomorphic timescales (10^0–10^6 years) the input is more likely affected by local or regional erosion rates (Gibson et al., 2017).

Rockwall slope erosion rates have been measured using ^{10}Be concentrations of medial moraine sediment for the Chhota Shigri catchment of Lahul, northern India (Scherler and Egholm, 2017) and Baltoro glacier catchment in the Central Karakoram, Pakistan (Seong et al., 2009). Slope erosion for Baltoro was shown to be an order of magnitude higher than rates inferred by sediment budgets, and half the fluvial incision and exhumation rates for the region. Seong et al., (2009) hypothesize that the difference between these erosion records indicates differing sensitivities to conditions responsible for erosion. Fluvial incision, for example, is argued to exceed slope erosion because of the influence of local/differential tectonism and/or isostatic uplift.

We combine this method with geomorphic and sedimentological analyses of Gangotri glacier medial moraines to constrain rates of rockwall slope erosion for the upper Bhagirathi catchment.

Field Methods

Detailed geomorphic maps of the upper Bhagirathi catchment were constructed in the field with the aid of Landsat ETM+ data (acquired in 2003), topographic maps generated from a 3-arc second (~30 m) STRM DEM and Google Earth imagery. Geomorphic and sedimentological

techniques described by Benn and Owen (2002) were applied to identify and differentiate between landforms and sediment deposits.

Six major medial moraines were identified on the surface of Gangotri glacier (Fig. 2). Each moraine was named, the initial term *SD* for the supraglacial debris moraine and a subscript letter from *A-F*. The moraine sourced from the Kirti tributary valley is referred to as SD_A, for example. The SD_{A-C} moraines are the focus of this study as they are the largest and most accessible moraines on the glacier, and extend throughout the ablation zone, making them most likely to reflect bedrock slope erosion rates of the upper Bhagirathi catchment. The traditional moraine nomenclature, e.g., M_{1-x}, was not used to avoid confusion with Gangotri terminal and lateral moraines.

Sediment samples from each moraine were collected where possible at intervals from the snout to ~3 km up-glacier. The moraines were inaccessible beyond this point due to major instabilities in both hillslopes and glacier surface. The samples were taken from high relief, stable and well-defined moraine ridges, to avoid input from external sources including lateral moraines and hillslope deposits. The sampling locations were ≥20 m^2 in area to avoid sampling from a single rockfall event. Detailed sedimentological and geomorphic descriptions of the moraine were taken at each location. Approximately 3 kg of sediment was collected for each sample, with a grain size range of <3 cm (clay-coarse gravels) applying bulk sediment sampling methods of Gale and Hoare (1991).

Two samples were collected from the SD_A moraine, three from SD_B and one from SD_C. The samples were numbered in ascending order for each moraine, from the furthest up-glacier to the closest to the snout of Gangotri glacier. G_{sup1} sample (subscript sup1), e.g., was collected at 4315

m asl, ~3 km from the terminus. The location of each sample was recorded using a handheld Garmin Etrex 30 GPS unit and then photographed.

Medial moraine sediment analysis

Particle size distribution was determined by dry sieving each sample into five size fractions using the Wentworth (1922) particle size classification, following the techniques of Allen (1981). These fractions include: coarse-medium gravel (8–32 mm), fine gravel (2–8 mm), coarse-medium sand (0.25–2 mm), fine sand (63–250 μm) and silt and clays (<63 μm).

Particle shape analysis of sediment with a grain size of <1 mm and a consistent lithology, typically involves the examination of 100 grains per sample or 50 grains per size fraction (Hambrey and Glasser, 2003; Owen et al., 2008; Hambrey et al., 2008; Lukas et al., 2013). Given the larger grain size range (0–3 cm) and variability in lithology, we analyzed 100 grains per size fraction, totaling 500 per sample, to facilitate the comparison with other records. The size fractions of each sample were prepared using dilute HCl acid (0.1%, >12 hours) and a deionized water rinse. The fine sands, and silts and clays were examined using a digital microscope and scanning electron microscope (SEM) respectively, in the Sedimentology Laboratories and Advanced Material Characterization Center (AMCC) at the University of Cincinnati.

Clast roundness for each size fraction was determined using the Powers (1953) visual estimation chart and modified criteria of Ballantyne and Benn (1994). Clast sphericity for each size fraction was determined using the visualization charts of Zingg (1935). The clast shape of each sample was derived using the Snead and Folk (1958) criteria; the three orthogonal axes (a, b and c axes) of 100 grains per size fraction were plotted using a Graham and Midgley (2000) ternary diagram.

We use the Benn and Ballantyne (1994) covariance plot methods to determine the origins and transport histories of the medial moraine sediment. This method plots the C_{40} indices (c:a axes ratio <0.4) and roundness index (RA and RWR, the percentage of very angular-angular and well rounded-rounded clasts respectively) of unclassified sediment alongside control samples of supraglacial, extraglacial (e.g. hillslope deposits), moraine, subglacial, meltout and fluvial sediment samples. Our samples are compared with control samples from high altitude alpine settings detailed in Lukas et al. (2012, 2013), in the absence of viable control samples for the Himalayan-Tibetan orogen. We recognize that there is great variability within glacial sedimentary environments and are therefore cautious when interpreting these plots.

The percentage of clast surface weathering was determined for 100 quartz sand grains (0.25–2 mm) for each sample using the visual estimation charts of Sheridan and Marshall (1987) and Owen et al. (2003). Each clast was assigned to a weathering class (<10, 10–20, 20–40, 40–60, 60–80 and 80–100%), and a mean surface weathering was calculated for each sample.

Approximately 10 g of the silt-clay fraction of each sample was treated with sodium pyrophosphate (0.02 N) and then centrifuged to disperse the clay component from the remainder of the sub-sample. The clay fraction of each sample was mounted onto three glass slides using the smear mount method outlined by Moore and Reynolds (1997) for air-dried, ethylene glycol solvation and oven dried (450°C) slide analysis. Each set of three sides was analyzed using the X-ray Diffractometer in the X-ray Laboratory at the University of Cincinnati. The clay mineralogy of each sample was identified using the databases of Chenn (1977) and Moore and Reynolds (1997). The percentage component for each clay mineral was calculated using methods of Underwood and Pickering (1996) and Mac.Diff. 4.2.5 software.

Be-10 production rates and geochemical analysis

Beryllium-10 production rates for the upper Bhagirathi catchment were calculated using methods outlined by Dortch et al. (2011). The production rates were calculated from a STRM DEM with a spatial resolution of 30 m, using a revised sea-level high-latitude spallogenic production rate of 4.08±0.23 Be atoms g^{-1} a^{-1} (Martin et al., 2017; http://calibration.ice-d.org/) and a ^{10}Be half-life of 1.36 Ma (Nishiizumi et al., 2007) in MATLAB R2017.a. The production rate for each pixel was corrected for topographic shielding and then averaged to derive the mean ^{10}Be production rate for the catchment.

The sieved fractions were once more combined, crushed and re-sieved to attain the 250–500 μm fraction. This process helps to avoid bias in the contribution of any one grain size to the geochemical analysis of the sample. Quartz isolation, dissolution, chromatography, isolation of Be and the preparation of BeO were undertaken in the Geochronology Laboratories at the University of Cincinnati using the community standards and chemical procedures described by Kohl and Nishiizumi (1992), Nishiizumi et al. (1994), and Dortch et al. (2009). After mounting into steel cathodes, the ^{10}Be/^{9}Be of each sample were measured using accelerator mass spectrometry at the Purdue Rare Isotope Measurement (PRIME) Laboratory at Purdue University (Sharma et al., 2000).

Portenga et al. (2015) have demonstrated that when native ^{9}Be is factored into ^{10}Be/^{9}Be ratios, irrespective of geologic setting, the resultant ^{10}Be concentrations and inferred erosion rates can be significantly altered (20-400 %). The native ^{9}Be measured in ~5 g fractions of clean quartz per Gangotri sample was negligible (<1 ppm), so no adjustment to the ^{10}Be/^{9}Be ratios was made. A procedural blank ^{10}Be/^{9}Be ratio correction of $3\pm1\times10^{-15}$ was made for each sample. Muongenic production is negligible for the timescales of processes characterized for this study (Brown et al., 1995; Braucher et al., 2003). Corrections for quartz content variability between samples was

considered unnecessary in this setting (Ahmad et al., 2001; Vance et al., 2003). Minimum rockwall slope erosion rates were calculated using the ^{10}Be concentrations and catchment-wide production rates by applying methods described in detail by Lal (1991), Granger et al. (1996), Balco et al. (2008) and Dortch et al. (2011).

Ward and Anderson (2011) suggested that ^{10}Be accumulation within moraine debris during supraglacial transport down-glacier is negligible in landscapes with denudation rates of ≤ 1 mm/a. Accordingly, no corrections to ^{10}Be concentrations for Gangotri glacier were necessary. As some catchment erosion rates in Garhwal exceed this threshold (0.13–5.37 mm/a; Vance et al., 2003; Lupker et al., 2013; Scherler et al., 2014), ^{10}Be accumulation during this phase of glacier surface transport was calculated using methods of Seong et al. (2009; Supplementary Item 1). The revised rates significantly exceed the original rates (>18.7−3.4 mm/a) and are not considered to reflect the rockwall slope erosion rates of the catchment accurately, and are therefore not referred to herein.

Medial moraines in the Himalayan-Tibetan orogen including Bhagirathi are primarily composed of rockfall debris; smaller rockfall events occurring frequently across time and space, interjected by larger and less frequent events (Dunning et al., 2014; Rowan et al., 2015). Despite much of the volumetric erosion being achieved by these larger events, this bias within the sediment source in favor of small rockfall events means that the resultant erosion rates should be considered minimum estimates. Unique sediment exchange processes in the supraglacial environment (Scherler et al., 2009; Ward and Anderson, 2011; Lukas et al., 2012, 2013; Lupker et al., 2012; Scherler et al., 2015), sediment storage and remobilization, shifting geomorphic regimes and ice/snow shielding (Bierman and Steig, 1996; Scherler et al., 2014; Fame et al., 2018) are also likely to affect the ^{10}Be concentrations, and mean that the derived erosion rates reflect minimum rates. Interpreting the ^{10}Be concentrations of sediments in medial moraines is made more

challenging because of the variability in production rates for alpine catchments and lack of uniformity in the ^{10}Be inventories at the bedrock surface, which vary over temporal and spatial scales. A detailed summary of this methodology and its assumptions are provided by Ward and Anderson (2011).

Topographic and geomorphic analyses

ASTER DEMs and Landsat ETM+ data were used in conjunction with GIS Spatial Analyst tools for additional topographic analyses including catchment slope, 3-km-radius relief, hypsometry and aspect. These parameters are defined for the glacial-periglacial realms of the upper Bhagirathi catchment only, as this is the area that pertains to the focus of our study. Topographic analyses of Chhota Shigri catchment in Lahul, northern India and Baltoro catchment in the Central Karakoram, Pakistan was also conducted to enable comparisons between slope erosion and catchment characteristics across the NW Himalaya.

Upper Bhagirathi catchment temperature reconstructions

The altitudinal-temperature gradient or adiabatic lapse rate ($\Delta T/\Delta Z$) for high relief mountain settings typically range between 6 and 11°C/km (Derbyshire et al., 1991; De Scally, 1997; Thayyen et al., 2005; Siddiqui and Maruthi, 2007; Bashir and Rasul, 2010; Pratap et al., 2013; Kattel et al., 2013, 2015). Conventional wisdom is that regional lapse rates better account for temporal and spatial variations, although their application within alpine settings such as the Himalayan-Tibetan orogen is particularly challenging due to the lack of weather stations (Blandford et al., 2008). We use an adiabatic environmental lapse rate of 7°C/km asl, a product of both an approximate median for the orogen, and a lapse rate derived from the local weather stations of Mukhim (~1900 masl) and Bhojbasa (~3780 masl). This lapse rate is used to estimate the summer and winter surface temperatures throughout the upper Bhagirathi catchment.

The optimum frost cracking envelope defined by Hales and Roering (2005) falls between mean annual temperatures of -8 and -3 °C. Bhagirathi catchment elevations which have surface temperatures within this range were determined using the chosen lapse rate and a 30-m-resolution SRTM DEM. The frost-cracking envelope was also calculated with respect to depth by modeling the thermal structure of the near surface of the catchment using methods outlined in detail by Anderson and Anderson (2010). A thermal diffusivity of 1.15 mm^2/s was used as it reflects an approximate midpoint in diffusivity values for the following substrates that characterize the catchment; regolith, landforms and deposits, and bedrock. This provides an estimate for the rate of heat transfer from the surface. The spatial distribution and depth of permafrost (0 °C; Brown, 1970) was also calculated for the catchment using the same methods as described above. Despite offering a reasonable assessment of the frost cracking and permafrost distribution, these simplified methodologies involve a series of assumptions about the physics, temperature data and geologic setting (Anderson and Anderson, 2010). Caution must therefore be exercised when interpreting this data, particularly because surface temperatures of Bhagirathi will have varied over space and time. These analyses aim to determine whether slope failure in the upper Bhagirathi catchment can be influenced by surface temperature and the associated periglacial weathering processes.

ELA and snowline altitude (SA) reconstructions

ELAs and ELA depressions (ΔELA) were calculated for the contemporary and past glacial stages within the upper Bhagirathi catchment using methods described by Osmaston (2005), Benn et al. (2005), Heyman (2014) and Sharma et al. (2016). To reduce the uncertainties inherent within these reconstructions, a mean ELA was calculated for each glacial stage from reconstructions derived from each of the following methods: area-altitude (AA); area accumulation ratio (AAR) with ratios of 0.4, 0.5 and 0.6; and toe-headwall accumulation ratio (THAR) with ratios of 0.4 and 0.5; Benn et al. 2005). This approach has been successfully applied in Ladakh, northern India

(Dortch et al., 2010; Orr et al., 2017, 2018; Saha et al., 2018) and the Karakoram (Seong et al., 2007), reflecting accurate estimates of the ELAs. Our study adopts methods strongly recommended by Porter (2001), whereby the mean ELA of a glacial stage also provides an estimation of the snowline altitude. The aim of these analyses is to evaluate the effect of the timing and nature of glaciation on the rates of bedrock slope erosion throughout the last glacial.

Medial moraine descriptions

Gangotri glacier system has six major medial moraines on its surface; the three investigated moraines of this study ($SD_{A\text{-}C}$) extend over 50% of the length of the glacier's ablation zone (Fig. 2; Table.1). The medial moraines are composed of supraglacial diamict, and like many alpine glaciers, the debris thickness is heterogeneous over space and time (10^1–10^4 years), ranging from a few millimeters to several meters thick (Owen, 1989; Schroder et al., 2000; Benn et al., 2012; Srivastava, 2012). This heterogeneity contributes to variations in the surface morphology, mass balance and flow velocities of the glacier (Benn and Owen, 2002; Rowan et al., 2005; Swift et al., 2005; Haritashya et al., 2006; Hambrey et al., 2008; Gibson et al., 2017), in addition to affecting the glacier's sensitivity to climatic and environmental change (Scherler et al., 2011a,b).

The moraine morphologies are characterized by irregular surface topographies, the result of variable diamict thicknesses, and distribution and orientation of steep relief ridges, depressions and ice cliffs. The widths of the moraines range from 50 to 650 m, widening towards the snout of Gangotri glacier (Fig. 2; Supplementary Item 2).

These supraglacial diamicts are composed of massive sandy boulder gravels with a finer sandy-silt matrix containing interstitial ice (Fig. 3; Supplementary Item 3). The subangular-very angular boulder gravels have surfaces that range from unweathered to moderately weathered. Striations or

chattermarks are not present on any clast size. Large boulders (>2−0.25 m) are located on or slightly offset from the moraine ridges with some evidence of varnish and previous toppling.

Finer sediment increases with proximity to the debris-ice interface, likely as a result of sorting through rainfall and meltwater flows (Hasnain and Thayyen, 1996). These fine sediments, and evidence of frost action on pebbles−boulders, indicate active periglacial weathering processes and continued sediment production and/or clast modification by interclast attrition and abrasion across the glacier surface (Owen et al., 2003; Benn and Evans, 2010; Benn et al., 2012). No clear englacial sediment horizons were identified in the field, despite some evidence of englacial silts and sands at the glacier surface. The exhumation of subglacial sediment to the englacial or supraglacial system is therefore likely to be very localized (Owen et al., 2003). Discontinuous soil development and tundra vegetation are restricted to the stable medial moraine ridges.

The diamicts are composed of biotite granite, tourmaline leucogranite, with some gneiss, mica schist and quartzite, reflecting the local bedrock (Searle et al., 1999; Srivastava, 2012). Sediment samples are composed of granites and schists, with the exception of the SD_A samples that include some gneiss clasts.

SD_A moraine

The SD_A medial moraine extends ~12 km from the Kirti tributary catchment to within ~500 m of the snout of Gangotri glacier (Fig. 2). A medial moraine from a Kirti sub-catchment coalesces with the main tributary moraine at 4670 m asl. SD_A narrows in width at the confluence (~600–300 m) between Kirti tributary and Gangotri glaciers, as a result ice deformation and shearing (Hubbard et al., 2004; Gibson et al., 2017).

The SD_A diamict has a unique rusty brown color, likely the result of the weathering of the local Augen gneiss or Vaikrita group gneiss bedrock slopes (Fig. 3B). Sharing the same source outcrops, the medial moraine (SD_E) of Ganohim glacier also has this coloration.

G_{sup1} (30.9°N, 79.09°E, 4315 m asl) was retrieved ~3 km from the glacier snout. G_{sup2} (30.9°N 79.08°E) was collected at 4280 m asl, ~500 m downstream and northwest of G_{sup1}.

SD_B moraine

SD_B is the centermost, gray medial moraine of Gangotri glacier that extends ~15 km from the modern ELA (4510–5160 m asl) to the glacier snout (Fig. 3B, 4). SD_B is the most stable moraine of this study, with proportionally fewer ice cliffs, ice collapse features and interstitial ice within the diamict matrix.

G_{sup3} (30.89°N, 79.09°E) was retrieved at 4325 m asl, ~300 m northeast of G_{sup1}, ~3 km from the glacier terminus. G_{sup4} (30.90°N, 79.09°E) was collected ~500 m northwest and down glacier from G_{sup3}, at 4285 m asl. G_{sup5} (30.92°N, 79.08°E) was sampled ~500 m from the glacier snout at 4130 m asl.

SD_C moraine

SD_C also extends ~15 km from the modern ELA to the glacier snout. The diamict has a slightly darker gray coloration to the SD_B moraine (Fig. 3D).

Due to access, only one sample could be retrieved from this moraine, ~500 m from the glacier snout. G_{sup6} (30.92°N, 79.08°E) was collected at 4130 m asl, slightly upstream from the confluence between the Raktavaran tributary catchment and Gangotri trunk glacier.

RESULTS

Medial moraine sediment analysis

Gangotri glacier medial moraine samples consist of medium-coarse sands and fine gravels; these fractions together account for 71−73% by weight of each sample. There are variations in the particle-size distributions between the moraines and between samples taken from specific moraines (Fig. 5; Supplementary Item 4). Caution must be exercised when interpreting shifts in particle size distribution with distance down-glacier, as only three or fewer samples are collected from each moraine.

Sediments from the SD_A moraine become progressively coarser down-glacier, the percentage component of fine gravels increasing from 30 to 55% between G_{sup1} and G_{sup2}, and the fraction of medium-coarse sands decreasing from 36 to 26% (Fig. 5). Depletion in the finer sediment fractions is also observed; sediment with particle sizes <0.25 mm (fine sand−clay) decrease from 28 to 11%. The supraglacial sediment of SD_A is marginally coarser than the other moraines of this study.

The particle size distribution of the SD_B moraine sediment fluctuates with distance down-glacier, other than a slight increase in the fine and medium-coarse gravel fractions. The percentage component of medium-coarse sands for this moraine range between 37 and 63%, and is the highest of this study.

The SD_C moraine has the largest percentage component of medium-coarse gravels of this study, at 14%.

No significant relationship can be identified between particle size distribution and proximity to the glacier snout when assessing down-glacier sediment transport as a whole. Whilst the percentage of medium-coarse gravels and silts-clays increase and decrease down-glacier respectively, the remaining fractions (fine sands−fine gravels) have fluctuating percentage distributions. The greatest proportion of fine sediment (silt-clay; <75 μm) for the SD_A and SD_B moraines are found in the samples located furthest from the glacier snout (G_{sup1}, G_{sup3}). This fine sediment fraction is likely either mobilized down-glacier by meltwater processes and rainfall or introduced by another source.

Comparisons between these records are restricted to sediment fractions <4 mm, due to the particle size range of available datasets. The percentage component of each particle size broadly decreases with particle size for medial moraine samples from Gangotri glacier and existing studies from the European Alps, Iceland and Norway (Fig. 6). There is some deviation from this trend for the SD_A and SD_B moraines, where the sediment is predominantly composed of medium-coarse sands. The percentage silt content of these moraines is either similar or higher than supraglacial sediment recovered from other glacial systems. Gangotri glacier medial moraine sediment is therefore largely finer than the supraglacial sediment from previous studies, based upon this particle size range alone.

Gangotri glacier medial moraine samples are largely made up of angular (32−48%) and subangular (19−46%) grains, with ≤1% of grains considered either rounded or well rounded (Fig. 7). Accordingly, grains of low sphericity constitute between 71 and 82% of each sample. No significant relationship can be identified between grain size and particle roundness or sphericity for any one moraine or sediment sample (Supplementary Item 5, 6).

The bladed (14−23%) and very bladed (30−40%) particle shape classes are the most prevalent for Gangotri glacier samples, where over 50% of grains per sample have c:a and b:a ratios <0.3 (Supplementary Item 7). Compact grains constitute <10% of each sample. The SD_A moraine sees a minor increase in the bladed and very bladed components of its samples with distance down-glacier, whilst SD_B sees a slight increase in the bladed and decrease in the very bladed fractions. The SD_C moraine records the highest percentage values of very bladed and very platy grains of this study, 40 and 28% respectively.

The covariance of clast shape and roundness indices are presented in RA-C_{40} and RWR-C_{40} plots for Gangotri glacier and previous studies in Fig. 8. Distinguishing between transport pathways must be approached with care due to the pronounced overlap in facies indices. The RA (85−94%) and C_{40} (75−96%) indices and large proportion of bladed and extremely bladed grains suggest that the medial moraines of this study share a supraglacial transport history (Benn and Owen 2002; Hubbard 2004; Lukas et al., 2013). Some extraglacial and moraine control samples also record RA values greater than 80%. The RWR indices for the medial moraines range between 6 and 15%, higher than the ~0% values typical for supraglacial samples. The more rounded component of the samples may reflect the input of sediment from other realms of the glacial system, or clast rounding by englacial and/or supraglacial transport, or the effects of meltwater on the glacier surface. The SD_C moraine's proximity to Raktavaran and Chaturangi tributary glaciers may result in the receipt of sediment from its subglacial, proglacial and fluvial system and therefore may explain the high RWR value (15%) of G_{sup6}.

Percentage surface weathering estimates of quartz grains for Gangotri glacier range from 30 to 100%, with mean surface weathering ranging from 66±22 to 78±17% (Fig. 9). A slight, yet negligible increase in surface weathering can be identified down glacier for the SD_A and SD_B moraines, and the glacier as a whole. A bimodal frequency distribution of surface weathering

(peaks at ~50% and 80−90%) transforms to a unimodal distribution (peak at 80%) with greater proximity to the glacier snout (Supplementary Item 8, 9).

The clay component of the SD_A G_{sup1} and G_{sup2} samples are made up of a mixed layer illite/smectite (97.1 and 97.7% of total sample, respectively) and a chlorite fraction (Supplementary Item. 10). The percentage smectite for the mixed layer group is 56% for G_{sup1} and 55% for G_{sup4}, and is likely to be the product of the preferential weathering of volcanic source rocks, namely the Augen or Vaikrita group gneiss. The illite and chlorite component of this moraine sediment is typical of a glacial setting and reflects the low-grade metamorphism of the Bhagirathi region (Birkeland 1974; Chamley 1989; Regmi et al., 2013). This mixed layer illite/smectite is also present in SD_B's G_{sup3} (25% smectite), making up 95.4% of the sample's clay fraction, the outstanding component being chlorite. The clay component of the remaining SD_B G_{sup3} and G_{sup5} samples is largely made up of illite, with 1.5 and 0.8% chlorite, respectively. Similarly, the G_{sup6} clay fraction from the SD_C moraine is composed of 98.2% illite and 1.8% chlorite.

Rockwall slope erosion rates of the upper Bhagirathi catchment

G_{sup1} and G_{sup2} from the SD_A moraine have ^{10}Be concentrations of 1.1±0.2 and 1.6±0.3 x10^4 at/g SiO_2, respectively. These concentrations infer bedrock slope erosion rates of 5.3±1.2 mm/a for the G_{sup1} sample, and 3.6±1.2 mm/a for G_{sup2} (Table. 2). The G_{sup3}, G_{sup4}, and G_{sup5} samples from the SD_B moraine have ^{10}Be concentrations of 2.7±0.3, 2.5±0.3 and 2.6±0.3 x10^4 at/g SiO_2 respectively. An inferred erosion rate of 2.1±0.4 mm/a is derived from G_{sup3}, 2.3±0.4 mm/a from G_{sup4}, and 2.2±0.4 mm/a from G_{sup5}. The SD_C G_{sup6} sample has a ^{10}Be concentration of 1.5±0.4x10^4 at/g SiO_2 and an inferred erosion rate of 3.8±1.1 mm/a.

Geomorphic analyses

The detailed geomorphic mapping of upper Bhagirathi (Fig. 2) reveals that the identification of discrete geomorphic zones within the catchment is not possible owing to the absence of the vertical stratification of landforms (Fig. 2; Supplementary Item 11). Terraces and fans occupy elevations <5000 m asl, whereas the remaining landforms extend the full extent of the upper Bhagirathi catchment.

The slopes of the upper Bhagirathi catchment range from 0 to 75°, gentle (<30°), moderate (31−45°) and steep (>46°) slopes occupying 38, 25 and 37% of the total catchment, respectively. The mean tributary catchment slopes of the study area range between 30 and 41° (Table. 1). Between 10 and 53% of the catchment areas are occupied by glaciers; the glacier surface slopes are included within this catchment slope analysis, which introduces a degree of uncertainty to these mean slope values. Catchment 3-km-radius relief ranges from 1.4±0.4 to 2.2±0.3 km.

Steep relief slopes that exceed 35° are largely unable to support regolith, snow or ice (Gruber and Haerberli, 2007; Nagai et al., 2013). Srivastava (2012) maintains that ~50% of the catchment's bedrock slopes have angles >60°. The steep topography of the catchment therefore means that it is susceptible to both rockfall and avalanching (Hewitt, 1988; Bookhagen et al., 2005; Dunning et al., 2007; Gruber and Haerberli 2007; Mitchell et al., 2007), which likely provides the primary source of supraglacial sediment on Gangotri glacier (Srivastava, 2012).

Ideal conditions for periglacial weathering processes including frost-shattering, cryofracturing, and frost heave are present throughout the upper Bhagirathi catchment. Optimum frost cracking conditions (-3−-8°C) within the catchment migrate from elevations of ~5680−6380 m asl during the summer, to ~3780−4480 m asl during the winter. This is consistent with the frost-cracking envelope between 4000−6000 m asl devised by Brozović et al. (1997) for the NW Himalaya.

These temperatures extend to a maximum depth of ~2.3 m into the near-surface between 3780 and 4430 m asl (Fig. 10).

Peaks which exceed ~6380 m asl (including Shivling, Meru and the Chaukhamba Massif) have surface temperatures which are lower than -8°C, which theoretically reduces the efficiency of periglacial weathering processes. The distribution and magnitude of these processes are affected by diurnal and seasonal cycles and climatic and microclimatic variations. With the gradual warming of temperatures over the last few glacial cycles, optimum frost cracking conditions are likely to have extended to lower elevations within the catchment than the present.

Transient or seasonal permafrost can occur at elevations between 3380 and 5280 m asl within the catchment; at higher elevations the permafrost can be permanent. Transient permafrost, which exacerbates slope instabilities and mass wasting (Fischer et al., 2006), may extend from the catchment slopes to the proglacial zone of Gangotri glacier and valley floor. Permafrost penetrates the near surface between 3080 and 3380 m asl, to a maximum depth of 0.8 m (Fig. 10).

ELA and SA reconstructions

The ELAs of contemporary glaciers in the Bhagirathi catchment range from 4880 to 5665 m asl (Table. 3), falling within the uncertainties of, and marginally above past estimates of 4510−5390 m asl (Owen and Sharma, 1998; Naithanu et al., 2001; Ahmad and Hasnain, 2004, Burbank et al., 2004; Srivastava, 2012; Singh et al., 2017).

Gangotri glacier has retreated ~30 km upstream over the past ~60 ka (Owen and Sharma, 1998; Burbank et al., 2004), the ELA rising from 4095±295 to 5160±160 m asl, giving an ΔELA of 1065±320 m. Over this timescale this is an impressive retreat of glacier ice; glacial studies across the Transhimalaya of northern India (Dortch et al., 2011; Orr et al., 2017, 2018) and the Tibetan

plateau (Heyman et al., 2014) document maximum ΔELAs between 240−290 and 280−494 m, respectively. This rate of recession has yet to be identified in Garhwal, where local glacial stages record ΔELAs <100 m within the past 1 ka, compared to an ΔELA of 465±140 m for Gangotri glacier. A net loss in glacier volume since 1.6 ka is indicated by the heights of the ice-contact Gangotri glacial stage moraines relative to the glacier surface. Approximately 50% of the total catchment is above the modern snowline altitude (5160±160 m asl).

DISCUSSION

Bhagirathi rockwall slope erosion

Medial moraine sediment characteristics for the lower ~3 km of the ablation zone of Gangotri glacier are broadly similar, despite the discrete origins of each landform. Particle shape analysis indicates a predominantly supraglacial transport history with possible contributions from other landscape realms, i.e. moraine, extraglacial. Clast roundness and surface weathering is attributed to periglacial weathering processes including freeze thaw, frost cracking and ice wedging, which dislodge angular rock fragments from the bedrock slopes and/or regolith (Benn and Lehmkuhl, 2000; Schroder et al., 2000; Benn et al., 2003; Hambrey et al., 2008; Lukas et al., 2012). Moisture availability, surface temperatures (Hales and Roering, 2007; Humphreys and Wilkinson, 2007; Moores et al., 2008; Dühnforth et al., 2010; Fischer et al., 2010, 2012; West et al., 2014; Eppes and Keanini, 2017) and rock mass strength (Augustinus, 1995; Wegmann et al., 1998; Murton et al., 2006; Eppes and McFadden, 2008) moderate the hillslope debris flux. The steep relief topography of the Bhagirathi catchment promotes hillslope-glacier coupling through mass wasting events including rockfalls and avalanching (Brozović et al., 1997; Anderson, 2005; Matsuoka and Murton, 2008; Foster et al., 2010; Scherler et al., 2011b). Rockfalls play a significant, if not principal role in the rockwall slope erosion, which is consistent with the observation that mass movements are the dominant mechanism for Himalayan landscape

denudation (Gabet et al., 2004; Dortch et al., 2009; Lupker et al., 2012). The frequency and magnitude of rockfall events over 10^5–10^3 year timescales are likely controlled by regional erosion rates, which are moderated by climate and/or tectonism (Molnar et al., 2007; Scherler et al., 2014; Gibson et al., 2017). The larger fine-sediment component to the samples from Gangotri glacier compared with other alpine glaciers (Fig. 6) may be explained by: 1) enhanced physical weathering of clasts; 2) input of fines from external sources; or 3) the preferential sampling of smaller grain sizes. Significant chemical weathering of moraine sediment is unlikely within these alpine environments, particularly in the absence of carbonate rocks (France-Lanord et al., 2003; Garzanti et al., 2007; Tripathy and Singh, 2010).

The ^{10}Be concentrations vary between the samples of each Gangotri glacier moraine and between individual landforms, despite sharing similar sediment characteristics (Fig. 11). No relationship is evident between ^{10}Be concentration and distance down-glacier. The range in ^{10}Be concentrations of our dataset ($1.1\pm0.2\text{x}10^4$–$2.7\pm0.3\text{x}10^4$ at/g SiO_2) may be due to insufficient sediment mixing, the prior or punctuated exposure to cosmic rays, shielding by snow, ice or regolith, or weathering (Seong et al., 2009; Ward and Anderson, 2011; Heyman et al., 2011).

The SD_A moraine records the lowest ^{10}Be concentrations, corresponding to the highest interpreted erosion rates of this study. The close proximity of SD_A to rockwall slopes and external sediment sources along the length of the landform, and the possible greater sensitivity of smaller catchments to external forcing, are two possible explanations for these lower nuclide concentrations. The concentration disparity between the SD_A samples may due to the sampling of isolated rockfall event(s) rather than amalgamated moraine sediment.

Similarly, the sedimentology and low ^{10}Be concentrations of SD_C's G_{sup6} may be the result of sediment input from proximal rockwall slopes at the snout of Gangotri glacier or contributions from Raktavaran and/or Chaturangi tributary glaciers.

The SD_B samples have the highest ^{10}Be concentrations of this study ($2.5\pm0.3 \times 10^4$–$2.7\pm0.3 \times 10^4$ at/g SiO_2), which each fall within uncertainty of each other, and record the lowest interpreted slope erosion rates (2.1±0.4–2.3±0.4 mm/a). The SD_B moraine extends the full length of the ablation zone of Gangotri glacier with no direct contact to the catchment slopes. Accordingly, the SD_B rates are considered to be the most representative of upper Bhagirathi catchment rockwall slope erosion. To test the robustness of our interpretations, it would be worthwhile to extend this investigation up-glacier and evaluate variations in ^{10}Be concentrations throughout the ablation zone, and across grain sizes.

The ELA reconstructions for the glacial stages show that the spatial extent of the glacier and periglacial realms has decreased significantly over the past 60 ka, which means that the slope area contributing debris directly to the glacier surface has reduced. Studies suggest that the timing and nature of glaciation and the associated geomorphic landscape change for the upper Bhagirathi catchment is governed by climate. The magnitude and rates of rockwall slope erosion are therefore not only intrinsically linked to climate through periglacial weathering processes, but also as a result of climate-driven glaciation affecting the extent of slope-glacier coupling. Accordingly, rates of rockwall slope erosion and the contribution of the periglacial realms to the denudation budget of the catchment is likely to have fluctuated throughout the last glacial.

Garhwal landscape denudation

Scherler et al. (2015) have shown that rates of fluvial incision in Garhwal during the late Pleistocene was greater than the present by a factor of ~2–4. Whether periglacial erosion has

remained constant across these timescales or followed the patterns of fluvial incision, the influence of rockwall slope erosion on the topographic evolution of upper Bhagirathi is likely have been maintained over time. Hillslope erosion in this alpine setting is likely to affect the sediment flux and storage of snow and ice from diurnal to millennial timescales, and then more broadly influence catchment configuration, microclimates (Bhambri et al., 2011; Srivastava, 2012), limit relief and affect the architectural organization of the local fault systems (Validya, 1991; Sorkhabi et al., 1996; Bali et al., 2003). The frequency and magnitude of rockfall events in Bhagirathi may have been affected, in part, by catchment-specific conditions, and external shifts in climate, geomorphic or tectonic regime. The global intensification of late Pleistocene glaciation, for example, caused extensive mass redistribution and localized incision throughout the Himalayan-Tibetan orogen (Zeitler et al., 2001; Brozović et al., 1997; Bookhagen et al., 2005; Hewitt, 2009; Whipple, 2009). This is likely to be similar in the Bhagirathi catchment where landscape denudation could be attributed to the changing glacier mass balance over time.

The rates of rockwall slope erosion largely exceed the averaged catchment-wide and exhumation rates of Bhagirathi and the Garhwal region (Fig. 11). Comparing these rates is challenging as they reflect landscape change through a variety of mechanisms and across different temporal and spatial scales. However, our erosion dataset supports the view that erosion of alpine headwaters outpace the wider drainage basin (Oskin and Burbank, 2005; Naylor and Gabet, 2007), and that the distribution and magnitude of erosion can vary significantly over short distances downstream (Scherler et al., 2014). The higher rockwall slope rates of 2.1±0.4−5.3±1.2 mm/a in the Bhagirathi catchment compared with the catchment-wide rates of 0.1±0.001−5.4±0.5 mm/a suggest that catchment headwaters are more sensitive to external forcing than the wider catchment. Alternatively, the difference in denudation rates may be because our dataset offers a higher resolution record of erosion than those on the catchment or mountain range scale, or that these latter records eliminate the ‘noise’ in sediment flux data over time, such as single mass

wasting events initiated by large and/or stochastic seismic events (Sadler and Jerolmack, 2014; Willenbring et al., 2013). The slope erosion rates of this study remain lower than the regional uplift rates of 4−5.7 mm/a (Barnard et al., 2004; Scherler et al., 2014), which may explain the preservation of high relief slopes within the study area.

Rockwall slope erosion of the NW Himalaya

Comparisons of ^{10}Be concentrations in medial moraine sediment of Gangotri glacier with similar datasets from Chhota Shigri in Lahul (Scherler and Egholm, 2017) and Baltoro glacier in the Central Karakoram (Seong et al., 2009) show that the ^{10}Be concentrations at these other localities exceed those in our study (Fig. 12). The SD_B samples that are considered to best reflect Bhagirathi slope erosion measure ^{10}Be concentrations >1x10^4 at/g SiO_2 lower than Chhota Shigri or Baltoro, and record erosion rates twice as fast. The ^{10}Be concentrations of the three study areas are compared with catchment parameters and regional climate records to decipher the possible drivers of rockwall slope erosion in the NW Himalaya (Fig. 12).

No significant relationship is evident between catchment area and ^{10}Be concentrations (Fig. 12). The catchment area does not account for the total surface area of the source bedrock slopes, a parameter that may influence these concentrations to a greater extent. Approximately 80, 50 and 53% of the total catchment area of Bhagirathi, Chhota Shigri and Baltoro respectively, are above the ELA/SA altitudes and nourish the glaciers through snow and ice avalanching. Changes to the snowline altitude over time likely affect the relative abundance of exposed bedrock and regolith-covered slopes and therefore dictate the hillslope debris flux. Similarly there is no correlation between ^{10}Be and glacier area, and by association, size of medial moraine.

No relationship is apparent between mean slope and ^{10}Be concentration, despite other studies being able to link these variables on a catchment scale and show that greater slope angles promote

a larger debris flux (Finlayson et al., 2002; Burbank et al., 2003; Ouimet et al., 2009; Scherler et al., 2011b, 2014). Although the slopes will broadly facilitate rockfall and avalanching (Luckman, 1977; Gruber and Haerberli, 2007; Bernhardt and Schulz, 2010; Nagai et al., 2013) and the eventual evacuation of sediment from the catchment, each of the study areas is also able to store extensive volumes of sediment in the form of landforms and sediment deposits (Fig. 2; Seong et al., 2009). These landforms typically have gentler slopes, which transfer sediment to the glacier surface via diffusive creep processes (Carson and Kirkby, 1972). Not only will these stores of sediment have implications for the sediment flux of the catchments, but also they may influence the ^{10}Be concentrations measured within medial moraine sediment.

The 3-km-radius relief of the study areas exceed ~1.6 km, the steeper relief catchments measuring the highest ^{10}Be concentrations, and therefore the lowest interpreted bedrock slope erosion rates. This suggests that rates of bedrock slope erosion can in some cases be insufficient to limit catchment relief in the NW Himalaya. A more likely explanation is that the 3-km-radius relief is largely dictated by the local uplift of the study areas.

The temperature data is recovered from weather stations outlying the study areas and therefore does not accurately reflect catchment temperatures. The ranges in annual recorded temperatures prevent any correlations being made between this climatic parameter and ^{10}Be. The high altitude setting of each study area with mean catchment elevations >4000 m asl (Fig. 12D) does however mean that the rockwall slopes of each catchment lie within the Brozović et al. (1997) 4000−6000 m asl frost cracking window for the NW Himalaya.

A tentative relationship lies between total annual rainfall and ^{10}Be concentrations, where higher rainfall coincides with higher interpreted rockwall slope erosion rates. This supports the extensive work on the coupling between precipitation and erosion in the Himalaya, where enhanced

moisture in the monsoon-influenced Lesser and Greater Himalaya is thought to drive more rapid landscape denudation, compared to the semi-arid interior of the orogen (Benn and Owen 1998, 2002; Harper and Humphrey, 2003; Bookhagen et al., 2005; Anders et al., 2006; Bookhagen and Burbank, 2006; Gabet et al., 2008; Owen, 2009). This relationship is not completely straightforward for our study areas however, as ^{10}Be concentrations shared by samples from Baltoro glacier (4.4 ± 0.3 x10^4−11.7 ± 2.2x10^4 at/g SiO_2) and Chhota Shigri ($3-6$x10^4 at/g SiO_2) experience contrasting annual rainfall of <500 and >900 mm, respectively. The complex climate-topography interactions of each study area prevent a conclusive relationship between erosion and this climatic parameter from being identified. This association does suggest however that rockwall slope erosion is sensitive to precipitation and therefore the glacial-periglacial realms of Himalayan catchments are likely to respond to major climatic events and/or environmental change over time.

Studies across the Himalayan-Tibetan orogen have drawn tentative links between erosion and climo-topography (Scherler et al., 2011a,b, 2014; Bookhagen et al., 2005; Bookhagen and Burbank, 2006; Gruber and Haeberli, 2007; Dortch et al., 2011). Our regional assessment of the NW Himalaya has demonstrated that no single discussed parameter provides a dominant control for bedrock slope erosion. We must therefore consider what other variables may be influencing landscape change in these high altitude settings.

Although glacial erosion is considered secondary to periglacial processes; glacier dynamics may affect the rates of rockwall slope erosion. Temperate glaciers, which occupy the monsoon-influenced Himalaya, erode the glacier bed through quarrying and abrasion, which can exploit fractures at the base of the glacier valley slopes (Benn and Evans, 2014; Benn and Owen, 2003). Glacier retreat and changes to mass balance can also lead to the debuttressing of these slopes. These processes can affect the hillslope debris flux and either contribute to, or trigger mass

wasting (Church and Slaymaker, 1989; Watanabe et al., 1998; Ballantyne, 2002a,b). In the semi-arid Himalaya, sub-polar glaciers frozen to the bed are unlikely to further slope denudation processes and therefore would maintain low erosion rates. Glacial velocity, hydrology and snow blow may also affect the rates of slope erosion over time (Matsuoka and Sakai, 1999, Mitchell and Montgomery, 2006; MacGregor et al., 2009; Scherler et al., 2011b; Barr and Spagnolo, 2015).

The large range of ^{10}Be concentrations and the relatively uniform rock mass strength across the study areas suggest the absence of a dominant lithological control to the rates of rockwall slope erosion. Investigating the jointing, structure and moisture content of the catchment walls would help to evaluate the ongoing damage of frost action and the susceptibility of the rock to failure (Hallet et al., 1999; Murton et al., 2006; Hales and Roering, 2007).

Studies throughout Garhwal and the NW Himalaya have underpinned a tectonic control within the distribution and magnitude of erosion, where erosion is strongly influenced by the Indo-Asian convergence and rock uplift patterns dictated by the geometry and shortening of the Main Himalayan Thrust (Burbank et al., 2003; Thiede et al., 2005; Scherler et al., 2014). Although contributing to this work is beyond the scope of this study, persistent seismicity throughout the Punjab, Himachal Pradesh and Uttarkhand districts of northern India may introduce a neotectonic control to landscape evolution (Bali et al., 2003; Scherler et al., 2014). In Garhwal for example, the 1991 Uttarkashi (M 6.1; Valdiya, 1991; Owen et al., 1996; Bali et al., 2003) and 1999 Chamoli (M 6.6; Rajendran et al., 2000) earthquakes occurred during the applicable timescales of the Bhagirathi erosion record and may have therefore triggered mass redistribution on a sufficient scale to affect the erosion rates of our study.

The mobilization and transfer of sediment from the valley walls to the glacier surface is an example of one of the primary stages in the evacuation of sediment from a glacerized catchment. Models of sediment transfer on the catchment scale argue that a shift in sediment flux requires a set of preconditioning factors and one or more forcing factor (Ballantyne, 2002a,b; McColl, 2012). This is true of the upper Bhagirathi catchment, where the preexisting landscape dynamics, which include catchment parameters, and transitions in climate, tectonic or geomorphic regime, are necessary to explain the nature and rates of bedrock slope erosion over time. Understanding the topographic evolution and configuration of Bhagirathi and glacierized catchments throughout the NW Himalaya is made particularly challenging as it involves processes that operate across a variety of temporal and spatial scales. Despite the controls of the evolution of alpine headwaters remaining elusive, this is the first study to quantify the rates of bedrock slope erosion in the upper Bhagirathi catchment, which has helped to demonstrate the importance of rockfall processes within mountain sedimentary systems.

CONCLUSION

Rockwall slope erosion has been defined for the upper Bhagirathi catchment by three medial moraines of Gangotri glacier. Bedrock slope erosion of the catchment is best reflected by the SD_B moraine interpreted rates, which range from 2.1±0.4 to 2.3±0.4 mm/a. Rockwall slope erosion would have likely varied over space and time, and responded to shifts in climate, geomorphic and/or tectonic regime throughout the late Quaternary.

The rockwall slope erosion rates exceed the averaged catchment-wide (0.1±0.001−5.4±0.5 mm/a) and erosional exhumation (1.5±0.5 mm/a) rates of Bhagirathi and the Garhwal region, indicating that erosion at the headwaters can outpace downstream reaches and the wider catchment. A possible explanation is that the high altitude periglacial settings of upper Bhagirathi have a

greater sensitivity to external forcing such a shift in climatic conditions, than the wider catchment or mountain range. Alternatively, the variance found between the rates of landscape denudation may be due to the difference in the temporal and spatial resolution of the erosion records.

Rockwall slope erosion rates are higher in upper Bhagirathi compared to the catchments of Chhota Shigri in the Lahul Himalaya and the Baltoro glacier in the Central Karakoram. Comparisons were made between the erosion datasets of these three study areas and catchment parameters and regional climate records, including catchment and glacier area, mean elevation and slope, 3-km-radius relief and annual temperature and rainfall. A tentative relationship is evident between erosion and rainfall, where more rapid slope erosion was recorded in the monsoon-influenced Lesser and Greater Himalaya, compared with the semi-arid interior of the orogen. No other individual catchment attribute was found to offer a control on the rates of slope erosion in the NW Himalaya.

We were unable to confidently link rockwall slope erosion with climo-topography. We conclude that bedrock slope erosion in the three study areas and then more broadly across the NW Himalaya is likely governed by individual catchment dynamics, which vary across space and time. The frequency and magnitude of rockfall and avalanche events is therefore determined by a set of preconditioning factors unique to each catchment, and one or more local and/or regional forcing factor.

By continuing to decipher the rates and controls of rockwall slope erosion, we will improve our understanding of the role and importance of periglacial processes in the morphological development of mountain ranges and contribute to future studies of sediment flux and wider landscape change across the orogen.

ACKNOWLEDGMENTS

A SEED grant from PRIME laboratory, Purdue University and a Research Fellowship Grant from the Graduate Student Governance Association of the University of Cincinnati helped to fund the AMS measurements of this project. ENO, LAO and SS thank the Department of Geology at the University of Cincinnati, Jim Benton and Jawaharlal Nehru University for logistical and fieldwork support. ENO thanks the Geological Society of America for a Graduate Student Research Grant to conduct fieldwork. ENO thanks Jeff Hannon, Sarah Hammer, Dr. Paula Marques Figueiredo and Dr. Warren Huff for their assistance with laboratory work.

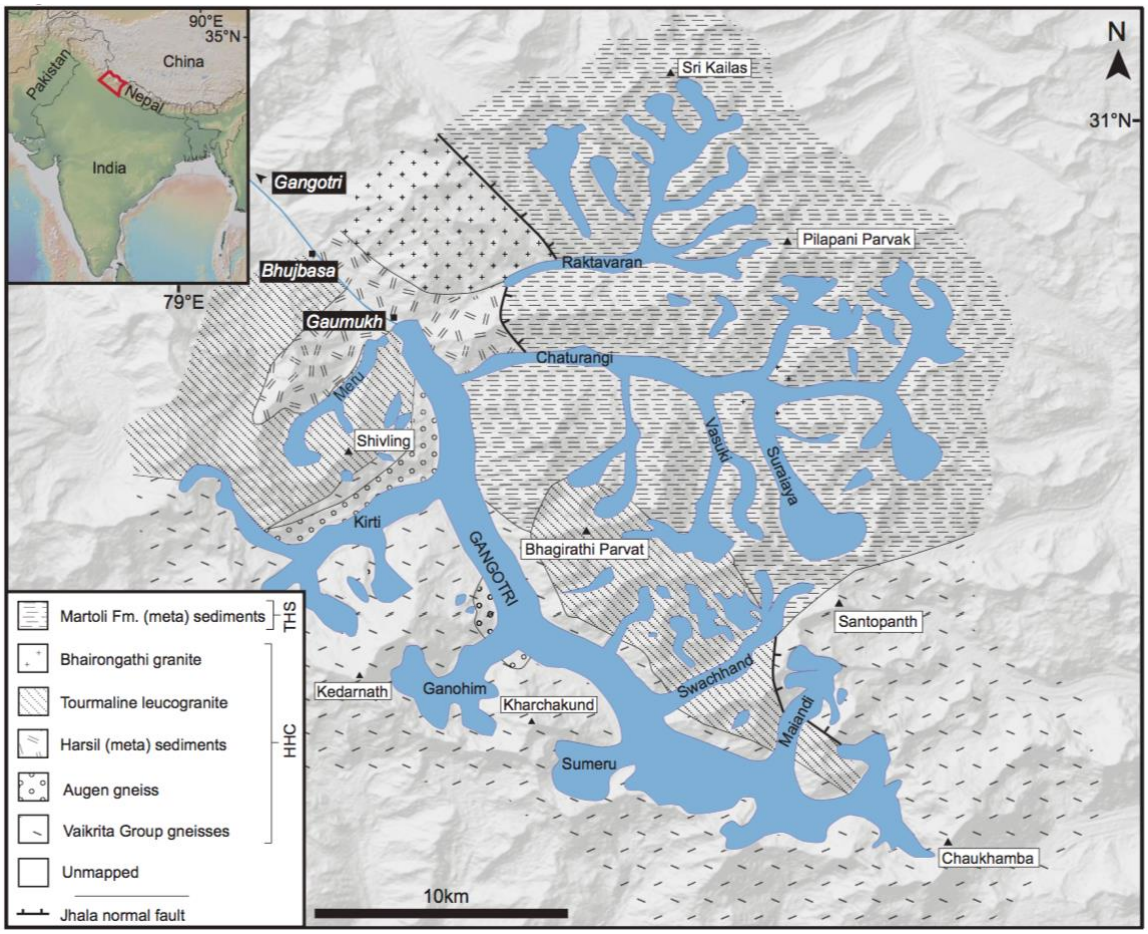

Fig. 1. Location of Gangotri glacier and tributary glaciers overlying a simplified geologic map of the upper Bhagirathi basin of Uttarkashi, northern India (adapted from Searle et al. 1999). Inset map illustrates the location of the state of Uttarakhand within the Himalayan-Tibetan orogen (base map from geomapap.org).

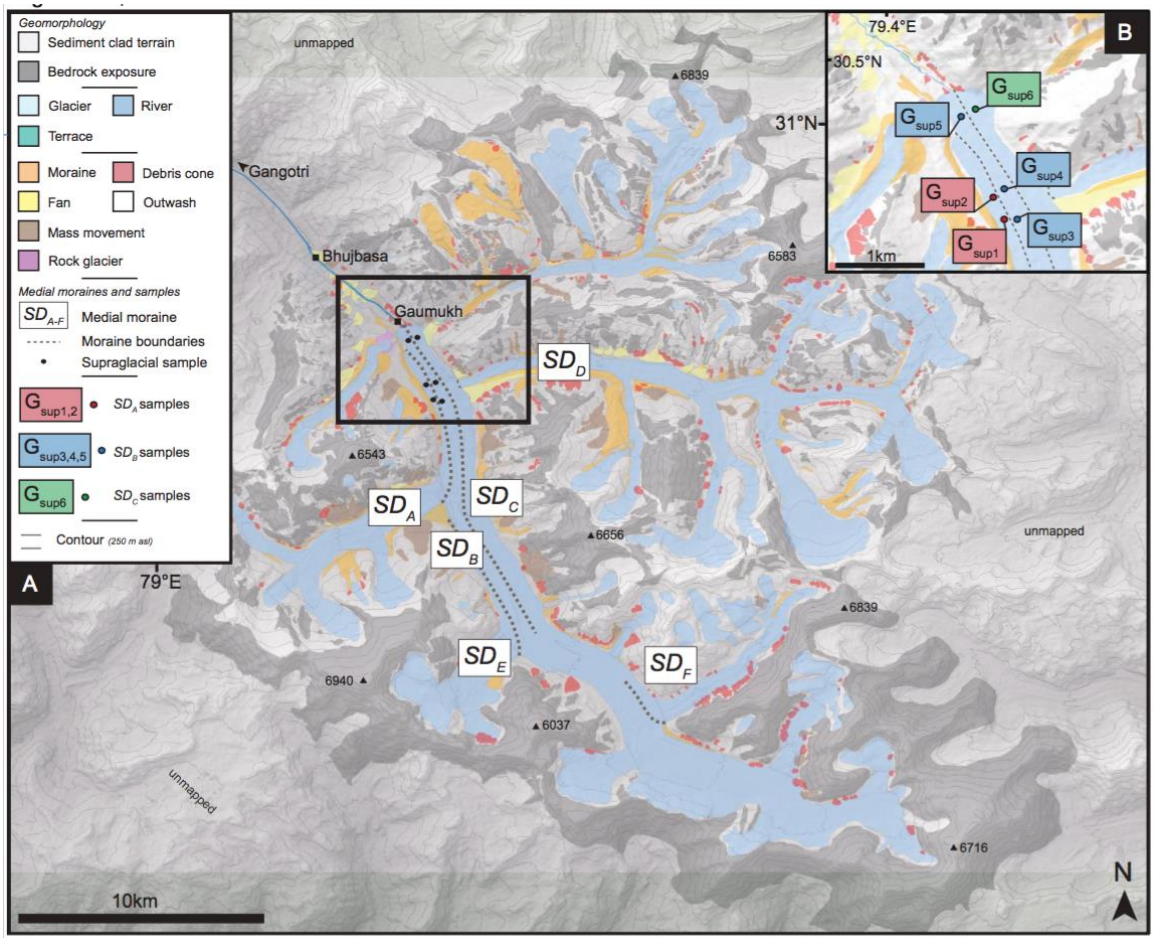

Fig. 2. A) Geomorphic map of the upper Bhagirathi catchment outlining the location of the five major supraglacial units of Gangotri glacier. Altitudinal zones of geomorphic landforms; moraine (~3900−6030 m asl), debris fan (~3890−5320 m asl), mass movement (4410−6020 m asl), rock glacier (~4440 m asl), debris cone (~3940−5900 m asl) and terrace (3890−4880 m asl). B) Sample locations for each of the three investigated supraglacial units of this study.

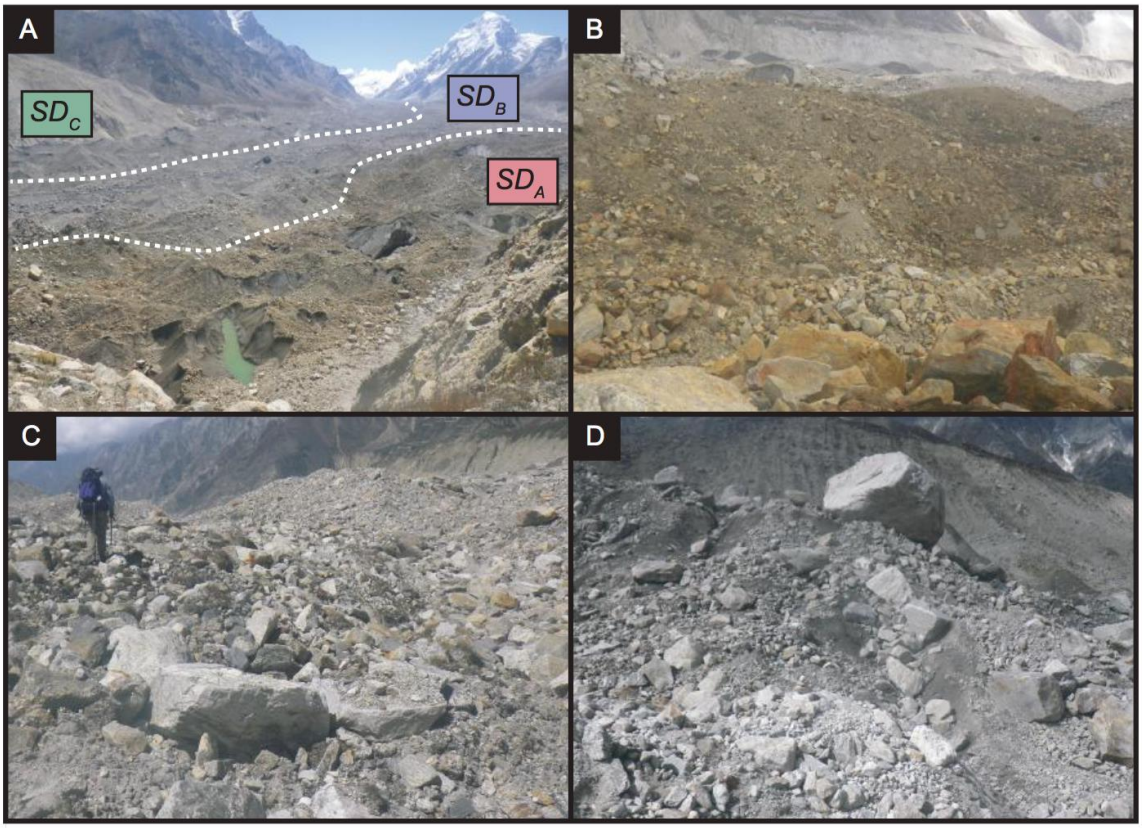

Fig. 3. Views of moraines in the study area. A) Gangotri glacier medial moraines. White dashed lines highlight boundaries between moraines. B) SD_A medial moraine. C) SD_B medial moraine. D) SD_C medial moraine.

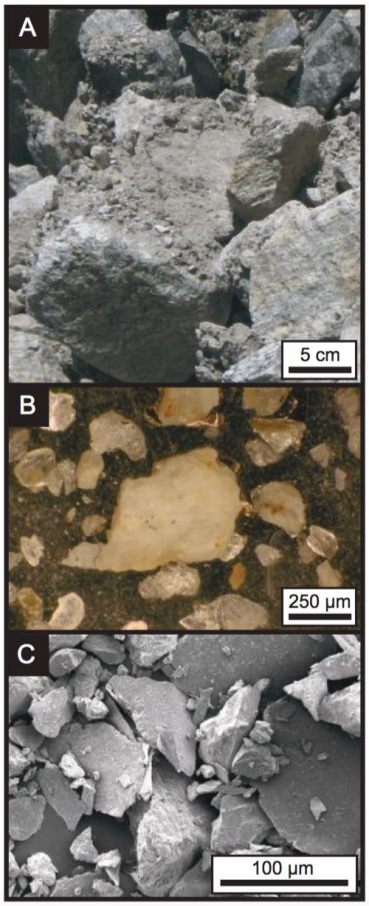

Fig. 4. Photomicrographs of the G_{sup4} sample from the SD_B medial moraine. A) Image of moraine surface at the G_{sup4} sampling site. B) Image of fine-coarse sand sediment fractions taken using digital microscope. C) SEM image (200x mag) of silt-clay fraction.

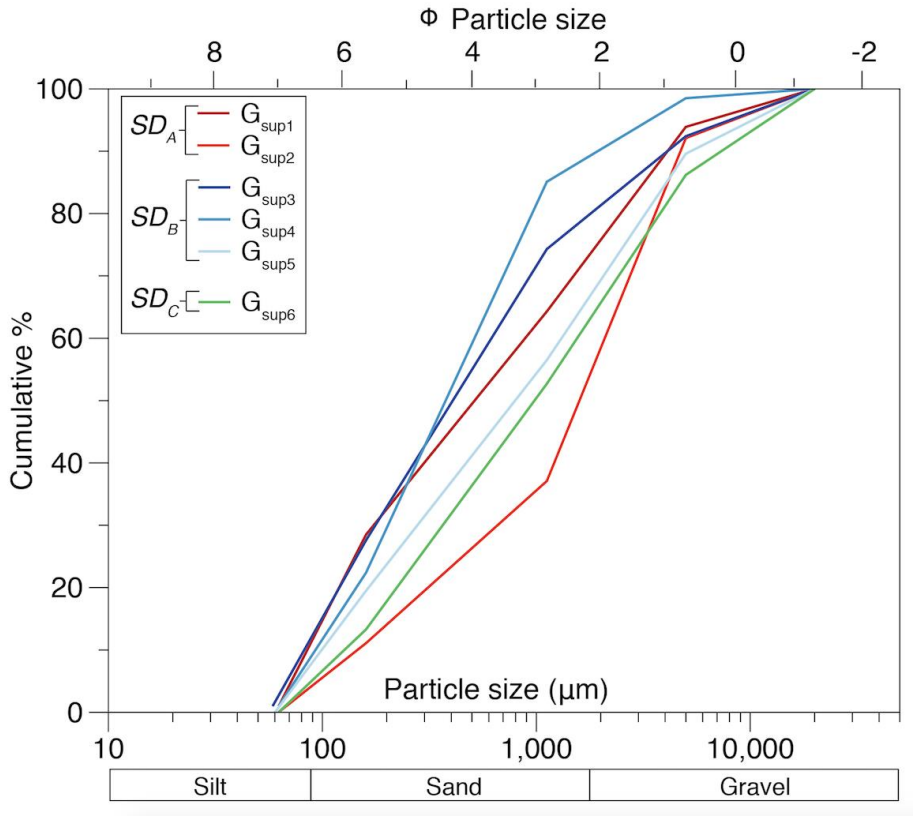

Fig. 5. Particle size distribution of Gangotri medial moraine samples.

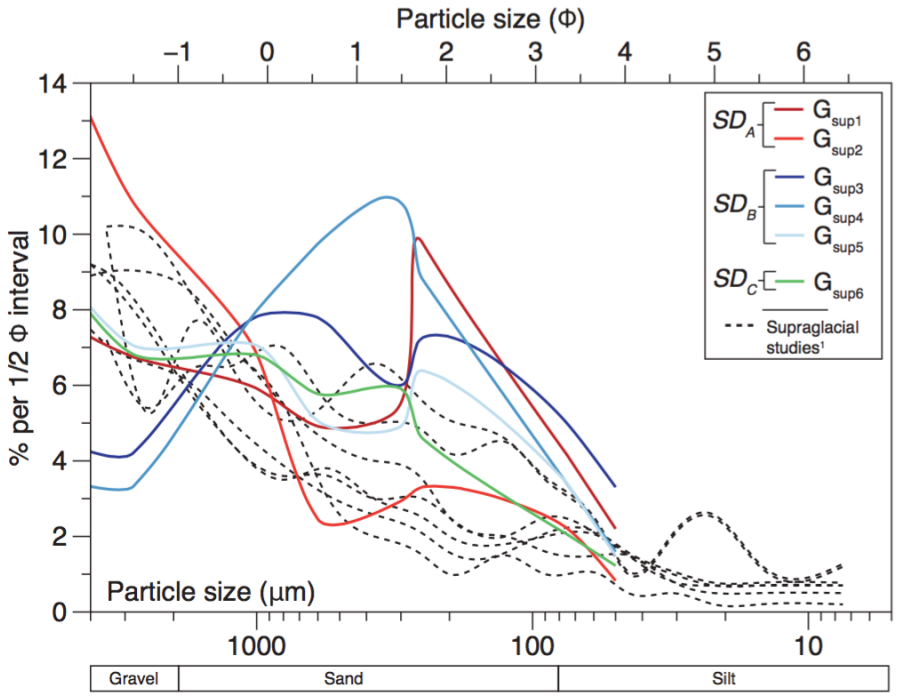

Fig. 6. Mean weight percentages per ½ Φ interval of medial moraine samples from Gangotri glacier and comparisons derived from Owen et al. (2003). These comparisons include supraglacial debris from Rakhiot, Chungphur and Glacier de Cheilon (Owen et al. 2003) in addition to Glacier de Tsidijore Nourve (Small 1983), Breidamerkurjokkull, Sore Buchananisen, and the Glacier d'Argentiere (Boulton 1978).

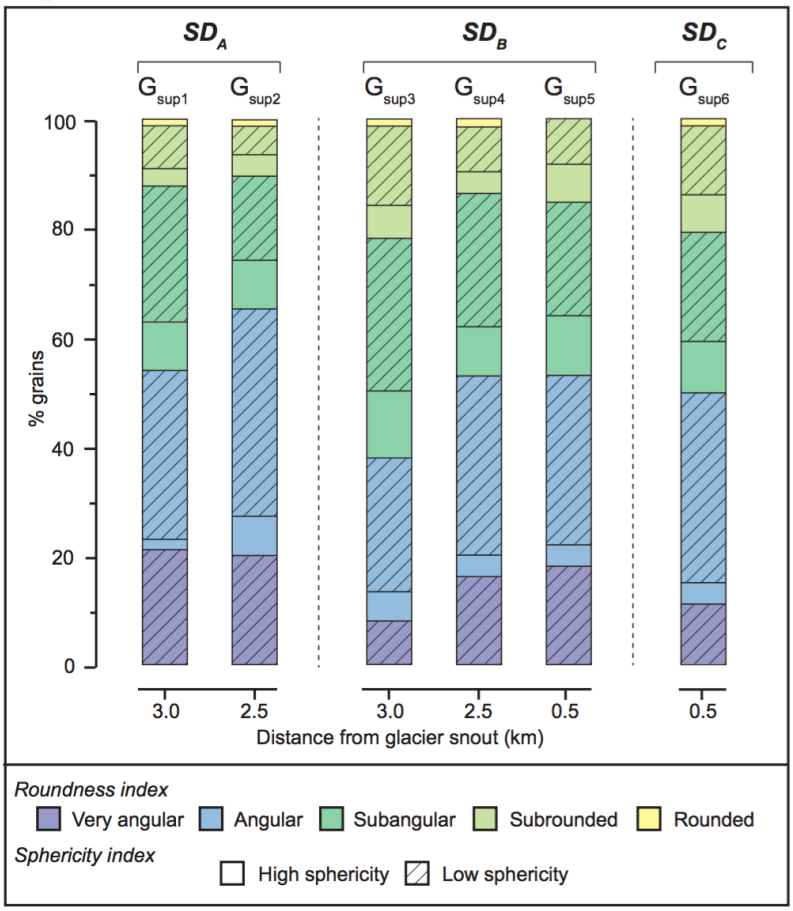

Fig. 7. Summary of particle roundness and sphericity for the medial moraine samples of Gangotri glacier.

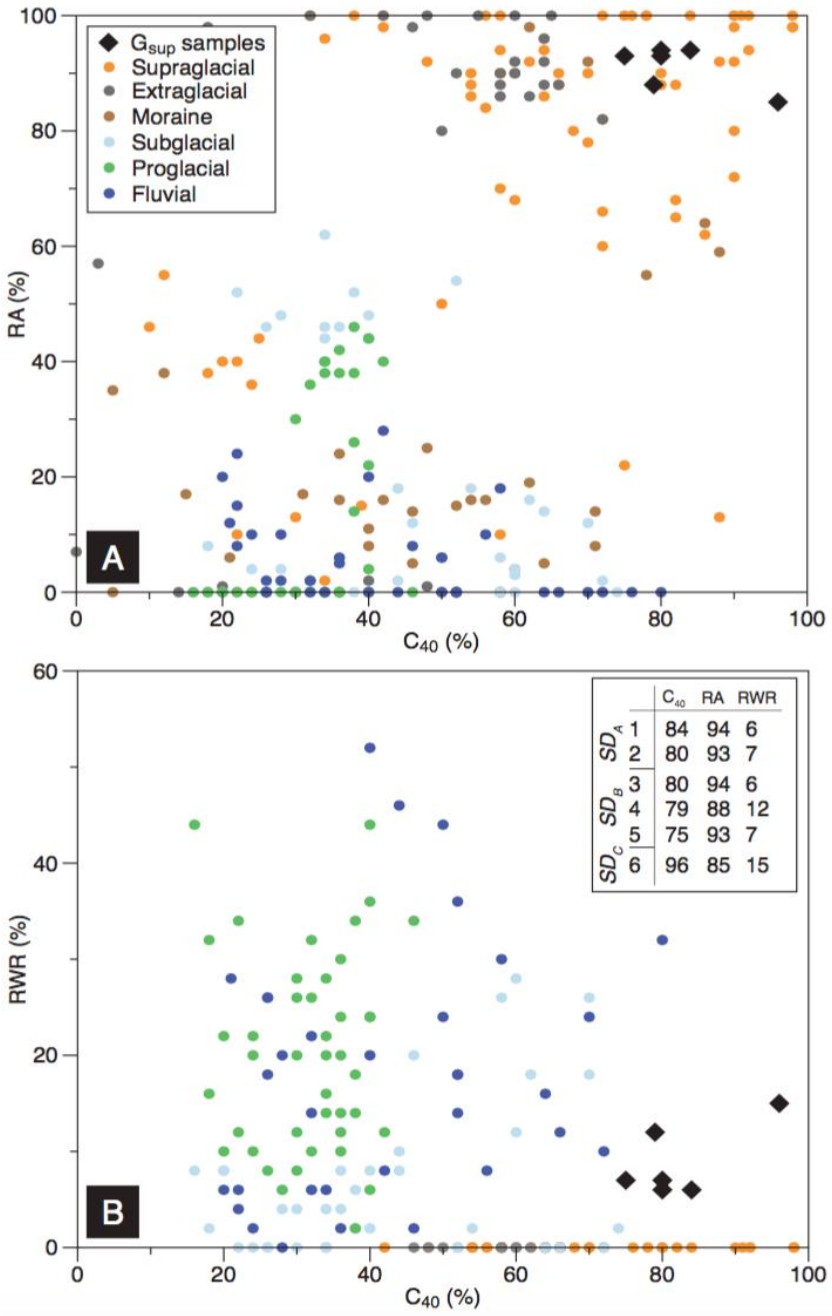

Fig. 8. Covariance plots of medial moraine samples from Gangotri glacier with a compilation of sediment samples from high altitude alpine catchments. Batal (Benn and Owen 2002), Khumbu (Hambrey et al. 2008), d'Arolla (Goodsell et al. 2005) and Findelen, Pasterze, Estelette, Tasman, Vadret and Fox glaciers (Lukas et al. 2013). A) Plot of RA-C_{40} index B) RWR-C_{40} index.

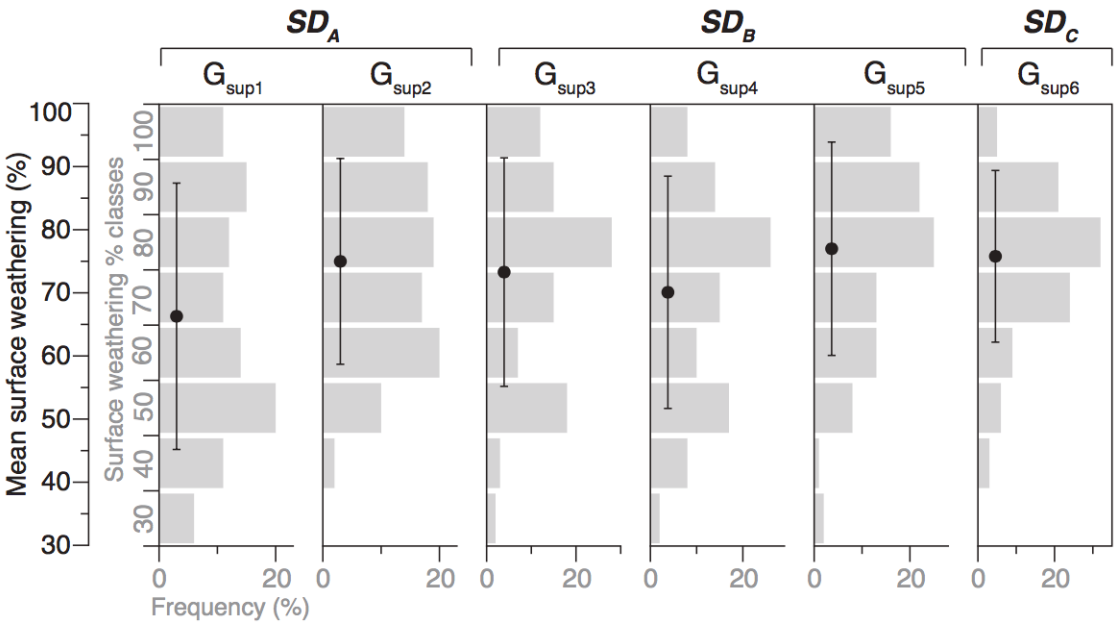

Fig. 9. Percentage surface weathering of quartz sand grains for the Gangotri glacier medial moraines.

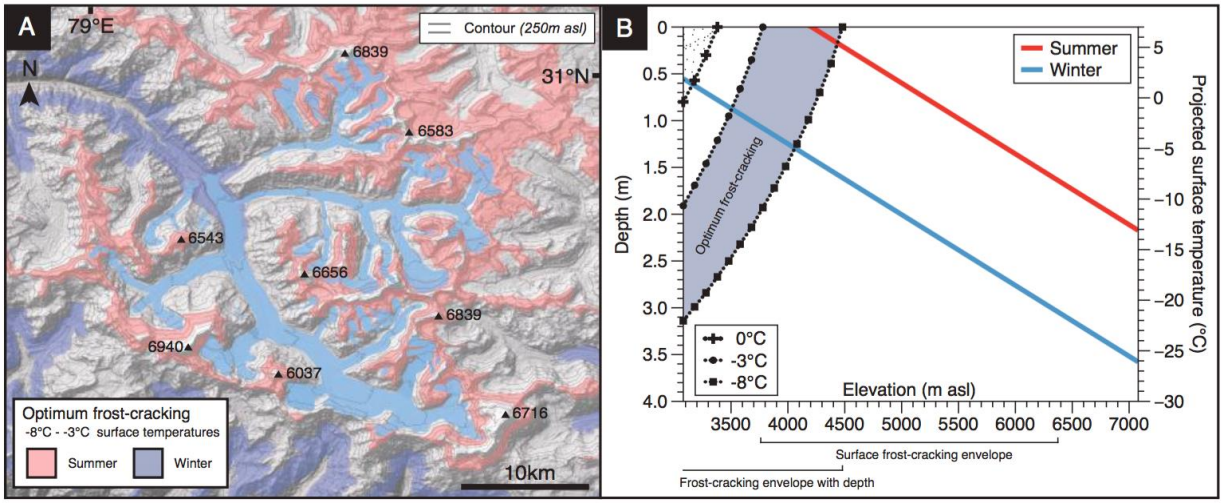

Fig. 10. Optimum frost shattering for the upper Bhagirathi catchment. A) Simplified map showing the regional distribution of the optimum frost shattering elevations during the summer and winter (temperature data from Bhambri et al. 2011 and CRU 2.0). B) Optimum frost cracking (blue shading) and permafrost boundaries with respect to depth and projected surface temperatures for the summer and winter within the basin elevations. Textured pattern represents elevations devoid of permafrost with depth.

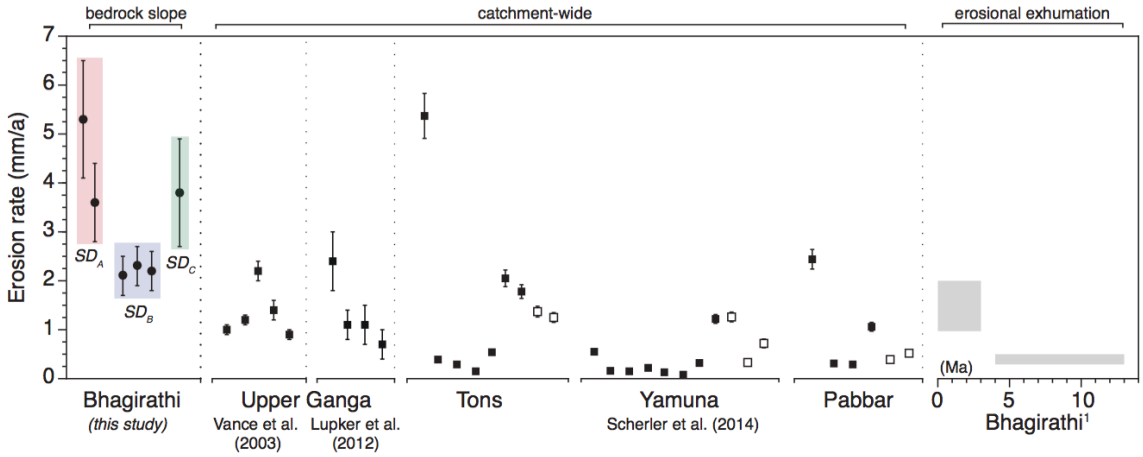

Fig. 11. Rates of erosion for the Garhwal Himalaya. 1: Erosional exhumation rates using thermochronometric methods from Sorkhabi et al. (1996), Searle et al. (1999), Thiede et al. (2009), Thiede and Ehlers (2013).

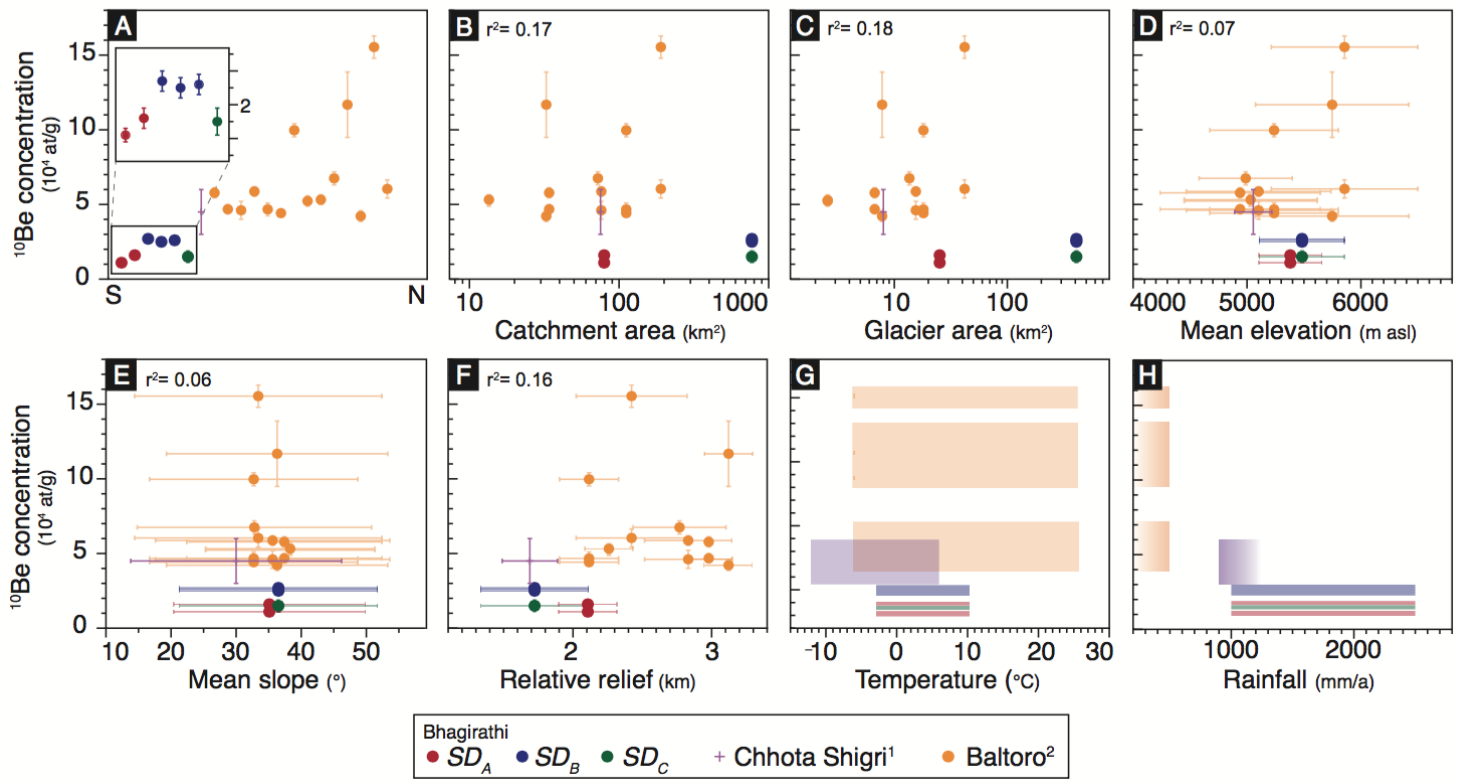

Fig. 12. Comparisons between ^{10}Be concentrations of the Bhagirathi, Chhota Shigri (1: Scherler and Egholm, 2017) and Baltoro (2: Seong et al., 2009) glaciers (uncertainties expressed to 1σ). A) ^{10}Be concentrations. Inset indicates the 1σ uncertainties of the Bhagirathi samples, B) Catchment area (r^2 value provided for all catchment data), C) Glacier area, D) Mean catchment elevation, E) Mean slope (slope calculated from 0.001km^2 catchment grid cells), F) 3-km-radius relief, G) Annual mean temperature for Bhagirathi (Bhambri et al., 2011), Chhota Shigri (Wagnon et al., 2007) and Baltoro (Mihalcea et al. 2006, 2008), H) Annual rainfall for Bhagirathi (Bhambri et al., 2011, Srivastava, 2012), Chhota Shigri and Baltoro (TRMM rainfall record [1998−2005]; Bookhagen and Burbank, 2006).

Table 1. Catchment and glacier characteristics of the upper Bhagirathi catchment (uncertainties are expressed to 1σ)

Catchment	Catchment characteristics						Glacier characteristics		
	Area (~km^2)	Relative relief[1] (km)	Max. slope[2] (°)	Mean slope[2] (°)	HI Index[3]	^{10}Be production rate (at/g/a)	Glacier area (~km^2)	Glacier head (m asl)	Glacier aspect (°)
Gangotri (trunk)	772.7	1.7±0.4	72	36.5±15.2	0.4	95.4±12.2	409.0	6000	330
Raktavaran	139.0	1.6±0.3	68	37.1±15.1	0.5	104.4±13.5	39.3	6280	260
Chaturangi	214.8	1.7±0.3	60	33.9±13.9	0.4	95.4±11.9	124.1	6125	270
Swachhand	39.3	1.7±0.3	57	31.2±13.8	0.4	102.8±13.3	15.1	5820	220
Maiandi	19.5	1.7±0.3	75	40.7±18.4	0.3	107.3±13.9	17.3	6000	200
Sumeru	12.3	1.4±0.4	57	29.6±15.7	0.4	90.6±11.7	12.2	5450	60
Ganohim	35.1	2.2±0.3	61	35.4±19.0	0.3	96.0±12.4	24.2	5735	45
Kirti	79.5	2.1±0.2	63	35.1±14.7	0.3	93.1±12.1	25.2	6300	45
Meru	23.6	2.0±0.3	61	37.5±18.3	0.4	87.0±11.3	8	5540	30

1: 3-km-radius relative relief
2: Slope calculated from 0.001km^2 catchment grid cells
3: Strahler (1952) Hypsometric Index (mean elevation- min elevation/relief)

Table 2. Gangotri glacier medial moraine sample AMS ratios, ^{10}Be concentrations and interpreted erosion rates.

Sample	Medial moraine	AMS ^{10}Be/^{9}Be ratio[1] (10^{-14})	^{10}Be concentration (10^{4} at/g)	Applicable time range[2] (a)	Erosion rate[3] (mm/a)
G_{sup1}	SD_A	1.1±0.2	1.1±0.2	112.4	5.3±1.2
G_{sup2}	SD_A	1.6±0.3	1.6±0.3	165.1	3.6±0.8
G_{sup3}	SD_B	2.7±0.3	2.7±0.3	280.9	2.1±0.4
G_{sup4}	SD_B	2.0±0.2	2.5±0.3	262.9	2.3±0.4
G_{sup5}	SD_B	2.3±0.3	2.6±0.3	272.6	2.2±0.4
G_{sup6}	SD_C	1.7±0.5	1.5±0.4	159.9	3.8±1.1

1: Ratios are corrected for background ^{10}Be detected in procedural blank ($0.3\pm0.1\times10^{-14}$)
2: Applicable time range follows Lal (1991).
3: Erosion rate calculated with mean ^{10}Be production rate for upper Bhagirathi catchment (95.4±12.2 at/g/a), ^{10}Be decay constant of $5.1\pm0.3\times10^{-7}$, and a ^{10}Be half-life of 1.36 Ma.

Table 3. Reconstructed ELAs for the upper Bhagirathi basin (uncertainty is expressed as 1σ)[1]

	Time	Area-Altitude	Area-Accumulation ratio			Toe-Headwall altitude ratio		Mean ELA	ΔELA
	(ka)	AA	AAR(0.4)	AAR(0.5)	AAR(0.6)	THAR(0.4)	THAR(0.5)	(m asl)	(m asl)
Contemporary glaciers									
Gangotri	-	5100	5210	5080	4960	5165	5440	5160±160	-
Raktavaran	-	5630	5790	5680	5560	5720	5620	5665±80	-
Chaturangi	-	5500	5650	5550	5430	5385	5665	5530±115	-
Swachhand	-	5290	5360	5280	5180	5325	5440	5310±85	-
Maiandi	-	5625	5730	5530	5400	5735	5885	5650±170	-
Sumeru	-	5155	5170	5130	5090	5170	5235	5160±50	-
Ganohim	-	5115	5200	5060	4920	5240	5375	5150±160	-
Kirti	-	4940	4920	4850	4770	5175	5350	5000±220	-
Meru	-	4875	5010	4870	4760	4830	4950	4880±90	-
Glacial stages									
Bhujbasa	~1.7−0.5	4770	4540	4760	4680	4615	4795	4695±100	465±140
Gangotri	~2.4–1.9	4750	4530	4750	4670	4605	4745	4675±90	485±145
Shivling	~5.2	4730	4530	4740	4650	4520	4710	4645±100	515±155
Sudarshan	21.0−16.0	4425	4700	4570	4410	4070	4360	4425±215	735±220
Bhagirathi	60.0-23.0	4025	4550	4290	3810	3770	4110	4095±295	1065±320

1: ELAs rounded to the nearest multiple of five.

REFERENCES

Ahmad, T., Harris, N., Bickle, M., Chapman, H., Bunbury, J., Prince, C., 2000. Isotopic constraints on the structural relationships between the lesser Himalayan series and the high Himalayan crystalline series, Garhwal Himalaya. Geological Society of America Bulletin, 112(3), p.467-477.

Ahmad, S., Hasnain, S.I., Arha C.D., Ramamurthy, V.S., Mathur, K.N., Bassi, U.K., 2004. Analysis of satellite imageries for characterization of glacio-morphological features of the Gangotri Glacier, Ganga headwater, Garhwal Himalayas. In Proceedings of Workshop on Gangotri Glacier Special Publication Series-Geological Survey of India (Vol. 80, p. 61-67).

Allen, T., 1981. Particle size, shape and distribution. In Particle size measurement (p. 103-164). Springer, Boston, MA.

Anders, A.M., Roe, G.H., Hallet, B., Montgomery, D.R., Finnegan, N.J., Putkonen, J., 2006. Spatial patterns of precipitation and topography in the Himalaya. Special Papers-Geological Society of America, 398, p.39.

Anderson S.P. 2005. Glaciers show direct linkage between erosion rate and chemical weathering fluxes. Geomorphology, 67(1-2), p.147-157.

Anderson, R.S., Anderson, S.P., 2010. Geomorphology: the mechanics and chemistry of landscapes. Cambridge University Press.

André, M.F., 1997. Holocene rockwall retreat in Svalbard: a triple-rate evolution. Earth Surface Processes and Landforms: The Journal of the British Geomorphological Group, 22(5), p.423-440.

Augustinus, P.C., 1995. Glacial valley cross-profile development: the influence of in situ rock stress and rock mass strength, with examples from the Southern Alps, New Zealand. Geomorphology, 14(2), p.87-97.

Balco, G., Stone, J., Lifton, N., Dunai, T., 2008. A complete and easily accessible means of calculating surface exposure ages or erosion rates from ^{10}Be and ^{26}Al measurements. Quaternary Geochronology, 3, p.174-195.

Bali, R., Awasthi, D.D., Tiwari, N.K., 2003. Neotectonic control on the geomorphic evolution of the Gangotri Glacier Valley, Garhwal Himalaya. Gondwana Research, 6(4), p.829-838.

Ballantyne, C.K., 2002a. Paraglacial geomorphology. Quaternary Science Reviews, 21(18-19), p.1935-2017.

Ballantyne, C.K., 2002b. A general model of paraglacial landscape response. The Holocene, 12(3), p.371-376.

Ballantyne, C.K., Benn, D.I., 1994. Paraglacial Slope Adjustment and Resedlmenfation following Recent Glacier Retreat, Fåbergstølsdalen, Norway. Arctic and Alpine Research, 26(3), p.255-269.

Barnard, P.L., Owen, L.A, Sharma, M.C., Finkel, R.C., 2001. Natural and human-induced landsliding in the Garhwal Himalaya of northern India. Geomorphology, 40(1-2), p.21-35.

Barnard, P., Owen, L., Finkel, R., 2004a. Style and timing of glacial and paraglacial sedimentation in a monsoon-influenced high Himalayan environment, the upper Bhagirathi Valley, Garhwal Himalaya. Sedimentary Geology, 165, p.199-221.

Barnard, P.L., Owen, L.A., Sharma, M.C., Finkel, R.C., 2004b. Late quaternary (Holocene) landscape evolution of a monsoon-influenced high Himalayan valley, Gori Ganga, Nanda Devi, NE Garhwal, Geomorphology, 61(1-2), p.91-110.

Barr, I.D., Spagnolo, M., 2015. Glacial cirques as palaeoenvironmental indicators: Their potential and limitations. Earth-science reviews, 151, p.48-78.

Barros, A.P., Chiao, S., Lang, T.J., Burbank, D., Putkonen, J., 2006. From weather to climate-seasonal and interannual variability of storms and implications for erosion processes in the Himalaya. Special Papers-Geological Society of America, 398, p.17.

Bashir, F., Rasul, G., 2010. Estimation of water discharge from Gilgit Basin using remote sensing, GIS and runoff modeling. Pakistan Journal of Meteorology, 6(12).

Benn. D., Evans, D.J., 2014. Glaciers and glaciation. Routledge.

Benn, D.I., Lehmkuhl, F., 2000. Mass balance and equilibrium-line altitudes of glaciers in high-mountain environments. Quaternary International, 65, p.15-29.

Benn, D., Owen, L., 1998. The role of the Indian summer monsoon and the mid-latitude westerlies in Himalayan glaciation: a review and speculative discussion. Journal of the Geological Society, 155, p.353–363.

Benn, D.I., Owen, L.A., 2002. Himalayan glacial sedimentary environments: a framework for reconstructing and dating former glacial extents in high mountain regions. Quaternary International, 97-98, p.3-26.

Benn, D.I., Owen, L.A., Osmaston, H.A., Seltzer, G.O., Porter, S.C., Mark, B.. 2005. Reconstruction of equilibrium-line altitudes for tropical and sub-tropical glaciers. Quaternary International, 138, p.8-21.

Benn, D.I., Bolch, T., Hands, K., Gulley, J., Luckman, A., Nicholson, L,, I,Quincey, D., Thompson, S., Toumi, R, Wiseman S. 2012. Response of debris-covered glaciers in the Mount Everest region to recent warming, and implications for outburst flood hazards. Earth-Science Reviews, 114(1-2), p.156-174.

Bernhardt, M., Schulz, K., 2010. SnowSlide: A simple routine for calculating gravitational snow transport. Geophysical Research Letters, 37(11).

Bhambri, R., Bolch, T., Chaujar, R.K., Kulshreshtha, S.C., 2011. Glacier changes in the Garhwal Himalaya, India, from 1968 to 2006 based on remote sensing. Journal of Glaciology, 57(203), p.543-556.

Bhambri, R,. Bolch, T., Chaujar, R.K., 2012. Frontal recession of Gangotri Glacier, Garhwal Himalayas, from 1965 to 2006, measured through highresolution remote sensing data. Current Science (00113891), 102(3).

Bhattacharya, A., Bolch, T., Mukherjee, K., Pieczonka, T., Kropacek, J., Buchroithner, M.F., 2016. Overall recession and mass budget of Gangotri Glacier, Garhwal Himalayas, from 1965 to 2015 using remote sensing data. Journal of Glaciology, 62(236), p.1115-1133.

Bierman, P., Nichols, K.K., 2004. Rock to sediment—slope to sea with ^{10}Be—rates of landscape change. Annual Review of Earth and Planetary Sciences, 32, p.215-255.

Bierman, P., Steig, E.J., 1996. Estimating rates of denudation using cosmogenic isotope abundances in sediment. Earth surface processes and landforms, 21(2), p.125-139.

Birkeland, P.W., 1974. Pedology, weathering, and geomorphological research. Oxford University Press, New York, N.Y.

Biswas, S., Coutand, I., Grujic, D., Hager, C., Stöckli, D., Grasemann, B., 2007. Exhumation and uplift of the Shillong plateau and its influence on the eastern Himalayas: New constraints from apatite and zircon (U-Th-[Sm])/He and apatite fission track analyses. Tectonics, 26(6).

Blandford, T.R., Humes, K.S., Harshburger, B.J., Moore, B.C., Walden, V.P., Ye, H., 2008. Seasonal and synoptic variations in near-surface air temperature lapse rates in a mountainous basin. Journal of Applied Meteorology and Climatology, 47(1), p.249-261.

Bookhagen, B., Burbank, D., 2006. Topography, relief and TRMM-derived rainfall variations along the Himalaya. Geophysical Research Letters, 33, 105.

Bookhagen, B., Thiede, R., Strecker, M., 2005. Late Quaternary intensified monsoon phases control landscape evolution in the northwest Himalaya. Geology 33, 1, 149-152.

Boulton, G.S., 1978. Boulder shapes and grain-size distributions of debris as indicators of transport paths through a glacier and till genesis. Sedimentology, 25(6), p.773-799.

Braucher, R., Brown, E.T., Bourlès, D.L., Colin, F., 2003. In situ produced 10Be measurements at great depths: implications for production rates by fast muons. Earth and Planetary Science Letters, 211(3-4), p.251-258.

Brown, R.J., 1970. Permafrost in Canada: its influence on northern development. University of Toronto Press.

Brown, E.T., Stallard, R.F., Larsen, M.C., Raisbeck, G,M., Yiou, F., 1995. Denudation rates determined from the accumulation of in situ-produced ^{10}Be in the Luquillo Experimental Forest, Puerto Rico. Earth and Planetary Science Letters, 129(1-4), p.193-202.

Brozović, N., Burbank, D.W., Meigs, A.J., 1997. Climatic limits on landscape development in the northwestern Himalaya. Science 276, p.571-574.

Burbank, D., Blythe, A., Putkonen, J., Pratt-Sitaula, B., Gabet, E., Oskin, M., Barros, A., Ojha, T., 2003. Decoupling of erosion and precipitation in the Himalayas. Nature 426, p.652-655.

Carson, M.A., Kirkby, M.J. ,1972. Hillslope form and process.

Chamley, H.,1989. Clay mineralogy. Springer, Berlin

Chen, P.Y., 1977. Table of key lines in X-ray powder diffraction patterns of minerals in clays and associated rocks. na.

Church, M., Slaymaker, O., 1989. Disequilibrium of Holocene sediment yield in glaciated British Columbia. Nature, 337(6206), p.452.

Craddock, W.H., Burbank, D.W., Bookhagen, B., Gabet, E.J., 2007. Bedrock channel geometry along an orographic rainfall gradient in the upper Marsyandi River valley in central Nepal. Journal of Geophysical Research: Earth Surface, 112(F3).

Derbyshire, E., Shi,Y., Li, J., Zheng, B., Li, S,. Wang, J., 1991. Quaternary glaciation of Tibet: the geological evidence. Quaternary Science Reviews. 10, 485-510.

de Scally, F.A., 1997. Deriving lapse rates of slope air temperature for meltwater runoff modeling in subtropical mountains: An example from the Punjab Himalaya, Pakistan. Mountain Research and Development, p.353-362.

Dobhal, D.P., Gergan, J.T., Thayyen, R.J., 2008. Mass balance studies of the Dokriani Glacier from to, Garhwal Himalaya, India. Bulletin of glaciological research, 25, p.9-17.

Dortch, J.M., Owen, L.A., Haneberg, W.C., Caffee, M.W., Dietsch, C., Kamp, U., 2009. Nature and timing of mega-landslides in northern India. Quaternary Science Reviews 28, p.1037-1056.

Dortch, J., Owen, L,. Caffee, M., 2010. Quaternary glaciation in the Nubra and Shyok valley confluence, northernmost Ladakh, India. Quaternary Research, 74, p.132-144.

Dortch, J., Owen, L., Schoenbohm, L., Caffee, M., 2011. Asymmetrical erosion and morphological development of the central Ladakh Range, northern India. Geomorphology 135, p.167-180.

Dühnforth, M., Anderson, R.S., Ward, D., Stock, G.M., 2010. Bedrock fracture control of glacial erosion processes and rates. Geology, 38(5), p.423-426.

Dunning, S.A., Mitchell, W.A., Rosser, N.J., Petley, D.N., 2007. The Hattian Bala rock avalanche and associated landslides triggered by the Kashmir Earthquake of 8 October 2005. Engineering Geology, 93(3-4), p.130-144.

Dutta, SS., Sangewar, C.V., Shukla, S.P., Chitranshi, A., Puri, V.M.K., Hampaiah, P., 2004. Some observation on physiography and geomorphology of Gangotri glacier area, Bhagirathi basin, Uttaranchal. Geological Survey of India Special Publication, 80, p.69-78.

Eppes, M.C., McFadden, L., 2008. The influence of bedrock weathering on the response of drainage basins and associated alluvial fans to Holocene climates, San Bernardino Mountains, California, USA. The Holocene, 18(6), p.895-905.

Eppes, M.C., Keanini, R., 2017. Mechanical Weathering and Rock Erosion by Climate-Dependent Subcritical Cracking. Reviews of Geophysics. 55, p.470–508.

Fame, M.L., Owen, L.A., Spotila, J.A., Dortch, J.M., Caffee, M.W., 2018. Tracking paraglacial sediment with cosmogenic 10 Be using an example from the northwest Scottish Highlands. Quaternary Science Reviews, 182, p. 20-36.

Finkel, R., Owen, L., Barnard, P., Caffee, M., 2003. Beryllium-10 dating of Mount Everest moraines indicates a strong monsoon influence and glacial synchroneity throughout the Himalaya. Geology 31, 6, p.561-564.

Finlayson, D.P., Montgomery, D.R., Hallet, B., 2002. Spatial coincidence of rapid inferred erosion with young metamorphic massifs in the Himalayas. Geology, 30(3), p.219-222.

Fischer, L., Kääb, A., Huggel, C., Noetzli, J., 2006. Geology, glacier retreat and permafrost degradation as controlling factors of slope instabilities in a high-mountain rock wall: the Monte Rosa east face. Natural Hazards and Earth System Sciences, 6(5), p.761-772.

Fischer, L., Amann, F., Moore, J.R., Huggel C. 2010. Assessment of periglacial slope stability for the 1988 Tschierva rock avalanche (Piz Morteratsch, Switzerland). Engineering Geology, 116(1-2), p.32-43.

Fischer, L., Purves, R.S., Huggel, C., Noetzli, J., Haeberli, W., 2012. On the influence of topographic, geological and cryospheric factors on rock avalanches and rockfalls in high-mountain areas. Natural Hazards and Earth System Sciences, 12(1), p.241.

Foster, D., Brocklehurst, S.H., Gawthorpe, R.L., 2010. Glacial-topographic interactions in the Teton Range, Wyoming. Journal of Geophysical Research: Earth Surface, 115(F1).

France-Lanord. C., Evans. M., Hurtrez, J.E., Riotte, J., 2003. Annual dissolved fluxes from Central Nepal rivers: budget of chemical erosion in the Himalayas. Comptes Rendus Geoscience, 335(16), p.1131-1140.

Frey, H., Paul, F., Strozzi, T., 2012. Compilation of a glacier inventory for the western Himalayas from satellite data: methods, challenges, and results. Remote Sens. Environ. 124, 832–843. GSI, 2007.

Gabet, E.J., Burbank, D.W., Putkonen, J.K., Pratt-Sitaula, B.A., Ojha, T., 2004. Rainfall thresholds for landsliding in the Himalayas of Nepal. Geomorphology, 63(3-4), p.131-143.

Gale, S.J., Hoare, P.G., 1991. Quaternary Sediments: Petrographic Methods for the Study of Unlithified Rocks. Wiley, Chichester.

Gantayat, P., Kulkarni, A.V., Srinivasan, J., 2014. Estimation of ice thickness using surface velocities and slope: case study at Gangotri Glacier, India. Journal of Glaciology, 60(220), p.277-282.

Garzanti, E., Vezzoli, G., Andò, S., Lavé, J., Attal, M., France-Lanord, C., DeCelles, P., 2007. Quantifying sand provenance and erosion (Marsyandi River, Nepal Himalaya). Earth and Planetary Science Letters, 258(3-4), p.500-515.

GeoMappApp (2014), Marine Geoscience Data System, Available from: http://www.geomappap.org (last accessed: 21/08. 2014).

Gibson, M.J., Glasser, N.F., Quincey, D.J., Mayer, C., Rowan, A.V., Irvine-Fynn, T.D., 2017. Temporal variations in supraglacial debris distribution on Baltoro Glacier, Karakoram between 2001 and 2012. Geomorphology, 295, p.572-585.

Goodsell, B., Hambrey, M.J., Glasser, N.F., 2005. Debris transport in a temperate valley glacier: Haut Glacier d'Arolla, Valais, Switzerland. Journal of Glaciology, 51(172), p.139-146.

Graham, D.J., Midgley, N.G., 2000. Graphical representation of particle shape using triangular diagrams: an Excel spreadsheet method. Earth Surface Processes and Landforms, 25(13), p.1473-1477.

Gruber, S., Haeberli, W., 2007. Permafrost in steep bedrock slopes and its temperature-related destabilization following climate change. Journal of Geophysical Research: Earth Surface, 112(F2).

Grujic, D., Coutand, I., Bookhagen, B., Bonnet, S., Blythe, A., Duncan, C., 2006. Climatic forcing of erosion, landscape, and tectonics in the Bhutan Himalayas. Geology, 34(10), p.801-804.

Hales, T.C., Roering, J.J., 2005. Climate-controlled variations in scree production, Southern Alps, New Zealand. Geology, 33(9), p.701-704.

Hales, T.C,, Roering, J.J., 2007. Climatic controls on frost cracking and implications for the evolution of bedrock landscapes. Journal of Geophysical Research: Earth Surface, 112(F2).

Hallet, B., Walder, J.S., Stubbs, C.W., 1991. Weathering by segregation ice growth in microcracks at sustained subzero temperatures: Verification from an experimental study using acoustic emissions. Permafrost and Periglacial Processes, 2(4), p.283-300.

Hambrey, M.J., Glasser, N.F., 2003. The role of folding and foliation development in the genesis of medial moraines: examples from Svalbard glaciers. The Journal of Geology, 111(4), p.471-485.

Hambrey, M.J., Quincey, D.J., Glasser, N.F., Reynolds, J.M., Richardson, S.J., Clemmens, S., 2008. Sedimentological, geomorphological and dynamic context of debris-mantled glaciers, Mount Everest (Sagarmatha) region, Nepal. Quaternary Science Reviews, 27(25-26), p.2361-2389.

Haritashya, U.K., Singh, P., Kumar, N., Gupta, R.P., 2006. Suspended sediment from the Gangotri Glacier: Quantification, variability and associations with discharge and air temperature. Journal of Hydrology, 321(1-4), p.116-130.

Hasnain, S.I., Thayyen, R.J., 1996. Sediment transport and solute variation in meltwaters of Dokriani Glacier (Bamak), Garhwal Himalaya. Journal of the Geological Society of India, 47(6), p.731-739.

Harper, J.T., Humphrey, N.F., 2003. High altitude Himalayan climate inferred from glacial ice flux. Geophysical Research Letters, 30(14).

Heimsath, A.M., McGlynn, R., 2008. Quantifying periglacial erosion in the Nepal high Himalaya. Geomorphology, 97(1-2), p.5-23.

Hewitt, K., 2009. Glacially conditioned rock-slope failures and disturbance-regime landscapes, Upper Indus Basin, northern Pakistan. Geological Society, London, Special Publications, 320(1), p.235-255.

Hewitt, K., 1988. Catastrophic landslide deposits in the Karakoram Himalaya. Science, 242(4875), p.64-67.

Heyman, J., 2014. Paleoglaciation of the Tibetan Plateau and surrounding mountains based on exposure ages and ELA depression estimates. Quaternary Science Reviews 91, p.30-41.

Heyman, J., Stroeven, A., Harbor, J., Caffee, M., 2011. Too young or too old: Evaluating cosmogenic exposure dating based on an analysis of compiled boulder exposure ages. Earth and Planetary Science Letters, 302, p.71-80.

Hubbard, B., Glasser, N., Hambrey, M., Etienne, J., 2004. A sedimentological and isotopic study of the origin of supraglacial debris bands: Kongsfjorden, Svalbard. Journal of Glaciology, 50(169), p.157-170.

Humphreys, G.S., Wilkinson, M.T., 2007. The soil production function: a brief history and its rediscovery. Geoderma, 139(1-2), p.73-78.

Kattel, D.B., Yao, T., Yang, K., Tian, L., Yang, G., Joswiak, D., 2013. Temperature lapse rate in complex mountain terrain on the southern slope of the central Himalayas. Theoretical and applied climatology, 113(3-4), p.671-682.

Kattel, D.B., Yao, T., Yang, W., Gao, Y., Tian, L., 2015. Comparison of temperature lapse rates from the northern to the southern slopes of the Himalayas. International Journal of Climatology, 35(15), p.4431-4443.

Kohl, C.P, Nishiizumi, K., 1992. Chemical isolation of quartz for measurement of in situ produced cosmogenic nuclides. Geochimica. Cosmochimica. Acta 56, p.3583–3587.

Lal, D., 1991. Cosmic ray labelling of erosion surfaces: in situ nuclide production rates and erosion models. Earth and Planetary Science Letters,104, p.429-439.

Luckman, B.H., 1977. The geomorphic activity of snow avalanches. Geografiska Annaler: Series A, Physical Geography, 59(1-2), p.31-48.

Lukas, S., Graf, A., Coray, S., Schlüchter, C., 2012. Genesis, stability and preservation potential of large lateral moraines of Alpine valley glaciers–towards a unifying theory based on Findelengletscher, Switzerland. Quaternary Science Reviews, 38, p.27-48.

Lukas, S., Benn, D.I,, Boston, C.M., Brook, M., Coray, S., Evans, D.J., Graf, A., Kellerer-Pirklbauer, A., Kirkbride, M.P., Krabbendam, M., Lovell, H., 2013. Clast shape analysis and clast transport paths

in glacial environments: A critical review of methods and the role of lithology. Earth-Science Reviews, 121, p.96-116.

Lupker, M., Blard, P.H., Lave, J., France-Lanord, C., Leanni, L., Puchol, N., Charreau, J., Bourlès, D., 2012. 10Be-derived Himalayan denudation rates and sediment budgets in the Ganga basin. Earth and Planetary Science Letters, 333, p.146-156.

MacGregor, K.R., Anderson, R.S., Waddington, E.D., 2009. Numerical modeling of glacial erosion and headwall processes in alpine valleys. Geomorphology, 103(2), p.189-204.

Martin, L., Blard, P., Balco, G., Laurent, V., 2017. The CREp program and the ICE-D production rate calibration database: A fully parameterizable and updated online tool to compute cosmic-ray exposure ages. Quaternary Geochronology, 38, p.25-49.

Matsuoka, N., 2001. Microgelivation versus macrogelivation: towards bridging the gap between laboratory and field frost weathering. Permafrost and Periglacial Processes, 12(3), p.299-313.

Matsuoka, N., Murton, J., 2008. Frost weathering: recent advances and future directions. Permafrost and Periglacial Processes, 19(2), p.195-210.

Matsuoka, N., Sakai, H., 1999. Rockfall activity from an alpine cliff during thawing periods. Geomorphology, 28(3-4), p.309-328.

Mihalcea C, Mayer C, Diolaiuti G, Lambrecht A, Smiraglia C, Tartari G. 2006. Ice ablation and meteorological conditions on the debris-covered area of Baltoro glacier, Karakoram, Pakistan. Annals of Glaciology, 43, p.292-300.

Mihalcea, C., Mayer, C., Diolaiuti, G., D'agata, C., Smiraglia, C., Lambrecht, A., Vuillermoz, E., Tartari, G., 2008. Spatial distribution of debris thickness and melting from remote-sensing and meteorological data, at debris-covered Baltoro glacier, Karakoram, Pakistan. Annals of Glaciology, 48, p.49-57.

Mitchell, S.G., Montgomery, D.R., 2006. Influence of a glacial buzzsaw on the height and morphology of the Cascade Range in central Washington State, USA. Quaternary Research, 65(1), p.96-107.

Mitchell, W.A., McSaveney, M.J., Zondervan A, Kim K, Dunning SA, Taylor PJ. 2007. The Keylong Serai rock avalanche, NW Indian Himalaya: geomorphology and palaeoseismic implications. Landslides, 4(3), p.245-254.

Molnar, P., Anderson, R.S., Anderson, S.P., 2007. Tectonics, fracturing of rock, and erosion. Journal of Geophysical Research: Earth Surface, 112(F3).

Moore, D.M., Reynolds Jr, R.C., 1997. X-ray Diffraction and the Identification and Analysis of Clay Minerals.

Moore, R.D., Fleming, S.W., Menounos, B., Wheate, R., Fountain, A., Stahl, K., Holm, K., Jakob, M., 2009. Glacier change in western North America: influences on hydrology, geomorphic hazards and water quality. Hydrological Processes, 23(1), p.42-61.

Moores, J.E., Pelletier, J.D., Smith, P.H., 2008. Crack propagation by differential insolation on desert surface clasts. Geomorphology, 102(3-4), p.472-481.

Murton, J.B., Peterson, R., Ozouf, J.C., 2006. Bedrock fracture by ice segregation in cold regions. Science, 314(5802), p.1127-1129.

Nagai, H., Fujita, K., Nuimura, T., Sakai, A., 2013. Southwest-facing slopes control the formation of debris-covered glaciers in the Bhutan Himalaya. The Cryosphere, 7(4), p.1303.

Naithani, A.K., Nainwal, H.C., Sati, K.K., Prasad, C., 2001. Geomorphological evidences of retreat of the Gangotri glacier and its characteristics. Current Science, p.87-94.

Naylor, S,, Gabet, E.J., 2007. Valley asymmetry and glacial versus nonglacial erosion in the Bitterroot Range, Montana, USA. Geology, 35(4), p.375-378.

Nishiizumi, K., Finkel, R.C., Caffee, M.W., Southon, J.R., Kohl, C.P., Arnold, J.R., Olinger, C.T., Poths, J., Klein, J., 1994. Cosmogenic production of ^{10}Be and ^{26}Al on the surface of the earth and underground. In Eighth International Conference on Geochronology, Cosmochronology and Isotope Geology: US Geological Survey Circular (Vol. 1107, p. 234).

Nishiizumi, K., Imamura, M., Caffee, M.W., Southon, J.R., Finkel, R.C., McAninch, J., 2007. Absolute calibration of ^{10}Be AMS standards. Nuclear Instruments and Methods in Physics Research Section B: Beam Interactions with Materials and Atoms, 258(2), p.403-413.

Orr, E.N., Owen, L., Murari, M., Saha, S., Caffee, M., 2017. The timing and extent of Quaternary glaciation of Stok, northern Zanskar Range, Transhimalaya, of northern India. Geomorphology 284, p.142-155.

Orr, E.N., Owen, L.A., Saha, S., Caffee, M.W., Murari, M.K., 2018. Quaternary glaciation of the Lato Massif, Zanskar Range of the NW Himalaya. Quaternary Science Reviews, 183, p.140-156.

Osmaston, H., 2005. Estimates of glacier equilibrium line altitudes by the Area× Altitude, the Area× Altitude Balance Ratio and the Area× Altitude Balance Index methods and their validation. Quaternary International, 138, p.22-31.

Oskin, M., Burbank, D.W., 2005. Alpine landscape evolution dominated by cirque retreat. Geology, 33(12), p.933-936.

Owen, L., 2009. Latest Pleistocene and Holocene glacier fluctuations in the Himalaya and Tibet. Quaternary Science Reviews 28, 21-22, p.2150-2164.

Owen, L.A., Derbyshire, E., 1989. The Karakoram glacial depositional system. Zeitschrift für Geomorphologie, 76(Suppl.), p.33-73.

Owen, L.A., Sharma, M.C., 1998. Rates and magnitudes of paraglacial fan formation in the Garhwal Himalaya: implications for landscape evolution. Geomorphology, 26(1-3), p.171-184.

Owen, L.A., Sharma, M.C., Bigwood, R., 1996. Mass movement hazard in the Garhwal Himalaya: the effects of the 20 October 1991 Garhwal earthquake and the July–August 1992 monsoon season. Geomorphology and Land Management in a Changing Environment. Wiley, Chichester, UK, p.69-88.

Owen, L.A., Derbyshire, E., Scott, C.H., 2003. Contemporary sediment production and transfer in high-altitude glaciers. Sedimentary Geology, 155(1-2), p.13-36.

Owen, L.A., Caffee, M.W., Finkel, R.C., Seong, B.S., 2008. Quaternary glaciation of the Himalayan–Tibetan orogen. Journal of Quaternary Science, 23, p.513–532.

Owen, L.A., 2009. Latest Pleistocene and Holocene glacier fluctuations in the Himalaya and Tibet. Quaternary Science Reviews, 28(21-22), p.2150-2164.

Ouimet, W.B., Whipple, K.X., Granger, D.E., 2009. Beyond threshold hillslopes: Channel adjustment to base-level fall in tectonically active mountain ranges. Geology, 37(7), p.579-582.

Placzek, C., Granger, D.E., Matmon, A., Quade, J., Ryb, U., 2014. Geomorphic process rates in the central Atacama Desert, Chile: insights from cosmogenic nuclides and implications for the onset of hyperaridity. American Journal of Science, 314(10), p.1462-1512.

Portenga, E.W., Bierman, P.R., 2011. Understanding Earth's eroding surface with 10 Be. GsA today, 21(8), p.4-10.

Portenga, E.W., Bierman, P.R., Duncan, C., Corbett, L.B., Kehrwald, N.M., Rood, D.H., 2015. Erosion rates of the Bhutanese Himalaya determined using in situ-produced 10Be. Geomorphology, 233, p.112-126.

Porter, S.C., 2000. Snowline depression in the tropics during the Last Glaciation. Quaternary science reviews, 20(10), p.1067-1091.

Pratap, B., Dobhal, D.P., Bhambri, R., Mehta, M., 2013. Near-surface temperature lapse rate in Dokriani Glacier catchment, Garhwal Himalaya, India. Himalayan Geology, 34, p.183-186.

Rajendran, K., Rajendran, C.P., Jain, S.K., Murty, C.V.R., Arlekar, J.N., 2000. The Chamoli earthquake, Garhwal Himalaya: field observations and implications for seismic hazard. CURRENT SCIENCE-BANGALORE-, 78(1), p.45-51.

Ranhotra, P.S., Bhattacharyya, A., 2013. Modern vegetational distribution and pollen dispersal study within Gangotri glacier valley, Garhwal Himalaya. Journal of the Geological Society of India, 82(2), p.133-142.

Regmi, A.D., Yoshida, K., Dhital, M.R., Devkota, K., 2013. Effect of rock weathering, clay mineralogy, and geological structures in the formation of large landslide, a case study from Dumre Besei landslide, Lesser Himalaya Nepal. Landslides, 10(1), p.1-13.

Rowan, A.V., Egholm, D.L., Quincey, D.J., Glasser, N.F., 2015. Modelling the feedbacks between mass balance, ice flow and debris transport to predict the response to climate change of debris-covered glaciers in the Himalaya. Earth and Planetary Science Letters, 430, p.427-438.

Saha, S., Owen, L.A., Orr, E.N., Caffee, M.W., 2018. Timing and nature of Holocene glacier advances at the northwestern end of the Himalayan-Tibetan orogen. Quaternary Science Reviews, 187, p.177-202.

Sadler, P.M., Jerolmack, D.J., 2014. Scaling laws for aggradation, denudation and progradation rates: the case for time-scale invariance at sediment sources and sinks. Geological Society, London, Special Publications, 404, p.SP404-7.

Sanders, J.W., Cuffey, K.M., Moore, J.R., MacGregor, K.R., Kavanaugh, J.L., 2012. Periglacial weathering and headwall erosion in cirque glacier bergschrunds. Geology, 40(9), p.779-782.

Satyabala, S.P., 2016. Spatiotemporal variations in surface velocity of the Gangotri glacier, Garhwal Himalaya, India: Study using synthetic aperture radar data. Remote sensing of environment, 181, p.151-161.

Scaillet B, Pêcher A, Rochette P, Champenois M. 1995. The Gangotri granite (Garhwal Himalaya): laccolithic emplacement in an extending collisional belt. Journal of Geophysical Research: Solid Earth, 100(B1), p.585-607.

Scherler, D., Egholm, D., 2017. Debris supply to mountain glaciers and how it effects their sensitivity to climate change–A case study from the Chhota Shigri Glacier, India (Invited)(206444). In 2017 Fall Meeting.

Scherler, D., Bookhagen, B., Strecker, M.R., von Blanckenburg, F., Rood, D., 2010. Timing and extent of late Quaternary glaciation in the western Himalaya constrained by 10Be moraine dating in Garhwal, India. Quaternary Science Reviews, 29(7-8), p.815-831.

Scherler, D., Bookhagen, B., Strecker, M.R., 2011a. Hillslope-glacier coupling: The interplay of topography and glacial dynamics in High Asia. Journal of Geophysical Research: Earth Surface, 116(F2).

Scherler, D., Bookhagen, B., Strecker, M.R., 2011b. Spatially variable response of Himalayan glaciers to climate change affected by debris cover. Nature geoscience, 4(3), p.156.

Scherler, D., Bookhagen, B., Strecker, M.R., 2014. Tectonic control on 10Be-derived erosion rates in the Garhwal Himalaya, India. Journal of Geophysical Research: Earth Surface, 119(2), p.83-105.

Scherler, D., Bookhagen, B., Wulf, H., Preusser, F., Strecker, M.R., 2015. Increased late Pleistocene erosion rates during fluvial aggradation in the Garhwal Himalaya, northern India. Earth and Planetary Science Letters, 428, p.255-266.

Schroder, J.F., Bishop, M.P., Copland, L., Sloan, V.F., 2000. Debris-covered glaciers and rock glaciers in the Nanga Parbat Himalaya, Pakistan. Geogr. Ann. 82A, 17–31

Schweinfurth, U., 1968. Vegetation of the Himalaya. V: Mountains and Rivers of India. In 21st International Geographical Congress, India. Calcutta, National Committee for Geography (p. 110-136).

Searle, M., 1986. Structural evolution and sequence of thrusting in the High Himalayan, Tibetan-Tethys and Indus suture zones of Zanskar and Ladakh, Western Himalaya. Journa of Structural Geology, 8,8, p.923-936.

Searle, M.P., Metcalfe, R.P., Rex, A.J., Norry, M.J., 1993. Field relations, petrogenesis and emplacement of the Bhagirathi leucogranite, Garhwal Himalaya. Geological Society, London, Special Publications, 74(1), p.429-444.

Searle, M., Parrish, R., Hodges, K., Hurford, A., Ayres, M., Whitehouse, M., 1997. Shisha Pangma Leucogranite, South Tibetan Himalaya: Field Relations, Geochemistry, Age, Origin, and Emplacement. Journal of Geology, 150, p.295-317.

Searle, M.P., Noble, S.R., Hurford, A.J., Rex, D.C., 1999. Age of crustal melting, emplacement and exhumation history of the Shivling leucogranite, Garhwal Himalaya. Geological Magazine, 136(5), p.513-525.

Seong, Y.B., Owen, L.A., Bishop, M.P., Bush, A., Clendon, P., Copland, L., Finkel, R., Kamp, U., Shroder, J.F., 2007. Quaternary glacial history of the Central Karakoram. Quaternary Science Reviews 26, p.3384–3405.

Seong, Y.B., Owen, L.A., Caffee, M.W., Kamp, U., Bishop, M.P., Bush, A., Copland, L., Shroder, J.F., 2009a. Rates of basin-wide rockwall retreat in the K2 region of the Central Karakoram defined by terrestrial cosmogenic nuclide 10Be. Geomorphology, 107(3-4), p.254-262.

Sharma, M.C., Owen, L.A., 1996. Quaternary glacial history of NW Garhwal, central Himalayas. Quaternary Science Reviews, 15(4), pp

Sharma, P., Bourgeois, M., Elmore, D., Granger, D., Lipschutz, M.E., Ma, X., Miller, T., Mueller, K., Rickey, F., Simms, P., Vog, S., (2000) PRIME lab AMS performance, upgrades and research applications. Nuclear Instruments and Methods in Physics Research, B 172, p.112-123.

Sheridan, M.F., Marshall, J.R., 1987. Comparative charts for quantitative analysis of grain textural elements on pyroclastics. In: Marshall, J.R. (Ed.), Clastic Particles. Van Nostrand-Reinhold, New York, p. 98 – 121.

Siddiqui, M.A., Maruthi, K.V., 2007. Detailed glaciological studies on Hamtah Glacier, Lahaul and Spiti District, HP Geol. Surv. India, 140, p.92-93.

Singh, P., Haritashya, U.K., Kumar, N., Singh, Y., 2006. Hydrological characteristics of the Gangotri glacier, central Himalayas, India. Journal of Hydrology, 327(1-2), p.55-67.

Singh, P., Haritashya, U.K., Kumar, N., 2007. Meteorological study for Gangotri Glacier and its comparison with other high altitude meteorological stations in central Himalayan region. Hydrology Research, 38(1), p.59-77.

Singh, P., Haritashya, U.K., Kumar, N., 2008. Modelling and estimation of different components of streamflow for Gangotri Glacier basin, Himalayas Hydrological sciences journal, 53(2), p.309-322.

Singh, D.S., Tangri, A.K., Kumar, D., Dubey. C.A., Bali, R., 2017. Pattern of retreat and related morphological zones of Gangotri Glacier, Garhwal Himalaya, India. Quaternary International, 444, p.172-181.

Small, R.J., 1983. Lateral moraines of Glacier de Tsidjiore Nouve: form, development, and implications. Journal of Glaciology, 29(102), p.250-259.

Sorkhabi, R.B., Stump, E., Foland, K.A., Jain, A.K., 1996. Fission-track and 40Ar39Ar evidence for episodic denudation of the Gangotri granites in the Garhwal Higher Himalaya, India. Tectonophysics, 260(1-3), p.187-199.

Sneed, E.D., Folk, R.L., 1958. Pebbles in the lower Colorado River, Texas a study in particle morphogenesis. The Journal of Geology, 66(2), p.114-150.

Srivastava, D., 2012. Status report on Gangotri glacier. Science and Engineering Research Board, Department of Science and Technology, New Delhi, Himalayan Glaciology Technical Report, 3, p.21-25.

Steck, A., Epard, J., Vannay, J., Hunziker, J., Girard, M., Morard, A,. Robyr, M. ,1998. Geological transect across the Tso Morari and Spiti areas- the nappe structures of the Tethys Himalayas. Eclogae Geologicae Helvetiae 91, p.103-121.

Swift, D.A., Nienow, P.W., Hoey, T.B., 2005. Basal sediment evacuation by subglacial meltwater: suspended sediment transport from Haut Glacier d'Arolla, Switzerland. Earth Surface Processes and Landforms, 30(7), p.867-883.

Tangri, A.K., (2002) Shrinking glaciers of Uttaranchal - cause of concern - hope for the future. Keynote address at NationaI Seminar on Geology and Natural Environment of Himalaya, Nainital.

Tangri, A.K., Chandra, R., Yadav, S.K.S., 2004, March. Temporal monitoring of the snout, equilibrium line and ablation zone of Gangotri glacier through remote sensing and GIS techniques–an attempt at deciphering the climatic variability. In Proceedings of Workshop on Gangotri glacier (p. 26-28).

Thayyen, R.J., Gergan, J.T., 2010. Role of glaciers in watershed hydrology: a preliminary study of a" Himalayan catchment". The Cryosphere, 4(1), p.115-128.

Thayyen, R.J., Gergan, J.T., Dobhal, D.P., 2005. Slope lapse rates of temperature in Din Gad (Dokriani glacier) catchment, Garhwal Himalaya, India. Bulletin of glaciological research, 22, p.31-37.

Thiede, R.C., Arrowsmith, J.R., Bookhagen, B., McWilliams, M.O., Sobel, E.R., Strecker, M.R., 2005. From tectonically to erosionally controlled development of the Himalayan orogen. Geology, 33(8), p.689-692.

Thiede, R.C., Bookhagen, B., Arrowsmith, J.R., Sobel, E.R., Strecker, M.R., 2004. Climatic control on rapid exhumation along the Southern Himalayan Front. Earth and Planetary Science Letters, 222(3-4), p.791-806.

Thiede, R.C., Ehlers, T.A., Bookhagen, B., Strecker, M.R., 2009. Erosional variability along the northwest Himalaya. Journal of Geophysical Research: Earth Surface, 114(F1).

Thiede, R.C., Ehlers, T.A., 2013. Large spatial and temporal variations in Himalayan denudation. Earth and Planetary Science Letters, 371, p.278-293.

Tripathy, G.R., Singh, S.K., 2010. Chemical erosion rates of river basins of the Ganga system in the Himalaya: Reanalysis based on inversion of dissolved major ions, Sr, and 87Sr/86Sr. Geochemistry, Geophysics, Geosystems, 11(3).

Underwood, M.B., Pickering, K.T., 1996. Clay-mineral provenance, sediment dispersal patterns, and mudrock diagenesis in the Nankai accretionary prism, southwest Japan. Clays and Clay Minerals, 44(3), p.339-356.

Valdiya, K.S., (1991) The Uttarkashi earthquake of 20 October:implications and lessons. Curr. Sci. v. 61, p. 801-803.

Vance, D., Bickle, M., Ivy-Ochs, S., Kubik, P.W., 2003. Erosion and exhumation in the Himalaya from cosmogenic isotope inventories of river sediments. Earth and Planetary Science Letters, 206(3-4), p.273-288.

Vannay, C., Grasemann, B., Rahn, M., Frank, W., Carter, A., Baudraz, V., Cosca, M., 2004. Miocene to Holocene exhumation of metamorphic crustal wedges in the NW Himalaya: Evidence for tectonic extrusion coupled to fluvial erosion. Tectonics, 23, p.1-24.

Wagnon, P., Lind, A., Arnaud, Y., Kumar, R., Sharma, P., Vincent, C., Pottakkal, J.G., Berthier, E., Ramanathan, A.,, Hasnain, S.I., Chevallier, P., 2007. Four years of mass balance on Chhota Shigri Glacier, Himachal Pradesh, India, a new benchmark glacier in the western Himalaya. Journal of Glaciology, 53(183), p.603-611.

Ward, D.J., Anderson, R.S., 2011. The use of ablation-dominated medial moraines as samplers for 10Be-derived erosion rates of glacier valley walls, Kichatna Mountains, AK. Earth Surface Processes and Landforms, 36(4), p.495-512.

Watanabe, T., Dali, L., Shiraiwa, T., 1998. Slope denudation and the supply of debris to cones in Langtang Himal, Central Nepal Himalaya. Geomorphology, 26(1-3), p.185-197.

Wegmann, M., Gudmundsson, G.H., Haeberli, W., 1998. Permafrost changes in rock walls and the retreat of Alpine glaciers: a thermal modelling approach. Permafrost and Periglacial Processes, 9(1), p.23-33.

Wentworth, C.K., 1922. A scale of grade and class terms for clastic sediments. The journal of geology, 30(5), p.377-392.

West, N.E., Kirby, P., Bierman, B.A., Clarke., 2014. Aspect-dependent variations in regolith creep revealed by meteoric ^{10}Be, Geology, 42(6), p.507–510.

Whipple, K.X., 2009. The influence of climate on the tectonic evolution of mountain belts. Nature geoscience, 2(2), p.97.

Willenbring, J.K., Codilean, A.T., McElroy, B., 2013. Earth is (mostly) flat: Apportionment of the flux of continental sediment over millennial time scales. Geology, 41(3), p.343-346.

Wulf, H., Bookhagen, B., Scherler, D., 2010. Seasonal precipitation gradients and their impact on fluvial sediment flux in the Northwest Himalaya. Geomorphology, 118, 1-2, p.13-21.

Zeitler, P.K., Koons, P.O., Bishop, M.P,. Chamberlain, C.P., Craw, D., Edwards, M.A., Hamidullah, S., Jan, M.Q., Khan, M.A., Khattak, M., Kidd, W.S., 2001. Crustal reworking at Nanga Parbat, Pakistan: Metamorphic consequences of thermal-mechanical coupling facilitated by erosion. Tectonics, 20(5), p.712-728.

Zingg, T., 1935. Beitrag zur Schotteranalyse, Scweizerische. Mineralogische und Petrographische Mitteilungen 15, 39 – 140

9. Rockwall slope erosion in the NW Himalaya

Elizabeth N. Orr[a*], Lewis A. Owen[a], Sourav Saha[a], Sarah Hammer[a], Marc W. Caffee[b,c]
[a] *Department of Geology, University of Cincinnati, Cincinnati, OH 45221, USA*
[b] *Department of Physics, Purdue University, West Lafayette, IN 47907, USA*
[c] *Department of Earth, Atmospheric and Planetary Sciences, Purdue University, West Lafayette, IN 47907, USA*

ABSTRACT

Steep north-south trending gradients in elevation, relief, rock uplift and precipitation make the NW Himalaya an excellent location to examine the relative roles of climate and tectonics in erosion and landscape evolution. We define the distribution and magnitude of periglacial rockwall slope erosion across 12 catchments in northern India using cosmogenic ^{10}Be concentrations in sediment from medial moraines. Beryllium-10 concentrations range from $5.3\pm0.8\text{x}10^4$ to $260.0\pm12.5\text{x}10^4$ at/g SiO_2, which yield erosion rates between 0.02 and 7.2±1.1 mm/a. Between ~0.02 and ~7 m of lateral erosion can therefore be achieved in this setting across a single millennia, and >2 km when extrapolated for the whole Quaternary. This erosion is therefore sufficient to affect catchment sediment flux and glacier dynamics, and help to set the pace of topographic change at the headwaters of catchments. We combine rockwall erosion records from Garhwal, Kullu, Lahul, Ladakh and Baltistan to create a regional erosion dataset. Rockwall slope erosion largely outpaces the local catchment-wide erosion rates and exhumation in the NW Himalaya. This demonstrates the importance of accounting for localized erosion ($<10^1$ km^2) and its effects on down-catchment reaches in studies of wider landscape change. The erosion of rockwall slopes is likely dictated by longstanding feedbacks between topography, geology, surface processes, climate and tectonics, which are specific to each catchment. The relative role of these parameters is likely to vary across space and time.

*Corresponding author. E. N. Orr: orreh@mail.uc.edu

Rockwall slope erosion rates become progressively less rapid with distance north from the Main Central Thrust and into the interior of the orogen. The distribution and magnitude of this erosion is most closely associated with records of Himalayan denudation and rock uplift. This suggests that tectonically driven uplift, rather than climate, provide a first order control on patterns of landscape change in the NW Himalaya, on geomorphic (10^2–10^5 years) to geologic (10^6 years) timescales. Precipitation is likely to play a secondary role in defining the spatial distribution of erosion.

Keywords: rock uplift; climate; periglacial erosion; cosmogenic isotopes; sediment flux

INTRODUCTION

A growing number of studies have underlined the importance of periglacial rockwall slope erosion in high altitude mountain settings, and its role in catchment sediment flux, relief production, topographic configuration and glacier dynamics (Heimsath and McGlynn, 2008; MacGregor et al., 2009; Seong et al., 2009; Ward and Anderson, 2011; Benn et al., 2012 Scherler and Egholm, 2017; Orr et al., *in review*). The lateral erosion of slopes has been shown to exceed rates of vertical incision through glacial and fluvial processes, and therefore to a greater extent than previously thought, contribute to denudation budgets and landscape change on the catchment and mountain range scale (Brocklehurst and Whipple, 2006; Foster et al., 2008).

Short and long-term erosion in the Himalayan-Tibetan orogen is understood to scale with tectonics (Burbank et al., 2003; Scherler et al., 2014; Godard et al., 2014), rainfall (Thiede et al., 2004; Grujic et al., 2006; Clift et al., 2008; Gabet et al. 2008; Wulf et al., 2010; Deeken et al., 2011) and/or topography (Vance et al., 2003; Scherler et al., 2011, 2014). Which of these parameters, if any, provide a first-order control on rates of rockwall slope erosion is unclear. The

Himalaya is an excellent location to evaluate these controls, given the south-north gradients in elevation, relief, rock uplift and precipitation (Bookhagen and Burbank, 2006, 2010; Scherler et al., 2011).

Orr et al. (*in review)* were the first to discuss the distribution of rockwall slope erosion throughout the NW Himalaya, and identified a tentative relationship between slope erosion and precipitation. Higher rates of erosion, e.g., were determined for catchments with enhanced monsoon precipitation. Rather than identifying a single control, their study instead suggests that rockwall slope erosion is more complex, and is therefore determined by the interaction between geology, tectonics, climate and topography, which are specific to each catchment. This opposes the view that in tectonically active mountain ranges, the strength of hillslope-glacier coupling is largely controlled by rock uplift and topographic steepness (Scherler et al., 2011; Gibson et al., 2017).

In this study, we seek to better define the distribution and magnitude of rockwall slope erosion in the NW Himalaya, by building upon the work of Orr et al. (*in review*) and quantifying erosion rates for a suite of 12 catchments. Rates of rockwall slope erosion are derived from ^{10}Be cosmogenic nuclide concentrations measured in sediment from medial moraines. Our new erosion dataset is combined with existing slope erosion records from Seong et al. (2009), Scherler and Egholm (2017) and Orr et al., (*in review*). This regional rockwall erosion dataset is compared to records of catchment-wide erosion and exhumation for the NW Himalaya to evaluate the extent to which slope erosion may differ to other records of landscape change, which have been averaged across various spatial and temporal scales. We compare patterns of slope erosion to those in geology, tectonics, climate and topography to resolve the primary controls of rockwall slope erosion in the NW Himalaya. Finally, we determine to what extent slope erosion and its controls, in this high-altitude and high relief setting, can contribute to the longstanding debate over the significance of climate versus tectonics in driving both short and long term landscape change.

REGIONAL SETTING

The Himalayan-Tibetan orogen has formed as the result of the continued continental collision and partial subduction between the Indian and Eurasian lithospheric plates (Searle et al., 1997). The Indus-Tsangpo Suture Zone defines the collision zone between these plates in the NW Himalaya and contains remnants of the Neo-Tethys Ocean, which include ophiolite mélanges. The suture zone marks the northern boundary of the Tethyan Himalaya; a unit of weakly metamorphosed Proterozoic−Paleogene sedimentary rocks including pelite and psammite (Searle, 1986; Steck et al., 1998; Schlup et al., 2003). Between the early Miocene and Pleistocene, deformation driven crustal shortening initiated the development of a sequence of foreland propogating thrust systems that divide the lithotectonic units that lie south of the Tethyan Himalaya. The South-Tibetan Detachment and the Main Central Thrust bound the Greater Himalaya Crystalline Core Zone to the north and south, respectively. This sequence is composed of Precambrian−Paleozoic high-grade metamorphic amphibolite-grade schist, gneiss and migmatites, which are intruded by Cambrian−Ordovician, Permian and Miocene granitic plutons (Frank et al., 1973; Searle and Fryer, 1986; Walker et al., 1999; Miller et al., 2001; Vannay et al., 2004). This unit has been divided into two sub-units: southern Greater Himalaya sequence (GHS-S) and northern Greater Himalaya sequence (GHS-N; DeCelles et al., 2001; Thiede and Ehlers 2013). South of the Main Central Thrust, the Lesser Himalaya sequence consists of medium-high grade mica schist and granitic gneiss, and low-grade Proterozoic metasedimentary rocks, which include phyllite, quartzite and limestone (Upreti, 1999; Miller et al., 2000; Vannay et al., 2004). The Sub-Himalaya is composed of detrital sediment eroded from the Himalayan arc between the Oligocene and Pliocene, and is bounded to the north and south by the Main Boundary Thrust and Main Frontal Thrust, respectively (Vannay et al., 2004).

Continued crustal shortening and thrust and strike-slip faulting throughout the orogen means that the NW Himalaya remains tectonically active (Hodges et al., 2004; Vannay et al., 2004; Bojar et al., 2005), even though some regions in northern India such as Ladakh, have undergone tectonic quiescence or dormancy since the early Miocene (Kristein et al., 2006, 2009). Hodges (2000), Yin and Harrison (2000) and Streule et al. (2009) provide further details of the Himalayan lithotectonic units and the timing of movement throughout the fault systems.

Two atmospheric systems primarily govern northwest Himalayan climate; the Indian summer monsoon that advects moisture from the Indian Ocean between late May and September, and the Northern Hemispheric westerlies, which bring moisture from the Mediterranean, Black and Caspian seas between December and March (Gadgil 2003; Lang and Barros 2004; Wulf et al., 2010; Mölg et al., 2013). A steep south-north precipitation gradient became established during the late Miocene, perpendicular to the strike of the mountain belt (~8 Ma; Qiang et al., 2001; Liu and Dong, 2013), due to the high elevation ranges of the Greater Himalaya inhibiting the northward migration of moisture to the interior of the orogen. Monsoon air masses are forced to ascend, condensate and form clouds along the Himalayan front, which creates a rainshadow down the leeside of this orographic barrier (Bookhagen et al., 2005a,b; Wulf et al., 2010). During times of increased monsoon strength, moisture is thought to penetrate farther into the interior of the orogen (Finkel et al., 2003 Bookhagen et al., 2005a,b; Wulf et al., 2010). The northern hemispheric westerlies operate at higher tropospheric levels to the Indian summer monsoon. The orographic capture of moisture transported by this atmospheric system is therefore focused in high elevation ranges (> 4500 m asl) as winter snowfall (Weiers 1995; Lang and Barros 2004). Today, total annual precipitation declines from ~1500−3000 mm in the Lesser and Greater Himalaya ranges, to <150 mm in the interior of the Tethyan Himlaya and Tibetan Plateau (Bookhagen and Burbank, 2006).

The distribution and magnitude of precipitation has been shown to vary both temporally and spatially throughout the Himalayan-Tibetan orogen during the late Quaternary (Burbank et al., 2003; Bookhagen et al., 2005a,b). Fluctuations in monsoon strength driven by changes in orbital insolation, the migration of the intertropical convergence zone, convective localized monsoon storms and sporadic heavy rainfall are thought to cause some of this variability (Finkel et al., 2003; Owen et al., 2008; Thomas et al., 2016). On the local-regional scale ($10^{2\text{-}4}$ km^2), topography and wind direction exert controls on the migration of moisture throughout the NW Himalaya (Bookhagen et al., 2005a,b), and create localized microclimates throughout individual mountain ranges (Benn and Owen, 1998; Bookhagen and Burbank, 2010; Wulf et al., 2010). Landscape change in the NW Himalaya is precipitation sensitive, where shifts in the availability and source of moisture has been shown to initiate changes to sediment flux, hillslope processes (Bookhagen et al., 2005; Bookhagen and Burbank, 2006; Sharma et al., 2017; Kumar et al., 2018; Orr et al. *in press*) and the timing of glaciation (Owen and Dortch, 2014; Saha et al., 2018).

The timing and forcing of glaciation can also vary across short distances (10^{1-2} km) in the NW Himalaya (Owen and Dortch 2014). Studies have shown that the nature of glaciation can be influenced by climatic factors such as shifts in the strength or behavior of regional and/or global atmospheric and oceanic systems (Owen and Sharma 1998; Watanabe et al., 1998; Solomina et al., 2015; 2016; Saha et al., 2018) and/or local geological factors such as topography and glacier type (Barr and Lovell 2014; Anderson et al., 2014). The Himalayan Holocene stages (HHs; Saha et al., 2018), semi-arid western Himalayan-Tibetan orogen stages (SWHTs; Dortch et al., 2013) and monsoonal Himalayan-Tibetan stages (MOHITs; Murari et al., 2014) provide regional syntheses of the glacial records throughout the NW Himalaya (Table 1).

Study areas

In this study, the Ladakh region refers to the Ladakh and Zanskar Ranges of Jammu and Kashmir in northern India. The Baltistan region encompasses the semi-arid Karakoram of Pakistan (Fig. 1). The Indian summer monsoon delivers two-thirds of the annual precipitation in the Ladakh and Zanskar Ranges (total: 87 mm/a; Table 1), whereas the westerlies provide the primary source of moisture to the Karakoram. Glaciers in the Ladakh region are small (1–10 km^2) cold-based sub-polar glaciers, which are precipitation sensitive and sublimation dominated (Benn and Owen, 2002).

Geomorphic studies recognize that the arid/semi-arid climatic setting of the Ladakh region is largely responsible for the preservation of very old landforms and sediment deposits (>400 ka; Owen et al., 2006; Hedrick et al., 2011; Orr et al., 2017, 2018, *in press*) and slow rates of landscape change (<0.07±0.01 mm/a; Dortch et al., 2011a; Dietsch et al., 2015, *in revisions*). Dortch et al. (2011) argue that the higher rates of catchment-wide erosion observed throughout the northern flanks of the Ladakh range (0.06±0.01−0.07±0.01 mm/a), compared to south-facing catchments (0.02±0.003−0.04±0.008 mm/a) is due to tectonic uplift along the active Karakoram fault and the tectonic tilting of the central range. This study suggests that catchment-wide erosion is unable to keep pace with regional uplift; erosion rates are at least an order of magnitude slower than the rates of uplift inferred by strath terrace incision (0.02±0.003−2.6±1.9 mm/a; Kristein et al., 2006, 2009; Dortch et al., 2011b; *ibid*). Bedrock incision rates of ~0.6 mm/a by rivers in some north-facing catchments over the past ~120 ka are equal to local rates of exhumation (0.4−0.6 mm/a). Dietsch et al. (2015) use cosmogenic nuclide concentrations in bedrock tors to demonstrate that periglacial weathering at catchment ridgelines in the Ladakh Range is greater in glaciated catchments than those that have remained unglaciated. Bedrock erosion rates in the periglacial domain of these catchments are higher than downstream reaches; interfluve bedrock

ridges yield erosion rates (<7.0±1.0x10^4 mm/a) an order of magnitude slower than the bedrock tors (50.0±5.0 x10^4−100.0±10x10^4 mm/a).

The investigated Gopal and Stok catchments are two north-facing transverse catchments in the high-altitude desert landscapes of the northern Zanskar Range in Ladakh, and each retain small valley glaciers (Fig. 1, 2; Table 1). Karzok and Mentok are northeast-trending catchments that drain the Rupshu Massif in central Zanskar of the Ladakh region. Cirque glaciers occupy the upper reaches of these catchments.

The Lahul region includes the Lahul-Spiti and Kullu districts of the Pir Panjal and Greater Himalaya ranges in the Himachal Pradesh of northern India. The majority of annual precipitation in this region is sourced from the Indian summer monsoon (950–1020 mm/a; Table 1), despite a large area of Lahul being in the rainshadow of the Himalayan front. Glaciers are large, temperate and melt dominated, and are fed by precipitation from the summer monsoon and westerlies (Benn and Owen, 2002; Su and Shi, 2002). Differential rates of fluvial incision during the Holocene range from 0.2±0.2 to 13.2±6.3 mm/a along the length of the Chandra valley in Lahul, and either equal, or exceed regional rates of tectonic uplift (Adams et al., 2009; Dortch et al., 2011a). These rates of fluvial incision are argued to reflect the variable valley response to past glaciation and the complex and active tectonic setting in Lahul. The Plio-Pleistocene Apatite Helium cooling ages for the GHS-S rocks in Lahul measure exhumation rates of ~1−2 mm/a from 2.5 Ma (Sorkhabi et al., 1999; Vannay et al., 2004; Adams et al., 2009).

The Urgos valley glacier extends throughout the upper reaches of a southeast trending tributary catchment of the Miyar basin in the Lahul-Spiti district (Fig. 2). Panchi is a north-facing catchment with a small valley glacier, located north of the Keylong and Darcha villages. Shitidar, Batal, Chhota Shigri and Hamtah are north facing tributary catchments with one−two valley

glaciers. Each catchment drains into the Chandra valley. Beas Kund is a southeast trending catchment located on the southern slopes of the Pir Panjal Range in the Kullu district. Two valley glaciers occupy this catchment.

The Indian summer monsoon also dominates annual precipitation in the Uttarkashi district of Uttarkhand in the Garhwal Himalaya, northern India, a region our study revisits. Catchment-wide erosion rates range from ~0.1 to 0.5 mm/a in the Lesser Himalaya and from ~1 to 2 mm/a in the Greater Himalaya (Vance et al., 2003; Scherler et al., 2014). Scherler et al. (2014) argue that the spatial variability in catchment erosion is primarily controlled by topographic steepness. This study and others conclude that the distribution of erosion is influenced by patterns of rock uplift (4−5.7 mm/a) which are dictated by the geometry and shortening of the Main Himalayan Thrust (Burbank et al., 2003; Barnard et al., 2004; Schlerer et al. 2014).

METHODOLOGY

A suite of 12 accessible catchments was selected for investigation along the south-north precipitation gradient of the NW Himalaya (Fig. 1, 2). Each catchment supports either a cirque or small valley glacier with distinct and well-preserved medial moraines. Geomorphic maps of the periglacial-glacial realms of these catchments were prepared in the field and then refined using Advanced Spaceborne Thermal Emission and Reflection Radiometer (ASTER) global digital elevation models (GDEMs; 30-m-resolution), Landsat Enhanced Thematic Mapper Plus (ETM+) imagery and Google Earth imagery. Topographic and geomorphic matrices including catchment area, 3-km-radius relief, mean slope, hypsometry and aspect were calculated using the Spatial Analyst Toolbox in ArcMap 10.1. These analyses were also conducted for the Baltoro catchment in the Central Karakoram of Pakistan (Seong et al., 2009) and the upper Bhagirathi catchment in

Garhwal, northern India (Orr et al., *in review*) to enable comparisons between rockwall slope erosion and catchment matrices throughout the NW Himalaya.

We define rates of rockwall slope erosion by measuring ^{10}Be concentrations in medial moraine sediment. Rockwall slope erosion is inversely proportional to the ^{10}Be concentrations measured in these landforms (Seong et al., 2009; Ward and Anderson 2011). The longer the rockwall slopes are exposed to cosmic rays before the debris is transferred to the glacier surface by rockfall processes, the greater the ^{10}Be concentration in the sediment and therefore the slower the inferred rockwall slope erosion rate. Details of this methodology and its assumptions are provided by Ward and Anderson (2011) and Orr et al. (*in review*).

Orr et al. (*in review*) argue that the rates of rockwall slope erosion in the upper Bhagirathi catchment are best represented by the erosion rates derived from the centermost SD_B medial moraine of Gangotri glacier. This is because the ^{10}Be concentrations of SD_B fall within uncertainty of each other, and that as the most stable of the three investigated moraines, it did not receive sediment input from lateral moraines or hillslopes along the ablation zone of the glacier. The study also suggests that multiple samples should be taken from each medial moraine and/or glacier to evaluate variability in slope erosion throughout the catchment. With these recommendations in mind, we collected between one and five samples from stable and well-defined medial moraine ridges for the 12 investigated catchments (Fig. 2, 3). The sample locations were $\geq$ 20 m^2 in area to avoid sampling from a single source slope or rockfall event. Approximately 3 kg of sediment with a grain size of <3 cm (clay-coarse gravels) were collected for each sample by applying bulk sediment sampling methods of Gale and Hoare (1991). Each sample was named using the initial term 'G' for 'glacier' and then an abbreviated term for the catchment name. The samples were numbered in ascending order from the glacier snout, for

glaciers with more than one sample. For example, the G_{Cht1} sample was located closest to the snout of Chhota Shigri in Lahul, whilst G_{Cht5} was located furthest up-glacier.

The extraction of quartz from the sediment samples and ^{10}Be sample preparation was conducted at the Geochronology Laboratories at the University of Cincinnati, applying the community standards and chemical procedures of Kohl and Nishiizumi (1992). The ^{10}Be/^{9}Be of the samples was measured using accelerator mass spectrometry at the Purdue Rare Isotope Measurement (PRIME) Laboratory at Purdue University (Sharma et al., 2000). Upon the recommendations of Portenga et al. (2015), native ^{9}Be measured in ~5g fractions of clean quartz from each sample was subtracted from the initial ratio. Ward and Anderson (2011) designed an analytical expression to quantify the accumulation of cosmogenic nuclides during the transport of sediment from the source slopes to the medial moraine. This study found that ^{10}Be accumulation during the burial, englacial transport and exhumation of sediment to the glacier surface was negligible in landscapes with denudation rates ≤ 1 mm/a. This model was implemented in our study because some of the records of erosion local to our investigated catchments, particularly in Garhwal, exceed this threshold (0.13–5.37 mm/a; Vance et al., 2003; Lupker et al., 2013; Scherler et al., 2014). Where necessary, the ^{10}Be accumulated during this transport was then subtracted from the total ^{10}Be sample concentration.

Berylium-10 production rates were calculated for each pixel of a 30-m resolution ASTER DEM using methods of Dortch et al. (2011) in MATLAB R2017.a. A revised sea-level high-latitude spallogenic production rate of 4.08±0.23 Be atoms/g/a (Martin et al., 2017; http://calibration.ice-d.org/) and ^{10}Be half-life of 1.36 Ma (Nishiizumi et al., 2007) was used, and corrections for topographic shielding for each pixel were made. The ^{10}Be production rate for each investigated catchment was calculated by taking a mean of the production rate values for the DEM pixels. Previous work has shown that shielding by snow can adjust nuclide concentrations in sediment

and boulders by ≤ 20% (Schildgen et al. 2005; Scherler et al., 2014). With snowline elevations below the rockwall slopes that are predominantly north facing, which encourages winter accumulation, snow shielding of the rockwall and supraglacial realm may affect the ^{10}Be concentrations in the medial moraine sediment. Widespread avalanching and minimal snow retention on the rockwall slopes reduce our concern about the effects of snow shielding. Moreover, any adjustment to the nuclide concentrations for snow shielding would be uniform throughout the study areas, and not disrupt the broad trends in the erosion dataset.

Rockwall slope erosion rates were calculated from the ^{10}Be concentrations and catchment production rates using the methods described in detail by Lal (1991), Granger et al. (1996), Balco et al. (2008) and Dortch et al. (2011a). A 1σ uncertainty was propagated through each of the erosion rate calculations.

We calculated the Pearson Correlation Coefficient values (p) between the ^{10}Be concentrations and topographic, climatic and geologic matrices, and conducted a Principle Component Analysis (PCA) to identify and evaluate the possible controls of rockwall slope erosion in the NW Himalaya (The R Core Team, 2018; Supplementary Item 1). A p-value of <0.01 (at >99% confidence level) was applied. This approach has been successfully applied in other studies to evaluate the nature and magnitude of the environmental response to climatic change (Edwards and Richardson 2004; Sagredo and Lowell, 2012; Seaby and Henderson, 2014). The topographic matrices include: catchment and glacier area, mean catchment, rockwall and glacier slope, catchment 3-km-radius relief, mean catchment elevation, snowline altitude and glacier aspect. Climatic variables include: total annual precipitation (weather stations [as referenced in Table 1] and TRMM [1998−2009]) and temperature (weather stations and CRU2.0 [as referenced in Table 1]), mean rockwall slope temperature and minimum catchment temperature. Catchment specific temperatures were calculated using an adiabatic lapse rate of 7°C/km asl and methods outlined in

Orr et al. (*in review*). Additional variables such as sample grain size and mean apatite fission track (AFT) cooling ages (referenced in Table 5) were also included within these analyses. The latter enables us to identify any correlation between modern erosion rates and regional denudation histories on the million-year timescale. Upper Bhagirathi was not included in these analyses because the rockwall slope erosion rates characterize an extensive basin system with numerous tributary catchments, rather than a single catchment. The catchment is examined in more detail in the discussion section below. Due to the relatively restricted dataset size and some variability in the precision and resolution of the data, strong yet erroneous associations between nuclide concentrations and catchment matrices can be made. We therefore identify and discuss the most significant parameters in slope erosion with this in mind. P-values were also calculated between nuclide concentrations and catchment parameters for Ladakh, Lahul and Kullu and Garhwal as discrete regions (Supplementary Item 3).

RESULTS

Catchment relief is relatively subdued in the Ladakh region study areas, despite the imposing, high-altitude mountain peaks and rockwalls (>5500 m asl) that mark the headwater limits of each catchment (Table 2). The mean rockwall slopes range between 26.3±12.4 and 35.2±15.5°. The topography of the Lahul Himalaya is more severe than Ladakh, even with lower mean elevations (<4500 m asl); the investigated catchments are larger (13.9−44.9km^2), and have steeper relative relief (1.2±0.3−1.8±0.5 km) and higher mean rockwall slopes (32.8±12.8−47.2±11.9°).

The ablation zone of the Lahul glaciers are either partially or completely covered by debris, whereas in Ladakh, <30% of the glacier surfaces are covered (Fig. 3; Table 3). Beryllium-10 sample concentrations for the Ladakh and Lahul catchments range from 6.1±0.7 to 260.0±12.5x10^4 at/g and 0.5±0.04 to 30.6±1.0x10^4 at/g, respectively (Fig. 2; Table 4). For each catchment, the accumulation of ^{10}Be during transport from source slopes to medial moraine has a

negligible impact on the derived slope erosion rates; the additional ^{10}Be was smaller than the total concentration error of each sample (Table 4; Supplementary Item 2). In the Batal catchment for example, 0.02x10^4 at/g of ^{10}Be accumulated during transit is subtracted from the total concentrations of G_{Bat1} (30.6±1.0x10^4 at/g) and G_{Bat2} (3.5±0.3x10^4 at/g; Fig. 4). Inherent ^{9}Be in each sample was either absent or very low. The Chhota Shigri G_{Cht4} sample measured the highest amount of ^{9}Be in this study at 160.7 ppm, which adjusted the derived erosion rate by <2 %.

In the northern Zanskar Range, the ^{10}Be concentrations of the Gopal (21.0±0.7x10^4 at/g) and Stok (6.1±0.7x10^4 at/g) samples infer rockwall slope erosion rates of 0.3±0.04 and 0.9±0.2 mm/a, respectively (Fig. 5; Table 4). Erosion rates of 0.5±0.1 and 0.6±0.1 mm/a for the Amda catchment are derived from ^{10}Be concentrations of 10.8±0.3x10^4 and 9.6±0.3x10^4 at/g. In central Zanskar, the Karzok samples record ^{10}Be concentrations from 260.0±12.5 to 213.0±3.5x10^4 at/g, which yield slope erosion rates between 0.003 and 0.02 mm/a. The adjacent Mentok catchment has a slope erosion rate of 0.2±0.03mm/a from a ^{10}Be sample concentration of 32.9±1.2x10^4 at/g.

The ^{10}Be sample concentrations from Urgos in Lahul (1.7±0.2, 0.7±0.0005 x10^4 at/g) infer rockwall slope erosion rates of 2.6±0.4 and 6.5±0.8 mm/a (Table 4). The rate of slope erosion in the Panchi catchment is 0.2±0.1 mm/a, derived from a ^{10}Be concentration of 19.4±4.5x10^4 at/g. For Shitidhar, the ^{10}Be concentration and derived erosion rate of G_{Sht1} is 3.2±0.4x10^4 at/g and 1.0±0.2 mm/a, respectively. The ^{10}Be sample concentrations range from 30.6±1.0 to 3.5±0.3 x10^4 at/g and the slope erosion rates range from 0.2±0.02 to 1.3±0.2 mm/a in the Batal catchment. The five samples from the Chhota Shigri catchment have ^{10}Be concentrations between 4.2±1.3 and 1.0±0.05x10^4 at/g, which yield slope erosion rates between 1.1±0.4 and 5.0±0.7 mm/a. The ^{10}Be sample concentrations range from 2.0±0.2x10^4 to 0.8±0.1x10^4 at/g and the slope erosion rates range from 2.0±0.3 to 5.0±1.0 mm/a in Hamtah. Beas Kund records the highest rates of slope

erosion in this study; ^{10}Be concentrations from 0.5±0.04 to 0.8±0.1 x10^4 at/g derive erosion rates between 4.1±0.8 and 7.2±1.1 mm/a (Table 3).

The strongest statistically significant relationships between ^{10}Be concentration and catchment matrices include mean rockwall slope, mean catchment and snowline elevation, total annual precipitation, mean annual temperature and mean AFT cooling age (Table 5). For the region specific analysis, ^{10}Be concentrations have a strong correlation with mean catchment (*p*: 5.0x10^4) and rockwall slope (0.001 x10^4) in Ladakh. Catchment parameters do not statistically correlate with nuclide concentrations for the Lahul and Kullu or Garhwal regions (Supplementary Item 3).

DISCUSSION

In view of the inherent complexities of periglacial-glacial environments and the application of cosmogenic nuclide analysis in these settings, the medial moraine ^{10}Be concentrations of each catchment are broadly in concert with one another (Fig. 5). No relationship is apparent between nuclide concentration and proximity of sample location to either a glacier margin or snout. Any internal variability in concentrations within the catchments is likely because the medial moraine sediment is poorly mixed and/or has a non-proportional sediment supply that is dominated by stochastic rockfall events (Small et al., 1997; Muzikar, 2008; Ward and Anderson, 2011). The ^{10}Be concentrations from the Lahul and Kullu catchments are broadly comparable to those from Garhwal, with the exception of Batal and Panchi at the southern margin of the GHS-N unit, where concentrations exceed 3.5±0.3x10^4 at/g. Nuclide concentrations from the Ladakh and Baltistan region catchments either equal or exceed those from northern Lahul (Table 4; Fig. 2, 5).

The strong variability in physical settings of the catchments prevent any meaningful interpretations or comparisons between specific erosion rates. Moreover, time-averaged nuclide

derived erosion rates come with large uncertainties when characterizing local areas ($\leq 10^1$ km^2), which has been shown to underestimate the true rates (Yanites et al., 2009; Willenbring et al., 2013; Sadler and Jerolmack, 2014). Instead, we focus on the broad trends of this first rockwall slope erosion dataset for the NW Himalaya. Rockwall slope erosion becomes progressively less rapid with distance north from the MCT; up to two orders of magnitude difference in erosion exist between Garhwal, Kullu and Lahul, and Ladakh and Baltistan (Fig. 5). The Urgos catchment slightly deviates from this trend with erosion rates of 2.6±0.4 and 6.5±0.8 mm/a, which are equivalent to those records in Kullu and southern Lahul. The elevated rates may be because the Miyar basin records annual precipitation that exceeds much of Lahul (snowfall: 120−400 cm/a; Patel et al., 2018), and therefore allows for more rapid erosion, or that the low ^{10}Be concentrations are due to the input of fresh debris from the large, steep relief lateral moraines along the Urgos glacier (Fig. 3E, F).

The applicable timescales of this time-averaged dataset, although varied (~0.1−26 ka), mean that the erosion rates encompass recognized shifts in climate, sediment flux, glacier mass balance and seismicity, which themselves operate across various timescales (10^6−10^1 years; Barnard et al., 2001; Finkel et al., 2008; Owen and Dortch, 2014; Scherler et al., 2015; Orr et al., *in press*). Between ~0.02 and 7 m of lateral rockwall slope erosion is possible for a single millenium in the NW Himalaya. When these rates are extrapolated for the whole Quaternary, ~2 km of rockwall retreat is accomplished in the NW Himalaya, which are similar projections to the Sierra Nevada in the Western USA (Brocklehurst and Whipple, 2002).

The magnitude of erosion, particularly in the GHS-S, is therefore sufficient to affect the strength of hillslope-glacier coupling, catchment sediment flux and contribute to topographic change such as the production of relief, the migration of catchment divides, and the reconfiguration of drainage basins (Oskin and Burbank, 2005; Naylor and Gabet, 2007; Heimsath and McGlynn,

2008; MacGregor et al., 2009 *ibid*). The slope erosion rates share a significant association with mean rockwall slope: the greater the mean slope, the more rapid the erosion (Fig. 6A, Table 5). This points to important feedbacks between these variables, where the slope angle and erosion rate limit one another. A similar relationship is recognized between relative relief and slope erosion; where catchments with the high-altitude peaks (>5800 m asl), narrow ridgelines and steep relief (>1.2±0.2 km), record the highest rates of erosion. Part of this is because catchments with rockwall slope erosion rates >1 mm/a have mean rockwall slopes that exceed the 35° threshold, above which slopes are unable to retain regolith, snow or ice (Gruber and Haerberli, 2007; Nagai et al., 2013). This means that rockfall and avalanching is pervasive. More extensive glacier debris cover in these catchments compared to those with slower erosion demonstrate that coupling between slope and glacier is enhanced in catchments with steep accumulation areas, and that slope is important in moderating hillslope debris flux (Regmi and Watanabe, 2009; Scherler et al., 2011; Table 3). Other studies also recognize the importance of slope in landscape change, some of which argue that slope gradients can be used to infer rates of background denudation (Portenga and Bierman, 2001; Finlayson et al., 2002; Burbank et al., 2003; Ouimet et al., 2009; Scherler et al., 2011, 2014).

The magnitude of rockwall slope erosion observed in the NW Himalaya not only demonstrates the importance of lateral erosion through periglacial processes, specifically frost cracking, in high-altitude alpine settings, but also the significance that localized erosion has for understanding wider landscape change (Small and Anderson 1998; Hales and Roering, 2005, 2007; Moore et al., 2009). The rates of slope erosion reflect, in part, the pace of topographic change at the catchment headwaters.

Rates of rockwall slope erosion in Garhwal and Ladakh are either equivalent to, or exceed by up to one order of magnitude, the local catchment-wide erosion and exhumation rates (Fig. 7).

Quaternary exhumation rates have ranged between ~0.1 and 3 mm/a in the study areas (Thiede et al., 2004; Theide and Ehlers, 2013). Catchment-wide rates for Lahul and Kullu are unavailable because much of the region remains glaciated (Owen and Dortch, 2014). Orr et al. (*in review*) caution that comparing these erosion datasets can be problematic as they refer to landscape change through a variety of erosional processes and across various spatial and temporal scales. Nevertheless, the magnitude difference in these rates show that erosion at catchment headwaters in the NW Himalaya largely outpace the wider drainage basins (Oskin and Burbank, 2005; Naylor and Gabet, 2007; Orr et al., *in review*), and that erosion can vary significantly across short distances downstream (Scherler et al., 2014). This is unsurprising as time-averaged rates for small areas such as catchment headwaters and rockwall slopes are sensitive to short-term local change, including single mass wasting events, and are therefore expected to record more rapid rates of erosion than a catchment-wide perspective. The Karzok catchment in central Zanskar, Ladakh deviates from this trend as the rockwall slope erosion either equals or is slower than the catchment-wide erosion and exhumation rates (Fig. 6). The preservation and gradual reworking of landforms and sediment deposits that date to > 400 ka is likely affected by the low background denudation recorded in this region (Hedrick et al., 2011; Dietsch et al., *in revisions*). A possible explanation is that sediment residence times exert a stronger control on the catchment-wide erosion signal in these ancient landscapes, than the scale and various surface processes operating in the applicable area.

Controls of slope erosion

Considerable efforts have been made in recent years to define the parameters that control hillslope stability, and therefore regulate the frequency and magnitude of mass wasting events (Matsuoka, 2001; Ballantyne, 2002; Hales and Roering, 2005; Regmi and Watanabe, 2009; Fischer et al., 2006, 2012 *ibid*). The interactions between topography, climate, hydrological and

geologic setting and cryosphere dynamics are shown to control rockfall activity. Of the catchment parameters which can be defined in the NW Himalaya with some precision, mean rockwall slope as already discussed, mean catchment and snowline elevation, total annual precipitation, mean annual temperature, and mean AFT cooling ages show the strongest correlation with ^{10}Be sample concentrations and/or apparent age, and therefore rockwall slope erosion rates (Fig. 6, 8; Table 5).

The close association between ^{10}Be concentration and mean catchment and snowline elevation is in part due to the scaling of production rates in high altitude settings (Lal, 1991; Balco et al., 2008). However these relationships remain when these concentrations are converted to apparent ages (Fig. 6; Table 5). Accordingly, catchments with the most rapid erosion rates have a greater proportion of the whole catchment above the snowline, and large glacier accumulation areas. Aided by steep slopes that are set in part by erosion, snow and ice entrained with debris is either absent from the rockwall or removed through avalanching. This supports the view that the extent of snow cover, whether set by climatic conditions or surface uplift, is important in moderating mass wasting processes, and can affect the strength of coupling between the rockwall and the glacier system (Scherler et al., 2011, 2014).

Projected surface temperatures of the rockwalls coincide with those considered optimal for mechanical weathering processes (-8 to -3°C), e.g. freeze-thaw, frost cracking and frost wedging (Brozović et al., 1997; Matsuoka and Sakai, 1999; Matsuoka, 2001; Hewitt, 2002; Hales and Roering, 2005; MacGregor et al., 2009; Table 1). The medial moraine sediment characteristics are consistent with sediment from the supraglacial realm, which have detached from source slopes by periglacial weathering processes (Benn and Lehmkuhl, 2000; Schroder et al., 2000; Benn and Owen, 2002; Hambrey et al., 2008; Lukas et al., 2012; Orr et al., *in review*; Table 3; Supplementary Item 4). Rates of periglacial erosion are likely further enhanced by seasonal and/or diurnal thermal variability in exposed bedrock surfaces of our investigated catchments,

which is determined in part by the topographic steepness (Gruber and Haerberli, 2007; Nagai et al., 2013). However, for high elevation catchments (> 4000 m asl) and/or rockwalls, which lack an insulating layer of snow, bedrock surfaces can cool to temperatures below -8 °C, which inhibit further mass wasting (Ward and Anderson, 2011). This is tentatively reflected in the relationship between mean annual temperature and rockwall slope erosion; the catchments with cooler regional temperatures record higher medial moraine ^{10}Be concentrations and therefore slower erosion rates (Fig. 6). The rockwall debris flux of each catchment is therefore likely influenced by the feedbacks between elevation, temperature and slope.

A strong negative relationship between ^{10}Be concentration and total annual precipitation supports the view that the distribution and magnitude of Himalayan erosion and denudation is partly a function of orographically focused monsoon rainfall (Bookhagen et al., 2005a; Theide et al., 2004; Bookhagen and Burbank, 2006; Gabet et al., 2006; Wulf et al., 2010; Dey et al., 2016; Fig. 6C, 7). The argument that precipitation provides a first-order control on the frequency and magnitude of mass wasting events in alpine settings is not uncommon (Hovius et al., 2000; Iverson, 2000; Dortch et al., 2009). Work by Eppes and Keanini (2017) argue that the proficiency of mechanical weathering processes such as sub-critical cracking is climate-dependent, and specifically limited by moisture. Although rockwall slope erosion is certainly influenced by the availability of moisture and is sensitive to the microclimatic conditions of each catchment, its distribution throughout the NW Himalaya cannot be fully explained by precipitation. A five-fold decline is precipitation is observed between the first topographic high of the Lesser Himalaya (900±400 m asl) and the interior ranges of the orogen (Bookhagen et al., 2005a,b; Bookhagen and Burbank, 2006; Fig. 7). If precipitation were the primary control of rockwall slope erosion we would expect to find that our maximum erosion rates coincide with maximum rainfall, and that a notable decline in these rates would be observed with distance into the Greater Himalayan interior. However, our results show that this is not the case. Scherler et al (2014) make a similar

observation, where the highest catchment-wide rates in Garhwal are also located north of the precipitation maxima. To further emphasize this point, there is an order of magnitude difference in the rockwall slope erosion rates between the GHS-N and the Tethyan Himalayan, yet a small decline in annual precipitation of < 300 mm.

Since the late Miocene the steep orographic barrier of the Himalaya has restricted the northward advancement of moisture (Bookhagen et al., 2005a; Wulf et al., 2010), therefore preventing any subsequent major shift in the overall intensity or distribution of precipitation (Bookhagen et al., 2005a; Bookhagen and Burbank, 2010; Boos and Kuang, 2010; Thiede and Ehlers, 2013). The overall pattern in slope erosion throughout the NW Himalaya is therefore unlikely to be an artifact of a previous climatic regime, despite short-term fluctuations in monsoon strength during the Quaternary potentially affecting rockfall activity on the catchment scale (Thompson et al., 1997; Gupta et al., 2003; Fleitmann et al., 2003; Demske et al., 2009). One major concern in evaluating the role of climate in long-term landscape change is that the denudation records are averaged across million year timescales and are therefore unable to account for the importance or variations in the Indian summer monsoon (Bookhagen et al., 2005a; Thiede and Ehlers, 2013). This study is able to show that erosion records that reflect landscape change on timescales that would be sensitive to fluctuations in monsoon strength (10^{2-5} years), i.e. slope and catchment-wide erosion, are not unilaterally controlled by precipitation.

Berylium-10 sample concentrations and therefore rockwall slope erosion rates are most closely associated with regional AFT cooling ages (Fig. 6D, 7; Table 5). Much attention has been paid to understanding the patterns of cooling ages and exhumations rates in the Himalaya, and the feedbacks between tectonics and climate that are responsible for the distribution and intensity of Himalayan denudation across million year timescales (Schelling and Arita, 1991; Srivastava and Mitra, 1994; Thiede and Ehlers, 2013). Many studies have argued that this denudation is

primarily governed by climate; orographic precipitation causes rapid erosion and exhumation along the Himalayan front and Lesser Himalaya (Zeitler et al., 2001; Thiede et al., 2004; Grujic et al., 2006; Biswas et al., 2007; Sharma et al., 2017; Kumar et al., 2018). However, young AFT ages (<10 Ma) and rapid rates of exhumation throughout the Lesser Himalaya and GHS-S instead reflect a close interaction between tectonics, denudation and monsoon-enhanced erosion, rather than just the latter (eg. Wobus et al., 2003; Thiede et al., 2004; Vannay et al., 2004). Coupling between climate and tectonics becomes less evident further into the Greater Himalayan interior; while the GHS-N becomes progressively more arid, the AFT ages remain <17 Ma and exhumation rates < 5mm/a (Thiede and Ehlers, 2013; Schlup et al., 2003; Fig. 7). The pattern in AFT ages and inferred exhumation histories for the NW Himalaya, like our rockwall slope erosion dataset, cannot therefore be fully explained by precipitation. Instead there is the growing argument that the patterns in Himalayan denudation are instead a function of tectonically controlled rock uplift; the result of crustal wedge deformation from the Indo-Eurasian collision and the flat-ramp-flat geometry of the Main Himalayan Thrust (e.g. Burbank et al., 2003; Bollinger et al., 2006; Herman et al., 2010; Robert et al., 2011; Godard et al., 2014). The lateral and vertical transport of rock over the ramp since the late Miocene has resulted in rapid and continuous exhumation, and the generation of steep topographic relief (Cattin and Avouac, 2000; Godard et al., 2004; Lavé and Avouac, 2000, 2001). Young AFT cooling ages and rapid rates of exhumation are therefore focused throughout the Lesser Himalaya and GHS-S (Fig. 7). This is consistent with the pattern in rockwall slope erosion, therefore indicating that tectonically driven rock uplift throughout the NW Himalaya is likely to provide a major control on patterns of denudation since the late Paleogene and late Quaternary records of erosion (Scherler et al., 2014; Orr et al., *in review*). Precipitation would therefore come as a secondary control.

Principle Component Analysis indicate that ~68% of the variance observed in rockwall slope erosion rates in the NW Himalaya can be explained by the six parameters discussed above (mean

rockwall slope, mean catchment and snowline elevation, total annual precipitation, mean annual temperature and mean AFT age; Fig. 8). Other parameters that were either less statistically significant or could not be included in these analyses are also likely to contribute slope erosion (Table 5). Rockwall lithology, rock strength and mass quality, and jointing and structure affect the thresholds for mass wasting and have been shown to govern hillslope debris flux and rates of erosion (Hallet et al., 1991; Augustinus, 1995; Anderson, 1998; Hales and Roering, 2005; MacGregor et al., 2009; Fischer et al., 2010). Rockfall activity in the investigated catchments is therefore very likely affected by the erodability of the rockwall and the periglacial processes acting upon it (Heimsath and McGlynn, 2008; Eppes and Keanini, 2017). The significance of this parameter in patterns of slope erosion on the regional scale is however less clear. Previous work has argued that the difference in rock strength between the crystalline sequences of the Lesser and Greater Himalaya is negligible, and therefore has little influence upon the denudation histories of the orogen (Burbank et al., 2003; Scherler et al., 2011, 2014).

Studies throughout High Asia have shown that geomorphic change, specifically mass wasting events, are closely associated with neotectonism including stochastic earthquakes and/or persistent microseismicity (Hovius et al., 2000; Rajendran et al., 2000; Bali et al., 2003; Menunier et al., 2008; Dortch et al., 2009; Lupker et al., 2012). The frequency of rockfall events and therefore rates of slope erosion in our investigated catchments is therefore likely to be influenced in part by local tectonic activity.

A further candidate for rockwall slope erosion control is glaciation and glacial erosion; vertical incision and the debuttressing of slopes lead to enhanced slope instability and failure (Naylor and Gabet, 2007; Heimsath and McGlynn, 2008; MacGregor et al., 2009; Fischer et al., 2010). Large, erosive temperate glaciers occupy catchments with rapid rates of rockwall slope erosion, while slower rates are from catchments with less erosive, sub-polar glaciers (Owen and Dortch, 2014).

The local glacial records for each investigated catchment confirm shifts in glacier mass balance throughout the Holocene (Saha et al., 2018; Table 1). Past retreat and expansion of glacier ice may have contributed to the evolution of the rockwalls; the downwasting of ice may encourage the unloading of slope debris, while a greater glacier volume may see an increase in glacial erosion processes acting upon the slope (Fischer et al., 2006; 2010, 2012).

Rather than a single control, we have demonstrated that rockwall slope erosion is instead more likely the result of longstanding feedbacks between topography, surface processes, climate and tectonics. This supports the initial findings of Orr et al. (*in review*), where the evolution of the rockwalls in the present day is determined by the unique expression of these feedbacks within each catchment. However, our erosion dataset does not account for any variability in the drivers or rate of rockfall activity throughout the applicable timescales (0.1−26 ka). The relative importance of each of these various parameters in slope erosion will therefore likely vary across spatial and temporal scales. The correlation between rockwall erosion and slope, e.g., which is recognized for the whole dataset, is not apparent in either Lahul and Kullu or Garhwal, if they are considered discrete regions. Only in Ladakh and Baltistan do the steepest catchment and rockwall slopes record the most rapid rates of erosion. No catchment parameters have strong correlations with slope erosion for either Lahul and Kullu or Garhwal. This may be because slope erosion is sensitive to other undefined parameters such as glaciation, or that deciphering erosion controls is not possible due to the inherent complexities of glaciated catchments in the NW Himalaya. An alternative explanation is that once a threshold for a parameter is met, slope erosion is then predominantly limited by this one parameter. During a period of enhanced rainfall or monsoon storm along the Himalayan front for example (Bookhagen et al., 2005b; Clift et al., 2008), catchments with strongly contrasting physical settings may display similar rockfall activity. The rainfall magnitude is sufficient to override any resistance to mass wasting, such as a strong, non-erosive rock type or shallow, low relief slopes. When averaged over time, these catchments will

share a similar record of erosion. This may offer an explanation for why single high-magnitude events such as these, are viewed to be responsible for a significant proportion of the total landscape change in a mountain environment (Hasnain 1996; Craddock et al., 2007; Wulf et al., 2010).

We have suggested that slope erosion is largely influenced by catchment-specific conditions that vary over temporal and spatial scales. However, our study is able to demonstrate that the broad spatial patterns in this erosion follow long-term trends in denudation throughout the NW Himalaya, and are therefore is broadly controlled by tectonically driven rock uplift. Precipitation is considered a secondary control. This suggests that periglacial rockfall processes are part of the erosional response to structural change throughout the Himalayan-Tibetan orogen, and play a significant role within topographic change at catchment headwaters and the mass balance of the orogen. Identifying a more significant tectonic control to landscape change than climate is becoming more common; work in the wider Himalaya and the northern Bolivian Andes suggest that denudation patterns do not follow gradients in precipitation (Burbank et al., 2003; Gasparini and Whipple, 2014; Godard et al., 2014; Scherler et al., 2014).

CONCLUSION

Rates of rockwall slope erosion are defined for 12 catchments in northern India, NW Himalaya and range between 0.02 and 7.2±1.1 mm/a. Rockwall slope erosion largely outpaces local catchment-wide erosion and exhumation, and is sufficient to affect catchment sediment flux, glacier dynamics and topographic change, such as the production of relief, the migration of catchment divides and the reconfiguration of drainage basins.

Erosion rates become progressively less rapid with distance north from the MCT; up to two orders of magnitude difference in erosion rates are observed between the Garhwal, Kullu and Lahul, and Ladakh and Baltistan. Rather than a single control, rockwall slope erosion on a catchment-by-catchment basis is largely influenced by longstanding feedbacks between topography, geology, surface processes, climate and tectonics. The relative roles of these parameters are likely to vary over various spatial and temporal scales.

Our study demonstrates that like records of denudation in the NW Himalaya, the broad trend in rockwall slope erosion cannot be fully explained by the distribution of precipitation. Instead slope erosion can be considered part of the erosional response to tectonically driven uplift, the product of Indo-Eurasian convergence and the geometry of overthrusting. The distribution and magnitude of erosion on geomorphic (10^2–10^5 years) and geologic (10^6 years) timescales in the NW Himalaya therefore indicates that tectonics, rather than climate, provide a first-order control on landscape evolution. Our study also demonstrates the importance of lateral rockwall slope erosion via periglacial processes in helping set the pace of topographic change at catchment headwaters of high altitude and high relief mountain ranges, and the significance that localized erosion has for understanding wider landscape change.

ACKNOWLEDGMENTS

ENO thanks the University of Cincinnati for providing tuition and stipend to support this work as part of ENO's doctoral thesis and the processing of samples for ^{10}Be dating. ENO would like to thank PRIME Laboratories at Purdue University for a seed grant for AMS measurements. ENO also extends thanks to National Geographic, the Geological Society of America and the Graduate Student Governance Association, University of Cincinnati for research grants to conduct fieldwork.

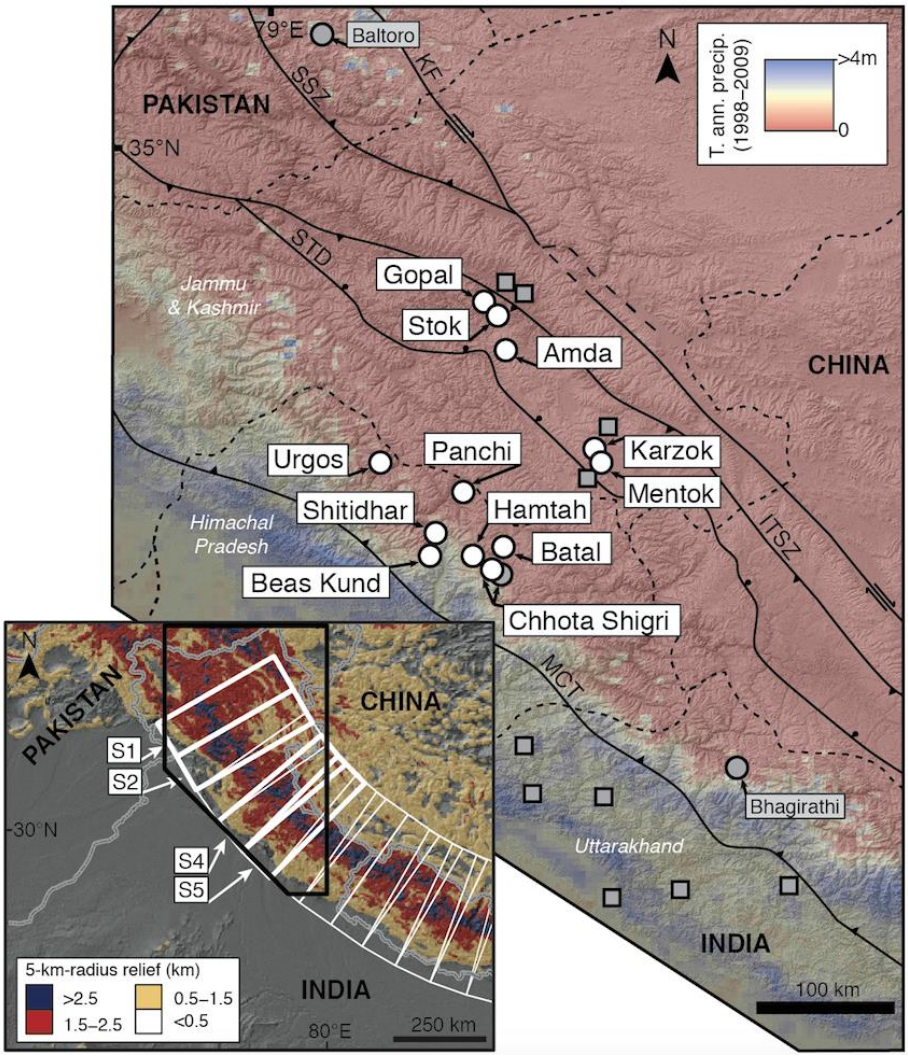

Fig. 1. Overview of the study area in the NW Himalaya. Hillshade map is overlain by total annual precipitation (TRMM 2B31; Bookhagen and Burbank, 2006). Major faults from Hodges (2000) and Schlup et al. (2003). White circles: investigated catchments of this study. Gray circles: location of published slope erosion rate studies (Seong et al., 2009; Scherler and Egholm 2017; Orr et al., *in review*). Squares with gray fill: catchment-wide erosion rate studies (Vance et al., 2003; Dortch et al., 2011; Schlerer et al., 2015; Dietsch et al., 2015, 2019). Inset map illustrates the location (black polygon) of the study areas (relief map with swath polygons [bold polygons S1, 2, 4, 5 are referred to in Fig. 7] modified from Bookhagen and Burbank 2006).

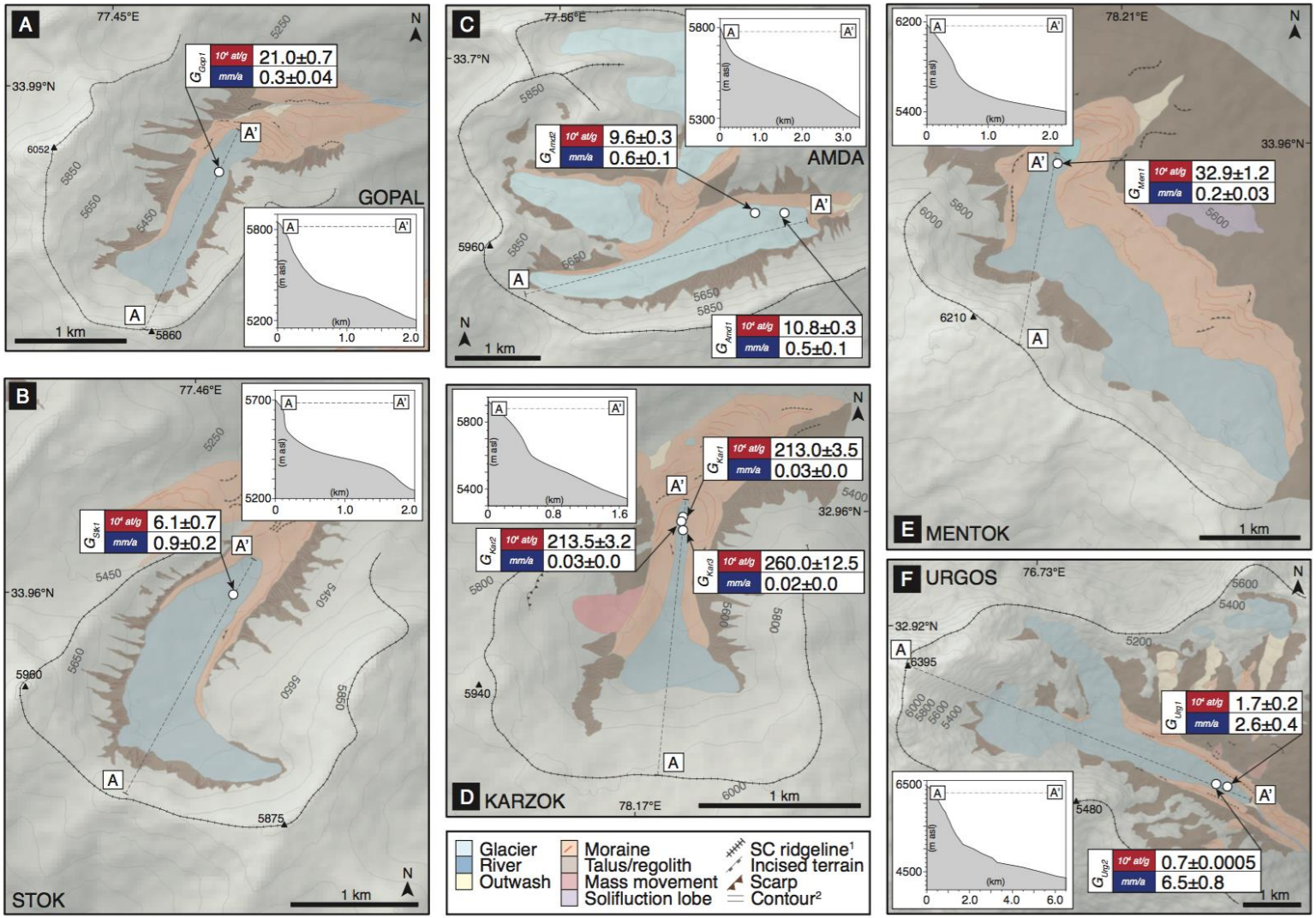

Fig. 2. Geomorphology of the study areas including sample ^{10}Be concentrations and rockwall slope erosion rates. 1: Catchment ridgeline (encompasses source rockwall slopes). 2: 100 m contour lines. Fan deposits in 3L are represented by dark yellow shading.

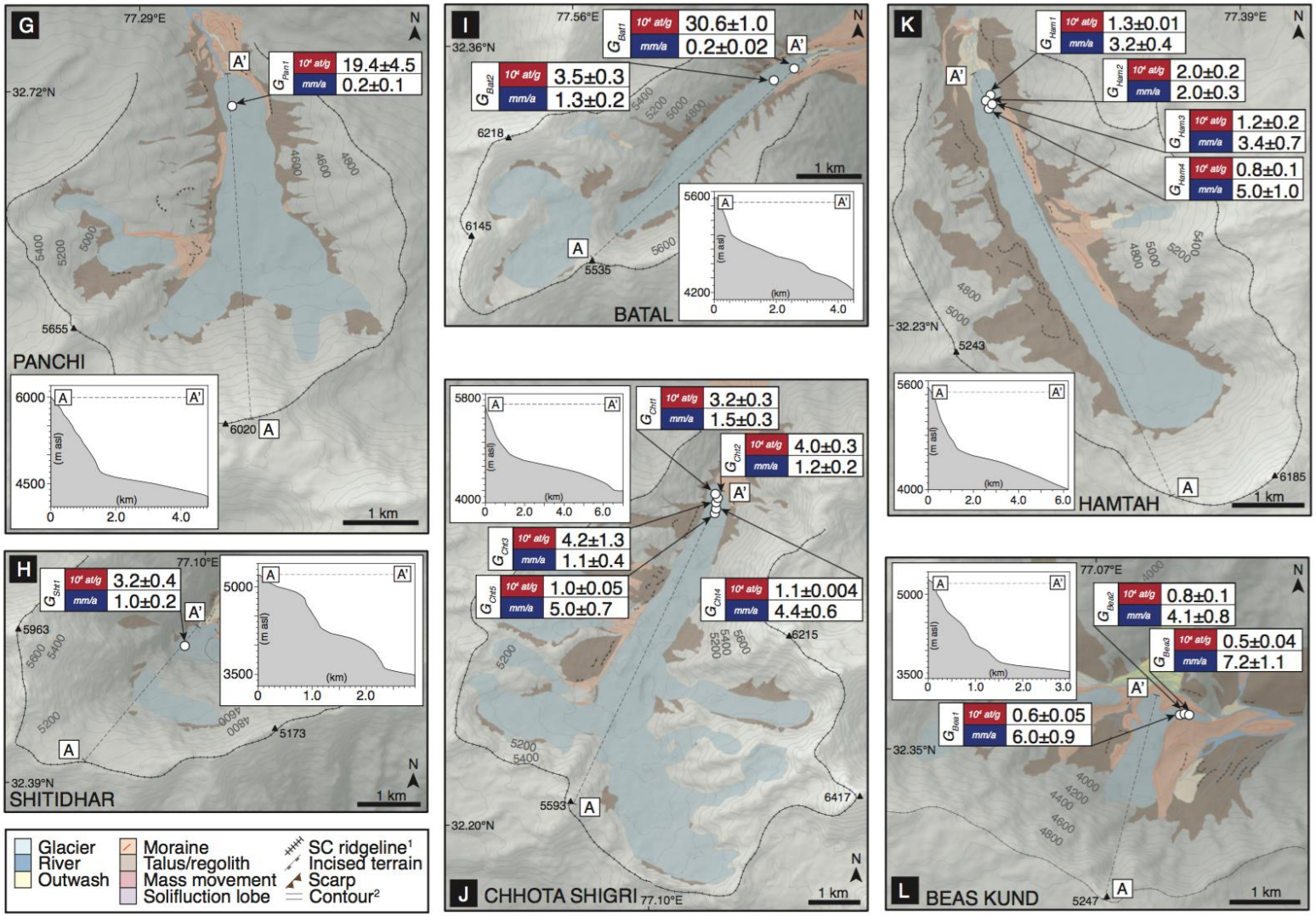
G
77.29°E
N
32.72°N
A'
G_{Pan1} 10⁴ at/g 19.4±4.5
mm/a 0.2±0.1
4600
4800
5400
5200
5000
5655
PANCHI
6000
4500
A
A'
(m asl)
(km)
0
2.0
4.0
6020
A
1 km
I
77.56°E
N
32.36°N
G_{Bat1} 10⁴ at/g 30.6±1.0
mm/a 0.2±0.02
A'
G_{Bat2} 10⁴ at/g 3.5±0.3
mm/a 1.3±0.2
5400
5200
5000
4800
6218
6145
5600
A
5535
BATAL
5600
4200
A
A'
(m asl)
(km)
0
2.0
4.0
1 km
K
77.39°E
N
G_{Ham1} 10⁴ at/g 1.3±0.01
mm/a 3.2±0.4
A'
G_{Ham2} 10⁴ at/g 2.0±0.2
mm/a 2.0±0.3
G_{Ham3} 10⁴ at/g 1.2±0.2
mm/a 3.4±0.7
G_{Ham4} 10⁴ at/g 0.8±0.1
mm/a 5.0±1.0
5400
5200
5000
4800
4800
5000
32.23°N
5243
5600
4000
A
A'
(m asl)
(km)
0
2.0
4.0
6.0
A
6185
HAMTAH
1 km
H
77.10°E
G_{Sht1} 10⁴ at/g 3.2±0.4
mm/a 1.0±0.2
A'
5963
5600
5400
5200
4800
A
5000
3500
A
A'
(m asl)
(km)
0
1.0
2.0
5173
32.39°N
N
SHITIDHAR
1 km
5800
4000
A
A'
(m asl)
(km)
0
2.0
4.0
6.0
G_{Chh1} 10⁴ at/g 3.2±0.3
mm/a 1.5±0.3
G_{Chh2} 10⁴ at/g 4.0±0.3
mm/a 1.2±0.2
A'
G_{Chh3} 10⁴ at/g 4.2±1.3
mm/a 1.1±0.4
G_{Chh5} 10⁴ at/g 1.0±0.05
mm/a 5.0±0.7
G_{Chh4} 10⁴ at/g 1.1±0.004
mm/a 4.4±0.6
6215
5600
5400
5200
5200
5400
5593
A
6417
32.20°N
N
J
CHHOTA SHIGRI
77.10°E
1 km
5000
3500
A
A'
(m asl)
(km)
0
1.0
2.0
3.0
G_{Bea2} 10⁴ at/g 0.8±0.1
mm/a 4.1±0.8
G_{Bea3} 10⁴ at/g 0.5±0.04
mm/a 7.2±1.1
A'
G_{Bea1} 10⁴ at/g 0.6±0.05
mm/a 6.0±0.9
77.07°E
N
32.35°N
4000
4200
4400
4600
4800
5247
A
L
BEAS KUND
1 km
Glacier
River
Outwash
Moraine
Talus/regolith
Mass movement
Solifluction lobe
SC ridgeline¹
Incised terrain
Scarp
Contour²

Fig. 2. cont

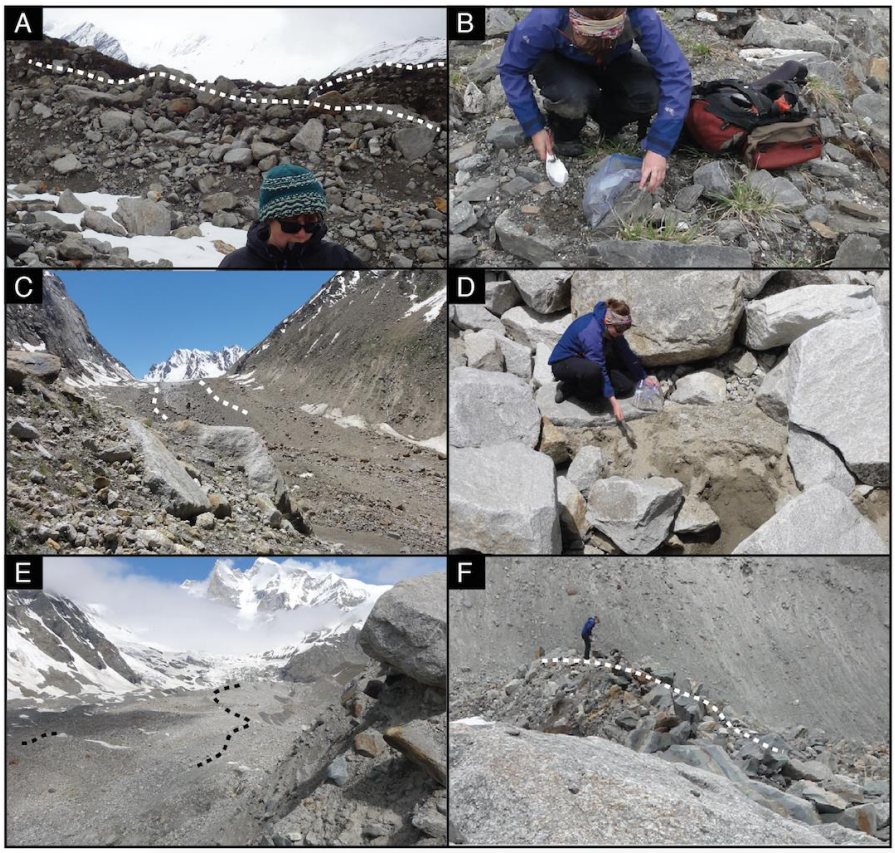

Fig. 3. Views of medial moraines and sampling locations for three investigated catchments (White and black dashed lines outline medial moraine ridges). A) Beas Kund medial moraine, B) Sampling of G_{Bea1} in Beas Kund, C) Chhota Shigri medial moraine, D) Sampling of G_{Cht5} of Chhota Shigri, E) Urgos medial moraine, F) Sampling of G_{Urg2}.

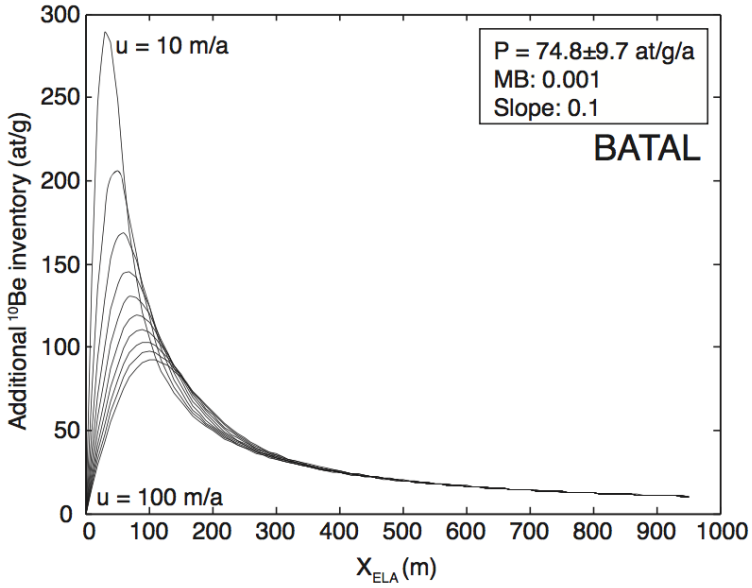

Fig. 4. Accumulation of ^{10}Be during burial, englacial transport and exhumation for the Batal catchment. Additional ^{10}Be inventory is 205 at/g. (u: mean glacier surface velocity [25±5 m/a]; ^{10}Be production rate: 74.8±9.7 at/g/a; mean X_{ELA}: 950 m; mass balance gradient: 0.001; slope: 0.1). See Supplementary Item 2 for analytical model details.

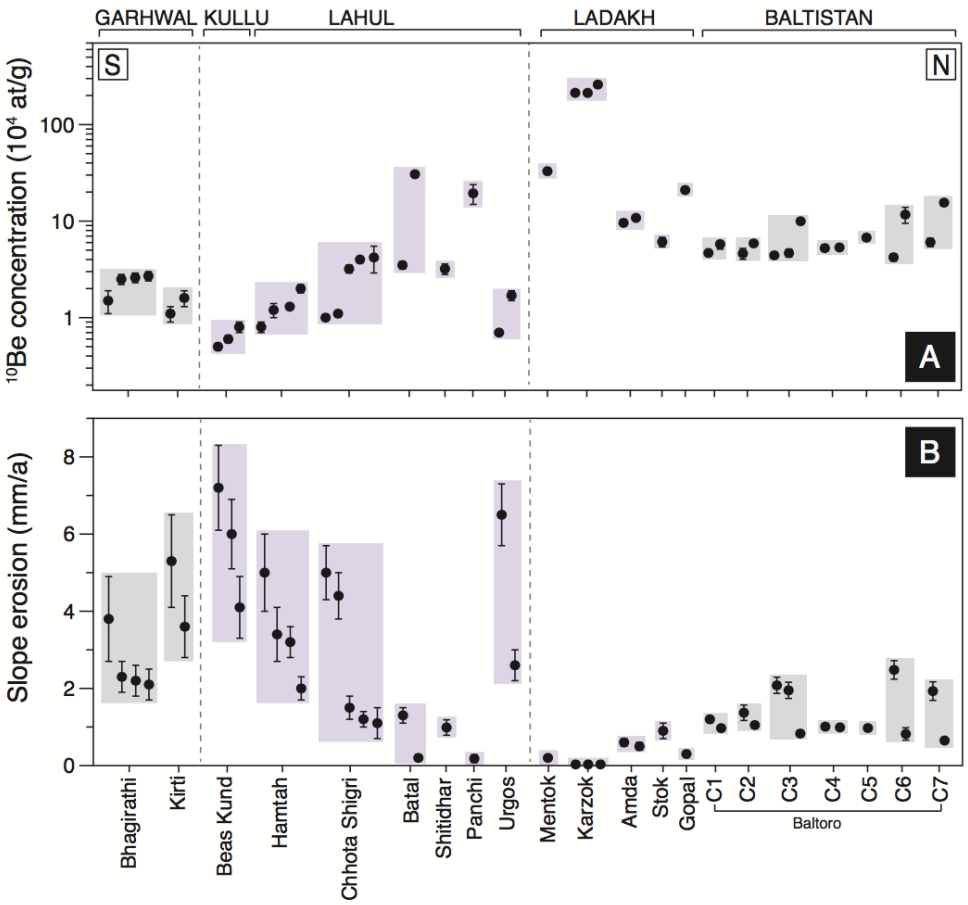

Fig. 5. Sample ^{10}Be concentrations (A) and rockwall slope erosion rates (B) for the NW Himalaya. Purple shading refers to the catchments of this study. The gray shading highlights the Garhwal and Baltoro catchments from Orr et al. (*in review*) and Seong et al. (2009), respectively.

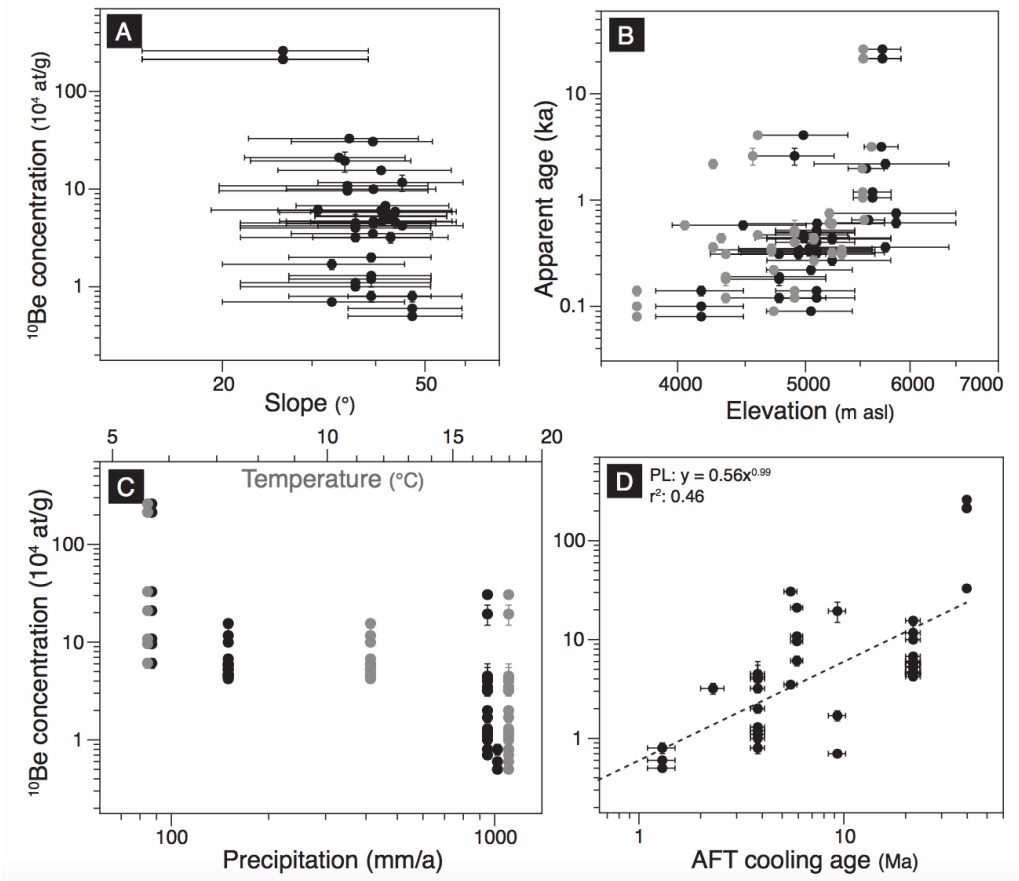

Fig. 6. Medial moraine ^{10}Be sample concentrations/apparent ages and catchment matrices. A) Mean rockwall slope. B) Apparent age of sample and mean elevation (black points) and snowline elevation (gray points). C) Total annual precipitation (black points) and mean annual temperature (gray points). D) Mean AFT cooling ages. The ^{10}Be concentrations and AFT ages are affected by the sampling elevations (PL: Power Law function). No significant adjustment to *p* or r^2 values is apparent when AFT ages are compared to applicable ages of the medial moraine sediment and are therefore not included in this study.

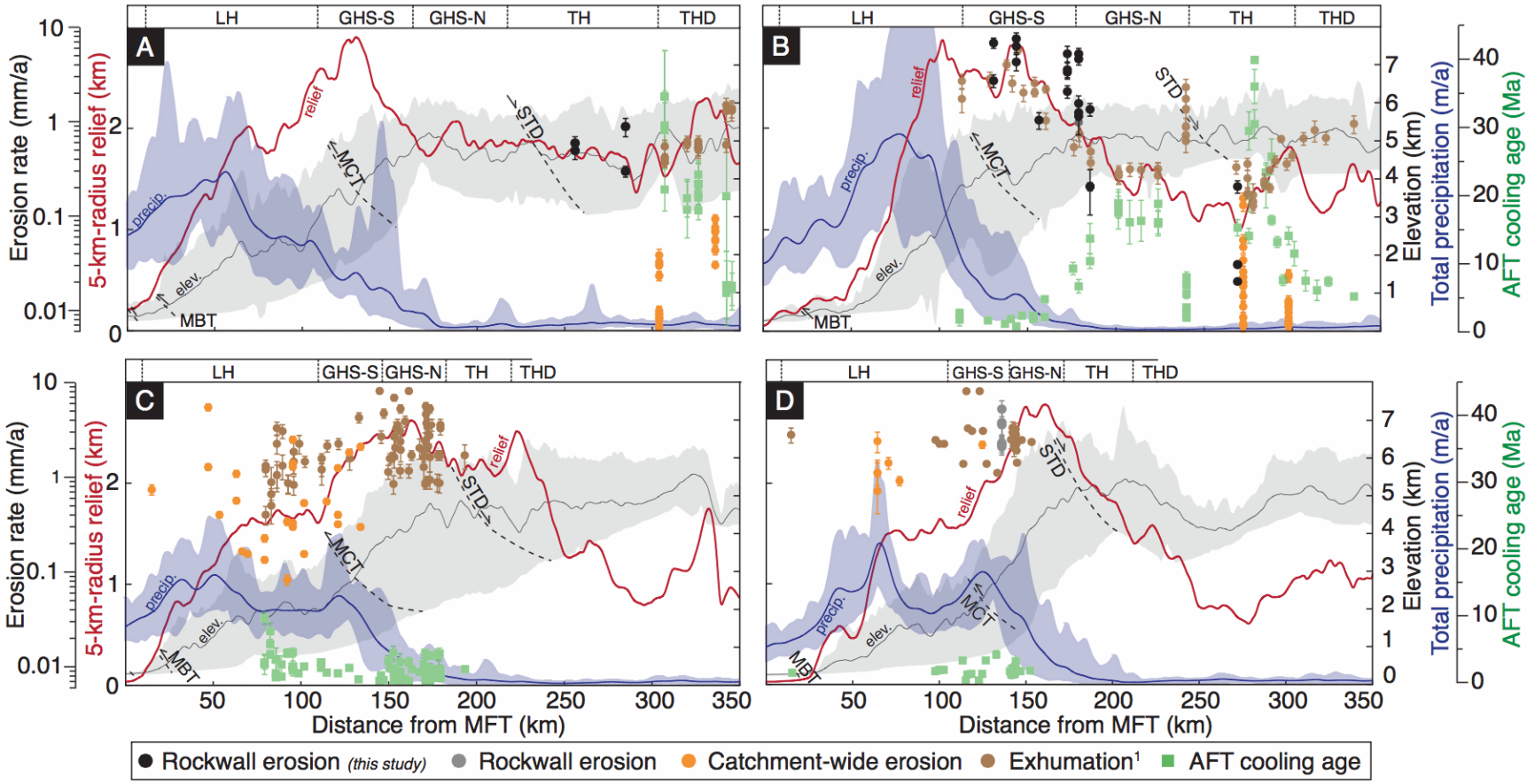

Fig. 7. Erosion, relief and precipitation of the NW Himalaya with distance from the MFT (datasets from Bookhagen and Burbank 2010). Swath locations outlined in Fig. 1. Exhumation[1]: Exhumation rates are inferred from AFT cooling ages as referenced below, an AFT cooling temperature of 120°C, and a geothermal gradient of 25°C/km. A) Swath 1. Slope erosion: this study; catchment-wide erosion: Dortch et al. (2011a), Dietsch et al. (2015); AFT cooling ages: Kristein et al. (2006, 2009). B) Swath 2. Slope erosion: this study, Scherler and Egholm (2017); catchment-wide erosion: Dietsch et al. (*in review*); AFT cooling ages: Schlup et al. (2003, 2011), Thiede et al. (2006), Walia et al. (2008). C) Swath 4. Catchment-wide erosion: Scherler et al. (2014); AFT cooling ages: Jain et

al. (2000), Thiede et al. (2004, 2005, 2009), Vannay et al. (2004). D) Swath 5. Slope erosion: Orr et al. (*in review*); catchment-wide erosion: Vance et al. (2003), Lupker et al. (2012); AFT cooling ages: Sorkhabi et al. (1996), Searle et al. (1999), Thiede et al. (2009).

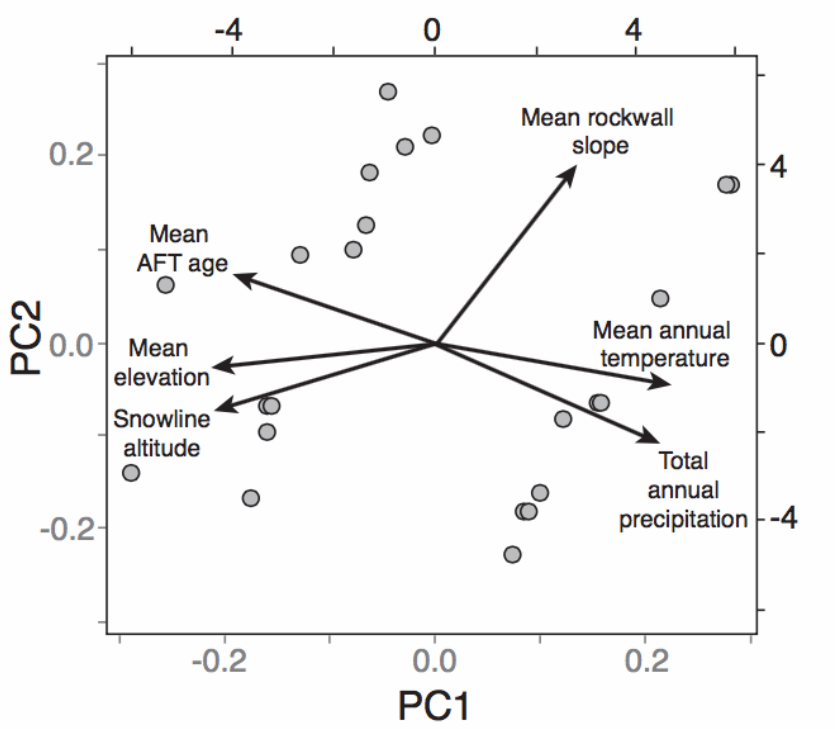

Fig. 8. PC1/PC2 plot for the matrices that characterize the investigation catchments and rockwall slope erosion rates. Matrices with strongest linear correlation with ^{10}Be sample concentrations are labeled. Proportion of variance: PC1 (0.68), PC2 (0.17), PC3 (0.07), PC4 (0.04).

Table 1. Details of the investigated catchments

	LOCATION[1]		CLIMATE				HOLOCENE GLACIAL RECORD	
Catchment	**Latitude** (°N)	**Longitude** (°E)	**Total annual precip.**[2, 3] (mm/a)	**Mean annual temp.**[4] (°C)	**Min. catch. temp.**[5] (~°C)	**Mean rockwall temp.**[5] (~°C)	**Local glacial stages**[6] (ka)	**Regional glacial stages**[7] (ka)
Ladakh								
Gopal	33.9865	77.4571	87 (<500)	5.6	-13.0	-10.6	M_{G1} (1.3±0.2 ka)	HH2 (~1.8−0.9 ka)
Stok	33.9678	77.4698	87 (<500)	5.6	-11.6	-9.7	M_{S1} (1.2±0.1 ka); M_{S2} (0.6±0.2 ka)	HH1 (<1 ka); HH2 (~1.8−0.9 ka)
Amda	33.6836	77.5925	87 (<500)	5.6	-12.3	-9.8	M_{A1} (0.3±0.1 ka); M_{A2C} (0.5±0.2 ka); M_{A3} (1.6±0.3 ka)	HH1 (<1 ka); HH2 (~1.8−0.9 ka)
Karzok	32.9681	78.1779	87 (<500)	5.6	-12.3	-10.2	M_{G1} (2.1±0.3 ka); M_{G2} (4.9±0.3 ka)	HH3 (~2.7−1.8 ka); HH5 (~6.9−4.3 ka)
Mentok	32.9354	78.2124	87 (<500)	5.6	-13.7	-11.6	M_{M1} (0.7±0.1 ka); M_{M2} (1.0±0.1 ka)	HH1 (<1 ka); HH2 (~1.8−0.9 ka)
Lahul-Spiti								
Urgos	32.8970	76.7679	950 (500−1000)	17.9	-14.2	-6.9	-	-
Panchi	32.7287	77.3009	950 (<500)	17.9	-12.1	-5.8	-	-
Shitidhar	32.4197	77.1074	950 (<500)	17.9	-10.7	-2.0	-	-
Batal	32.3640	77.6032	950 (<500)	17.9	-12.1	-5.8	-	-
Chhota Shigri	32.2663	77.5288	950 (<500)	17.9	-12.8	-5.5	-	-
Hamtah	32.2680	77.3572	950 (500−1000)	17.9	-12.8	-5.8	M_{H1} (0.2±0.1 ka); M_{H3} (10.4±0.3 ka)	HH1 (<1 ka); HH7 (~10.9−9.3 ka)
Kullu								
Beas Kund	32.3532	77.0890	1020 (500−1000)	17.9	-14.9	-5.8	-	-

1: Catchment coordinates taken from glacier snout.
2: Total annual precipitation. Rainfall data from local weather stations. Leh Meteorological Station (34.18°N, 77.58°E, 3500 m asl; CRUTEM4 1876−1990, Jones et al., 2012; Osborn and Jones, 2014): Gopal, Stok, Amda, Karzok and Mentok. Chhota Shigri weather station (32.28°N, 77.53°E, 3900 m asl; 1980−2005; Wagnon et al., 2007; Azam et al., 2014): Urgos, Panchi, Shitidhar, Batal, Chhota and Hamtah. Bhuntar Observatory(1969−2012; 31.8°N, 77.1°E, 1130 m asl; Azam et al., 2014): Beas Kund
3: (x) TRMM2B31 (1998−2009) annual rainfall data (Bookhagen and Burbank, 2010)
4:Temperature data from local weather stations. Leh Meteorological Station (34.18°N, 77.58°E, 3500 m asl; CRUTEM4 1876−1990, Jones et al., 2012; Osborn and Jones, 2014): Gopal, Stok, Amda, Karzok and Mentok. Chhota Shigri weather station (32.28°N, 77.53°E, 3900 m asl; 1980−2005; Wagnon et al., 2007; Azam et al., 2014): Urgos, Panchi, Shitidhar, Batal, Chhota Shigri, Hamtah and Beas Kund.
5: Temperatures estimated using local weather station data and an adiabatic lapse rate ($\Delta T/\Delta Z$) of 7°C/km Derbyshire et al., 1991; De Scally, 1997; Thayyen et al., 2005; Bashir and Rasul, 2010; Pratap et al., 2013; Kattel et al., 2013, 2015).

6: Local glacial stages from the northwestern end of the Himalayan-Tibetan orogen. Gopal: Saha et al. (2018); Stok: Orr et al. (2017), Saha et al. (2018); Amda: Orr et al. (2018), Saha et al. (2018); Karzok and Mentok: Hedrick et al. (2014), Saha et al., (2018); Hamtah: Saha et al. (2018).
7: Regional glacial stages from Saha et al. (2018). Holocene regional glacial stages for Ladakh include SWHTS 2A (12.2±0.8 ka), 1C (3.8±0.6 ka), 1B (1.7±0.2 ka) and 1A (0.4±0.1 ka) from Dortch et al. (2013). Regional stages for Lahul-Spiti and Kullu include MOHITS 2A (12.9±0.9 ka), 1K (11.4±0.7 ka), 1J (10.1±0.5 ka), 1I (9.1±0.3 ka), 1H (8.1±0.8 ka), 1G (7.7±0.6 ka), 1F (5.4±0.6 ka), 1E (3.5±0.4 ka), 1D (2.3±0.1 ka),1C (1.5±0.2 ka), 1B (0.7±0.1 ka) and 1A (0.4±0.1 ka) from Murari et al. (2014

Table 2. Catchment and glacier characteristics of the catchment (uncertainties are expressed to 1σ).

Catchment	CATCHMENT CHARACTERISTICS						GLACIER CHARACTERISTICS				
	Area (~km^2)	**Max. elevation** (m asl)	**Relative relief**[1] (km)	**Mean slope**[2] (°)	**HI Index**[3]	**Rockwall area** (~km^2)	**Mean rockwall slope** (°)	**Glacier area** (~km^2)	**Glacier aspect** (°)	**Mean slope**[2] (°)	**Modern ELA/SE**[4] (m asl)
Gopal	4.9	5920	1.0±0.1	27.3±12.6	0.4	4.2	33.9±11.8	0.7	22.5	13.4±6.9	5420±10
Stok	4.1	5930	0.7±0.1	26.6±12.4	0.5	3.1	30.8±11.8	1	45	14.4±6.7	5440±10
Amda	7	6000	0.8±0.2	26.9±15.7	0.5	5.3	35.2±15.5	1.7	90	12.4±6.6	5525±15
Karzok	3.9	5970	0.9±0.1	25.9±12.2	0.5	3.6	26.3±12.4	0.3	360	18.8±10.9	5550±10
Mentok	10.3	6200	0.9±0.2	21.1±13.6	0.4	7.6	35.5±13.0	2.7	22.5	13.8±7.8	5610±40
Urgos	30.3	6290	1.2±0.2	28.3±13.9	0.4	26.6	32.8±12.8	3.7	90	13.4±8.5	4830±25
Panchi	20.5	5945	1.3±0.3	29.5±14.0	0.4	16	34.8±12.1	4.5	360	14.7±8.7	4560±15
Shitidhar	22.2	5945	1.8±0.5	39.1±14.5	0.4	20.7	42.8±12.7	1.5	22.5	18.7±7.3	4050±10
Batal	13.9	5770	1.4±0.2	34.3±14.6	0.4	11.4	39.5±12.2	2.5	22.5	15.2±7.8	4700±15
Chhota Shigri	44.9	5600	1.3±0.3	29.4±15.8	0.5	31.6	36.5±14.8	13.3	360	16.2±9.2	4905±25
Hamtah	33.1	6155	1.2±0.3	32.2±14.9	0.4	28.3	39.2±12.2	4.8	360	10.6±6.0	4450±20
Beas Kund	17.6	5140	1.6±±0.3	35.3±16.3	0.4	16.6	47.2±11.9	1	360	13.1±8.7	3725±20

1: 3-km-radius relative relief
2: Slope calculated from 0.001km^2 catchment grid cells
3: Strahler (1952) Hypsometric Index (mean elevation- min elevation/relief)
4: Mean of equilibrium line altitudes (ELA)/snowline elevation (SE) calculated using Area-altitude (AA), Area-accummulation ratio (AAR: 0.4,0.5,0.6) and Toe-headwall ratio (THAR: 0.4,0.5) methods from Benn et al. (2005) and Osmaston (2005).

Table 3. Medial moraine morphology and sediment descriptions

	D.C[1]	Medial moraine description	Supraglacial diamict description
Gopal	R	-Subdued moraine ridge; heterogeneous debris thickness (<5 mm−2 m).	-Sandy-boulder gravels with silt matrix; angular-sub angular clasts of leucogranite and granitic gneiss.
Stok	R	-Subdued moraine ridge; heterogeneous debris thickness (<5 mm−2 m); some soil development.	-Bouldery gravels; angular-sub angular clasts of leucogranite, grantic gneiss and schist.
Amda	R	-Moraine deposits along northern flank of Amda Kangri; heterogeneous debris thickness (<30 cm); some soil development and xerophytic shrubs.	-Sandy gravels with silt matrix containing interstitial ice; angular-sub angular clasts of leucogranite and schist.
Karzok	R	-Subdued moraine ridge (<10 m wide); heterogeneous debris thickness (<5 mm−10 m)	-Bouldery gravels with sandy matrix; very angular- sub angular clasts of leucograntic, gneiss and schist.
Mentok	R	-Moraine deposits at Mentok Kangri snout; heterogeneous debris thickness (<5 mm−3 m).	-Bouldery gravels with sandy matrix; very angular- sub angular clasts of leucograntic, gneiss and schist.
Urgos	C	-Distinct, steep relief medial moraine ridges; depressions and ice collapse features; heterogeneous debris thickness (<5 mm−5 m); discontinuous soil development, tundra vegetation and large boulders (>2−0.25 m) along and slightly offset from ridges.	-Sandy-boulder gravels with silt matrix containing interstitial ice; angular-sub angular clasts of leucogranite and granitic gneiss.
Panchi	C	-Steep relief medial moraine ridge; surface depressions; large ice cliff at glacier snout; restricted soil development.	-Sandy gravels with a silty-sand matrix; angular-sub rounded clasts of schist.
Shitidhar	P	-Subdued moraine deposits; heterogeneous debris thickness (<5 mm−2 m).	-Gravelly boulders with sandy matrix; very angular- angular clasts of leucograntic, gneiss and schist.
Batal	C	-Steep relief medial moraine ridge; ice cliffs; heterogeneous debris thickness (<5 mm−2 m); restricted soil development.	-Sandy-boulder gravels with silt matrix, angular-sub angular schistose clasts.
Chhota Shigri	C	-Distinct moraine ridges along length of ablation zone; heterogeneous debris thickness (<1cm−1 m); large boulders (>5 m) located along moraine ridge; soil development and tundra vegetation.	-Bouldery gravels with sandy-silt matrix, angular-sub rounded clasts of granite, granitic gneiss and schist.
Hamtah	C	-Distinct moraine ridges along length of ablation zone; heterogeneous debris thickness (<5mm−>5 m); soil development and tundra vegetation.	-Bouldery gravels with sandy-silt matrix, angular-sub rounded clasts of granitic gneiss and schist.
Beas Kund	P	-Steep relief medial moraine ridge, heterogeneous debris thickness (<5mm− 2 m); soil development restricted to moraine ridges	-Sandy-boulder gravels; angular- sub angular clasts of granite and gneiss.

1: Debris cover: C- Complete debris coverage of the glacier ablation zone; P- Partial coverage (>30% of ablation zone surface); R- Restricted coverage (<30% of ablation zone surface)

Table. 4. Medial moraine sample details, ^{10}Be concentrations and interpreted slope erosion rates for the study areas.

		LOCATION			COSMOGENIC ^{10}BE DATA						SLOPE EROSION RATE			
	Catchment	Lat.	Long.	Elev.	Quartz mass	^{9}Be carrier mass, conc.	Native ^{9}Be	AMS ^{10}Be/^{9}Be ratio[1]	^{10}Be conc.	^{10}Be accumm. transport[2]	^{10}Be production rate	Erosion rate	Adjusted erosion rate[3]	Applicable time range[2]
		(°N)	(°E)	(m asl)	(g)	(g, mg/g)	(ug/g)	(10^{-15})	(10^{4} at/g)	(10^{4} at/g)	(at/g/a)	(mm/a)	(mm/a)	(ka)
G_{Gop1}	Gopal	33.9865	77.4570	5294	23.3326	0.3496, 1.0082	0	208.2±7.0	21.0±0.7	0.03	105.6±13.7	0.3±0.04	0.3±0.04	1.98
G_{Stk1}	Stok	33.9668	77.4684	5339	6.4552	0.3496, 1.0082	0	17.1±2.3	6.1±0.7	0.03	92.8±12.0	0.9±0.2	0.9±0.2	0.65
G_{Amd1}	Amda	33.6833	77.5910	5340	25.8515	0.3490, 1.0255	0	120.0±5.2	10.8±0.3	0.03	90.5±11.7	0.5±0.1	0.5±0.1	1.19
G_{Amd2}	Amda	33.6837	77.5909	5410	30.8093	0.3507, 1.0038	0	126.8±4.2	9.6±0.3	0.03	90.5±11.7	0.6±0.1	0.6±0.1	1.05
G_{Kar1}	Karzok	32.9668	78.1775	5362	22.6878	0.3492, 1.0255	0	2022.4±34.3	213.0±3.5	0.02	99.3±12.9	0.03±0.00	0.03±0.00	21.43
G_{Kar2}	Karzok	32.9665	78.1776	5367	13.2533	0.3506, 1.0038	0	1205.0±18.8	213.5±3.2	0.02	99.3±12.9	0.03±0.00	0.03±0.00	21.49
G_{Kar3}	Karzok	32.9663	78.1776	5371	27.3612	0.3507. 1.0038	0.03	3027.6±146.2	260.0±12.5	0.02	99.3±12.9	0.02±0.00	0.02±0.00	26.26
G_{Men1}	Mentok	32.9332	78.2107	5506	29.3919	0.3497, 1.0255	0	406.4±16.3	32.9±1.2	0.03	103.4±13.4	0.2±0.03	0.2±0.03	3.17
G_{Urg1}	Urgos	32.8990	76.7646	4420	17.6703	0.3505, 1.0038	0.03	16.3±2.4	1.7±0.2	0.02	74.2±9.6	2.6±0.4	2.6±0.4	0.22
G_{Urg2}	Urgos	32.8999	76.7635	4434	20.0819	0.3491, 1.0038	0.4	9.5±1.0	0.7±0.0005	0.02	74.2±9.6	6.3±0.8	6.5±0.8	0.09
G_{Pan1}	Panchi	32.7244	77.3020	4349	0.3987	0.3508, 1.0082	0	3.7±1.2	19.4±4.5	0.02	74.4±9.6	0.2±0.1	0.2±0.1	2.60
G_{Sht1}	Shitidhar	32.4159	77.1049	3568	4.6600	0.3494, 1.0082	0	6.8±1.2	3.2±0.4	0.01	55.5±7.2	1.0±0.2	1.0±0.2	0.58
G_{Bat1}	Batal	32.3628	77.6012	4310	11.3517	0.3505, 1.0082	0	147.4±5.3	30.6±1.0	0.02	74.8±9.7	0.2±0.02	0.2±0.02	4.08
G_{Bat2}	Batal	32.3609	77.5981	4368	6.3124	0.3495, 1.0082	0	9.8±1.3	3.5±0.3	0.02	74.8±9.7	1.3±0.2	1.3±0.2	0.47
G_{Cht1}	Chhota Shigri	32.2639	77.5283	4273	27.0872	0.3488, 1.0255	31.5	39.9±5.3	3.2±0.3	0.02	80.3±10.4	1.5±0.3	1.5±0.3	0.40
G_{Cht2}	Chhota Shigri	32.2635	77.5283	4281	26.4000	0.3496, 1.0038	0	46.1±4.5	4.0±0.3	0.02	80.3±10.4	1.2±0.2	1.2±0.2	0.49
G_{Cht3}	Chhota Shigri	32.2629	77.5285	4292	27.4440	0.3501, 1.0822	0	49.0±16.5	4.2±1.3	0.02	80.3±10.4	1.1±0.4	1.1±0.4	0.52
G_{Cht4}	Chhota Shigri	32.2621	77.5287	4316	18.7804	0.3487, 1.0255	160.7	12.0±1.5	1.1±0.004	0.02	80.3±10.4	4.3±0.6	4.4±0.6	0.14
G_{Cht5}	Chhota Shigri	32.2611	77.5282	4336	29.3671	0.3509, 1.0038	0	14.0±1.3	1.0±0.05	0.02	80.3±10.4	4.9±0.7	5.0±0.7	0.12
G_{Ham1}	Hamtah	32.2643	77.3583	4085	27.9648	0.3493, 1.0255	0.04	17.9±1.5	1.3±0.01	0.02	65.6±8.5	3.1±0.4	3.2±0.4	0.19
G_{Ham2}	Hamtah	32.2640	77.3579	4083	26.2989	0.3492, 1.0038	0	24.5±3.2	2.0±0.2	0.02	65.6±8.5	1.9±0.3	2.0±0.3	0.31
G_{Ham3}	Hamtah	32.2635	77.3585	4091	25.0875	0.3511, 1.0255	0.02	15.5±3.4	1.2±0.2	0.02	65.6±8.5	3.3±0.7	3.4±0.7	0.18
G_{Ham4}	Hamtah	32.2626	77.3582	4095	29.8146	0.3492, 1.0038	0	11.8±2.2	0.8±0.1	0.02	65.6±8.5	4.9±1.0	5.0±1.0	0.12
G_{Bea1}	Beas Kund	32.3543	77.0858	3604	26.9295	0.3496, 1.0038	0.02	6.8±0.9	0.6±0.05	0.02	53.7±6.9	5.8±0.9	6.0±0.9	0.10
G_{Bea2}	Beas Kund	32.3536	77.0863	3594	25.8173	0.3499, 1.0038	3.13	9.2±1.5	0.8±0.1	0.02	53.7±6.9	4.1±0.8	4.1±0.8	0.14
G_{Bea3}	Beas Kund	32.3534	77.0864	3579	24.7578	0.3510, 1.0038	0.04	5.3±0.8	0.5±0.04	0.02	53.7±6.9	6.9±1.0	7.2±1.1	0.08

1:^{10}Be/^{9}Be ratios are corrected for background ^{10}Be detected in full procedural blanks (G_{Amd1}, G_{Kar1}, G_{Men1}; $G_{Cht2,4}$, G_{Ham1}, G_{Kar1}, G_{Men1}: 3.14±1.43x10^{-15}; G_{Cht3}: 3.14±2.47x10^{-15}; G_{Amd2}, $G_{Kar}2$, $_{GCht2,5}$, $G_{Ham2,4}$: 1.55±0.64x10^{-15}; G_{Bea1-3}: 4.15±0.39x10^{-15}; G_{Kar3}, $G_{Urg1,2}$: 3.41±1.08x10^{-15}; G_{Gop1}, G_{Stk1}, G_{Pan1}, G_{Sht1}, $G_{Bat1,2}$: 4.15±3.9x10^{-16}.

2: Accumulation of ^{10}Be during burial, englacial transport and exhumation is calculated using methods detailed in Ward and Anderson (2011; see Supplementary Item 1)

3: Erosion rate which has been adjusted for ^{10}Be accumulation during transport from source bedrock slope to medial moraine.

Table. 5. Pearson's Correlation Coefficient values (p) between ^{10}Be concentrations and catchment parameters. (See Supplementary Item 3 for the extended dataset).

Catchment characteristics								**Glacier characteristics**				**Climatic conditions**					**G. Set.**
Max. grain size *(2)*	Catch. area *(>10)*	Rockwall area *(>10)*	Peak elevation *(>10)*	Mean elevation *(>10)*	Snowline elevation *(>10)*	Catch. relief *(>10)*	Catch. slope *(>10)*	Rockwall slope *(>10)*	Glacier area *(>10)*	Glacier aspect *(>10)*	Mean glacier slope *(>10)*	Glacier velocity *(5)*	Mean annual precip[1] *(4)*	Mean annual temp.[2] *(3)*	Min. catch. temp[3]. *(3)*	Mean rockwall temp[3]. *(>10)*	Mean AFT age[4] *(8)*
6558.0	47.5	213.8	1957.0	0.004 [47.4]	0.05 [13]	2077.0	91.7	0.6	263.2	3867.0	385.5	5619.0	0.1	0.001	8055.0	71.1	0.001

( ): Class size; [ ]: P-values between applicable sample age and matrices

1: Total annual precipitation (see Table 1).

2: Temperature data from local weather stations (Table 1).

3: Temperatures estimated using local weather station data and an adiabatic lapse rate ($\Delta T/\Delta Z$) of 7°C/km (Derbyshire et al., 1991; De Scally, 1997; Thayyen et al., 2005; Siddiqui and Maruthi, 2007; Bashir and Rasul, 2010; Pratap et al., 2013; Kattel et al., 2013, 2015).

4: Mean of AFT ages from Sorkhabi et al. (1996), Searle et al. (1999), Jain et al. (2000), Schlup et al. (2003, 2011), Thiede et al. (2004, 2005, 2006, 2008, 2009), Vannay et al. (2004), Kristein et al. (2006, 2009), Walia et al. (2008) and van der Beek et al. (2009).

REFERENCES

Adams, B., Dietsch, C., Owen, L.A., Caffee, M.W., Spotila, J., Haneberg, W.C., 2009. Exhumation and incision history of the Lahul Himalaya, northern India, based on (U–Th)/He thermochronometry and terrestrial cosmogenic nuclide methods. Geomorphology, 107(3-4), p.285-299.

Anderson, R.S., 1998. Near-surface thermal profiles in alpine bedrock: Implications for the frost weathering of rock. Arctic and Alpine Research, 30(4), pp.362-372.

Anderson, L.S., Roe, G.H., Anderson, R.S., 2014. The effects of interannual climate variability on the moraine record. Geology, 42(1), p.55-58.

Augustinus, P.C., 1995. Glacial valley cross-profile development: the influence of in situ rock stress and rock mass strength, with examples from the Southern Alps, New Zealand. Geomorphology, 14(2), p.87-97.

Azam, M.F., Wagnon, P., Vincent, C., Ramanathan, A.L., Favier, V., Mandal, A., Pottakkal, J.G., 2014. Processes governing the mass balance of Chhota Shigri Shigri Glacier (western Himalaya, India) assessed by point-scale surface energy balance measurements. The Cryosphere, 8(6), p.2195-2217.

Balco, G., Stone, J., Lifton, N., Dunai, T., 2008. A complete and easily accessible means of calculating surface exposure ages or erosion rates from ^{10}Be and ^{26}Al measurements. Quaternary Geochronology, 3, p.174-195.

Bali R, Awasthi D.D, Tiwari N.K. 2003. Neotectonic control on the geomorphic evolution of the Gangotri Glacier Valley, Garhwal Himalaya. Gondwana Research 6(4). p. 829-838.

Ballantyne, C.K., 2002. Paraglacial geomorphology. Quaternary Science Reviews, 21(18-19), p.1935-2017.

Barnard, P., Owen, L., Finkel, R., 2004. Style and timing of glacial and paraglacial sedimentation in a monsoon-influenced high Himalayan environment, the upper Bhagirathi Valley, Garhwal Himalaya. Sedimentary Geology, 165, p.199-221.

Barr, I.D.,Lovell, H., 2014. A review of topographic controls on moraine distribution. Geomorphology, 226, p.44-64.

Bashir, F.,Rasul, G., 2010. Estimation of water discharge from Gilgit Basin using remote sensing, GIS and runoff modeling. Pakistan Journal of Meteorology, 6(12).

Benn D.I, Lehmkuhl F. 2000. Mass balance and equilibrium-line altitudes of glaciers in high-mountain environments. Quaternary International 65. p.15-29.

Benn, D., Owen, L., 1998. The role of the Indian summer monsoon and the mid-latitude
westerlies in Himalayan glaciation: a review and speculative discussion. Journal of the Geological Society, 155, p.353–363.

Benn, D.I., Owen, L.A., 2002. Himalayan glacial sedimentary environments: a framework for reconstructing and dating former glacial extents in high mountain regions. Quaternary International, 97-98, p.3-26.

Benn D.I, Owen L.A, Osmaston H.A, Seltzer G.O, Porter S.C, Mark B. 2005. Reconstruction of equilibrium-line altitudes for tropical and sub-tropical glaciers. Quaternary International 138: 8-21.

Benn, D.I., Bolch, T., Hands, K., Gulley, J., Luckman, A., Nicholson, L.I., Quincey, D., Thompson, S., Toumi, R.,Wiseman, S., 2012. Response of debris-covered glaciers in the Mount Everest region to recent warming, and implications for outburst flood hazards. Earth-Science Reviews, 114(1-2), p.156-174.

Biswas S, Coutand I, Grujic D, Hager C, Stöckli D, Grasemann B. 2007. Exhumation and uplift of the Shillong plateau and its influence on the eastern Himalayas: New constraints from apatite and zircon (U-Th-[Sm])/He and apatite fission track analyses. Tectonics 26(6).

Bojar, A.V., Fritz, H., Nicolescu, S., Bregar, M., Gupta, R.P., 2005. Timing and mechanisms of Central Himalayan exhumation: discriminating between tectonic and erosion processes. Terra Nova, 17, 5, p.427-433.

Bollinger, L., Henry, P., Avouac, J.P., 2006. Mountain building in the Nepal Himalaya: Thermal and kinematic model. Earth and Planetary Science Letters, 244(1-2), pp.58-71.

Bookhagen, B., Burbank, D., 2006. Topography, relief and TRMM-derived rainfall variations along the Himalaya. Geophysical Research Letters, 33, 105.

Bookhagen, B., Burbank, D., 2010. Toward a complete Himalayan hydrological budget: Spatiotemporal distribution of snowmelt and rainfall and their impact on river discharge. Journal of Geophysical Research 115, F3, p.1-25.

Bookhagen, B., Thiede, R., Strecker, M., 2005a. Late Quaternary intensified monsoon phases control landscape evolution in the northwest Himalaya. Geology 33, 1, 149-152.

Bookhagen, B., Thiede, R.C., Strecker, M.R., 2005b. Abnormal monsoon years and their control on erosion and sediment flux in the high, arid northwest Himalaya. Earth and Planetary Science Letters, 231(1-2), p.131-146.

Boos, W.R., Kuang, Z., 2010. Dominant control of the South Asian monsoon by orographic insulation versus plateau heating. Nature, 463(7278), p.218.

Boulton G.S. 1978. Boulder shapes and grain-size distributions of debris as indicators of transport paths through a glacier and till genesis. Sedimentology 25(6). p.773-799.

Brocklehurst, S.H., Whipple, K.X., 2002. Glacial erosion and relief production in the Eastern Sierra Nevada, California. Geomorphology, 42(1-2), p.1-24.

Brocklehurst, S.H., Whipple, K.X., 2006. Assessing the relative efficiency of fluvial and glacial erosion through simulation of fluvial landscapes. Geomorphology, 75(3-4), p.283-299.

Brozovic, N., Burbank, D.W., Meigs, A.J., 1997. Climatic limits on landscape development in the northwestern Himalaya. Science 276, p.571-574.

Burbank, D., Blythe, A., Putkonen, J., Pratt-Sitaula, B., Gabet, E., Oskin, M., Barros, A., Ojha, T., 2003. Decoupling of erosion and precipitation in the Himalayas. Nature 426, p.652-655.

Cattin, R., Avouac, J.P., 2000. Modeling mountain building and the seismic cycle in the Himalaya of Nepal. Journal of Geophysical Research: Solid Earth, 105(B6), p.13389-13407.

Clift, P., Giosan, L., Blusztajn, J., Campbell, I., Allen, C., Pringle, M., Tebrez, A., Danish, M., Rabbani, M., Alizai, A., Carter, A., Luckge, A., 2008. Holocene erosion of the Lesser Himalaya triggered by intensified summer monsoon. Geology 36, p.79-82.

Craddock, W.H., Burbank, D.W., Bookhagen, B., Gabet, E.J., 2007. Bedrock channel geometry along an orographic rainfall gradient in the upper Marsyandi River valley in central Nepal. Journal of Geophysical Research: Earth Surface, 112(F3).

DeCelles, P.G., Robinson, D.M., Quade, J., Ojha, T.P., Garzione, C.N., Copeland, P., Upreti, B.N., 2001. Stratigraphy, structure, and tectonic evolution of the Himalayan fold-thrust belt in western Nepal. Tectonics, 20(4), p.487-509.

Deeken, A., Thiede, R.C., Sobel, E.R., Hourigan, J.K., Strecker, M.R., 2011. Exhumational variability within the Himalaya of northwest India. Earth and Planetary Science Letters, 305(1-2), p.103-114.

Demske, D., Tarasov, P.E., Wünnemann, B., Riedel, F., 2009. Late glacial and Holocene vegetation, Indian monsoon and westerly circulation in the Trans-Himalaya recorded in the lacustrine pollen sequence from Tso Kar, Ladakh, NW India. Palaeogeography, Palaeoclimatology, Palaeoecology, 279(3), p.172-185.

Derbyshire, E., Shi, Y., Li, J., Zheng, B., Li, S., Wang, J., 1991. Quaternary glaciation of Tibet: the geological evidence. Quaternary Science Reviews. 10, p.485-510.

de Scally, F.A., 1997. Deriving lapse rates of slope air temperature for meltwater runoff modeling in subtropical mountains: An example from the Punjab Himalaya, Pakistan. Mountain Research and Development, p.353-362.

Dey, S., Thiede, R.C., Schildgen, T.F., Wittmann, H., Bookhagen, B., Scherler, D., Jain, V., Strecker, M.R., 2016. Climate-driven sediment aggradation and incision since the late Pleistocene in the NW Himalaya, India. Earth and Planetary Science Letters, 449, p.321-331.

Dietsch, C., Dortch, J., Reynhout, S., Owen, L., Caffee, M., 2015. Very slow erosion and topographic evolution of the Southern Ladakh Range, India. Earth Surface Processes and Landforms, 40, 3, p.389-402.

Dietsch, C., Hedrick, K., Owen, L., Caffee, M., (2018, submitted). Slow erosion rates in an arid, high-altitude Himalayan extensional setting, Zanskar, northern India.

Dortch, J.M., Owen, L.A., Haneberg, W.C., Caffee, M.W., Dietsch, C., Kamp, U., 2009. Nature and timing of mega-landslides in northern India. Quaternary Science Reviews 28, p.1037-1056.

Dortch, J.M., Dietsch, C., Owen, L.A., Caffee, M.W. and Ruppert, K., 2011b. Episodic fluvial incision of rivers and rock uplift in the Himalaya and Transhimalaya. Journal of the Geological Society, 168(3), p.783-804.

Dortch, J., Owen, L., Schoenbohm, L., Caffee, M., 2011a. Asymmetrical erosion and morphological development of the central Ladakh Range, northern India. Geomorphology 135, p.167-180.

Dortch, J., Owen, L., Caffee, M., 2013. Timing and climatic drivers for glaciation across semi-arid western Himalayan-Tibetan orogen. Quaternary Science Reviews 78, p.188-208.

Edwards, M., Richardson, A.J., 2004. Impact of climate change on marine pelagic phenology and trophic mismatch. Nature, 430(7002), p.881.

Eppes, M.C., Keanini, R., 2017. Mechanical Weathering and Rock Erosion by Climate-Dependent Subcritical Cracking. Reviews of Geophysics. 55, p.470–508.

Finkel, R., Owen, L., Barnard, P., Caffee, M., 2003. Beryllium-10 dating of Mount Everest moraines indicates a strong monsoon influence and glacial synchroneity throughout the Himalaya. Geology 31, 6, p.561-564.

Finlayson D.P, Montgomery D.R, Hallet B. 2002. Spatial coincidence of rapid inferred erosion with young metamorphic massifs in the Himalayas. Geology 30(3), p.219-222.

Fischer, L., Kääb, A., Huggel, C., Noetzli, J., 2006. Geology, glacier retreat and permafrost degradation as controlling factors of slope instabilities in a high-mountain rock wall: the Monte Rosa east face. Natural Hazards and Earth System Sciences, 6(5), p.761-772.

Fischer, L., Amann, F., Moore, J.R., Huggel, C., 2010. Assessment of periglacial slope stability for the 1988 Tschierva rock avalanche (Piz Morteratsch, Switzerland). Engineering Geology, 116(1-2), p.32-43.

Fischer, L., Purves, R.S., Huggel, C., Noetzli, J., Haeberli, W., 2012. On the influence of topographic, geological and cryospheric factors on rock avalanches and rockfalls in high-mountain areas. Natural Hazards and Earth System Sciences, 12(1), p.241.

Fleitmann, D., Burns, S.J., Mudelsee, M., Neff, U., Kramers, J., Mangini, A., Matter, A., 2003. Holocene forcing of the Indian monsoon recorded in a stalagmite from southern Oman. Science 300, p.1737–1739

Foster, D., Brocklehurst, S.H., Gawthorpe, R.L., 2008. Small valley glaciers and the effectiveness of the glacial buzzsaw in the northern Basin and Range, USA. Geomorphology, 102(3-4), p.624-639.

Frank, W., Hoinkes, G., Miller, C., Purtscheller, F., Richter, W., Thöni, M., 1973. Relations between metamorphism and orogeny in a typical section of the Indian Himalayas. Tschermaks mineralogische und petrographische Mitteilungen, 20(4), p.303-332.

Gabet, E.J., Burbank, D.W., Putkonen, J.K., Pratt-Sitaula, B.A., Ojha, T., 2004. Rainfall thresholds for landsliding in the Himalayas of Nepal. Geomorphology, 63(3-4), p.131-143.

Gadgil, S., 2003. The Indian monsoon and its variability. Annual Review of Earth and Planetary Sciences, 31(1), pp.429-467.

Gale S.J, Hoare P.G. 1991. Quaternary Sediments: Petrographic Methods for the Study of Unlithified Rocks. Wiley, Chichester.

Gasparini, N.M., Whipple, K.X., 2014. Diagnosing climatic and tectonic controls on topography: Eastern flank of the northern Bolivian Andes. Lithosphere, 6(4), p.230-250.

Gibson M.J, Glasser N.F, Quincey D.J, Mayer C, Rowan A.V, Irvine-Fynn, T.D. 2017. Temporal variations in supraglacial debris distribution on Baltoro Glacier, Karakoram between 2001 and 2012. Geomorphology 295: 572-585.

Godard, V., Cattin, R., Lavé, J., 2004. Numerical modeling of mountain building: Interplay between erosion law and crustal rheology. Geophysical Research Letters, 31(23).

Godard, V., Bourlès, D.L., Spinabella, F., Burbank, D.W., Bookhagen, B., Fisher, G.B., Moulin, A., Léanni, L., 2014. Dominance of tectonics over climate in Himalayan denudation. Geology, 42(3), p.243-246.

Gupta, A.K., Anderson, D.M., Overpeck, J.T., 2003. Abrupt changes in the Asian southwest monsoon during the Holocene and their links to North Atlantic Ocean. Nature 421, p.354–357.

Gruber, S., Haeberli, W., 2007. Permafrost in steep bedrock slopes and its temperature-related destabilization following climate change. Journal of Geophysical Research: Earth Surface, 112(F2).

Grujic D, Coutand I, Bookhagen B, Bonnet S, Blythe A, Duncan C. 2006. Climatic forcing of erosion, landscape, and tectonics in the Bhutan Himalayas. Geology 34(10): 801-804.

Granger, D.E., Kirchner, J.W., Finkel, R., 1996. Spatially averaged long-term erosion rates measured from in situ-produced cosmogenic nuclides in alluvial sediment. The Journal of Geology, 104(3), p.249-257.

Hales, T.C., Roering, J.J., 2005. Climate-controlled variations in scree production, Southern Alps, New Zealand. Geology, 33(9), p.701-704.

Hales, T.C., Roering, J.J., 2007. Climatic controls on frost cracking and implications for the evolution of bedrock landscapes. Journal of Geophysical Research: Earth Surface, 112(F2).

Hallet, B, Walder, J.S., Stubbs, C.W, 1991. Weathering by segregation ice growth in microcracks at sustained subzero temperatures: Verification from an experimental study using acoustic emissions. Permafrost and Periglacial Processes 2(4): p.283-300.

Hambrey M.J, Quincey D.J, Glasser N.F, Reynolds J.M, Richardson S.J. Clemmens, S. 2008. Sedimentological, geomorphological and dynamic context of debris-mantled glaciers, Mount Everest (Sagarmatha) region, Nepal. Quaternary Science Reviews 27(25-26): p.2361-2389.

Hasnain, S.I., 1996. Factors controlling suspended sediment transport in Himalayan glacier meltwaters. Journal of Hydrology, 181(1-4), p.49-62.

Hedrick, K., Seong, Y., Owen, L., Caffee, M., Dietsch, C., 2011. Towards defining the transition in style and timing of Quaternary glaciation between the monsoon-influenced Greater Himalaya and the semi-arid Transhimalaya of Northern India. Quaternary International,236, p.21-33.

Heimsath, A.M., McGlynn, R., 2008. Quantifying periglacial erosion in the Nepal high Himalaya. Geomorphology, 97(1-2), p.5-23.

Herman, F., Copeland, P., Avouac, J.P., Bollinger, L., Mahéo, G., Le Fort, P., Rai, S., Foster, D., Pêcher, A., Stüwe, K., Henry, P., 2010. Exhumation, crustal deformation, and thermal structure of the Nepal Himalaya derived from the inversion of thermochronological and

thermobarometric data and modeling of the topography. Journal of Geophysical Research: Solid Earth, 115(B6).
Hewitt, K., 2002. Altitudinal organization of Karakoram geomorphic processes and depositional environments. In Himalaya to the sea (p. 118-133). Routledge.
Hodges, K.V., 2000. Tectonics of the Himalaya and southern Tibet from two perspectives. Geological Society of America Bulletin 112, 3, p.324-350.
Hodges, K.V., Wobus, C., Ruhl, K., Schildgen, T., Whipple, K., 2004. Quaternary deformation, river steepening, and heavy precipitation at the front of the Higher Himalayan ranges. Earth and Planetary Science Letters, 220, 3-4, p.379-389.
Hovius, N., Stark, C.P., Hao-Tsu, C., Jiun-Chuan, L., 2000. Supply and removal of sediment in a landslide-dominated mountain belt: Central Range, Taiwan. The Journal of Geology, 108(1), p.73-89.
Iverson, R.M., 2000. Landslide triggering by rain infiltration. Water resources research, 36(7), pp.1897-1910.
Jain, A.K., Kumar, D., Singh, S., Kumar, A., Lal, N., 2000. Timing, quantification and tectonic modelling of Pliocene–Quaternary movements in the NW Himalaya: evidence from fission track dating. Earth and Planetary Science Letters, 179(3-4), p.437-451.
Jones, P.D., Lister, D.H., Osborn, T.J., Harpham, C., Salmon, M., Morice, C.P., 2012. Hemispheric and large-scale land-surface air temperature variations: An extensive revision and an update to 2010. Journal of Geophysical Research: Atmospheres, 117(D5).
Kattel, D.B., Yao, T., Yang, K., Tian, L., Yang, G., Joswiak, D., 2013. Temperature lapse rate in complex mountain terrain on the southern slope of the central Himalayas. Theoretical and applied climatology, 113(3-4), p.671-682.
Kohl, C.P., Nishiizumi, K., 1992. Chemical isolation of quartz for measurement of in situ produced cosmogenic nuclides. Geochimica. Cosmochimica. Acta 56, p.3583–3587.
Kirstein, L.A., Sinclair, H., Stuart, F.M., Dobson, K., 2006. Rapid early Miocene exhumation of the Ladakh batholith, western Himalaya. Geology, 34(12), p.1049-1052.
Kirstein, L.A., Foeken, J.P.T., Van Der Beek, P., Stuart, F.M., Phillips, R.J., 2009. Cenozoic unroofing history of the Ladakh Batholith, western Himalaya, constrained by thermochronology and numerical modelling. Journal of the Geological Society, 166(4), p.667-678.
Kumar, A., Gupta, A.K., Bhambri, R., Verma, A., Tiwari, S.K., Asthana, A.K.L., 2018. Assessment and review of hydrometeorological aspects for cloudburst and flash flood events in the third pole region (Indian Himalaya). *Polar Science*.
Lavé, J., Avouac, J.P., 2000. Active folding of fluvial terraces across the Siwaliks Hills, Himalayas of central Nepal. Journal of Geophysical Research: Solid Earth, 105(B3), p.5735-5770.
Lavé, J., Avouac, J.P., 2001. Fluvial incision and tectonic uplift across the Himalayas of central Nepal. Journal of Geophysical Research: Solid Earth, 106(B11), p.26561-26591.
Lal, D., 1991. Cosmic ray labelling of erosion surfaces: in situ nuclide production rates and erosion models. Earth and Planetary Science Letters,104, p.429-439.
Lang, T.J., Barros, A.P., 2004. Winter storms in the central Himalayas. Journal of the Meteorological Society of Japan. Ser. II, 82(3), p.829-844.
Liu, X., Dong, B., 2013. Influence of the Tibetan Plateau uplift on the Asian monsoon-arid environment evolution. Chinese Science Bulletin, 58(34), p.4277-4291.
Lukas S, Graf A, Coray S, Schlüchter C. 2012. Genesis, stability and preservation potential of large lateral moraines of Alpine valley glaciers–towards a unifying theory based on Findelengletscher, Switzerland. Quaternary Science Reviews 38: p. 27-48.
Lupker M, Blard P.H, Lave J, France-Lanord C, Leanni L, Puchol N, Charreau J, Bourlès D. 2012. ^{10}Be-derived Himalayan denudation rates and sediment budgets in the Ganga basin. Earth and Planetary Science Letters 333: p.146-156.

MacGregor K.R, Anderson R.S, Waddington, E.D. 2009. Numerical modeling of glacial erosion and headwall processes in alpine valleys. Geomorphology 103(2): p.189-204.
Martin, L., Blard, P., Balco, G., Laurent, V., 2017. The CREp program and the ICE-D production rate calibration database: A fully parameterizable and updated online tool to compute cosmic-ray exposure ages. Quaternary Geochronology, 38, p.25-49.
Matsuoka N. 2001. Microgelivation versus macrogelivation: towards bridging the gap between laboratory and field frost weathering. Permafrost and Periglacial Processes 12(3): p.299-313.
Matsuoka N, Sakai H. 1999. Rockfall activity from an alpine cliff during thawing periods. Geomorphology 28(3-4): p.309-328.
Meunier, P., Hovius, N., Haines, J.A., 2008. Topographic site effects and the location of earthquake induced landslides. Earth and Planetary Science Letters, 275(3-4), p.221-232.
Miller, C., Klötzli, U., Frank, W., Thöni, M., Grasemann, B., 2000, Proterozoic crustal evolution in the NW Himalaya (India) as recorded by circa 1.80 Ga mafic and 1.84 Ga granitic magmatism: Precambrian Research, v. 103, p. 191–206.
Miller, C., Thöni, M., Frank, W., Grasemann, B., Klötzli, U., Guntli, P. and Draganits, E., 2001. The early Palaeozoic magmatic event in the Northwest Himalaya, India: source, tectonic setting and age of emplacement. Geological Magazine, 138(3), p.237-251.
Mölg, T., Maussion, F.,Scherler, D., 2014. Mid-latitude westerlies as a driver of glacier variability in monsoonal High Asia. Nature Climate Change, 4(1), p.68.
Moore, R.D., Fleming, S.W., Menounos, B., Wheate, R., Fountain, A., Stahl, K., Holm, K., Jakob, M., 2009. Glacier change in western North America: influences on hydrology, geomorphic hazards and water quality. Hydrological Processes, 23(1), p.42-61.
Murari, M.K., Owen, L.A., Dortch, J.M., Caffee, M.W., Dietsch, C., Fuchs, M., Haneberg, W.C., Sharma, M.C., Townsend-Small, A., 2014. Timing and climatic drivers for glaciation across monsoon-influenced regions of the Himalayan–Tibetan orogen. Quaternary Science Reviews, 88, p.159-182.
Muzikar, P., 2008. Cosmogenic nuclide concentrations in episodically eroding surfaces: Theoretical results. Geomorphology, 97(3-4), p.407-413.
Nagai, H., Fujita, K., Nuimura, T., Sakai, A., 2013. Southwest-facing slopes control the formation of debris-covered glaciers in the Bhutan Himalaya. The Cryosphere, 7(4), p.1303.
Naylor, S., Gabet, E.J., 2007. Valley asymmetry and glacial versus nonglacial erosion in the Bitterroot Range, Montana, USA. Geology, 35(4), p.375-378.
Nishiizumi K, Imamura M, Caffee M.W, Southon J.R, Finkel R.C, McAninch J. 2007. Absolute calibration of 10Be AMS standards. Nuclear Instruments and Methods in Physics Research Section B: Beam Interactions with Materials and Atoms 258(2): p.403-413.
Orr, E., Owen, L., Murari, M., Saha, S., Caffee, M., 2017. The timing and extent of Quaternary glaciation of Stok, northern Zanskar Range, Transhimalaya, of northern India. Geomorphology 284, p.142-155.
Orr, E.N., Owen, L.A., Saha, S., Caffee, M.W., Murari, M.K., 2018. Quaternary glaciation of the Lato Massif, Zanskar Range of the NW Himalaya. Quaternary Science Reviews, 183, p.140-156.
Osborn, T.J., Jones, P., 2014. The CRUTEM4 land-surface air temperature data set: construction, previous versions and dissemination via Google Earth. Earth System Science Data, 6(1), p.61-68.
Osmaston H. 2005. Estimates of glacier equilibrium line altitudes by the Area× Altitude, the Area× Altitude Balance Ratio and the Area× Altitude Balance Index methods and their validation. Quaternary International 138: 22-31.
Oskin M, Burbank, D.W. 2005. Alpine landscape evolution dominated by cirque retreat. Geology 33(12): p.933-936.

Ouimet W.B, Whipple K.X, Granger, D.E. 2009. Beyond threshold hillslopes: Channel adjustment to base-level fall in tectonically active mountain ranges. Geology 37(7): p.579-582.

Owen, L., Dortch, J., 2014. Nature and timing of Quaternary glaciation in the Himalayan-Tibetan orogen. Quaternary Science Reviews 88, p.14-54.

Owen, L.A., Sharma, M.C., 1998. Rates and magnitudes of paraglacial fan formation in the Garhwal Himalaya: implications for landscape evolution. Geomorphology, 26(1-3), p.171-184.

Owen L.A, Derbyshire E, Scott C.H. 2003. Contemporary sediment production and transfer in high-altitude glaciers. Sedimentary Geology 155(1-2): p.13-36.

Owen, L., Caffee, M., Bovard, K., Finkel, R., Sharma, M., 2006. Terrestrial cosmogenic nuclide surface exposure dating of the oldest glacial successions in the Himalayan orogen: Ladakh Range, northern India. GSA Bulletin, 118, 3-4, p.383-392.

Owen, L.A., Caffee, M.W., Finkel, R.C., Seong, B.S., 2008. Quaternary glaciation of the Himalayan–Tibetan orogen. Journal of Quaternary Science, 23, p.513–532.

Patel, L.K., Sharma, P., Fathima, T.N., Thamban, M., 2018. Geospatial observations of topographical control over the glacier retreat, Miyar basin, Western Himalaya, India. *Environmental earth sciences*, *77*(5), p.190.

Portenga E.W, Bierman, P.R. 2011. Understanding Earth's eroding surface with 10 Be. GsA today 21(8): p.4-10.

Portenga E.W, Bierman P.R, Duncan C, Corbett L.B, Kehrwald N.M, Rood, D.H. 2015. Erosion rates of the Bhutanese Himalaya determined using in situ-produced ^{10}Be. Geomorphology 233: p.112-126.

Pratap, B., Dobhal, D.P., Bhambri, R., Mehta, M., 2013. Near-surface temperature lapse rate in Dokriani Glacier catchment, Garhwal Himalaya, India. Himalayan Geology, 34, p.183-186.

Qiang, X.K., Li, Z.X., Powell, C.M., Zheng, H.B., 2001. Magnetostratigraphic record of the Late Miocene onset of the East Asian monsoon, and Pliocene uplift of northern Tibet. Earth and Planetary Science Letters,187, 1-2, p.83-93.

Rajendran, K., Rajendran, C.P., Jain, S.K., Murty, C.V.R.,Arlekar, J.N., 2000. The Chamoli earthquake, Garhwal Himalaya: field observations and implications for seismic hazard. CURRENT SCIENCE-BANGALORE-, 78(1), pp.45-51.

Regmi, D., Watanabe, T., 2009. Rockfall activity in the Kangchenjunga area, Nepal Himalaya. Permafrost and Periglacial Processes, 20(4), p.390-398.

Robert, X., Van Der Beek, P., Braun, J., Perry, C., Mugnier, J.L., 2011. Control of detachment geometry on lateral variations in exhumation rates in the Himalaya: Insights from low-temperature thermochronology and numerical modeling. Journal of Geophysical Research: Solid Earth, 116(B5).

Sadler P.M, Jerolmack, D.J. 2014. Scaling laws for aggradation, denudation and progradation rates: the case for time-scale invariance at sediment sources and sinks. Geological Society, London, Special Publications 404: p.404-7.

Saha, S., Owen, L.A., Orr, E.N., Caffee, M.W., 2018. Timing and nature of Holocene glacier advances at the northwestern end of the Himalayan-Tibetan orogen. Quaternary Science Reviews, 187, p.177-202.

Sagredo, E.A., Lowell, T.V., 2012. Climatology of Andean glaciers: A framework to understand glacier response to climate change. Global and Planetary Change, 86, p.101-109.

Schelling, D., Arita, K., 1991. Thrust tectonics, crustal shortening, and the structure of the far-eastern Nepal Himalaya. Tectonics, 10(5), p.851-862.

Scherler D, Bookhagen B, Strecker M.R. 2011. Hillslope-glacier coupling: The interplay of topography and glacial dynamics in High Asia. Journal of Geophysical Research: Earth Surface: 116(F2).

Scherler, D., Bookhagen, B., Strecker, M.R., 2014. Tectonic control on 10Be-derived erosion rates in the Garhwal Himalaya, India. Journal of Geophysical Research: Earth Surface, 119(2), p.83-105.

Scherler, D., Bookhagen, B., Wulf, H., Preusser, F., Strecker, M.R., 2015. Increased late Pleistocene erosion rates during fluvial aggradation in the Garhwal Himalaya, northern India. Earth and Planetary Science Letters, 428, p.255-266.

Scherler, D., Egholm, D,. 2017. Debris supply to mountain glaciers and how it effects their sensitivity to climate change–A case study from the Chhota Shigri Shigri Glacier, India (Invited)(206444). In 2017 Fall Meeting.

Schildgen, T.F., Phillips, W.M., Purves, R.S., 2005. Simulation of snow shielding corrections for cosmogenic nuclide surface exposure studies. Geomorphology, 64(1-2), p.67-85.

Schlup, M., Carter, A., Cosca, M., Steck, A., 2003. Exhumation history of eastern Ladakh revealed by 40Ar/39Ar and fission-track ages: the Indus River- Tso Morari transect, NW Himalayas. Journal of the Geological Society, 160, p.385-399.

Schlup, M., Steck, A., Carter, A., Cosca, M., Epard, J.L., Hunziker, J., 2011. Exhumation history of the NW Indian Himalaya revealed by fission track and 40Ar/39Ar ages. *Journal of Asian Earth Sciences*, *40*(1), p.334-350.

Schroder J.F, Bishop M.P, Copland L, Sloan V.F. 2000. Debris-covered glaciers and rock glaciers in the Nanga Parbat Himalaya, Pakistan. Geografiska Annaler: Series A, 82A, p. 17–31.

Seaby, R., Henderson, P., 2014."Community Analysis Package 5.0."

Searle, M., 1986. Structural evolution and sequence of thrusting in the High Himalayan, Tibetan-Tethys and Indus suture zones of Zanskar and Ladakh, Western Himalaya. Journa of Structural Geology, 8,8, p.923-936.

Searle, M.P., Fryer, B.J., 1986. Garnet, tourmaline and muscovite-bearing leucogranites, gneisses and migmatites of the Higher Himalayas from Zanskar, Kulu, Lahoul and Kashmir. Geological Society, London, Special Publications, 19(1), p.185-201.

Searle M.P, Noble S.R, Hurford A.J, Rex, D.C. 1999. Age of crustal melting, emplacement and exhumation history of the Shivling leucogranite, Garhwal Himalaya. Geological Magazine 136(5): p. 513-525.

Searle, M., Parrish, R., Hodges, K., Hurford, A., Ayres, M., Whitehouse, M., 1997. Shisha Pangma Leucogranite, South Tibetan Himalaya: Field Relations, Geochemistry, Age, Origin, and Emplacement. Journal of Geology, 150, p.295-317.

Seong Y.B, Owen L.A, Caffee M.W, Kamp U, Bishop M.P, Bush A, Copland L, Shroder, J.F. 2009. Rates of basin-wide rockwall retreat in the K2 region of the Central Karakoram defined by terrestrial cosmogenic nuclide ^{10}Be. Geomorphology 107(3-4): p. 254-262.

Sharma, P., Bourgeois, M., Elmore, D., Granger, D., Lipschutz, M.E., Ma, X., Miller, T., Mueller, K., Rickey, F., Simms, P., Vogt, S. 2000 PRIME lab AMS performance, upgrades and research applications. Nuclear Instruments and Methods in Physics Research, B 172, p.112-123.

Sharma, S., Shukla, A.D., Bartarya, S.K., Marh, B.S., Juyal, N., 2017. The Holocene floods and their affinity to climatic variability in the western Himalaya, India. *Geomorphology*, *290*, p.317-334.

Small R.J. 1983. Lateral moraines of Glacier de Tsidjiore Nouve: form, development, and implications. Journal of Glaciology 29(102): p. 250-259.

Small, E.E., Anderson, R.S., 1998. Pleistocene relief production in Laramide mountain ranges, western United States. Geology, 26(2), p.123-126.

Small, E.E., Anderson, R.S., Repka, J.L., Finkel, R., 1997. Erosion rates of alpine bedrock summit surfaces deduced from in situ ^{10}Be and ^{26}Al. Earth and Planetary Science Letters, 150(3-4), p.413-425.

Solomina, O.N., Bradley, R.S., Hodgson, D.A., Ivy-Ochs, S., Jomelli, V., Mackintosh, A.N., Nesje, A., Owen, L.A., Wanner, H., Wiles, G.C., Young, N.E., 2015. Holocene glacier fluctuations. Quaternary Science Reviews, 111, p.9-34.

Solomina, O.N., Bradley, R.S., Jomelli, V., Geirsdottir, A., Kaufman, D.S., Koch, J., McKay, N.P., Masiokas, M., Miller, G., Nesje, A., Nicolussi, K., 2016. Glacier fluctuations during the past 2000 years. Quaternary Science Reviews, 149, p.61-90.

Sorkhabi, R.B., Stump, E., Foland, K.A., Jain, A.K., 1996. Fission-track and 40Ar39Ar evidence for episodic denudation of the Gangotri granites in the Garhwal Higher Himalaya, India. Tectonophysics, 260(1-3), p.187-199.

Sorkhabi, R.B., Stump, E., Foland, K., Jain, A.K., 1999. Tectonic and cooling history of the Garhwal Higher Himalaya (Bhagirathi Valley): constraints from thermochronological data. Geodynamics of the NW Himalaya. Gondwana Research Group Memoir, 6, p.217-235.

Srivastava, P., Mitra, G., 1994. Thrust geometries and deep structure of the outer and lesser Himalaya, Kumaon and Garhwal (India): Implications for evolution of the Himalayan fold-and-thrust belt. Tectonics, 13(1), p.89-109.

Strahler, A.N., 1952. Hypsometric (area-altitude) analysis of erosional topography. Geological Society of America Bulletin, 63(11), p.1117-1142.

Steck, A., Epard, J., Vannay, J., Hunziker, J., Girard, M., Morard, A., Robyr, M., 1998. Geological transect across the Tso Morari and Spiti areas- the nappe structures of the Tethys Himalayas. Eclogae Geologicae Helvetiae 91, p.103-121.

Streule, M.J., Searle, M.P., Waters, D.J., Horstwood, M.S., 2010. Metamorphism, melting, and channel flow in the Greater Himalayan Sequence and Makalu leucogranite: Constraints from thermobarometry, metamorphic modeling, and U-Pb geochronology. Tectonics. 29, p.5.

Su, Z., Shi, Y., 2002. Response of monsoonal temperate glaciers to global warming since the Little Ice Age. Quaternary International, 97, p.123-131.

Thayyen, R.J., Gergan, J.T., Dobhal, D.P., 2005. Slope lapse rates of temperature in Din Gad (Dokriani glacier) catchment, Garhwal Himalaya, India. Bulletin of glaciological research, 22, p.31-37.

Thiede, R.C., Bookhagen, B., Arrowsmith, J.R., Sobel, E.R., Strecker, M.R., 2004. Climatic control on rapid exhumation along the Southern Himalayan Front. Earth and Planetary Science Letters, 222(3-4), p.791-806.

Thiede, R.C., Arrowsmith, J.R., Bookhagen, B., McWilliams, M.O., Sobel, E.R., Strecker, M.R., 2005. From tectonically to erosionally controlled development of the Himalayan orogen. Geology, 33(8), p.689-692.

Thiede, R.C., Arrowsmith, J.R., Bookhagen, B., McWilliams, M., Sobel, E.R., Strecker, M.R., 2006. Dome formation and extension in the Tethyan Himalaya, Leo Pargil, northwest India. Geological Society of America Bulletin, 118(5-6), p.635-650.

Thiede, R.C., Ehlers, T.A., Bookhagen, B., Strecker, M.R., 2009. Erosional variability along the northwest Himalaya. Journal of Geophysical Research: Earth Surface, 114(F1).

Thiede, R.C., Ehlers, T.A., 2013. Large spatial and temporal variations in Himalayan denudation. Earth and Planetary Science Letters, 371, p.278-293.

Thomas, E.K., Huang, Y., Clemens, S.C., Colman, S.M., Morrill, C., Wegener, P., Zhao, J., 2016. Changes in dominant moisture sources and the consequences for hydroclimate on the northeastern Tibetan Plateau during the past 32 kyr. Quaternary Science Reviews, 131, p.157-167.

Thompson, L.O., Yao, T., Davis, M.E., Henderson, K.A., Mosley-Thompson, E., Lin, P.N., Beer, J., Synal, H.A., Cole-Dai, J., Bolzan, J.F., 1997. Tropical climate instability: The last glacial cycle from a Qinghai-Tibetan ice core. Science, 276(5320), p.1821-1825.

Upreti, B., 1999. An overview of the stratigraphy and tectonics of the Nepal Himalaya. Journal of Asian Earth Science, 17, 5-6, p.577-606.

Vance, D, Bickle, M, Ivy-Ochs, S., Kubik, P.W, 2003. Erosion and exhumation in the Himalaya from cosmogenic isotope inventories of river sediments. Earth and Planetary Science Letters, 206(3-4), p.273-288.

Van Der Beek, P., Van Melle, J., Guillot, S., Pêcher, A., Reiners, P.W., Nicolescu, S., Latif, M., 2009. Eocene Tibetan plateau remnants preserved in the northwest Himalaya. Nature Geoscience, 2(5), p.364.

Vannay, C., Grasemann, B., Rahn, M., Frank, W., Carter, A., Baudraz, V., Cosca, M., 2004. Miocene to Holocene exhumation of metamorphic crustal wedges in the NW Himalaya: Evidence for tectonic extrusion coupled to fluvial erosion. Tectonics, 23, p.1-24.

Walia, M., Yang, T.F., Liu, T.K., Kumar, R., Chung, L., 2008. Fission track dates of Mandi granite and adjacent tectonic units in Kulu–Beas valley, NW Himalaya, India. Radiation Measurements, 43, p.S343-S347.

Walker, J.D., Martin, M.W., Bowring, S.A., Searle, M.P., Waters, D.J., Hodges, K.V., 1999. Metamorphism, melting, and extension: Age constraints from the High Himalayan slab of southeast Zanskar and northwest Lahaul. The Journal of Geology, 107(4), p.473-495.

Ward D.J, Anderson, R.S. 2011. The use of ablation-dominated medial moraines as samplers for ^{10}Be-derived erosion rates of glacier valley walls, Kichatna Mountains, AK. Earth Surface Processes and Landforms 36(4): p.495-512.

Watanabe, T., Dali, L., Shiraiwa, T., 1998. Slope denudation and the supply of debris to cones in Langtang Himal, Central Nepal Himalaya. Geomorphology, 26(1-3), p.185-197.

Weiers, S., 1995. On the climatology of the NW Karakorum and adjacent areas: Statistical analyzes including weather satellite images and a Geographical Information System (GIS). In commission with F. Dümmler.

Willenbring, J.K., Gasparini, N.M., Crosby, B.T., Brocard, G., 2013. What does a mean mean? The temporal evolution of detrital cosmogenic denudation rates in a transient landscape. Geology, 41(12), p.1215-1218.

Wobus, C.W., Hodges, K.V.,Whipple, K.X., 2003. Has focused denudation sustained active thrusting at the Himalayan topographic front?. Geology, 31(10), p.861-864.

Wulf, H., Bookhagen, B., Scherler, D., 2010. Seasonal precipitation gradients and their impact on fluvial sediment flux in the Northwest Himalaya. Geomorphology, 118, 1-2, p.13-21.

Yanites, B.J., Tucker, G.E., Anderson, R.S., 2009. Numerical and analytical models of cosmogenic radionuclide dynamics in landslide-dominated drainage basins. Journal of Geophysical Research: Earth Surface, 114(F1).

Yin, A., Harrison, T.M., 2000. Geologic evolution of the Himalayan-Tibetan orogen. Annual Review of Earth and Planetary Science, 28, 1, p.211-280.

Zeitler, P.K., Koons, P.O., Bishop, M.P., Chamberlain, C.P., Craw, D., Edwards, M.A., Hamidullah, S., Jan, M.Q., Khan, M.A., Khattak, M., Kidd, W.S., 2001. Crustal reworking at Nanga Parbat, Pakistan: Metamorphic consequences of thermal-mechanical coupling facilitated by erosion. Tectonics, 20(5), p.712-728.

10. Climate-driven late Quaternary fan surface abandonment in the NW Himalaya

Elizabeth N. Orr[a*], Lewis A. Owen[a], Sourav Saha[a], Marc W. Caffee[b,c]

[a] *Department of Geology, University of Cincinnati, Cincinnati, OH 45221, USA*
[b] *Department of Physics, Purdue University, West Lafayette, IN 47907, USA*
[c] *Department of Earth, Atmospheric and Planetary Sciences, Purdue University, West Lafayette, IN 47907, USA*

ABSTRACT

The timing of surface abandonment for ten alluvial/debris-flow fans across contrasting climatic settings in the NW Himalaya of northern India are defined using cosmogenic ^{10}Be surface exposure dating. Debris-flow fans in the Garhwal, Kullu and Lahul regions of the monsoon-influenced Greater Himalaya were largely abandoned during the Mid−Late Holocene. Large alluvial fans and smaller debris-flow fans in the semi-arid Ladakh region of the Greater and Tethyan Himalaya have surface ages which extend throughout the last glacial. Regional events of landform abandonment and incision are defined for the monsoon-influenced western Himalaya ranges (MWHR) and the semi-arid western Himalaya ranges (SWHR) over the past ~120 ka. In the MWHR and SWHR these regional events are limited to the Holocene and from ~40 ka, respectively. The timing of fan surface abandonment and regional landform abandonment events coincide with periods of weakening monsoon strength and cooling, and local and regional glacier advances. The nature and timing of fan stabilization and abandonment in the NW Himalaya is determined by the interaction between climate and internal catchment dynamics including

*Corresponding author. E. N. Orr: orreh@mail.uc.edu
L.A. Owen: owenls@ucmail.uc.edu, S. Saha: sahasv@mail.uc.edu, M. W. Caffee: mcaffee@purdue.edu

sediment supply and topography. Regional incision events from the MWHR and SWHR regions are recognized across various climatic conditions due to the ubiquitous nature of erosion in mountain settings. Climate-driven processes and glaciation are important drivers in fan sedimentation, catchment sediment flux and the topographic evolution of the NW Himalaya during the late Quaternary.

Keywords: sediment flux; glaciation; climate; topographic controls; cosmogenic isotopes

INTRODUCTION

Alluvial/debris-flow fans are widespread throughout mountain environments. These landforms radiate from locations at points of gradient lowering along mountain fronts and where catchments become unconfined, invariably at the mouth. In high-altitude, high-relief settings such as the Himalayan-Tibetan orogen, alluvial/debris-flow fans serve as temporary stores of poorly sorted deposits including debris-flow, glaciofluvial, fluvial, lacustrine and aeolian sediment (Ballantyne 2002a,b; Barnard et al., 2006b). Alluvial/debris-flow fans are not simply fluvial in nature; debris/mud flow, snow avalanching and other diffusive hillslope processes also contribute to their formation (Ballantyne 2002a, Nicholas and Quine 2007). We refer to these landforms as 'fans' in our study.

In the Himalayan-Tibetan orogen, most fans are understood to form and evolve as part of the landscape response to a shift in climate or environmental conditions (Owen and Sharma 1998; Kumar Singh et al., 2001; Barnard et al., 2004a,b, 2006a,b; Srivastava et al., 2008). Studies have shown that fans frequently form as the result of enhanced catchment sediment flux following deglaciation. The climate-driven downwasting and retreat of glacier ice causes the unloading of hillslope debris, and the reworking and redistribution of glacigenic sediment to the catchment

mouth. Fans in the Himalaya are found to aggrade in this way on timescales of 10^4–10^1 years after the onset of deglaciation (Owen and Sharma 1998; Watanabe et al., 1998; Ballantyne 2002a).

Shifts in catchment sediment flux and the aggradation of fans can also be the result of processes and events that enhance hillslope instability. The regeneration or readvance of a glacier can exacerbate instabilities by steepening and/or debuttressing hillslopes through glacial erosion (Watanabe et al., 1998; Ballantyne et al., 2002a; Barnard et al., 2006b; Hewitt, 2009). Further adjustments to slope stability can occur through periglacial weathering processes, permafrost degradation, changes in runoff regime and extreme storm and flood events (Gruber and Haeberli 2007; Hales and Roering 2007; Eppes and McFadden 2008; Heimsath and McGlynn 2008). In addition to climate, other variables that are also likely to contribute to the formation and evolution of fans include: sediment supply, source catchment lithology, seismic events and changes to base level (Ritter et al., 1995; Pope and Wilkinson 2005; Hobley et al., 2010; Scherler et al., 2014). Deciphering the relative role of any one of these variables in the development of these landforms is challenging in rapidly denuding mountain settings such as the Himalaya, particularly as each factor will likely vary over space and time.

There are few quantitative studies that define the timing of fan development and stabilization in the Himalaya. Our understanding of the evolution of these landforms and the wider catchment, and the influence of climate and/or tectonism within these sedimentary systems is therefore incomplete. Improvements in dating methods, particularly cosmogenic nuclide surface exposure dating, enable better constraints on the age of fan surfaces (Dühnforth et al., 2007; Blisniuk et al., 2012; Cesta and Ward 2017). Cosmogenic nuclide surface exposure ages define the timing of fan surface abandonment, and a period of landform stability following its formation across timescales of 10^4–10^1 years (Pope and Wilkinson 2005; Owen et al., 2014).

Well-preserved fans in the NW Himalaya provide an excellent opportunity to assess the controls of fan formation in a high-relief mountain setting, as well as evaluate how these controls may vary between areas of contrasting climatic regime. We report 18 new and 29 recalculated ^{10}Be fan surface ages for a suite of ten fans across the Greater Himalaya ranges of northern India. This study focuses on three new study areas: the Kullu and Chandra valleys in the monsoon-influenced Kullu and Lahul regions in Himachal Pradesh, and the Karzok valley is located in semi-arid Ladakh in Jammu and Kashmir (Fig. 1). We also revisit the study areas of Tangtse valley in Ladakh, and the Bhagirathi and Gori Ganga valleys in the warm-wet Garhwal region of Uttarkhand. We compare the fan surface ages in our study with local and regional climate and glacial records to evaluate the contributions of climate and climate-driven surface processes in the timing of fan aggradation and stabilization in the NW Himalaya, throughout the late Quaternary.

Regional landform abandonment and incision events are defined for the monsoon-influenced Lesser and Greater Himalaya, and the semi-arid interior ranges of the Greater and Tethyan Himalaya using geomorphic records throughout the NW Himalaya (Fig. 1). This record is compared to the fan surface ages of our study to explore possible patterns or times of regional landscape change in response to climate. We also discuss the effect of preservation bias within geomorphic evidence in the understanding of landscape change throughout the NW Himalaya.

REGIONAL SETTING

The regional geologic setting of the study area is the consequence of the continued collision and partial subduction between the Indian and Eurasian continental lithospheric plates, commencing at ~55 Ma (Searle et al., 1997). In the NW Himalaya, the Indus-Tsangpo Suture Zone marks the collision zone between these continental plates and the northern boundary of the Tethyan Himalaya. Deformation driven crustal shortening from the early Miocene to the Pleistocene

initiated the development of a series of foreland propagating thrust systems that divide the Himalayan lithotectonic units south of the Tethyan Himalaya, into the High Himalaya crystalline sequence, the Lesser Himalaya sequence, sub-Himalaya and foreland basin (Searle, 1986; Steck et al., 1998; Schlup et al., 2003; Vannay et al., 2004; Thakur et al., 2014).

The climate in the NW Himalaya is primarily governed by the mid-latitude westerlies that bring most of the precipitation during the winter from the Mediterranean, Black and Caspian seas (Mölg et al., 2013), and the south Asian summer monsoon (SASM) that advects moisture from the Indian Ocean bringing enhanced summer precipitation to the high altitude southern frontal ranges of the orogen (Benn and Owen 1998, 2002; Bookhagen and Burbank 2006, 2010; Owen 2009). The imposing orographic barrier of the Himalaya creates a steep precipitation gradient, perpendicular (S−N) to the strike of the mountain belt (Qiang et al., 2001; Liu and Dong, 2013). The northward decline in annual precipitation today falls from ~1500−3000 mm in the Lesser and Greater Himalaya ranges to <150 mm in the interior of the Tibetan Plateau (TRMM 1998−2005, Bookhagen and Burbank, 2006). Strong variability in climate throughout the late Quaternary is considered to have a significant influence upon the rate and magnitude of landscape change (Prell and Kutzbach, 1987; Gasse et al., 1996; Shi et al., 2001; Bookhagen et al., 2005; Bookhagen and Burbank, 2006; Wulf et al., 2010) and nature and timing of glaciation (Owen and Dortch, 2014) in the Himalayan-Tibetan orogen.

There is growing contention around whether the morphostructural and landscape evolution of the mountain belt is the result of climate-topography interactions and/or underlying tectonism. Most studies argue that the spatial distribution of erosion is a function of orographically focused monsoon rainfall (Bookhagen et al., 2005; Bookhagen and Burbank 2006; Gabet et al., 2006; Wulf et al., 2010). This relationship is not straightforward however because the distribution and magnitude of precipitation on the regional scale varies both spatially and temporally, and local

microclimates are retained throughout individual mountain ranges. Moreover, sporadic heavy rainfall has been argued to govern the sediment flux of Himalayan catchments (Hasnain 1996; Craddock et al., 2007; Wulf et al., 2010). The opposing view is that patterns in erosion are instead determined by structurally controlled rock uplift (Lavé and Avouac 2001; Burbank et al., 2003; Thiede et al., 2004; Scherler et al., 2014).

Most Greater Himalaya glaciers today are large, temperate and melt-dominated, and are fed by monsoonal precipitation (Benn and Owen, 2002; Su and Shi, 2002). Glaciers in the semi-arid Greater Himalaya are usually small (1–10 km^2) cold-based sub-polar types: precipitation-sensitive and sublimation-dominated (Benn and Owen, 2002). Evidence of three to four glacial stages per catchment is typically preserved throughout the western Himalaya (Owen and Dortch, 2014). The glacial records of the NW Himalaya are synthesized by the following regional chronostratigraphies: the semi-arid western Himalayan-Tibetan orogen stages (SWHTs) of Dortch et al. (2013), monsoonal Himalayan-Tibetan stages (MOHITs) of Murari et al. (2014), and Himalayan Holocene stages (HHs) of Saha et al. (2018). Dortch et al. (2013) and Owen and Dortch (2014) argue that the nature, timing and forcing of glaciation varies over short distances (10^1-10^2 km) within individual mountain ranges. Broadly, glacier advances in the NW Himalaya are moderated by monsoon strength (Owen and Sharma 1998; Watanabe et al., 1998). Our study areas were selected because the local glacial successions have been dated using cosmogenic nuclides (Table. 1).

The Kullu valley study area is located on the southern slopes of the Pir Panjal Range of the Greater Himalaya in the Kullu district of Himachal Pradesh (Fig. 1; Table 1). This large transverse drainage system extends ~60 km from the source of the Solang Nala and Beas rivers (~3400 m asl) to the village of Larji (~1000 m asl). The study area is limited to the upper reaches

of the Kullu valley (>1700 m asl) where bajada-style fan complexes sourced from the eastern and western tributaries occupy the valley (Owen et al., 1995).

The Chandra valley is a large longitudinal drainage system in the Lahul-Spiti district of Himachal Pradesh, in the rainshadow of the Pir Panjal Range (Fig. 1; Table 1). The study area extends along the northwest flowing Chandra River from Koksar (32.4141°N, 77.2351°E) to Sissu (32.4805°N, 77.1220°E), and is characterized by highly dissected fans along the valley floor.

The Karzok valley is located in the high altitude semi-arid desert of the Zanskar Range, Ladakh in Jammu and Kashmir (Fig. 1; Table 1). The study area is composed of a series of northeast trending tributary catchments draining the Rupshu Massif. A broad bajada extends along the flank of the massif.

METHODOLOGY

Our investigated valleys have small glaciated and non-glaciated tributary catchments that contain a wealth of well-preserved Quaternary deposits and landforms. Fans composed of diamicts and gravels are particularly abundant in these study areas (Derbyshire and Owen, 1990; Owen et al., 1995; Barnard et al., 2004a,b; Barnard et al., 2006b).

Field Methods

Detailed geomorphic maps of each study area were made in the field aided by Landsat Enhanced Thematic Mapper Plus (ETM+) imagery (30 m resolution), topographic maps generated from Advanced Spaceborne Thermal Emission and Reflection Radiometer (ASTER) global digital elevation models (V002, 30 m resolution), and Google Earth imagery. Landforms and sediments

were described and differentiated using geomorphic and sedimentological methods and criteria of Benn and Owen (2002).

Topographic and geomorphic metrics for the study areas and investigated fans were calculated from an ASTER V002 derived DEM (30 m resolution) using the Spatial Analyst toolbox in ESRI's ArcMap 10.1 (Table 1).

Fans in each study area were assigned names based on their source catchment and where appropriate were numbered from oldest to youngest (1 to n) based on their morphostratigraphic position within the catchments (Hughes et al., 2005; Hughes, 2010). As an example, $Qf_{_GOMUCHE03}$ (Qf = Quaternary fan) is located furthest downstream (subscript 03) from the Gomuche tributary catchment (subscript GOMUCHE).

The best-preserved fans with clearly defined proximal and distal zones with little evidence of surface denudation, deflation or human modification were selected for further investigation and ^{10}Be dating. The investigated fans include: $Qf_{_SARAI}$ from the Kullu valley; $Qf_{_SISSU}$ and $Qf_{_TELING}$ from the Chandra valley; and $Qf_{_MENTOKa}$ and $Qf_{_MENTOKb}$ from the Karzok valley.

Three to five boulders of quartz-bearing lithologies were sampled for ^{10}Be dating on each fan surface. Approximately 500 g of rock with a thickness of 1−5 cm was removed from each boulder surface using a hammer and chisel. The sampled boulders were described and photographed (Appendix 1), and their locations recorded using a handheld Garmin Etrex 30 GPS unit. Topographic shielding was measured at 10° azimuths from the boulder surface to the horizon using a compass and inclinometer.

Large tabular boulders with varnish and/or lichen cover, well set into the fan surface were

preferentially selected for sampling; sampling large boulders reduces the likelihood of selecting ones that have recently toppled or been exhumed (Benn and Owen, 2002; Heyman et al., 2011). Boulders were avoided if there was with evidence of strong weathering, pitting, fracturing, exfoliation or shielding from regolith. Likewise, boulders adjacent to or within areas with evidence of human modification of the landscape were not sampled. Boulders were only sampled from the distal zones of each fan to restrict the likelihood of them being derived from adjacent slopes through rockfalls. Boulders in ephemeral channels were also avoided.

The ^{10}Be age of each fan surface was defined by the range of boulder exposure ages. The age range defines the timing of the abandonment of the fan surface, and cessation of fan aggradation (Pope and Wilkinson 2005; Owen et al., 2014; Cesta and Ward 2016). A broad range of ^{10}Be ages may be the result of inheritance, boulder weathering, toppling or shielding, or that multiple sedimentation events characterize the fan surface (Zehfuss et al., 2001; Blisniuk et al., 2012; Hedrick et al., 2013). No statistical treatment of the ^{10}Be ages was possible due to the restricted size of the dataset, and distribution of ages for each landform.

Laboratory Methods

Crushing and sieving of the rock samples, quartz isolation, dissolution, chromatography, isolation of Be and the preparation of BeO was performed at the Geochronology Laboratories at the University of Cincinnati, using the chemical procedures and community standards of Kohl and Nishiizumi (1992) and Nishiizumi et al. (1994), modified by Dortch et al. (2009). The isolated BeO was mounted onto steel cathodes and the ^{10}Be/^{9}Be sample ratios were measured using accelerator mass spectrometry (AMS) at the Purdue Rare Isotope Measurement Laboratories (PRIME) at Purdue University (Sharma et al. 2000).

^{10}Be Fan Exposure Ages

The ^{10}Be boulder exposure ages were calculated using the Cosmic Ray Exposure program calculator (CREp) of Martin et al. (2017), using the LSD scaling model (Lifton et al., 2014) with the ERA40 atmospheric model (Uppala et al., 2005) and Lifton VDM 2016 geomagnetic database. This calculation scheme accounts for nuclide-specific production rate sensitivities to temporal and spatial variability in geomagnetic and solar inputs (Lifton et al., 2014), and has been successfully applied throughout the NW Himalaya, particularly for the Holocene (Orr et al., 2018; Saha et al., 2018). Published ^{10}Be ages of the revisited Garhwal (Barnard et al., 2004a,b) and Ladakh (Brown et al., 2002, 2003; Dortch et al., 2011c) fans were recalculated using these same methods, to allow for comparisons between fan records. The exposure ages were calculated assuming zero erosion. The effect of erosion is considered negligible owing to the very low 0.5−2.3 m/Ma rates measured throughout the Ladakh Range of northern India (Dortch et al., 2011b; Dietsch et al., 2015).

Regional landform abandonment and incision events in the NW Himalaya

Probability density functions of phases of landform abandonment and incision for the monsoon influenced Lesser and Greater Himalaya ranges (MWHR: monsoon western Himalayan ranges) and semi-arid interior ranges of the Greater Himalaya and Tethyan Himalaya (SWHR: semi-arid western Himalayan ranges) were defined by numerically dated river terrace, strath terrace and fan surfaces from existing geomorphic studies (Fig. 1). Previously published numerical cosmogenic ages were recalculated using the same calculation scheme as was used for our new fan ages. The MWHR region includes the Lahul, Kullu, Simla, Uttarkashi and Garhwal districts of northern India, whilst SWHR spans the Ladakh region of northern India and the Karakoram ranges of northeastern Pakistan. Regional events in landform abandonment and incision are defined by ≥3 ages. Landform abandonment events refer to times of restricted sedimentation where landforms stabilize.

LANDFORM DESCRIPTIONS

The *Qf_SARAI* (32.3095°N, 77.1568°E) fan in the Kullu valley study area is sourced from the Sarai tributary; a steep relief unglaciated catchment with a parallel drainage system. The fan is located at the confluence between the Solang Nala and Beas River at ~2300 m asl (Table 2, 3; Fig. 2). The source catchment of the *Qf_SISSU* fan (32.4827°N, 77.1176°E) in the Chandra valley study area is located adjacent to the Sissu Nala catchment (Fig. 3A−C). This steep relief catchment has preserved evidence of past glaciation, but presently is not glaciated. *Qf_TELING* (32.4357°N, 77.1926°E) is sourced from the Teling tributary, ~6 km northwest from Koksar (Fig. 3D−F). This glaciated amphitheater preserves an abundance of landforms and sediment deposits including moraines, talus and mass movements. In the Karzok valley study area, *Qf_MENTOKa* (32.9647°N, 78.2381°E) is the most easterly fan of the bajada, sourced from a Mentok catchment that has a cirque glacier. A similar morphology is shared by the second Mentok tributary catchment located directly adjacent to, and to the northwest of the first: the source catchment for *Qf_MENTOKb* (32.9701°N, 78.2301°E; Table 2, 3; Fig. 4).

RESULTS

New and recalculated fan surface ^{10}Be Ages

Fan surfaces in the Kullu and Chandra valley study areas have ^{10}Be boulder ages <12 ka, the majority <4 ka. ^{10}Be ages for the Karzok valley fan surfaces range between ~110 and 12 ka (Fig. 5; Table 4; Appendix 1).

The Kullu valley *Qf_SARAI* fan surface has ^{10}Be ages between 7.8±1.1 and 2.8±0.2 ka (uncertainties for all ages are quoted to 1σ). The *Qf_SISSU* and *Qf_TELING* fan surfaces in the Chandra valley study

area have ^{10}Be age ranges of 10.9±0.6−2.4±0.3 ka and 11.8±1.6−0.6±0.1 ka, respectively. In the Karzok valley study area, *Qf_MENTOKa* has ^{10}Be ages between 110.8±2.2 and 64.5±0.5 ka, whilst the *Qf_MENTOKb fan* surface has ages from 66.1±1.3 to 12.6±0.3 ka. No ages are discounted from the dataset because the restricted number and distribution of ^{10}Be ages for each landform prevents the identification of age outliers.

The recalculated ages for the *Rilkot1* fan surface in the Gori Ganga valley, northeast Garhwal range from 1.8±0.2 to 0.9±0.1 ka (Appendix 2). In the Bhagirathi valley, *Gaumukh1* and *Gaumukh2* fan surfaces have ^{10}Be ages that range from 5.5±0.2 to 3.1±0.2 ka and 1.5±0.3 to 1.2±0.2 ka, respectively. Additional fan surfaces with only one exposure age were also recalculated for this valley (*Bhuj Kharak1*: 3.27±0.47 ka; *Kedar Kharak1*: 9.8±0.6 ka; *Rudugaira1*: 7.8±0.5 ka), but are not referred to herein. The surface ages for the northern Ladakh *Tangtse1* and *Tangtse2* range from 38.6±2.6 to 19.0±1.5 ka and 14.3±1.5 to 2.1±0.2 ka, respectively.

Regional landform abandonment and incision events for the NW Himalaya

Records of landform abandonment are recognized in the MWHR region throughout the past ~50 ka, with regional events at 1.4±0.5 and 0.6±0.2 ka (Fig. 6; Appendix 3, 4). Records of incision extend from ~70 to 0.6 ka, with regional incision events at 6.9±3.7, 3.6±1.0, 1.8±0.6 and 1.0±0.1 ka. In the SWHR region of the NW Himalaya, records of landform abandonment extend over the past 56 ka and >110 ka. Regional events occur at 31.5±5.1 and 20.0±5.3 ka. Records of incision are recognized throughout the past ~120 ka, with regional events occurring at 35.9±5.8, 13.7±3.9 and 2.2±1.7 ka.

DISCUSSION

The *Rilkot1* (1.8±0.2−0.9±0.1 ka), *Gaumukh1* (5.5±0.3−3.1±0.3 ka) and *Gaumukh2* (1.5±0.3−1.2±0.3 ka) debris-flow fans in Garhwal have fan surfaces dating to the Mid−Late Holocene, at a time of increasing aridity and relative cooling (Gasse et al., 1996; Fleitmann et al., 2003, 2007; Dykoski et al., 2005; Wang et al., 2005; Herzschuh et al., 2006; Hu et al., 2008; Dong et al., 2010; Leipe et al., 2014; Rawat et al., 2015; Hudson et al., 2016; Srivastava et al., 2017; Fig. 6). These conditions are the result of a decline in monsoon intensity and the strengthening of the mid-latitude westerlies due to cooling in the North Atlantic (Clift et al., 2012; Leipe et al., 2014). Local glacial stages are recognized ~1−2 ka before the stabilization and abandonment of these surfaces; *Rilkot1* postdates the m_2 stage (4.4±0.1−1.9±0.3 ka) and *Gaumukh1* and *Gaumukh2* follow the Shivling (~5.2 ka) and Gangotri (~2.4−1.9 ka) stages, respectively (Sharma and Owen, 1996; Barnard et al., 2004b; Srivastava, 2012). Srivastava et al. (2017) argue that the prevailing cold and dry conditions were punctuated by short-term warm-wet periods between ~5.4 and 3.8 ka. The Garhwal fans are therefore likely to have evolved during these periods of glacial advance or enhanced temperature and precipitation, before being abandoned thereafter.

The $Qf_{_SARAI}$ debris-flow fan surface (7.8±1.2−2.8±0.3 ka) in the Kullu valley was also abandoned during this period of increasing aridity and relative cooling in the Mid−Late Holocene (as referenced above). Although no local glacial stages have been recognized south of Pir Panjal at this time, the Sarai source catchment preserves a succession of moraines from past glacial advances (Owen et al., 2001). Studies have shown that an enhancement in the strength of the monsoon during the late glacial and Early Holocene caused glaciers to advance along the southern Himalayan front (Owen et al., 2001; Bookhagen et al., 2005; Saha et al., 2018). The evolution of $Qf_{_SARAI}$ is likely, in part, affected by this glaciation.

The spread in ^{10}Be ages for the *Qf_SARAI* is likely the result of inheritance, which is a particular problem when dating young fan surfaces and/or those composed of older reworked sediment (Gosse et al., 2003; Wittmann and von Blanckenburg, 2009; Owen et al., 2011; Blisnuik et al., 2012; Hedrick et al., 2013). Boulder weathering, exhumation, toppling and shielding by sediment, snow or ice also affects the ^{10}Be inventory of a boulder surface, producing exposure ages younger than the timing of its emplacement on the landform's surface. These geological factors and other post-depositional landform disturbance by slope processes, fluvial reworking or anthropogenic activity can produce a distribution of ^{10}Be ages on an individual fan surface.

The *Qf_SISSU* (10.9±0.8−2.4±0.3 ka) and *Qf_TELING* (11.8±1.7−0.6±0.1 ka) debris-flow fans in the Chandra valley have a broad range of fan surface ages from the Early to Late Holocene (Fig. 6). During the last glacial maximum (LGM: 24−18; Mix et al., 2001), a large ~200-km-long, 400−600 thick glacier occupied the Chandra valley and tributaries. Deglaciation of the valley extended from ~19−16 ka (Euguster et al., 2017). *Qf_SISSU* and *Qf_TELING* formed after this glacier retreat; the older ^{10}Be ages (*Qf_SISSU*: 10.9±0.8 ka; *Qf_TELING:* 11.8±1.7 ka) likely contain inheritance from the LGM. The remaining Late Holocene ages indicate that the fans were abandoned during the continued decline in relative temperatures and humidity throughout the epoch. The Teling catchment is glaciated in the present day, but both catchments retain evidence of past glacial advances. The Chandra valley fans likely formed and/or evolved in response to local glaciation.

The broad distribution of ^{10}Be ages for the Karzok valley alluvial fans (*Qf_MENTOKa*: 110.8±5.5−64.5±2.9 ka; *Qf_MENTOKb*: 66.1±3.6−12.6±0.7 ka) might reflect either single or multiple phases of fan surface stabilization and abandonment during the late Pleistocene (Fig. 6). We argue that the landforms were abandoned during single events and that the range in ^{10}Be ages is

the result of inheritance, due to the lack of an exposure age gradient evident across the fan surfaces. Local geomorphic studies confirm that geological materials may contain inherited ^{10}Be due to the preservation of old landforms and sediment, and low rates of landscape change in the semi-arid western Himalaya (Hedrick et al., 2011; Dortch et al., 2011b; Orr et al., 2017, 2018). The stable position and lack of weathering features for the Men_F04 boulder suggests that the young 12.6±0.7 ka age for *Qf*$_{_MENTOKb}$ is due to the recent exhumation of the boulder. The timing of Karzok fan abandonment extends across times of fluctuating climatic conditions (Fig. 6). Several local glacial stages including Kar$_{_M1}$ (132.5±36.8 ka; Saha et al., 2018) and KM1−3 (72.0±31.0 ka; Hedrick et al., 2011; Dortch et al., 2013) may have contributed to the formation of this extensive bajada, however the causes of fan stabilization and abandonment remain unclear.

The *Tangtse1* debris-flow fan formed after the most recent glaciation of the Tangtse valley at 35.8±3.0ka (Brown et al., 2002, 2003; Dortch et al., 2011c; Fig. 6). The fan surface ages have a bimodal distribution; the older ages (45.1±4.7−32.2±2.6 ka) are likely the result of inheritance from this previous period of glaciation, or earlier. The remaining exposure ages are similar in age to the local Ladakh 2 glacial stage (22.9±0.7 ka; Dortch et al., 2013) and the period of reduced monsoon strength and effective moisture associated with the LGM (Fig. 6).

The *Tangtse2* debris-flow fan formed after the Pangong Tso outburst flood at 11.1±1.0 ka, which was a large flood event that reworked the majority of the landforms and sediment deposits that occupied the Tangtse valley floor at that time (Dortch et al., 2011c). The late-glacial ages for the fan surface therefore reflect inherited ^{10}Be. The remaining ^{10}Be ages suggest that *Tangtse2* was abandoned during the cooling temperatures and increasing aridity of the Mid−Late Holocene (Fig. 6).

Fan surface abandonment throughout the NW Himalaya

The Mid−Late Holocene fan surfaces of this study are predominantly limited to the debris-flow fans of the MWHR region. The SWHR region presents greater complexity, with the preservation of fan surfaces with abandonment ages from 110.8±5.5 to 2.1±0.3 ka. Preservation bias favors Holocene aged fan surfaces in the MWHR because elevated rates of erosion in this region rapidly rework and overprint landforms and sediment deposits over timescales of 10^4−10^1 years (Gabet et al., 2004; Wulf et al., 2010; Murari et al., 2014). The lower rates of landscape change in the semi-arid interior ranges help to preserve a longer fan record (Dortch et al., 2011a,b; Dietsch et al., 2015; Jonell et al., 2018).

The source catchments of the debris-flow fans of this study have mean slopes >30°, above which slopes are unable to securely retain regolith, snow or ice (Table 2). The steep topography of these catchments is conducive to diffusive hillslope processes, as well as stochastic high-magnitude mass-wasting events (Gruber and Haerberli, 2007; Dortch et al., 2009; Nagai et al., 2013). The narrow valley floor and steep relief hillslopes of the Chandra valley restrict the extent to which the $Qf__{SISSU}$ and $Qf__{TELING}$ can aggrade out into the trunk valley. The fans are further truncated and dissected by the Chandra River and tributaries. In contrast, the Karzok valley tributary catchments which are of comparable size to the former, have shallower mean slopes (<20°) and channel profiles (10°), which allow for large, gently sloping (<8°) alluvial fans to aggrade throughout the valley (Table 2). These examples demonstrate the importance of topography in determining the type, size and morphology of fans in the NW Himalaya.

With the exception of the Karzok fans, the timing of fan abandonment throughout the NW Himalaya coincides with periods of relative cooling and increasing aridity (Fig. 6). During warm, wet conditions, fans aggrade and evolve as sediment is released and then transferred throughout the catchments. As the climate then transitions to cooler and drier conditions, aggradation ceases

or becomes more restricted, and the fan surface stabilizes. Fans can also develop in response to single high-magnitude events such as storms and outburst floods or rapid fluctuations in precipitation (10^4–10^2 years; Hasnain 1996; Craddock et al., 2007; Wulf et al., 2010).

The fan surface ages coincide with one or more local glacial stages and between one and five regional glacial stages (Fig. 6). Periods of late Quaternary glaciation throughout the Himalayan-Tibetan orogen were cooler and drier than the present day (Burbank et al, 2003). Our study therefore proposes that fans evolve during interglacial periods or phases of deglaciation during a higher intensity monsoon, and then as glacial conditions become reestablished, the fans stabilize. As an example, fan aggradation, which includes the MWHR fans of this study, occurred in the NW Himalaya as part of the landscape response to a period of glacier retreat during the Mid−Holocene. This more restricted glaciation followed a time of extensive glacial advances during the Early Holocene, which has been argued to be the result of the northerly migration of the ITCZ and an enhanced summer monsoon (Fleitmann et al., 2003, 2007; Dykoski et al., 2005; Wang et al., 2005; Herzschuh, 2006; Hu et al., 2008; Leipe et al., 2014). Enhanced cooling due to the strengthening of the mid-latitude westerlies by the Mid−Holocene likely caused a reduction in fan sedimentation and the stabilization and abandonment of fan surfaces. This example highlights the sensitivity of fans in the NW Himalaya to glacial advances and/or associated shifts in local−regional climate.

The nature and timing of fan evolution and abandonment in the NW Himalaya is determined by the interaction between climate and internal catchment dynamics such as topography, sediment supply and catchment lithology. Seismic events or shifts in base level are additional external forcing which may prompt further mass redistribution in these high-altitude settings (Owen et al., 1996; Hobley et al., 2010).

Regional records of landform abandonment and incision

The regional timing of landform abandonment for the SWHR and MWHR broadly accompany periods of weakening monsoon and relative cooling (Gasse et al., 1996; Fleitmann et al., 2003, 2007; Dykoski et al., 2005; Wang et al., 2005; Herzschuh et al., 2006; Hu et al., 2008; Dong et al., 2010; Leipe et al., 2014; Rawat et al., 2015; Hudson et al., 2016; Srivastava et al., 2017; Fig. 6). This suggests that on the regional scale, landforms aggrade and evolve during warm and wet conditions before a shift to cool arid conditions forces the stabilization and abandonment of the landforms. Regional incision events are less straightforward, as they are recognized across various climatic conditions. The ubiquitous nature of erosion in these active alpine settings is perhaps the reason for this (Barnard et al., 2006b). The contrasting geomorphic regimes of the NW Himalaya causes a similar bias in the records of landform abandonment and incision in favor of Holocene events, as has been observed in the fan record of this study.

The $Qf_{_TELING}$, *Gaumukh2* and *Tangtse1* fan surface ages overlap with regional events of landform abandonment for the MWHR and SWHR regions, respectively (Fig. 6). A greater correspondence is evident however between the fans of this study and regional incision events. This correlation is likely because of the greater number of incision records available in the NW Himalaya, compared to landform abandonment records. Some landform abandonment and incision events within the regions of the MWHR (landform abandonment at 1.4±0.5 ka, incision at 1.0±0.1 ka) and the SWHR (landform abandonment at 31.5±5.1 ka, incision at 35.9±5.9 ka) are synchronous. This alludes to the existence of region-scale cycles of aggradation and incision throughout the NW Himalaya. Unlike parts of the Himalaya and other mountain systems, cycles of aggradation and incision at particular intervals (i.e. 40, 100 k cycles) are not recognized in the NW Himalaya (Pratt et al., 2002; Srivastava et al., 2008; Tofelde et al., 2017)

The MWHR and SWHR regional landform abandonment and incision events each occur alongside between two and seven regional glacial stages (MWHR landform abandonment [MOHITS 1B, 1C; HH1, 2] and incision [MOHITS 1C−1K; HH1, 2, 4−7]; SWHR landform abandonment [SWHTS 2D−2F] and incision [SWHTS 1B, 1C, 2A−2D, 2F; HH2, 3] Dortch et al., 2013; Murari et al., 2014; Saha et al., 2018; Fig. 6). This overlap is anticipated due to the duration of these geomorphic events, and the number of glacial records available throughout the inherently glaciated NW Himalaya. The most significant regional incision event for both MWHR and SWHR occurs at the time of extensive glaciation at the onset and early millennia of the Holocene (Fig. 6). This incision event likely reflects enhanced glacial and fluvial erosion during this glaciation and its association phase of deglaciation. More broadly, these regional records of geomorphic change illustrate the climatic-dependence of landscape change throughout the NW Himalaya.

CONCLUSION

The timing of fan surface abandonment has been defined for ten fans in the NW Himalaya; fan surface ages range from 110.8±5.5−64.5±2.9 ka to 1.8±0.2−0.9±0.1 ka. Debris-flow fans in the Garhwal, Kullu and Lahul regions of the monsoon-influenced Greater Himalaya are largely abandoned during the Holocene. In the Ladakh region of the Greater and Tethyan Himalaya, large alluvial fans and debris-flow fans have surface ages which extend throughout the last glacial. The type, size and morphology of the fans are shown to be influenced by the topography and fluvial channel behaviors of the source catchments and trunk valleys.

Regional landform abandonment and incision events for the MWHR and SWHR are defined over the past ~120 ka. In the MWHR, regional geomorphic events are restricted to the Holocene, while in the SWHR they are recognized from ~40 ka. The fans of this study and the regional

geomorphic records present preservation bias, where elevated rates of erosion and sediment reworking in the MWHR mean that the landforms retained in these catchments are restricted to the Holocene. The lower rates of landscape change in the SWHR enable the preservation of longer geomorphic records.

The timing of fan surface abandonment for the ten fans of this study and the regional events of landform abandonment throughout the NW Himalaya accompany periods of weakening monsoon strength and relative cooling. The landforms aggrade and evolve during warm-wet conditions before a shift to cool and arid conditions forces the stabilization and abandonment of the landforms. Regional incision events are recognized across various climatic conditions throughout the late Quaternary, likely due to the ubiquitous nature of erosion in these active alpine settings.

The fan surface ages are coincident with one or more local glacial stages and between one and five regional glacial stages. Fan formation and evolution extends throughout interglacial periods and times of deglaciation, before stabilizing once cool-arid glacial conditions return. The nature and timing of the fan evolution and abandonment is determined by the interaction between internal catchment dynamics and climate. Regional geomorphic events defined for the MWHR and SWHR regions also coincide with between two and seven regional glacial stages. This further illustrates the critical role played by glaciation and glacial processes in local and regional landscape change. More broadly, this study demonstrates the importance of climate-driven processes in the sediment flux and topographic evolution of the NW Himalaya.

ACKNOWLEDGMENTS

ENO and LAO thank the University of Cincinnati for providing tuition and stipend to support this work as part of ENO's doctoral thesis and the processing of samples for ^{10}Be dating. ENO and SS thank the Geological Society of America and the Graduate Student Governance Association, University of Cincinnati for research grants to conduct fieldwork. MWC acknowledges support from NSF (EAR-1560658). We should like to thank Dr. Paul Bierman, Dr. Nick Lancaster and Dr. Alan Gillespie for their detailed, constructive suggestions and comments on our manuscript.

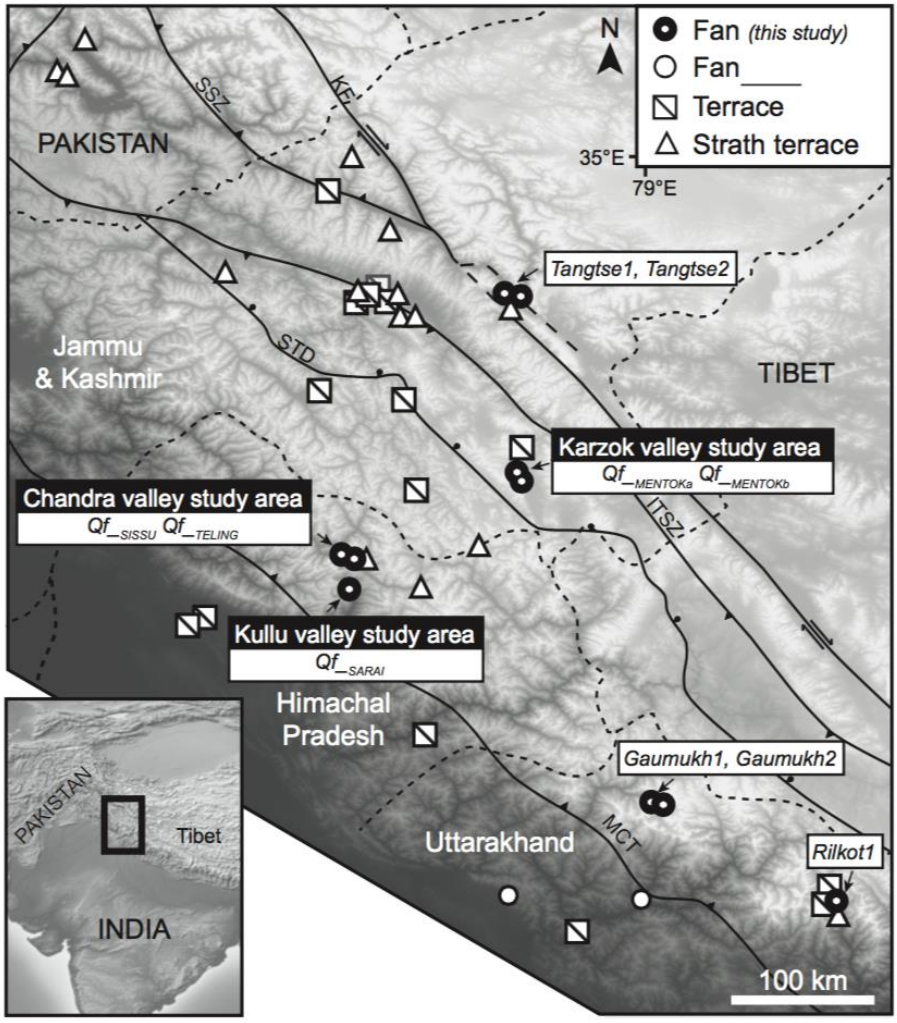

Fig. 1. Location of the study areas overlying a digital elevation model. Geologic structures from Hodges (2000; ITSZ- Indus-Tsangpo Suture Zone; KF- Karakoram Fault; MCT- Main Central Thrust; SSZ- Shyok Suture Zone; STD, South Tibetan Detachment). Fans of this study: Gori Ganga, Nanda Devi, NE Garhwal (*Rilkot1*; Barnard et al., 2004a); upper Bhagirathi valley, Garhwal (*Bhuj Kharak1, Kedar Kharak1, Rudugaira1, Gaumukh1, Gaumukh2*; Barnard et al., 2004b); Kullu valley ($Qf_{_SARAI}$); Chandra valley ($Qf_{_SISSU}$, $Qf_{_TELING}$); Karzok valley ($Qf_{_MENTOKa}$, $Qf_{_MENTOKb}$); Tangtse valley, Ladakh (*Tangtse1*, *Tangtse2*; Brown et al., 2002, 2003; Dortch et al. 2011c). Fan studies from Kumar Singh et al. (2001), Srivastava (2017). Terrace studies from Barnard et al. (2004a,b); Bookhagen et al. (2006); Dortch et al., (2011a); Blöthe et al. (2014); Scherler et al. (2015); Dey et al. (2016). Strath terrace studies from Burbank et al. (1996), Leland et al. (1998), Barnard et al. (2001, 2004a,b), Seong et al. (2007), Adams et al. (2009), Dortch et al. (2011a,b). Inset map illustrates the location of the overall study area within the Himalayan-Tibetan orogen (base map from geomapapp.org).

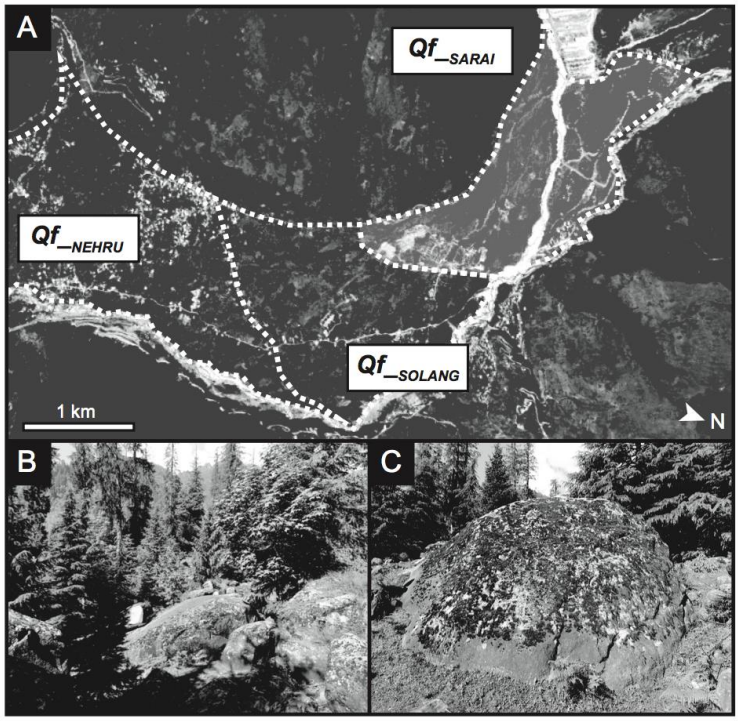

Fig. 2. Kullu valley fans and typical sampled boulders. A) Google Earth image of the Kullu valley (along Beas River from 2460 to 2030 m asl). *Qf_SOLANG* underlies *Qf_SARAI* and is sourced from the Sarai and/or Solang valleys. The Nehru Kund natural spring is located at the *Qf_NEHRU* fan (white dashed lines denote fan margins). B) View facing east down the fan. C) Lichen covered sampled boulder Sar_F03.

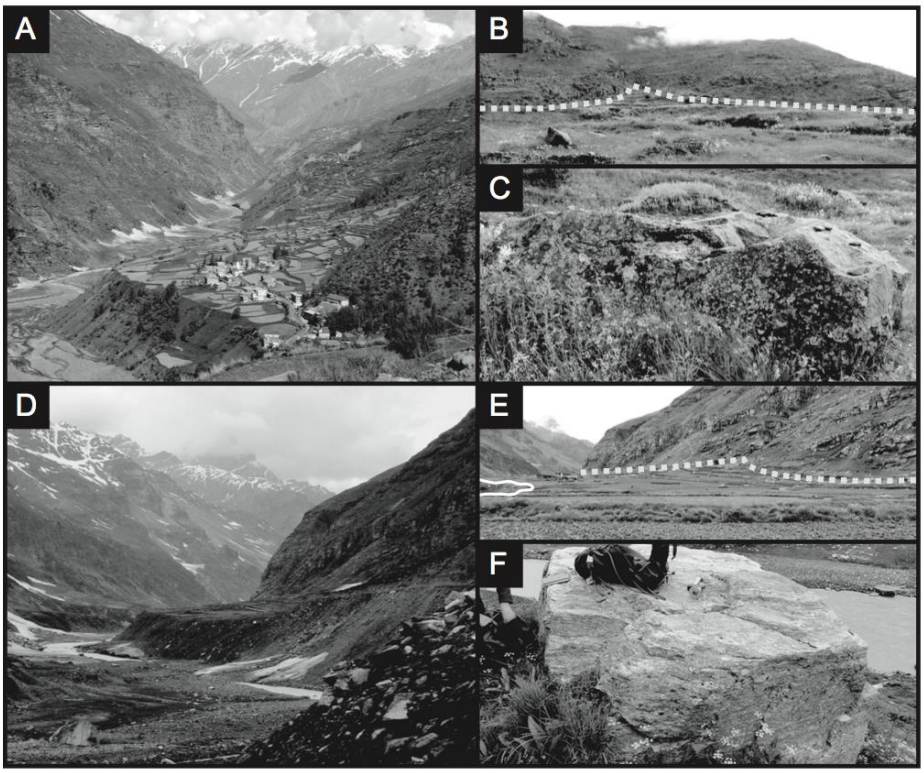

Fig. 3. Fans in the Chandra valley and examples of typical boulders that were sampled for ^{10}Be dating. A) View facing west towards *Qf_SISSU*. B) Image of the *Qf_SISSU* fan apex, extent (white dashed lines) and surface. C) Sampled boulder Sis_F03. D) View facing west of the *Qf_TELING* fan. E) *Qf_TELING* apex and fan surface (white dashed and solid lines denote fan perimeter and distal toe of the fan, respectively). F) Sampled boulder Sis_F07.

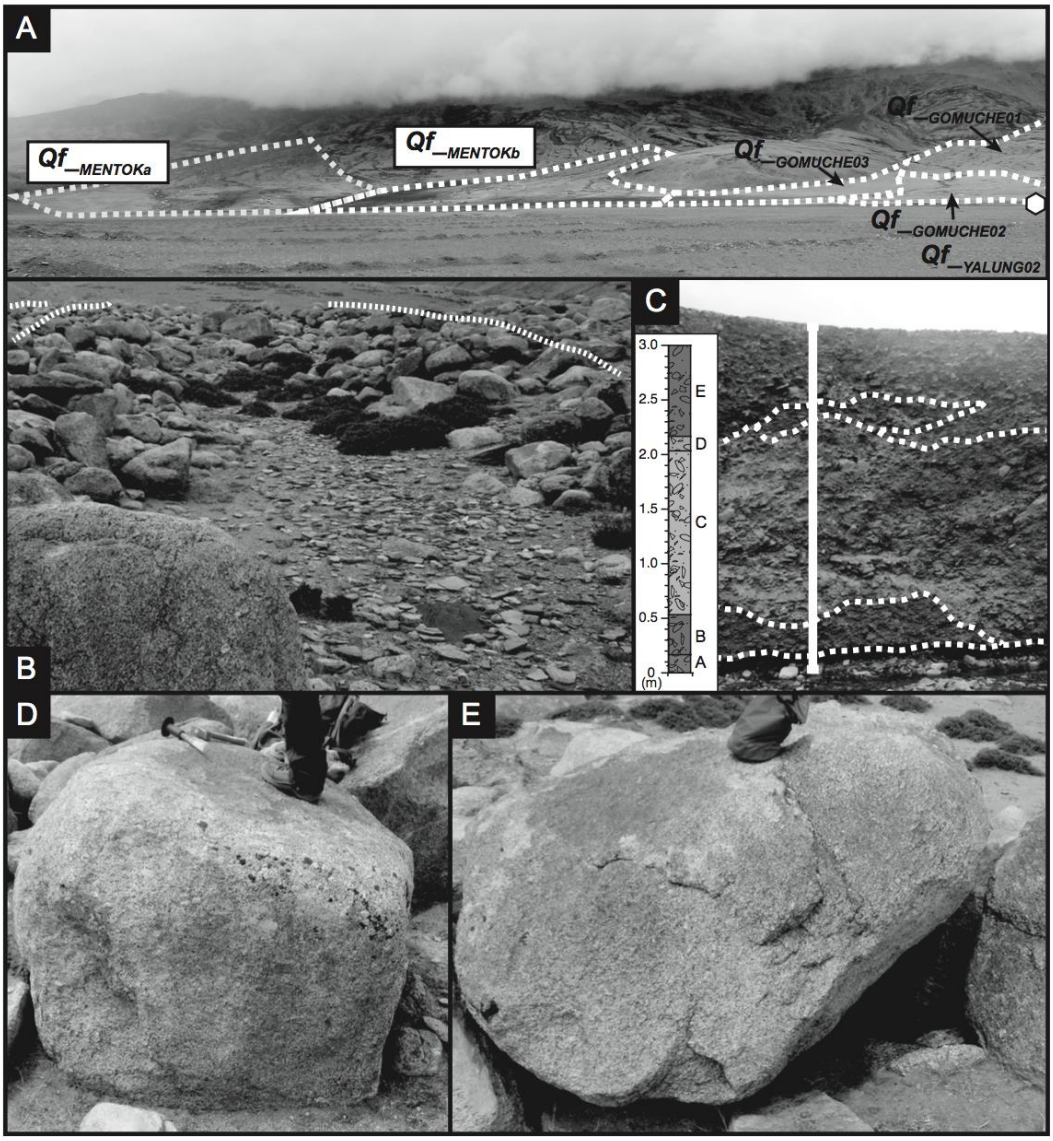

Fig. 4. Views of the Karzok valley and typical sampled boulders. A) View facing east of the Karzok valley from *Qf_YALUNG02*. Dashed white lines delineate the fan extents. B) View of boulder ridges (dashed white lines) and abandoned channels on *Qf_MENTOKb* surface. C) Stream cut revealing multiple units of diamict upstream from the studied fans, with inset stratigraphic log (units labeled to F, from base to the surface). White dashed lines delineate the unit boundaries. Refer to A for location (white pentagon). D) Sampled boulder Men_F03 from *Qf_MENTOKa*. E) Sampled boulder Men_F06 from *Qf_MENTOKb*.

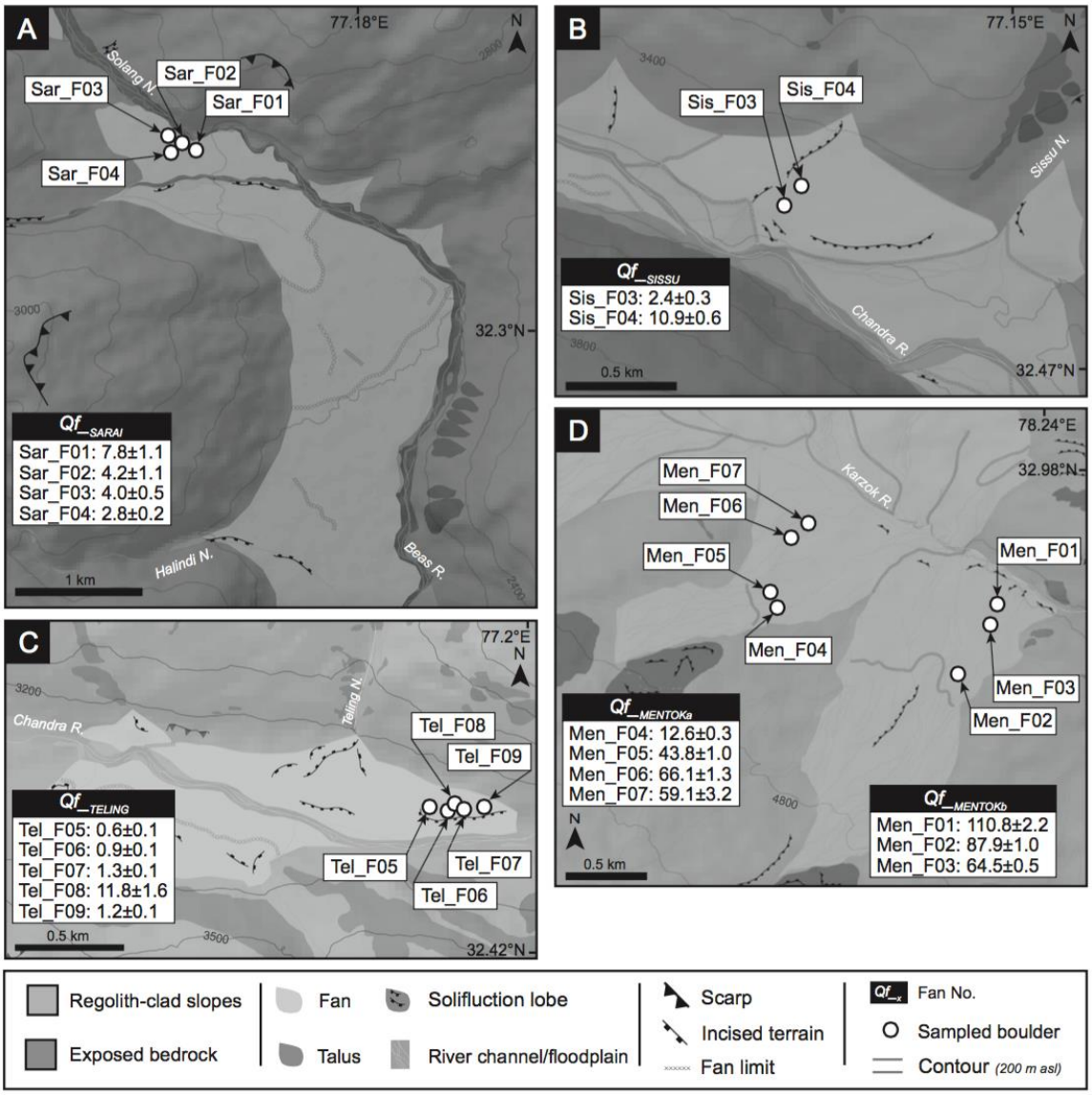

Fig 5. Geomorphology of the fan study areas showing the ^{10}Be sampling sites and ages (ka). See Fig. 3 for location of each map. A) *Qf_SARAI* study area (includes the fan and surrounding features). B) *Qf_SISSU* study area. C) Qf_TELING study area. D) *Qf_MENTOKa* and *Qf_MENTOKb* study area.

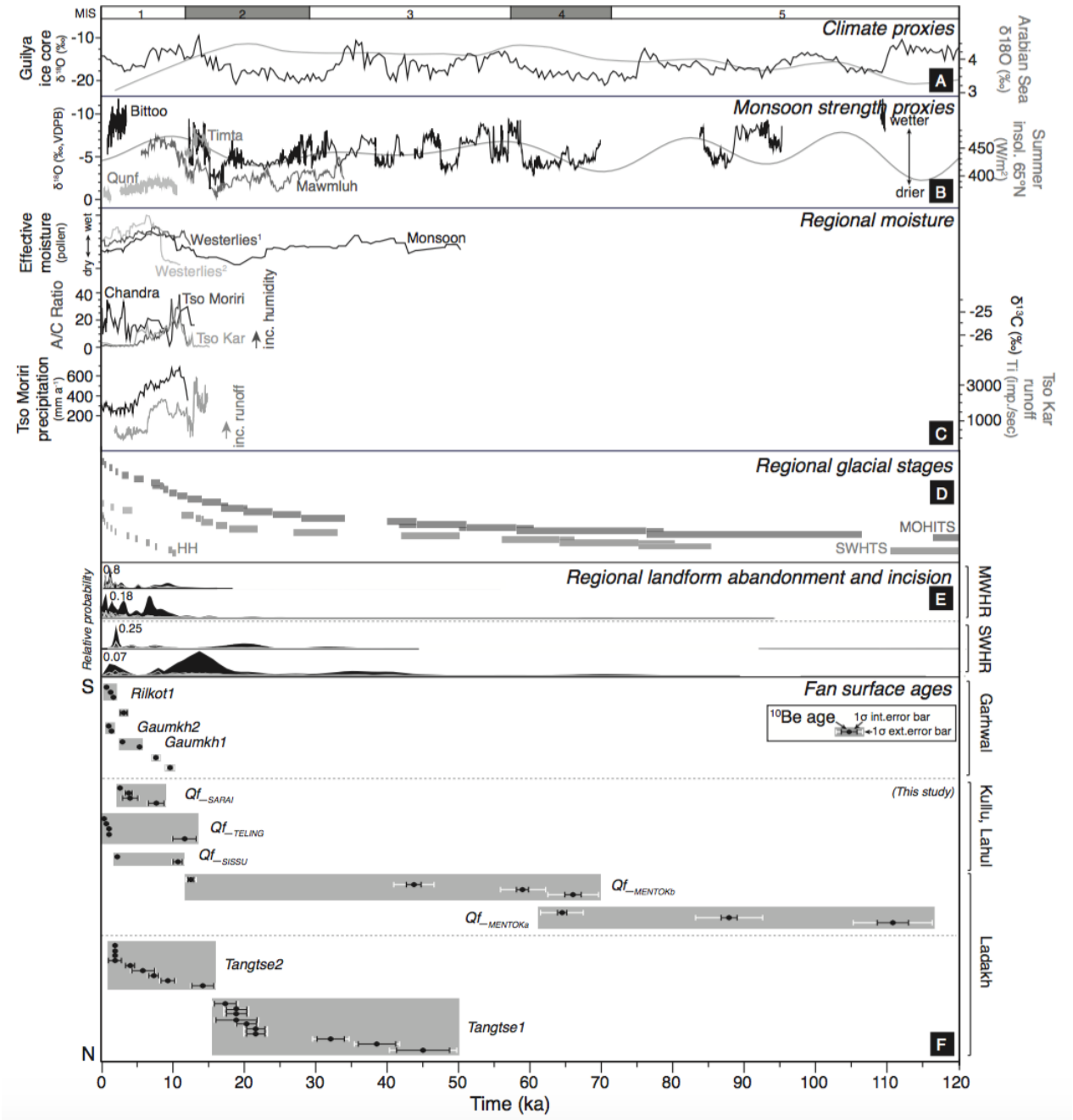

Fig. 6. Late Quaternary paleoclimatic, paleoenvironmental, glacial and geomorphic records for the NW Himalaya and Tibet. A) Climatic proxies including the Guliya ice core $\delta^{18}O$ record (Thompson et al., 1997). B) 65° N insolation (Leuschner and Sirocko, 2003), the Arabian Sea Core 722 $\delta^{18}O$ record (Clemens et al., 1996; Lisiecki and Raymo, 2005) and monsoon strength proxies including cave records from Qunf in Oman (Fleitmann et al., 2003), and Bittoo (Kathayat et al., 2016), Mawmluh (Dutt et al., 2015), Timta (Sinha et al., 2005; VDPB: Vienna Pee Dee Belemnite) in India, plus summer insolation for 65°N (Berger and Loutre, 1991). C) Regional moisture proxies including central Asian pollen records of monsoon (Herzchuh, 2006) and mid-latitude westerlies moisture transport (Herzchuh, 2006; Chen et al., 2008).

Paleoenvironmental and paleohydrologic records for Tso Moriri (Leipe et al., 2014; Mishra et al., 2015), Tso Kar (Demske et al., 2009; Wünnemann et al., 2010), and $\delta^{13}C$ peat-lake sequence for the Chandra valley (Rawat et al., 2015). D) Regional glacial stages for the NW Himalaya. Himalayan Holocene (HH) stages from Saha et al. (2018), Semi-Arid Western Himalayan-Tibetan stages (SWHTs) from Dortch et al. (2013) and Monsoonal Himalayan-Tibetan stages (MOHITs) from Murari et al. (2014). E) Regional events of landform abandonment (upper) and incision (lower) for the NW Himalaya. Probability density distribution plots for the MWHR (landform abandonment = Barnard et al., 2004a,b; Scherler et al., 2015. incision = Barnard et al., 2004a,b; Bookhagen et al., 2006b; Adams et al., 2009; Dortch et al., 2011b; Dey et al., 2016) and SWHR (landform abandonment = Brown et al., 2002, 2003; Dortch et al., 2011b; Blöthe et al., 2014. incision = Leland et al., 1998; Brown et al., 2002, 2003; Seong et al., 2007; Dortch et al., 2011a, b). Fan ^{10}Be ages of this study are not included in these PDFs. F) Fan chronologies for the NW Himalaya defined by TCN dating for Ladakh, Lahul, Kullu and recalculated for Garhwal (Barnard et al., 2004a,b) and northern Ladakh (Brown et al., 2002, 2003; Dortch et al., 2011c).

Table 1. Climate and glacial records for the Kullu, Chandra and Karzok valley study areas.

	CLIMATE			GLACIAL RECORD
	Mean annual precipitation (mm)	Mean annual temperature range (°C)	Vegetation	
Kullu valley study area*	2000−3000	-4−11	Dense broad leaved, coniferous and sub-alpine forest	15.5±0.5 ka (Rhotang Pass Stage), 12.2±1.6−10.6±0.3 ka (Solang Stage; Owen et al., 2001)
Chandra valley study area†	(a) >500 (predom. >900) (b) 400−800	(a) -12−6 (b) -15−7	Alpine herbs, sedges, grasses and sub-alpine forest	15.3±1.6 ka (Batal Stage; Murari et al., 2014), 12.4±1.2 ka (Kulti Stage; Murari et al., 2014), 10.4±0.3 ka (mH3), 0.2±0.1 ka (mH1a; Saha et al., 2018) LGM deglaciation: ~20− 14 ka (Euguster et al., 2016)
Karzok valley study area§	(a) ~115 (b) 40−100	(a) -2.8−24.7	Xerophytic shrubs and grasses	311.0±8.0 ka (KM-0), 126.0±8.0 ka (PM-0), 72.0±31.0 ka (KM1-3), 47.0±12.0 ka (PM-1), 2.7±2.3 ka (PM-2), 0.3±0.2 ka (PM-3; Hedrick et al., 2011; Dortch et al., 2013) 4.9±0.3 ka (KM-4/mG2), 2.1±0.2 ka (mM2), 1.0±0.1 ka (mM1), 0.7±0.1 ka (mM1; Hedrick et al., 2011; Dortch et al., 2013; Saha et al., 2018)

*: Kullu valley: Dhundi weather station (32.2530°N, 77.1299°E, 2850 m asl; Snow and Avalanche Establishment [SASE] 1993−2001; Gusain et al., 2004), TRMM (1998−2005; Bookhagen and Burbank 2006), vegetation from Rawat et al. (2015).
†: Chandra valley: (a) Chhota Shigri weather station (32.2867°N, 77.5365°E, 3900 m asl; 1980−2005; Wagnon et al., 2007; Azam et al., 2014); (b) TRMM (1998−2005; Bookhagen and Burbank 2006), Patseo weather station (32.7538°N, 77.2610°E, 3780 m asl; Snow and Avalanche Establishment [SASE] 1993−2001; Gusain et al., 2004); vegetation from Rawat et al. (2015).
§: Karzok valley: (a) Leh weather station (34.1800°N, 77.5800°E, 3500 m asl; CRUTEM4 1876−1990, Jones et al., 2012; Osborn and Jones, 2014); (b) TRMM (1998−2005; Bookhagen and Burbank 2006)

Table 2. Source catchment and fan metrics for the Kullu, Chandra and Karzok valley study areas.

	CATCHMENT CHARACTERISTICS							FAN CHARACTERISTICS					
Fan No.	Headwall	Area	Aspect	Relative Relief*	Mean slope†	HI index§	Channel profile	Apex	Area	Aspect	Mean slope	Mean channel depth#	Mean channel width#
	(m asl)	(km^2)	(°)	(m)	(°)		(°)	(m asl)	(km^2)	(°)	(°)	(m)	(m)
Kulllu valley													
Qf_SARAI	5060	18.8	90	250	35	0.4	15	2510	1.5	115	8	0.7	48.3
Chandra valley													
Qf_SISSU	5730	12.2	205	195	30	0.5	18	3210	0.7	225	15	10.8	13.8
Qf_TELING	5710	17.9	205	250	35	0.6	16	3190	0.5	205	11	3.1	18.3
Karzok valley													
Qf_MENTOKa	6200	17.8	45	130	18	0.5	10	4880	1.9	20	8	2.3	5.9
Qf_MENTOKb	6090	17.1	45	130	19	0.5	10	4790	1.2	45	6	2	5.1

*: Mean relative relief derived from 0.13km^2 catchment grid cells. Catchment relative relief (m): Qf_SARAI (2276); Qf_SISSU (2772); Qf_TELING (2619); Qf_MENTOKa (1642); Qf_MENTOKb (1520)
†: Slope derived from 0.001km^2 catchment grid cells
§: Strahler (1952) Hypsometric index (mean elevation- min elevation/relief)
#: Mean depth and width derived from 10 channel cross section profiles between apex and distal zone of fan.

Table 3. Fan and surface boulder descriptons for the Kullu, Chandra and Karzok valley study areas.

Fan No.	Landform description	Surface boulder description
Kullu valley		
$Qf_{_SARAI}$	• Slightly weathered, matrix (sand) supported bouldery gravel diamicton. • No morphostratigraphically younger units or sub-lobes on surface. Overlies older fan at Palchan (Fig. 2A). • Solang Nala and Beas River truncate northern margins of mid and distal zones. • Sarai Nala incises into fan revealing cut banks and terraces. • Shallow, sinuous ephemeral and/or abandoned channels across fan surface. • Montane forests and grasslands, well-developed soils for agricultural land use. • Human settlement and infrastructure across fan surface.	• Distributed across northern extent of fan. Anthropogenic boulder clearing evident on southern flank. • Granitic, subangular−subrounded boulders (≤10 m; Fig. 2B,C). • Tabular, well-set boulders with no landform degradation/ erosion at boulder margins. • Slight-moderately weathered (minor exfoliation). Rock varnish and lichen present.
Chandra valley		
$Qf_{_SISSU}$	• Slight-moderately weathered bouldery gravel diamicton with sandy-silt matrix. • Overlies a morphostratigraphically older fan at Sissu. • Small sub-lobe extends from the distal region of fan at tributary-river confluence. • Chandra River and tributaries have incised, entrenched and truncated the eastern extent of fan. • Alpine tundra, developed soils for agricultural land use. • Human settlement and infrastructure (inc. irrigation) across fan surface (Fig. 3A).	• Distributed across mid-distal zones of fan. • Angular-subrounded granites and siltstones (≤10 m). • Tabular, well-set boulders with no landform degradation/erosion at boulder margins (Fig. 3B,C). • Slight-moderate weathered (minor exfoliation). Rock varnish and lichen present.
$Qf_{_TELING}$	• Slight-moderately weathered bouldery gravel diamicton with sandy-silt matrix. • Increased surface degradation on the western fan flank. • No morphostratigraphically younger units or sublobes on surface. • Teling Nala and Chandra River have incised and truncated the fan. • Alpine tundra, developed soils for agricultural land use. • Human settlement and infrastructure.	• Distributed across mid-distal zones of fan. • Granitic angular-subrounded boulders (≤10 m). • Tabular, well-set boulders with no landform degradation/erosion at boulder margins (Fig. 3F). • Slight-moderately weathered (minor exfoliation). Rock varnish and lichen present.
Karzok valley		
$Qf_{_MENTOKa}$	• Surface characterized by two depositional units (upper, lower) with consistent descriptions. • Moderate-highly weathered, matrix (sandy-silt) supported sandy gravel diamicton with boulders. • Northeastern distal flank of fan underlies $Qf_{_MENTOKb}$. No morphostratigraphically younger units or sub-lobes identified on fan surface (Fig. 4A). • Distal zone truncated by the Karzok River. • Sinuous tributary transforms into a large braided system across fan surface. Channels are shallow, ephemeral and/or abandoned. • Alpine tundra including xerophytic shrubs and grasses. Poor soil development.	• Distributed across mid-distal zones of fan. Boulder ridges trend down-fan at channel margins. • Granitic subangular-subrounded boulders (≤3 m). • Tabular, well-set boulders with some landform degradation/erosion at boulder margins (Fig. 4D). • Moderate-highly weathered (cavernous weathering, pitting and exfoliation). Rock varnish present.
$Qf_{_MENTOKb}$	• Surface characterized by two depositional units (upper, lower) with consistent descriptions. • Moderate-highly weathered, matrix (sandy-silt) supported sandy gravel diamicton with boulders. • No morphostratigraphically younger units or sub-lobes identified on fan surface (Fig. 4A). • Distal zone truncated by the Karzok River. • Sinuous tributary transforms into a large braided system across fan surface. Channels are shallow, ephemeral and/or abandoned (Fig. 4B). • Alpine tundra including xerophytic shrubs and grasses. Poor soil development. • Nomadic human settlement at distal zone of fan.	• Distributed across mid-distal zones of fan (anthropogenic boulder clearing evident in lower distal zone). Boulder ridges trend down-fan at channel margins. • Granitic subangular-subrounded boulders (≤3 m). • Tabular, well-set boulders with some landform degradation/erosion at boulder margins (Fig. 4E). • Moderate-highly weathered (cavernous weathering, pitting and exfoliation). Rock varnish present.

Table 4: Sample details and ^{10}Be ages (uncertainty is expressed as 1σ) for the fans of the study areas.

Sample name	Fan	Location		Altitude	Boulder size			Lithology*	Weathering†	ST§	TSF#	Quartz mass	^{9}Be carrier mass,conc.	^{10}Be/^{9}Be AMS ratio**	^{10}Be conc.	LSD age ±1σ int. (ext.)††
		Latitude (°N)	Longitude (°E)	(m asl)	Length (m)	Width (m)	Height (m)			(cm)		(g)	(g, mg/g)	(10^{-14})	(10^{6} atoms/g)	(ka)
Kullu valley																
Sar_F01	$Qf_{_SARAI}$	32.3138	77.1618	2440	3.9	2.5	1.6	L. granite	SW/MB	1	0.94	26.59	0.3501, 1.0038	14.10±2.03	0.13±0.02	7.8±1.1 (1.2)
Sar_F02	$Qf_{_SARAI}$	32.3138	77.1612	2453	7.7	7.2	0.8	L. granite	SW/DB	1	0.95	11.18	0.3503, 1.0038	2.91±0.81	0.06±0.02	4.2±1.1 (1.1)
Sar_F03	$Qf_{_SARAI}$	32.3136	77.1610	2463	4.9	3.0	1.6	L. granite	SW/MB	3	0.96	15.11	0.3503, 1.0038	3.74±0.50	0.06±0.008	4.0±0.5 (0.5)
Sar_F05	$Qf_{_SARAI}$	32.3136	77.1620	2437	6.4	4.0	2.3	L. granite	SW-MW/DB	2	0.95	15.40	0.349, 1.0038	2.60±0.19	0.04±0.003	2.8±0.2 (0.3)
Chandra valley																
Sis_F03	$Qf_{_SISSU}$	32.4808	77.1163	3100	6.0	1.5	2.0	Siltstone	SW/DB	2	0.91	3.69	0.3512, 1.0038	0.78±0.09	0.05±0.005	2.4±0.3 (0.3)
Sis_F04	$Qf_{_SISSU}$	32.4806	77.1161	3095	3.4	2.0	1.3	Siltstone	SW/MB	2	0.91	1.40	0.3493, 1.0038	1.51±0.11	0.25±0.02	10.9±0.6 (0.8)
Tel_F05	$Qf_{_TELING}$	32.4326	77.1960	3132	3.9	0.3	1.5	L. granite	SW/DB	2	0.91	19.27	0.3492, 1.0038	1.11±0.11	0.01±0.001	0.6±0.1 (0.1)
Tel_F06	$Qf_{_TELING}$	32.4326	77.1969	3133	9.0	2.5	2.5	L. granite	SW-MW/DB	2	0.92	15.24	0.3504, 1.0038	1.28±0.18	0.02±0.003	0.9±0.1 (0.1)
Tel_F07	$Qf_{_TELING}$	32.4326	77.1972	3128	4.1	2.8	0.7	L. granite	SW/MB	1	0.91	21.59	0.3492, 1.0038	2.65±0.17	0.03±0.002	1.3±0.1 (0.1)
Tel_F08	$Qf_{_TELING}$	32.4328	77.1970	3136	5.7	2.5	2.0	L. granite	SW-MW/MB	2	0.91	9.89	0.3495, 1.0038	12.10±1.85	0.29±0.04	11.8±1.6 (1.7)
Tel_F09	$Qf_{_TELING}$	32.4328	77.1981	3137	4.7	4.0	1.5	L. granite	SW/DB	2	0.92	16.35	0.3501, 1.0038	1.93±0.13	0.03±0.002	1.2±0.1 (0.1)
Karzok valley																
Men_F01	$Qf_{_MENTOKa}$	32.9679	78.2420	4633	4.5	3.0	0.7	Granite	MW/MB	1	1.00	29.88	0.3499, 1.0232	1020.00±24.40	8.14±0.19	110.8±2.2 (5.5)
Men_F02	$Qf_{_MENTOKa}$	32.9638	78.2400	4664	1.6	0.9	1.0	Granite	MW/DB	2	0.99	20.67	0.3506, 1.0038	541.00±6.55	6.16±0.07	87.9±1.0 (4.7)
Men_F03	$Qf_{_MENTOKa}$	32.9669	78.2417	4639	1.8	1.3	1.6	Granite	SW-MW/DB	2	0.99	22.21	0.3487, 1.0038	428.00±6.55	4.51±0.05	64.5±0.5 (2.9)
Men_F04	$Qf_{_MENTOKb}$	32.9680	78.2294	4673	1.5	1.0	1.7	P. granite	MW-HW/MB	2	0.98	16.35	0.3500, 1.0038	54.50±1.26	0.78±0.02	12.6±0.3 (0.7)
Men_F05	$Qf_{_MENTOKb}$	32.9687	78.2289	4673	1.4	1.1	0.9	P. granite	SW/MB	2	1.00	21.77	0.3504, 1.0800	283.00±6.4	3.28±0.07	43.8±1.0 (2.8)
Men_F06	$Qf_{_MENTOKb}$	32.9707	78.2303	4656	1.5	0.7	0.7	Granite	MW/DB	2	1.00	25.35	0.3490, 1.0038	513.00±11.20	4.74±0.10	66.1±1.3 (3.6)
Men_F07	$Qf_{_MENTOKb}$	32.9708	78.2306	4650	2.1	1.4	0.8	Granite	MW/MB	2	1.00	9.67	0.3490, 1.0038	169.00±2.73	4.10±0.07	59.1±0.9 (3.2)

*: Lithology: L. granite- leaucogranite, P. granite- Porphyritic granite.

†: Boulder weathering characteristics: SW- slightly weathered (no pitting), MW- moderately weathered (some pitting, moderate exfoliation), HW- Highly weathered (exfoliated sheets can be manually pulled off the rock), SB- slightly buried, MB- moderately buried, DB- deeply buried.

§: Sample thickness

#: Topographic Shielding Factor

**: ^{10}Be/^{9}Be ratios are corrected for background ^{10}Be detected in full procedural blanks (Sar_F01−05, Men_F05: 1.87±0.94x10^{-15}; Sis_F03, 04, Men_F07: 4.2±0.17x10^{-15}; Tel_F05−09: 1.22±0.43x10^{-15}; Men_F02−04,06: 17.0±5.0x10^{-15}; KO20−23, Men_F01: 32.0±2.0x10^{-15}.

††: LSD age (internal/external errors quoted) is calculated using the Balco et al. (2008) calibration dataset (^{10}Be decay constant of 5.1±0.3x10^{-7}), and Lifton et al. (2014) calculation scheme with the Lifton 2016 VDM geomagnetic database. Production rate for the CREP calculator is 4.13±0.2 ^{10}Be atoms/grams SiO_2/year (Martin et al., 2016) with a ^{10}Be half-life of 1.36Ma. Density of 2.7 g cm^3, AMS Standard of 07KNSTD. Ages rounded to 1 decimal place.

REFERENCES

Adams, B., Dietsch, C., Owen, L.A., Caffee, M.W., Spotila, J., Haneberg, W.C., 2009. Exhumation and incision history of the Lahul Himalaya, northern India, based on (U–Th)/He thermochronometry and terrestrial cosmogenic nuclide methods. Geomorphology, 107(3-4),p.285-299. https://doi.org/10.1016/j.geomorph.2008.12.017

Azam, M.F., Wagnon, P., Vincent, C., Ramanathan, A.L., Favier, V., Mandal, A., Pottakkal, J.G., 2014. Processes governing the mass balance of Chhota Shigri Glacier (western Himalaya, India) assessed by point-scale surface energy balance measurements. The Cryosphere, 8(6), p.2195-2217. https://doi.org/10.5194/tc-8-2195-2014

Balco, G., Stone, J., Lifton, N., Dunai, T., 2008. A complete and easily accessible means of calculating surface exposure ages or erosion rates from ^{10}Be and ^{26}Al measurements. Quaternary Geochronology, 3, p.174-195. https://doi.org/10.1016/j.quageo.2007.12.001.

Ballantyne, C.K., 2002a. Paraglacial geomorphology. Quaternary Science Reviews, 21(18-19), p.1935-2017. https://doi.org/10.1016/S0277-3791(02)00005-7

Ballantyne, C.K., 2002b. A general model of paraglacial landscape response. The Holocene, 12(3), p.371-376. https://doi.org/10.1191/0959683602hl553fa

Barnard, P., Owen, L., Finkel, R., 2004a. Style and timing of glacial and paraglacial sedimentation in a monsoon-influenced high Himalayan environment, the upper Bhagirathi Valley, Garhwal Himalaya. Sedimentary Geology, 165, p.199-221. https://doi.org/10.1016/j.sedgeo.2003.11.009

Barnard, P.L., Owen, L.A., Sharma, M.C., Finkel, R.C., 2004b. Late quaternary (Holocene) landscape evolution of a monsoon-influenced high Himalayan valley, Gori Ganga, Nanda Devi, NE Garhwal, Geomorphology, 61(1-2), p.91-110. https://doi.org/10.1016/j.geomorph.2003.12.002

Barnard, P., Owen, L., Finkel, R., Asahi, K., 2006a. Landscape response to deglaciation in a high relief, monsoon-influenced alpine environment, Langtang Himal, Nepal. Quaternary Science Reviews 25, p.2162-2176. https://doi.org/10.1016/j.quascirev.2006.02.002

Barnard, P.L., Owen, L.A., Finkel, R.C., 2006b. Quaternary fans and terraces in the Khumbu Himal south of Mount Everest: their characteristics, age and formation. Journal of the Geological Society, 163(2), p.383-399. https://doi.org/10.1144/0016-764904-157

Benn, D., Owen, L., 1998. The role of the Indian summer monsoon and the mid-latitude westerlies in Himalayan glaciation: a review and speculative discussion. Journal of the Geological Society, 155, p.353–363. https://doi.org/10.1144/gsjgs.155.2.0353

Benn, D.I., Owen, L.A., 2002. Himalayan glacial sedimentary environments: a framework for reconstructing and dating former glacial extents in high mountain regions. Quaternary International, 97-98, p.3-26. https://doi.org/10.1016/S1040-6182(02)00048-4

Berger, A., Loutre, M.F., 1991. Insolation values for the climate of the last 10 million years. Quaternary Science Reviews, 10(4), p.297-317. https://doi.org/10.1016/0277-3791(91)90033-Q

Blisniuk, K., Oskin, M., Fletcher, K., Rockwell, T., Sharp, W., 2012. Assessing the reliability of U-series and ^{10}Be dating techniques on alluvial fans in the Anza Borrego Desert, California. Quaternary Geochronology, 13, p.26-41. https://doi.org/10.1016/j.quageo.2012.08.004

Blöthe, J.H., Munack, H., Korup, O., Fülling, A., Garzanti, E., Resentini, A., Kubik, P.W., 2014. Late Quaternary valley infill and dissection in the Indus River, western Tibetan Plateau margin. Quaternary Science Reviews, 94, p.102-119. https://doi.org/10.1016/j.quascirev.2014.04.011

Bookhagen, B., Burbank, D., 2006. Topography, relief and TRMM-derived rainfall variations along the Himalaya. Geophysical Research Letters, 33, 105. https://doi.org/10.1029/2006GL026037

Bookhagen, B., Burbank, D., 2010. Toward a complete Himalayan hydrological budget: Spatiotemporal distribution of snowmelt and rainfall and their impact on river discharge. Journal of Geophysical Research 115, F3, p.1-25. https://doi.org/10.1029/2009JF001426

Bookhagen, B., Thiede, R., Strecker, M., 2005. Late Quaternary intensified monsoon phases control landscape evolution in the northwest Himalaya. Geology 33, 1, 149-152. https://doi.org/10.1130/G20982.1

Brown, E.T., Bendick, R., Bourles, D.L., Gaur, V., Molnar, P., Raisbeck, G.M., Yiou, F., 2002. Slip rates of the Karakorum fault, Ladakh, India, determined using cosmic ray exposure dating of debris flows and moraines. Journal of Geophysical Research: Solid Earth, 107(B9), doi.org/10.1029/2000JB000100.

Brown, E.T., Bendick, R., Bourles, D.L., Gaur, V., Molnar, P., Raisbeck, G.M., Yiou, F., 2003. Early Holocene climate recorded in geomorphological features in Western Tibet. Palaeogeography, Palaeoclimatology, Palaeoecology, 199(1-2), p.141-151. https://doi.org/10.1016/S0031-0182(03)00501-7

Burbank, D., Blythe, A., Putkonen, J., Pratt-Sitaula, B., Gabet, E., Oskin, M., Barros, A., Ojha, T., 2003. Decoupling of erosion and precipitation in the Himalayas. Nature 426, p.652-655.

Cesta, J.M., Ward, D.J., 2016. Timing and nature of alluvial fan development along the Chajnantor Plateau, northern Chile. Geomorphology, 273, p.412-427. https://doi.org/10.1016/j.geomorph.2016.09.003

Chen, F., Yu, Z., Yang, M., Ito, E., Wang, S., Madsen, D.B., Huang, X., Zhao, Y., Sato, T., Birks, H.J.B., Boomer, I., 2008. Holocene moisture evolution in arid central Asia and its out-of-phase relationship with Asian monsoon history. Quaternary Science Reviews, 27(3-4), p.351-364. https://doi.org/10.1016/j.quascirev.2007.10.017

Clemens, S.C., Murray, D.W., Prell, W.L., 1996. Nonstationary phase of the Plio-Pleistocene Asian monsoon. Science, 274(5289), p.943-948. https://doi.org/10.1126/science.274.5289.943

Clift, P.D., Carter, A., Giosan, L., Durcan, J., Duller, G.A.T., Macklin, M.G., Alizai, A., Tabrez, A.R., Danish, M., VanLaningham, S., Fuller, D.Q., 2012. U-Pb zircon dating evidence for a Pleistocene Sarasvati River and capture of the Yamuna River. Geology 40, 211–214. https://doi.org/10.1130/G32840.1

Craddock, W.H., Burbank, D.W., Bookhagen, B., Gabet, E.J., 2007. Bedrock channel geometry along an orographic rainfall gradient in the upper Marsyandi River valley in central Nepal. Journal of Geophysical Research: Earth Surface, 112(F3), doi.org/10.1029/2006JF000589.

Demske, D., Tarasov, P.E., Wünnemann, B., Riedel, F., 2009. Late glacial and Holocene vegetation, Indian monsoon and westerly circulation in the Trans-Himalaya recorded in the lacustrine pollen sequence from Tso Kar, Ladakh, NW India. Palaeogeography, Palaeoclimatology, Palaeoecology, 279(3), p.172-185. https://doi.org/10.1016/j.palaeo.2009.05.008

Derbyshire, E., Owen, L.A., 1990. Quaternary alluvial fans in the Karakoram Mountains. Alluvial Fans: a Field Approach. Wiley, Chichester, p.27-53.

Dey, S., Thiede, R.C., Schildgen, T.F., Wittmann, H., Bookhagen, B., Scherler, D., Jain, V., Strecker, M.R., 2016. Climate-driven sediment aggradation and incision since the late Pleistocene in the NW Himalaya, India. Earth and Planetary Science Letters, 449, p.321-331. https://doi.org/10.1016/j.epsl.2016.05.050

Dietsch, C., Dortch, J., Reynhout, S., Owen, L., Caffee, M., 2015. Very slow erosion and topographic evolution of the Southern Ladakh Range, India. Earth Surface Processes and Landforms, 40, 3, p.389-402. https://doi.org/10.1002/esp.3640

Dong, J., Wang, Y., Cheng, H., Hardt, B., Edwards, R.L., Kong, X., Wu, J., Chen, S., Liu, D., Jiang, X., Zhao, K., 2010. A high-resolution stalagmite record of the Holocene East Asian monsoon from Mt Shennongjia, central China. Holocene 20, 257–264. https://doi.org/10.1177/0959683609350393

Dortch, J.M., Owen, L.A., Haneberg, W.C., Caffee, M.W., Dietsch, C., Kamp, U., 2009. Nature and timing of large landslides in northern India. Quaternary Science Reviews 28, p.1037-1056. https://doi.org/10.1016/j.quascirev.2008.05.002

Dortch, J.M., Dietsch, C., Owen, L.A., Caffee, M.W. and Ruppert, K., 2011a. Episodic fluvial incision of rivers and rock uplift in the Himalaya and Transhimalaya. Journal of the Geological Society, 168(3), p.783-804. https://doi.org/10.1144/0016-76492009-158

Dortch, J., Owen, L., Schoenbohm, L., Caffee, M., 2011b. Asymmetrical erosion and morphological development of the central Ladakh Range, northern India. Geomorphology 135, p.167-180. https://doi.org/10.1016/j.geomorph.2011.08.014

Dortch, J.M., Owen, L.A., Caffee, M.W. and Kamp, U., 2011c. Catastrophic partial drainage of Pangong Tso, northern India and Tibet. Geomorphology, 125(1), p.109-121. https://doi.org/10.1016/j.geomorph.2010.08.017

Dortch, J., Owen, L., Caffee, M., 2013. Timing and climatic drivers for glaciation across semi-arid western Himalayan-Tibetan orogen. Quaternary Science Reviews 78, p.188-208. https://doi.org/10.1016/j.quascirev.2013.07.025

Dühnforth, M., Densmore, A.L., Ivy-Ochs, S., Allen, P.A. and Kubik, P.W., 2007. Timing and patterns of debris flow deposition on Shepherd and Symmes creek fans, Owens Valley, California, deduced from cosmogenic ^{10}Be. Journal of Geophysical Research: Earth Surface, 112(F3). https://doi.org/10.1029/2006JF000562

Dutt, S., Gupta, A.K., Clemens, S.C., Cheng, H., Singh, R.K., Kathayat, G., Edwards, R.L., 2015. Abrupt changes in Indian summer monsoon strength during 33,800 to 5500 years BP. Geophysical Research Letters 42, p.5526–5532. https://doi.org/10.1002/2015GL064015

Dykoski, C.A., Edwards, R.L., Cheng, H., Yuan, D., Cai, Y., Zhang, M., Lin, Y., Qing, J., An, Z., Revenaugh, J., 2005. A high-resolution, absolute-dated Holocene and deglacial Asian monsoon record from Dongge Cave, China. Earth and Planetary Science Letters 233, 71–86. https://doi.org/10.1016/j.epsl.2005.01.036

Eppes, M.C., McFadden, L., 2008. The influence of bedrock weathering on the response of drainage basins and associated alluvial fans to Holocene climates, San Bernardino Mountains, California, USA. The Holocene, 18(6), p.895-905. https://doi.org/10.1177/0959683608093526

Eugster, P., Scherler, D., Thiede, R.C., Codilean, A.T., Strecker, M.R., 2016. Rapid Last Glacial Maximum deglaciation in the Indian Himalaya coeval with midlatitude glaciers: New insights from ^{10}Be-dating of ice-polished bedrock surfaces in the Chandra Valley, NW Himalaya. Geophysical Research Letters, 43(4), p.1589-1597. https://doi.org/10.1002/2015GL066077

Fleitmann, D., Burns, S.J., Mangini, A., Mudelsee, M., Kramers, J., Villa, I., Neff, U., Al-Subbary, A.A., Buettner, A., Hippler, D., Matter, A., 2007. Holocene ITCZ and Indian monsoon dynamics recorded in stalagmites from Oman and Yemen (Socotra). Quaternary Science Reviews 26, 170–188. https://doi.org/10.1016/j.quascirev.2006.04.012

Fleitmann, D., Burns, S.J., Mudelsee, M., Neff, U., Kramers, J., Mangini, A., Matter, A., 2003. Holocene forcing of the Indian monsoon recorded in a stalagmite from southern Oman. Science 300, p.1737–1739. https://doi.org/10.1126/science.1083130

Gabet, E.J., Burbank, D.W., Putkonen, J.K., Pratt-Sitaula, B.A., Ojha, T., 2004. Rainfall thresholds for landsliding in the Himalayas of Nepal. Geomorphology, 63(3-4), p.131-143. https://doi.org/10.1016/j.geomorph.2004.03.011

Gasse, F., Fontes, J.C., Van Campo, E., Wei, K., 1996. Holocene environmental changes in Bangong Co basin (Western Tibet). Part 4: discussion and conclusions. Palaeogeography, Palaeoclimatology, Palaeoecology, 120(1-2), p.79-92. https://doi.org/10.1016/0031-0182(95)00035-6

GeoMappApp (2014), Marine Geoscience Data System, Available from: http://www.geomappap.org (last accessed: 21/08.2014).

Gosse, J., McDonald, E., Finkel, R., 2003, March. Cosmogenic nuclide dating of arid region alluvial fans. In Geological Society of America Abstracts with Programs (Vol. 35, No. 3, p. 8).

Gruber, S., Haeberli, W., 2007. Permafrost in steep bedrock slopes and its temperature-related destabilization following climate change. Journal of Geophysical Research: Earth Surface, 112(F2), doi.org/10.1029/2006JF000547.

Gusain, H.S., Singh, A., Ganju, A., Singh, D., 2004. Characteristics of the seasonal snow-cover of Pir Panjal and Great Himalayan ranges in Indian Himalaya. Proceedings of the International Symposium on Snow Monitoring and Avalanches -2004, Manali, p.97-102.

Hales, T.C., Roering, J.J., 2007. Climatic controls on frost cracking and implications for the evolution of bedrock landscapes. Journal of Geophysical Research: Earth Surface, 112(F2), doi.org/10.1029/2006JF000616.

Hasnain, S.I., Thayyen, R.J., 1996. Sediment transport and solute variation in meltwaters of Dokriani Glacier (Bamak), Garhwal Himalaya. Journal of the Geological Society of India, 47(6), p.731-739.

Hedrick, K., Seong, Y., Owen, L., Caffee, M., Dietsch, C., 2011. Towards defining the transition in style and timing of Quaternary glaciation between the monsoon-influenced Greater Himalaya and the semi-arid Transhimalaya of Northern India. Quaternary International, 236, p.21-33. https://doi.org/10.1016/j.quaint.2010.07.023

Hedrick, K., Owen, L.A., Rockwell, T.K., Meigs, A., Costa, C., Caffee, M.W., Masana, E., Ahumada, E., 2013. Timing and nature of alluvial fan and strath terrace formation in the Eastern Precordillera of Argentina. Quaternary Science Reviews, 80, p.143-168. https://doi.org/10.1016/j.quascirev.2013.05.004

Heimsath, A.M., McGlynn, R., 2008. Quantifying periglacial erosion in the Nepal high Himalaya. Geomorphology, 97(1-2),p.5-23. https://doi.org/10.1016/j.geomorph.2007.02.046

Herzschuh, U., 2006. Palaeo-moisture evolution in monsoonal Central Asia during the last 50,000 years. Quaternary Science Reviews, 25(1-2), p.163-178. https://doi.org/10.1016/j.quascirev.2005.02.006

Hewitt, K., 2009. Glacially conditioned rock-slope failures and disturbance-regime landscapes, Upper Indus Basin, northern Pakistan. Geological Society, London, Special Publications, 320(1), p.235-255. https://doi.org/10.1144/SP320.15

Heyman, J., Stroeven, A., Harbor, J., Caffee, M., 2011. Too young or too old: Evaluating cosmogenic exposure dating based on an analysis of compiled boulder exposure ages. Earth and Planetary Science Letters, 302, p.71-80. https://doi.org/10.1016/j.epsl.2010.11.040

Hobley, D., Sinclair, H., Cowie, P., 2010. Processes, rates, and timescales of fluvial response in an ancient postglacial landscape of the northwest Indian Himalaya. Geological Society of America Bulletin, 122, p.1569–1584. https://doi.org/10.1130/B30048.1

Hu, C., Henderson, G.M., Huang, J., Xie, S., Sun, Y., Johnson, K.R., 2008. Quantification of Holocene Asian monsoon rainfall from spatially separated cave records. Earth and Planetary Science Letters 266, 221–232. https://doi.org/10.1016/j.epsl.2007.10.015

Hudson, A.M., Olsen, J.W., Quade, J., Lei, G., Huth, T.E., Zhang, H., 2016. A regional record of expanded Holocene wetlands and prehistoric human occupation from paleowetland

deposits of the western Yarlung Tsangpo valley, southern Tibetan Plateau. Quat. Res. (United States) 86, 13–33. https://doi.org/10.1016/j.yqres.2016.04.001

Hughes, P., 2010. Geomorphology and Quaternary Stratigraphy: The roles of morpho-, litho- and allostratigraphy.Geomorphology123,p.189-199. https://doi.org/10.1016/j.geomorph.2010.07.025

Hughes, P., Gibbard, P., Woodwad, J., 2005. Quaternary glacial records in mountain regions: a formal stratigraphical approach. Episodes 28, p.85-92.

Jonell, T.N., Owen, L.A., Carter, A., Schwenniger, J.L., Clift, P.D., 2018. Quantifying episodic erosion and transient storage on the western margin of the Tibetan Plateau, upper Indus River. Quaternary Research, 89, p.281–306. https://doi.org/10.1017/qua.2017.92

Jones, P.D., Lister, D.H., Osborn, T.J., Harpham, C., Salmon, M. and Morice, C.P., 2012. Hemispheric and large-scale land-surface air temperature variations: An extensive revision and an update to 2010. Journal of Geophysical Research: Atmospheres, 117(D5). https://doi.org/10.1029/2011JD017139

Kathayat, G., Cheng, H., Sinha, A., Spötl, C., Edwards, R.L., Zhang, H., Li, X., Yi, L., Ning, Y., Cai, Y., Lui, W.L., 2016. Indian monsoon variability on millennial-orbital timescales. Scientific Reports, 6, p.24374.

Kohl, C.P., Nishiizumi, K., 1992. Chemical isolation of quartz for measurement of in situ produced cosmogenic nuclides. Geochimica Cosmochimica Acta 56, p.3583–3587. https://doi.org/10.1016/0016-7037(92)90401-4

Kumar Singh, A., Parkash, B., Mohindra, R., Thomas, J.V., Singhvi, A.K., 2001. Quaternary alluvial fan sedimentation in the Dehradun valley piggyback basin, NW Himalaya: tectonic and palaeoclimatic implications. Basin Research, 13(4), p.449-471.

Kumar, A., Srivastava, P., 2017. The role of climate and tectonics in aggradation and incision of the Indus River in the Ladakh Himalaya during the late Quaternary. Quaternary Research, 87(3), p.363-385. https://doi.org/10.1017/qua.2017.19

Lavé, J., Avouac, J.P., 2001. Fluvial incision and tectonic uplift across the Himalayas of central Nepal. Journal of Geophysical Research: Solid Earth, 106(B11), p.26561-26591. https://doi.org/10.1029/2001JB000359

Leland, J., Reid, M.R., Burbank, D.W., Finkel, R., Caffee, M., 1998. Incision and differential bedrock uplift along the Indus River near Nanga Parbat, Pakistan Himalaya, from ^{10}Be and ^{26}Al exposure age dating of bedrock straths. Earth and Planetary Science Letters, 154(1-4), p.93-107. https://doi.org/10.1016/S0012-821X(97)00171-4

Lee, S.Y., Seong, Y.B., Owen, L. a., Murari, M.K., Lim, H.S., Yoon, H. Il, Yoo, K.C., 2014. Late Quaternary glaciation in the Nun-Kun massif, northwestern India. Boreas 43, p.67–89. https://doi.org/10.1111/bor.12022

Leipe, C., Demske, D., Tarasov, P.E., 2014. A Holocene pollen record from the northwestern Himalayan lake Tso Moriri: implications for palaeoclimatic and archaeological research. Quaternary International, 348, p.93-112. https://doi.org/10.1016/j.quaint.2013.05.005

Leuschner, D., Sirocko, F., 2003. Orbital insolation forcing of the Indian Monsoon- a motor for global climate changes? Paleogeography, Paleoclimatology, Paleoecology, 197, p.83-95. https://doi.org/10.1016/S0031-0182(03)00387-0

Lifton, N., Sato, T., Dunai, T., 2014. Scaling in situ cosmogenic nuclide production rates using analytical approximations to atmospheric cosmic-ray fluxes. Earth and Planetary Science Letters, 386, p.149-160. https://doi.org/10.1016/j.epsl.2013.10.052

Lisiecki, L., Raymo, M., 2005. A Pliocene-Pleistocene stack of 57 globally distributed benthic δ^{18}O records. Paleoceanography, 20, p.1. https://doi.org/10.1029/2004PA001071

Liu, X., Dong, B., 2013. Influence of the Tibetan Plateau uplift on the Asian monsoon-arid environment evolution. Chinese Science Bulletin, 58(34), p.4277-4291. . https://doi.org/10.1007/s11434-013-5987-8

Martin, L., Blard, P., Balco, G., Laurent, V., 2017. The CREp program and the ICE-D production rate calibration database: A fully parameterizable and updated online tool to compute cosmic-ray exposure ages. Quaternary Geochronology, 38, p.25-49. https://doi.org/10.1016/j.quageo.2016.11.006

Mishra, P.K., Anoop, A., Schettler, G., Prasad, S., Jehangir, A., Menzel, P., Naumann, R., Yousuf, A.R., Basavaiah, N., Deenadayalan, K., Wiesner, M.G., 2015. Reconstructed late Quaternary hydrological changes from Lake Tso Moriri, NW Himalaya. Quaternary International, 371, p.76-86. https://doi.org/10.1016/j.quaint.2014.11.040

Mix, A.C., Bard, E., Schneider, R., 2001. Environmental processes of the ice age: land, ocean, glaciers (EPILOG). Quaternary Science Reviews 20, p.627–657. https://doi.org/10.1016/S0277-3791(00)00145-1

Mölg, T., Maussion, F., Scherer, D., 2014. Mid-latitude westerlies as a driver of glacier variability in monsoonal High Asia. Nature Climate Change, 4(1), p.68. https://doi.org/10.1038/nclimate2055

Murari, M.K., Owen, L.A., Dortch, J.M., Caffee, M.W., Dietsch, C., Fuchs, M., Haneberg, W.C., Sharma, M.C., Townsend-Small, A., 2014. Timing and climatic drivers for glaciation across monsoon-influenced regions of the Himalayan–Tibetan orogen. Quaternary Science Reviews, 88, p.159-182. https://doi.org/10.1006/qres.1999.2108

Nagai, H., Fujita, K., Nuimura, T., Sakai, A., 2013. Southwest-facing slopes control the formation of debris-covered glaciers in the Bhutan Himalaya. The Cryosphere, 7(4), p.1303. https://doi.org/10.5194/tc-7-1303-2013

Nicholas, A.P., Quine, T.A., 2007. Modeling alluvial landform change in the absence of external environmental forcing. Geology, 35(6), p.527-530. https://doi.org/10.1130/G23377A.1

Nishiizumi, K., Finkel, R.C., Caffee, M.W., Southon, J.R., Kohl, C.P., Arnold, J.R., Olinger, C.T., Poths, J., Klein, J., 1994. Cosmogenic production of ^{10}Be and ^{26}Al on the surface of the earth and underground. In Eighth International Conference on Geochronology, Cosmochronology and Isotope Geology: US Geological Survey Circular, 1107, p. 234. https://doi.org/10.1016/j.nimb.2007.01.297

Orr, E., Owen, L., Murari, M., Saha, S., Caffee, M., 2017. The timing and extent of Quaternary glaciation of Stok, northern Zanskar Range, Transhimalaya, of northern India. Geomorphology 284, p.142-155. https://doi.org/10.1016/j.geomorph.2016.05.031

Orr, E.N., Owen, L.A., Saha, S., Caffee, M.W., Murari, M.K., 2018. Quaternary glaciation of the Lato Massif, Zanskar Range of the NW Himalaya. Quaternary Science Reviews, 183, p.140-156. https://doi.org/10.1016/j.quascirev.2018.01.005

Owen, L.A., Benn, D.I., Derbyshire, E., Evans, D.J.A., Mitchell, W.A., Thompson, D., Richardson, S., Lloyd, M., Holden, C., 1995. The geomorphology and landscape evolution of the Lahul Himalaya, Northern India. Zeitschrift für Geomorphologie, 39, p.145-174. https://ci.nii.ac.jp/naid/10009483085/

Owen, L., 2009. Latest Pleistocene and Holocene glacier fluctuations in the Himalaya and Tibet. Quaternary Science Reviews 28, 21-22, p.2150-2164. https://doi.org/10.1016/j.quascirev.2008.10.020

Owen, L., Dortch, J., 2014. Nature and timing of Quaternary glaciation in the Himalayan-Tibetan orogen. Quaternary Science Reviews 88, p.14-54. https://doi.org/10.1016/j.quascirev.2013.11.016

Owen, L.A., Sharma, M.C., 1998. Rates and magnitudes of paraglacial fan formation in the Garhwal Himalaya: implications for landscape evolution. Geomorphology, 26(1-3), p.171-184. https://doi.org/10.1016/S0169-555X(98)00057-9

Owen, L.A., Gualtieri, L.Y.N., Finkel, R.C., Caffee, M.W., Benn, D.I., Sharma, M.C., 2001. Cosmogenic radionuclide dating of glacial landforms in the Lahul Himalaya, northern India: defining the timing of Late Quaternary glaciation. Journal of Quaternary Science, 16(6), p.555-563. https://doi.org/10.1002/jqs.621

Owen, L.A., Frankel, K.L., Knott, J.R., Reynhout, S., Finkel, R.C., Dolan, J.F., Lee, J., 2011. Beryllium-10 terrestrial cosmogenic nuclide surface exposure dating of Quaternary landforms in Death Valley. Geomorphology, 125(4), p.541-557. https://doi.org/10.1016/j.geomorph.2010.10.024

Owen, L.A., Clemmens, S.J., Finkel, R.C., Gray, H., 2014. Late Quaternary alluvial fans at the eastern end of the San Bernardino Mountains, Southern California. Quaternary Science Reviews, 87, p.114-134. https://doi.org/10.1016/j.geomorph.2010.10.024

Pope, R.J., Wilkinson, K.N., 2005. Reconciling the roles of climate and tectonics in Late Quaternary fan development on the Spartan piedmont, Greece. Geological Society, London, Special Publications, 251(1), p.133-152. https://doi.org/10.1144/GSL.SP.2005.251.01.10

Pratt, B., Burbank, D.W., Heimsath, A., Ojha, T., 2002. Impulsive alluviation during early Holocene strengthened monsoons, central Nepal Himalaya. Geology, 30(10), p.911-914. https://doi.org/10.1130/0091-7613(2002)030<0911:IADEHS>2.0.CO;2

Qiang, X.K., Li, Z.X., Powell, C.M., Zheng, H.B., 2001. Magnetostratigraphic record of the Late Miocene onset of the East Asian monsoon, and Pliocene uplift of northern Tibet. Earth and Planetary Science Letters, 187, 1-2, p.83-93. https://doi.org/10.1016/S0012-821X(01)00281-3

Rawat, S., Gupta, A.K., Srivastava, P., Sangode, S.J., Nainwal, H.C., 2015. A 13,000 year record of environmental magnetic variations in the lake and peat deposits from the Chandra valley, Lahaul: Implications to Holocene monsoonal variability in the NW Himalaya. Palaeogeography, Palaeoclimatology, Palaeoecology 440, 116–127. https://doi.org/10.1016/j.palaeo.2015.08.044

Ritter, J.B., Miller, J.R., Enzel, Y., Wells, S.G., 1995. Reconciling the roles of tectonism and climate in Quaternary alluvial fan evolution. Geology, 23(3), p.245-248. https://doi.org/10.1130/0091-7613(1995)023<0245:RTROTA>2.3.CO;2

Saha, S., Owen, L.A., Orr, E.N., Caffee, M.W., 2018. Timing and nature of Holocene glacier advances at the northwestern end of the Himalayan-Tibetan orogen. Quaternary Science Reviews, 187, p.177-202. https://doi.org/10.1016/j.quascirev.2018.03.009

Scherler, D., Bookhagen, B., Strecker, M.R., 2014. Tectonic control on ^{10}Be-derived erosion rates in the Garhwal Himalaya, India. Journal of Geophysical Research: Earth Surface, 119(2), p.83-105. https://doi.org/10.1002/2013JF002955

Scherler, D., Bookhagen, B., Wulf, H., Preusser, F., Strecker, M.R., 2015. Increased late Pleistocene erosion rates during fluvial aggradation in the Garhwal Himalaya, northern India. Earth and Planetary Science Letters, 428, p.255-266. https://doi.org/10.1016/j.epsl.2015.06.034

Schlup, M., Carter, A., Cosca, M., Steck, A., 2003. Exhumation history of eastern Ladakh revealed by 40Ar/39Ar and fission-track ages: the Indus River- Tso Morari transect, NW Himalayas. Journal of the Geological Society, 160, p.385-399. https://doi.org/10.1144/0016-764902-084

Searle, M., 1986. Structural evolution and sequence of thrusting in the High Himalayan, Tibetan-Tethys and Indus suture zones of Zanskar and Ladakh, Western Himalaya. Journa of Structural Geology, 8,8, p.923-936. https://doi.org/10.1016/0191-8141(86)90037-4

Seong, Y.B., Owen, L.A., Bishop, M.P., Bush, A., Clendon, P., Copland, L., Finkel, R., Kamp, U., Shroder, J.F., 2007. Quaternary glacial history of the Central Karakoram. Quaternary Science Reviews 26, p.3384–3405. https://doi.org/10.1016/j.quascirev.2007.09.015

Sharma, P., Bourgeois, M., Elmore, D., Granger, D., Lipschutz, M.E., Ma, X., Miller, T., Mueller, K., Rickey, F., Simms, P., Vogt, S. (2000) PRIME lab AMS performance, upgrades and research applications. Nuclear Instruments and Methods in Physics Research, B 172, p.112-123. https://doi.org/10.1016/S0168-583X(00)00132-4

Shi, Y., Yu, G., Liu, X., Li, B., Yao, T., 2001. Reconstruction of the 30–40 ka BP enhanced Indian monsoon climate based on geological records from the Tibetan Plateau. Palaeogeography, Palaeoclimatology, Palaeoecology, 169(1-2), p.69-83. https://doi.org/10.1016/j.quascirev.2017.07.017

Simpson, G., Castelltort, S., 2012. Model shows that rivers transmit high-frequency climate cycles to the sedimentary record. Geology, 40(12), p.1131-1134. https://doi.org/10.1130/G33451.1

Sinha, A., Cannariato, K.G., Stott, L.D., Li, H.C., You, C.F., Cheng, H., Edwards, R.L., Singh, I.B., 2005. Variability of Southwest Indian summer monsoon precipitation during the Bølling-Allerød. Geology, 33(10), p.813-816. https://doi.org/10.1130/G21498.1

Srivastava, D., 2012. Status report on Gangotri glacier. Science and Engineering Research Board, Department of Science and Technology, New Delhi, Himalayan Glaciology Technical Report, 3, p.21-25.

Srivastava, P., Tripathi, J.K., Islam, R., Jaiswal, M.K., 2008. Fashion and phases of late Pleistocene aggradation and incision in the Alaknanda River Valley, western Himalaya, India. Quaternary Research, 70(1), p.68-80. https://doi.org/10.1016/j.yqres.2008.03.009

Srivastava, P., Agnihotri, R., Sharma, D., Meena, N., Sundriyal, Y.P., Saxena, A., Bhushan, R., Sawlani, R., Banerji, U.S., Sharma, C., Bisht, P., Rana, N., Jayangondaperumal, R., 2017. 8000-year monsoonal record from Himalaya revealing reinforcement of tropical and global climate systems since mid-Holocene. Scientific Reports 7, 1–10. https://doi.org/10.1038/s41598-017-15143-9.

Strahler, A.N., 1952. Hypsometric (area-altitude) analysis of erosional topography. Geological Society of America Bulletin, 63(11), p.1117-1142. https://doi.org/10.1130/0016-7606(1952)63[1117:HAAOET]2.0.CO;2

Steck, A., Epard, J., Vannay, J., Hunziker, J., Girard, M., Morard, A., Robyr, M., 1998. Geological transect across the Tso Morari and Spiti areas- the nappe structures of the Tethys Himalayas. Eclogae Geologicae Helvetiae 91, p.103-121. https://doi.org/10.1007/s00015-003-1091-

Su, Z., Shi, Y., 2002. Response of monsoonal temperate glaciers to global warming since the Little Ice Age. Quaternary International, 97, p.123-131. https://doi.org/10.1016/S1040-6182(02)00057-5

Thakur, V., Joshi, M., Sahoo, D., Suresh, N., Jayangondapermal, R., Singh, A., 2014. Partitioning of convergence in Northwest Sub-Himalaya: estimation of late Quaternary uplift and convergence rates across the Kangra reentrant, North India. International Journal of Earth Science. 103, p.1037-1056. https://doi.org/10.1007/s00531-014-1016-7

Thiede, R.C., Bookhagen, B., Arrowsmith, J.R., Sobel, E.R., Strecker, M.R., 2004. Climatic control on rapid exhumation along the Southern Himalayan Front. Earth and Planetary Science Letters, 222(3-4), p.791-806. https://doi.org/10.1016/j.epsl.2004.03.015

Thompson, L.O., Yao, T., Davis, M.E., Henderson, K.A., Mosley-Thompson, E., Lin, P.N., Beer, J., Synal, H.A., Cole-Dai, J., Bolzan, J.F., 1997. Tropical climate instability: The last glacial cycle from a Qinghai-Tibetan ice core. Science, 276(5320), p.1821-1825. https://doi.org/10.1126/science.276.5320.1821

Uppala, S.M., Kållberg, P.W., Simmons, A.J., Andrae, U., Bechtold, V.D., Fiorino, M., Gibson, J.K., Haseler, J., Hernandez, A., Kelly, G.A., Li, X., 2005. The ERA-40 re-analysis. Quarterly Journal of the royal meteorological society, 131(612), p.2961-3012. https://doi.org/10.1256/qj.04.176

Vannay, C., Grasemann, B., Rahn, M., Frank, W., Carter, A., Baudraz, V., Cosca, M., 2004. Miocene to Holocene exhumation of metamorphic crustal wedges in the NW Himalaya: Evidence for tectonic extrusion coupled to fluvial erosion. Tectonics, 23, p.1-24. https://doi.org/10.1029/2002TC001429

Wagnon, P., Linda, A., Arnaud, Y., Kumar, R., Sharma, P., Vincent, C., Pottakkal, J.G., Berthier, E., Ramanathan, A., Hasnain, S.I., Chevallier, P., 2007. Four years of mass balance on Chhota Shigri Glacier, Himachal Pradesh, India, a new benchmark glacier in the western Himalaya. Journal of Glaciology, 53(183), p.603-611. https://doi.org/10.3189/002214307784409306

Wang, Y., Cheng, H., Edwards, R.L., He, Y., Kong, X., An, Z., Wu, J., Kelly, M.J., Dykoski, C.A., Li, X., 2005. The Holocene Asian Monsoon : Links to Solar Changes and North Atlantic Climate 854–858. https://doi.org/10.1126/science.1106296

Watanabe, T., Dali, L., Shiraiwa, T., 1998. Slope denudation and the supply of debris to cones in Langtang Himal, Central Nepal Himalaya. Geomorphology, 26(1-3), p.185-197. https://doi.org/10.1016/S0169-555X(98)00058-0

Wittmann, H., Von Blanckenburg, F., 2009. Cosmogenic nuclide budgeting of floodplain sediment transfer. Geomorphology, 109(3-4), p.246-256. https://doi.org/10.1016/j.geomorph.2009.03.006

Wulf, H., Bookhagen, B., Scherler, D., 2010. Seasonal precipitation gradients and their impact on fluvial sediment flux in the Northwest Himalaya. Geomorphology, 118, 1-2, p.13-21. https://doi.org/10.1016/j.geomorph.2009.12.003

Wünnemann, B., Demske, D., Tarasov, P., Kotlia, B.S., Reinhardt, C., Bloemendal, J., Diekmann, B., Hartmann, K., Krois, J., Riedel, F., Arya, N., 2010. Hydrological evolution during the last 15 kyr in the Tso Kar lake basin (Ladakh, India), derived from geomorphological, sedimentological and palynological records. Quaternary Science Reviews, 29(9-10), p.1138-1155. https://doi.org/10.1016/j.quascirev.2010.02.017

Zehfuss, P.H., Bierman, P.R., Gillespie, A.R., Burke, R.M., Caffee, M.W., 2001. Slip rates on the Fish Springs fault, Owens Valley, California, deduced from cosmogenic ^{10}Be and ^{26}Al and soil development on fan surfaces. Geological Society of America Bulletin, 113(2), p.241-255. https://doi.org/10.1130/0016-7606(2001)113<0241:SROTFS>2.0.CO;2

11. Supplementary Items

11.1 Supplementary Geomorphic Maps

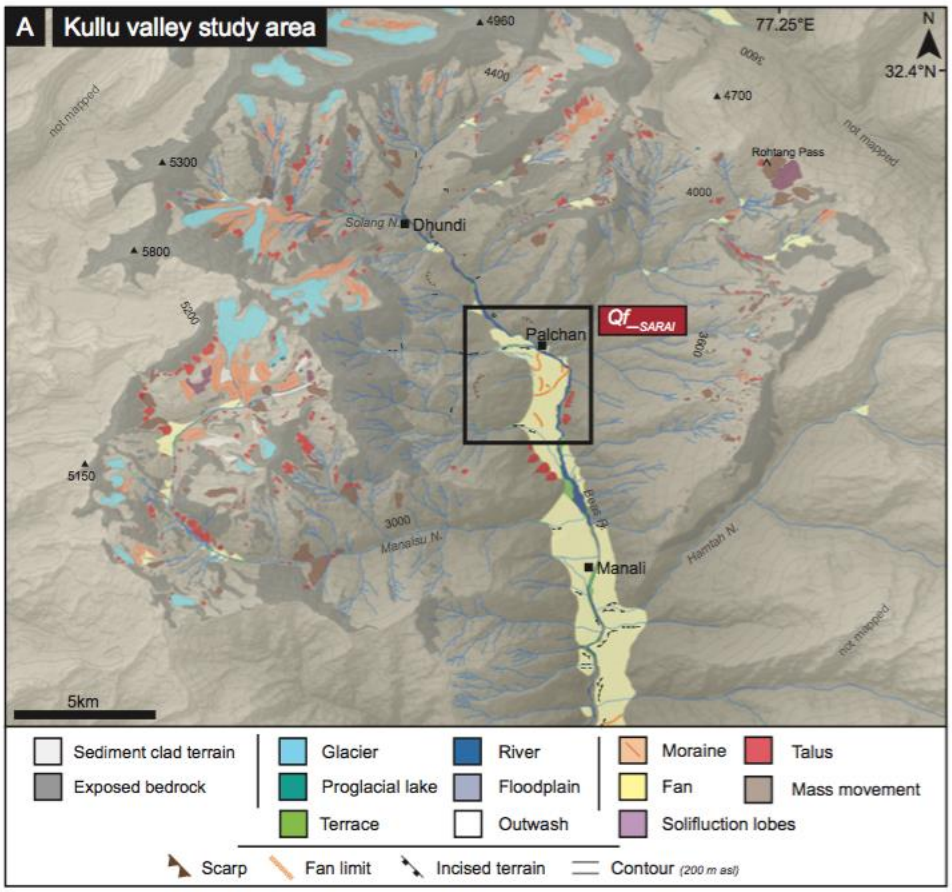

SI_0. Geomorphology and locations of the Kullu, Chandra and Karzok study areas (*Focus 3*). Black rectangles outline the detailed geomorphic maps shown in Fig 7. A) Kullu valley study area. B) Chandra valley study area. C) Karzok valley study area. Inset hillshade map shows the location of the study area (dashed black polygon) and the *Kar_M1* moraine (includes ^{10}Be boulder sample locations).

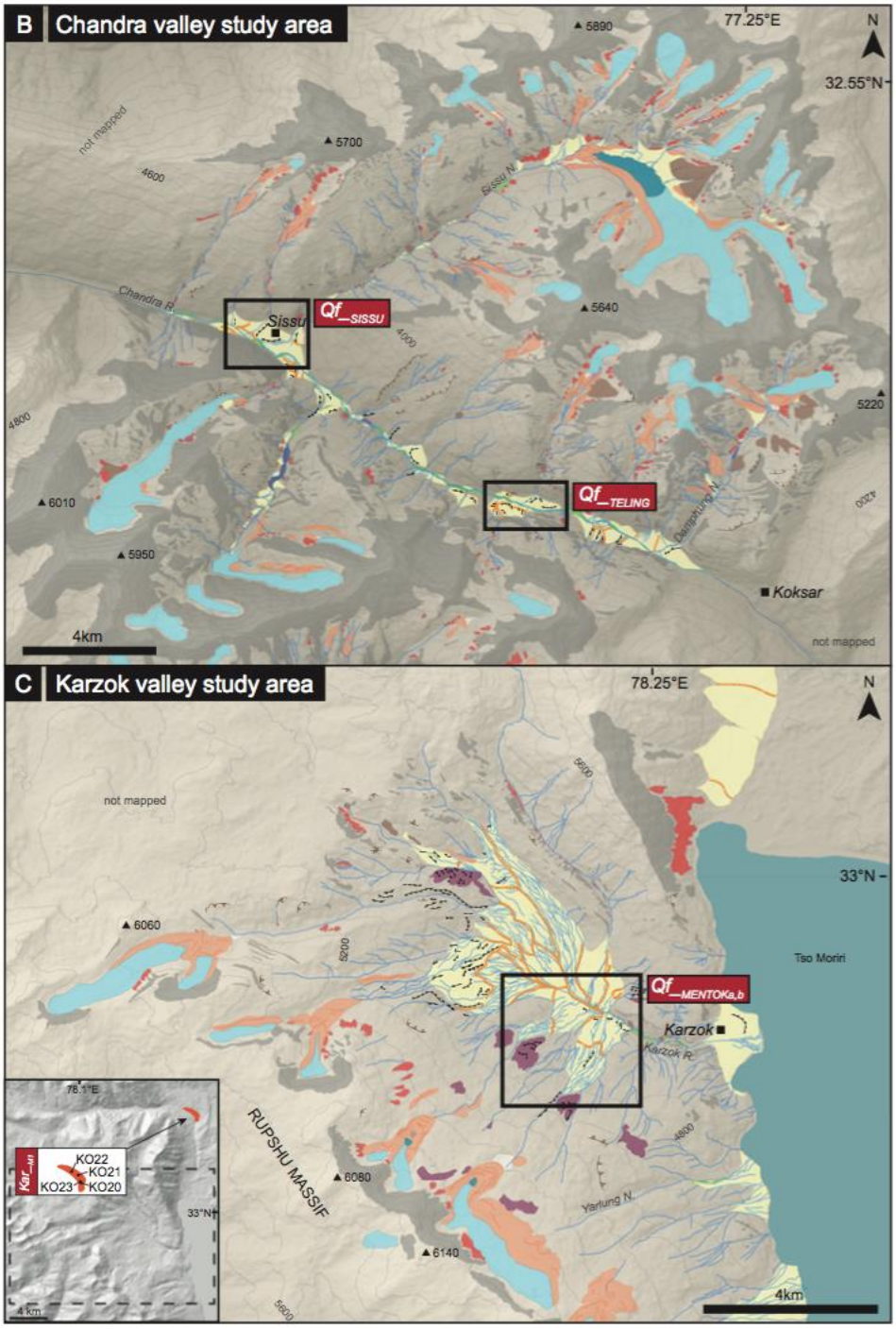
B Chandra valley study area
77.25°E
N
32.55°N
▲5890
▲5700
not mapped
4600
Sissu N.
Chandra R.
Sissu
Qf_SISSU
▲5640
4000
5220
4800
▲6010
▲5950
Qf_TELING
Dempjung N.
Koksar
4km
not mapped
C Karzok valley study area
78.25°E
N
not mapped
5800
33°N
▲6060
5000
Tso Moriri
Qf_MENTOKa,b
Karzok
Karzok R.
78.1°E
KO22
KO21
KO23
KO20
33°N
RUPSHU MASSIF
4800
▲6080
Yarlung N.
▲6140
4km
5800

SI_0. cont.

11.2. Supplementary Items (Manuscript 1)

Supplementary Item 1. Adjusted ^{10}Be concentrations and interpreted bedrock slope erosion rates for the upper Bhagirathi catchment

	Medial moraine	**Max. distance of debris transport[1]** (km)	**Max. ^{10}Be inheritance during debris transport[2]**				**^{10}Be inheritance during debris transport[3]**			
			Duration of transport (a)	^{10}Be production (10^4 at/g)	Adjusted ^{10}Be conc. (10^4 at/g)	Adjusted erosion rate (mm/a)	Duration of transport (a)	^{10}Be production (10^4 at/g)	Adjusted ^{10}Be conc. (10^4 at/g)	Adjusted erosion rate (mm/a)
G_{sup1}	SD_A	9	450	4.3	-3.2	-	188	0.8	0.3	18.2
G_{sup2}	SD_A	12	475	4.5	-3.0	-	198	0.8	0.8	7.4
G_{sup3}	SD_B	12.5	600	5.7	-3.1	-	250	1.0	1.7	3.4
G_{sup4}	SD_B	9.5	625	6.0	-3.5	-	260	1.0	1.4	3.9
G_{sup5}	SD_B	14.5	725	6.9	-4.3	-	302	1.2	1.4	4.1
G_{sup6}	SD_C	14.5	725	6.9	-5.4	-	302	1.2	0.3	18.7

1:Estimated using a SRTM DEM (30 m resolution), measuring from the highest elevation of the medial moraine to the sampling location.
2: Inheritance during transport calculated with mean production rate of 95.4±12.2 at/g/a and a glacier surface velocity of 20 m/a (Bhattacharya et al., 2016).
3: Inheritance during transport calculated with a production rate of 40 at/g/a and a glacier surface velocity of 48±4.8 m/a (Bhattacharya et al., 2016).
−: Estimated ^{10}Be production on medial moraine exceeds ^{10}Be concentration measured. Erosion rates are not derived.

Supplementary Item 2. Cross-sections of Gangotri medial moraines at sampling locations. Sections are referenced to the highest point in each profile. Refer to Fig. 2 for the sampling locations.

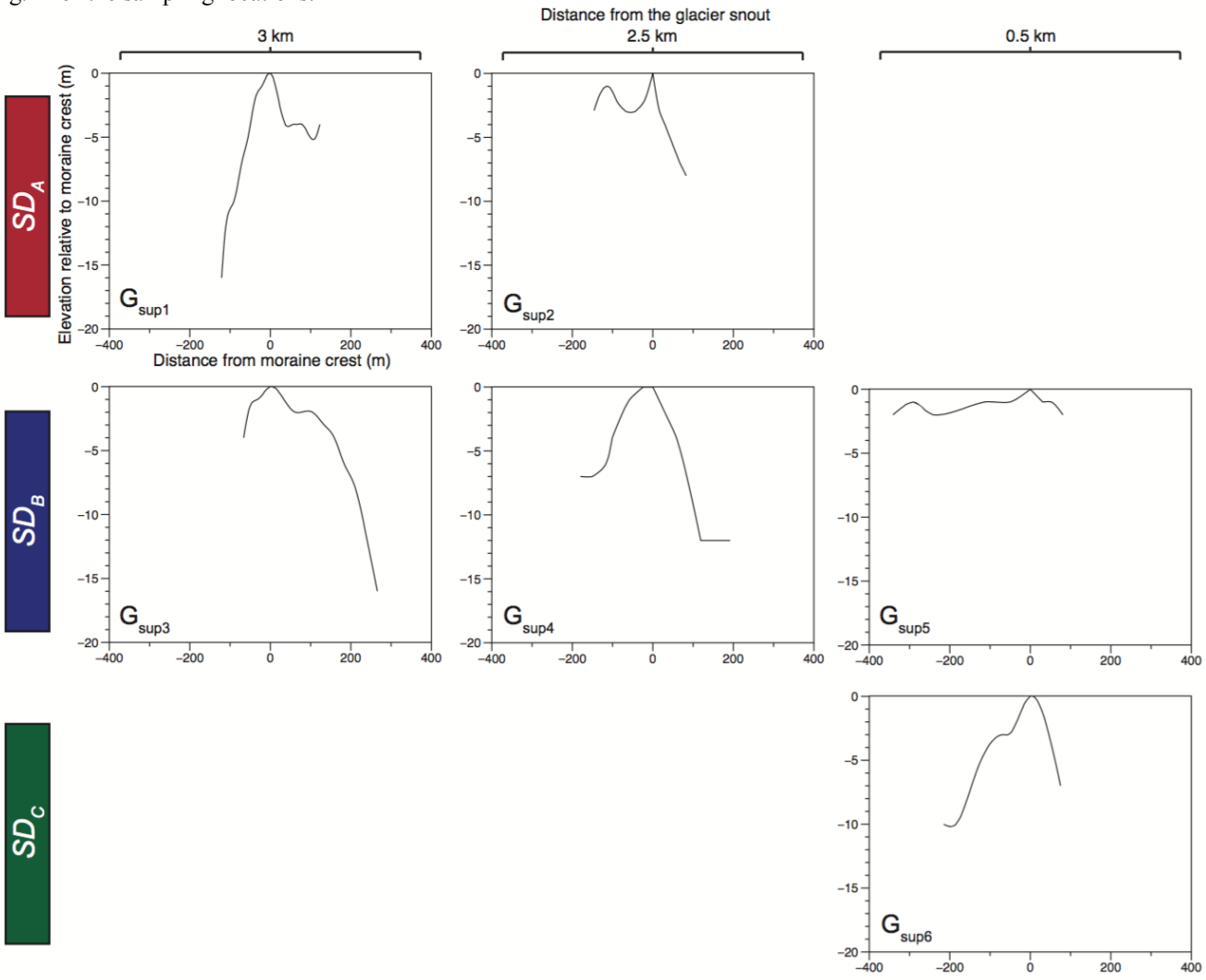

Supplementary Item 3. SEM images of Gangotri medial moraine samples. G_{sup1} i) 350x mag ii) 500x mag iii) 1000x mag. G_{sup2} i) 80x mag, ii) 350x mag, iii) 500x mag. G_{sup3} i) 120x mag, ii) 200x mag, iii) 650x mag. G_{sup4} i) 150x mag, ii) 120x mag, iii) 250x mag. G_{sup5} i) 120x mag, ii) 350x mag, iii) 500x mag. G_{sup6} i) 100x mag, ii) 200x mag, iii) 1000x mag.

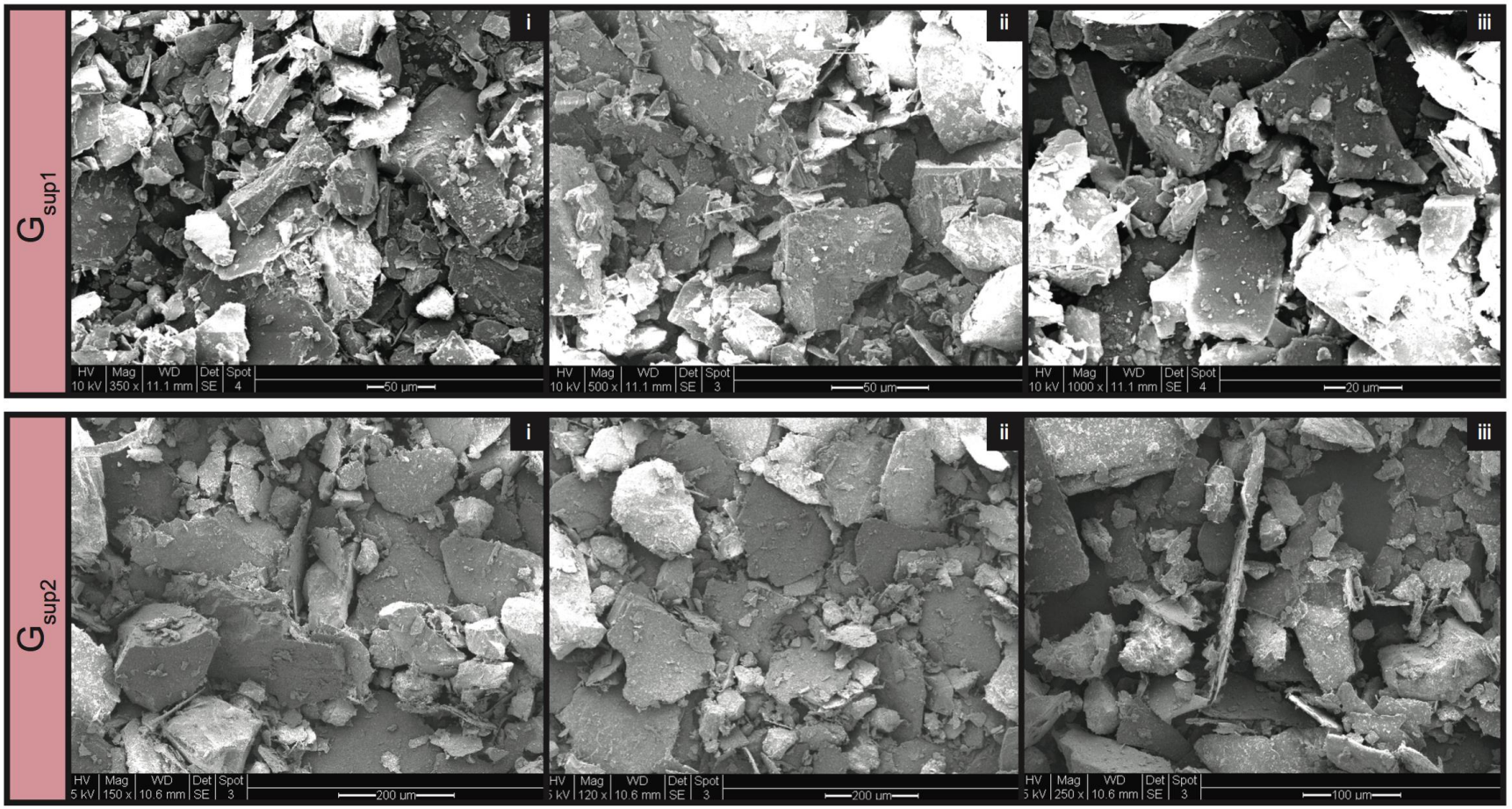

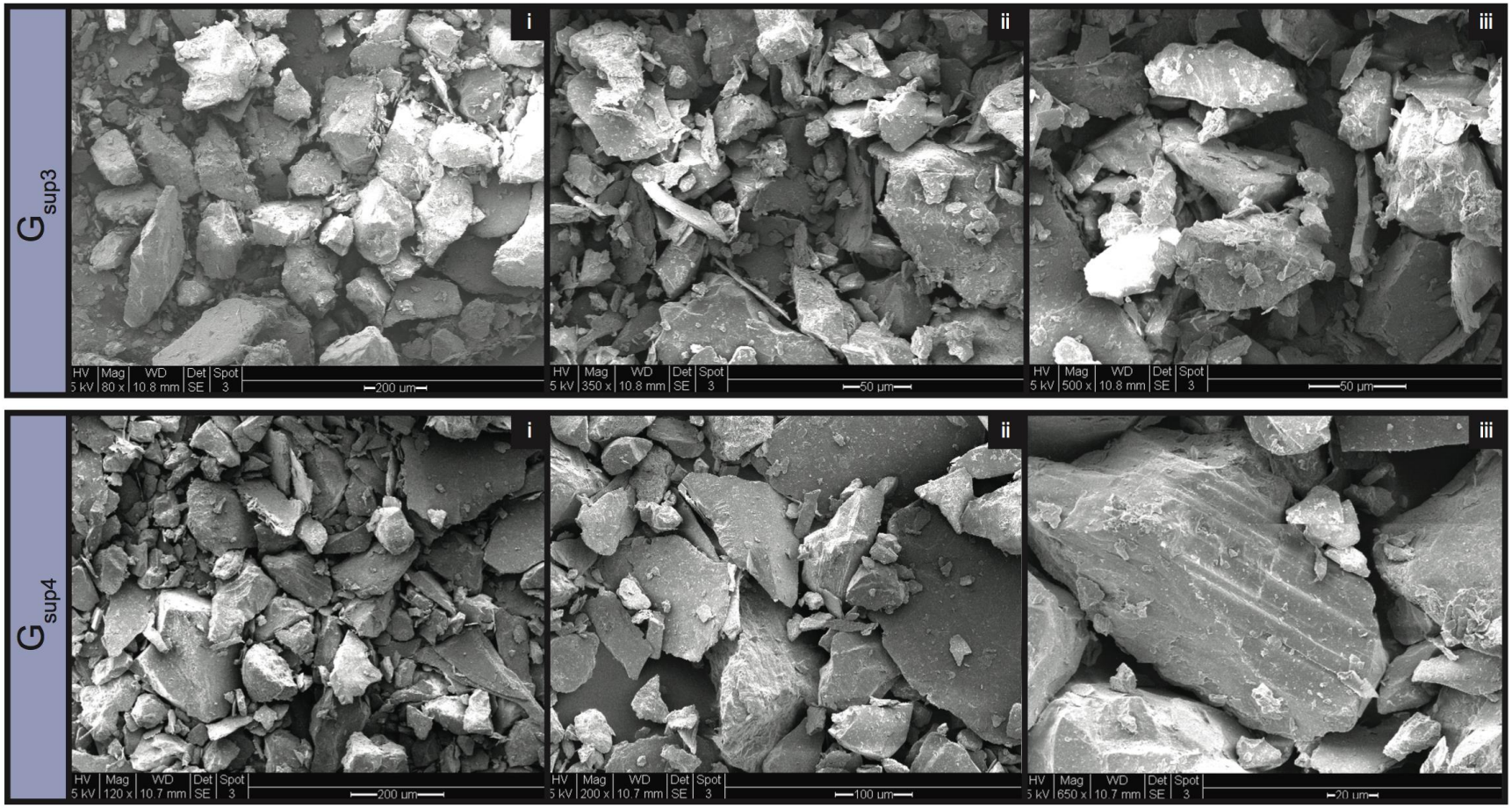
G sup3
i
HV 5 kV | Mag 80 x | WD 10.8 mm | Det SE | Spot 3
200 µm
ii
HV 5 kV | Mag 350 x | WD 10.8 mm | Det SE | Spot 3
50 µm
iii
HV 5 kV | Mag 500 x | WD 10.8 mm | Det SE | Spot 3
50 µm
G sup4
i
HV 5 kV | Mag 120 x | WD 10.7 mm | Det SE | Spot 3
200 µm
ii
HV 5 kV | Mag 200 x | WD 10.7 mm | Det SE | Spot 3
100 µm
iii
HV 5 kV | Mag 650 x | WD 10.7 mm | Det SE | Spot 3
20 µm

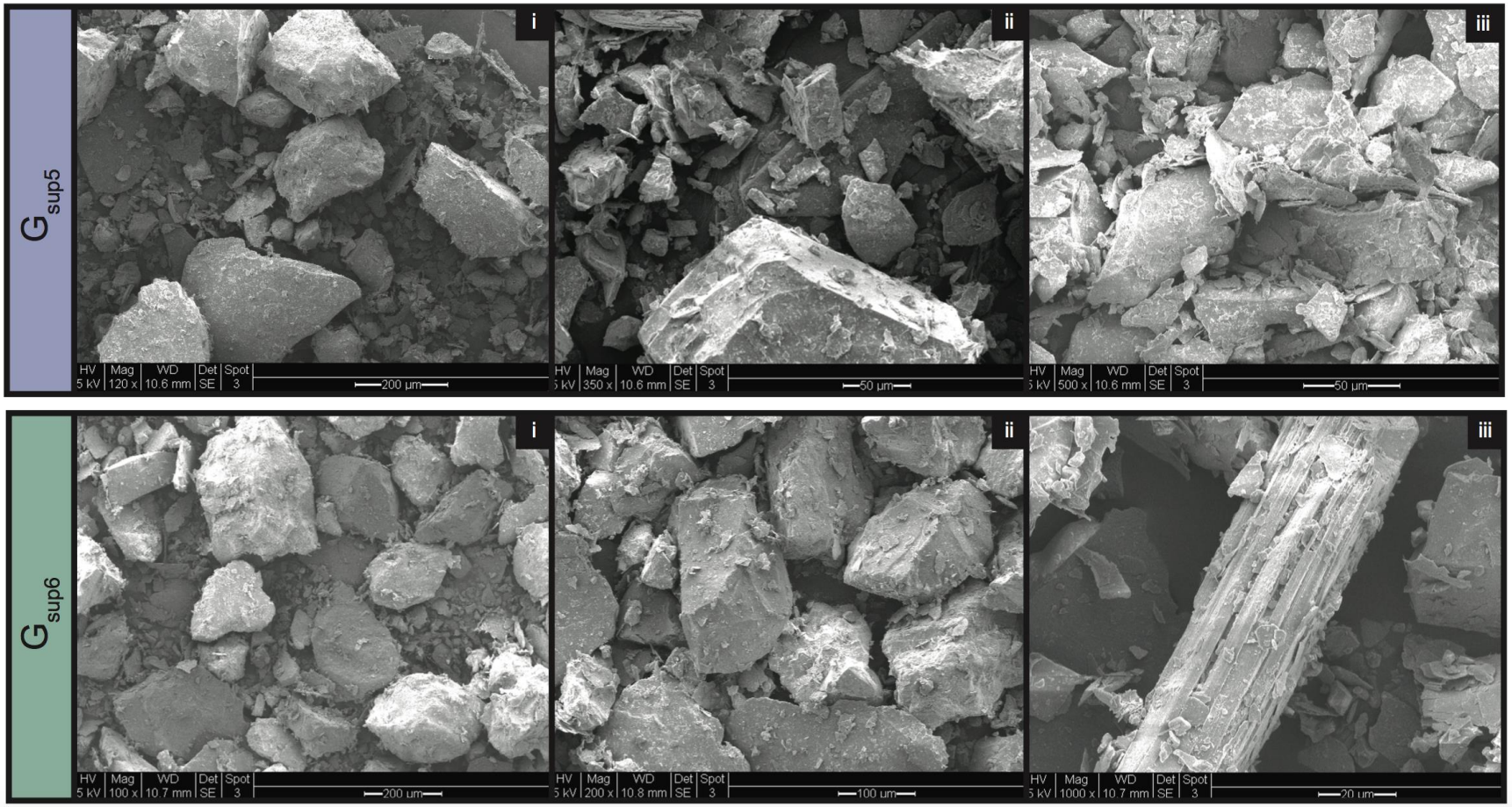
G_{sup5}
i
HV 5 kV | Mag 120 x | WD 10.6 mm | Det SE | Spot 3
200 µm
ii
HV 5 kV | Mag 350 x | WD 10.6 mm | Det SE | Spot 3
50 µm
iii
HV 5 kV | Mag 500 x | WD 10.6 mm | Det SE | Spot 3
50 µm
G_{sup6}
i
HV 5 kV | Mag 100 x | WD 10.7 mm | Det SE | Spot 3
200 µm
ii
HV 5 kV | Mag 200 x | WD 10.8 mm | Det SE | Spot 3
100 µm
iii
HV 5 kV | Mag 1000 x | WD 10.7 mm | Det SE | Spot 3
20 µm

Supplementary Item 4. Percentage grain size distribution of Gangotri medial moraine samples.

	Grain size[1]	***SD*$_A$**		***SD*$_B$**			***SD*$_C$**
	(mm)	G_{sup1} (%)	G_{sup2} (%)	G_{sup3} (%)	G_{sup4} (%)	G_{sup5} (%)	G_{sup6} (%)
Coarse gravel	16-32	1.3	1.5	2.1	0	3.4	4.2
Medium gravel	8-16	4.7	6.4	5.5	1.5	7	9.6
	Total	6	7.9	7.6	1.5	10.4	13.8
Fine gravel	4-8	16.1	33.3	9.7	6.7	20	19.9
V. fine gravel	2-4	13.5	21.7	8.4	6.7	14.1	13.6
	Total	29.6	55	18.1	13.4	34.1	33.5
V. coarse sand	1-2	11.8	13.7	15.6	16	14.1	13.6
Coarse sand	0.5-1	9.8	4.9	15.6	19.5	10.1	11.6
Medium sand	0.25-0.5	14.2	7.4	15.6	27.3	12.9	14.3
	Total	35.8	26	46.8	62.8	37.1	39.5
Fine sand	0.125-0.25	15.8	5.1	11	12.6	9.7	6.7
V. fine sand	0.075-0.125	8.3	4.4	10	6.7	6.8	4.1
	Total	24.1	9.5	21	19.3	16.5	10.8
Silt and clay	<0.075	4.4	1.6	6.6	3.2	3	2.5

1: Wentworth (1922)

Supplementary Item 5. Particle shape details for Gangotri medial moraine samples.

	Angularity Index[1]						**Spherity Index[2]**		**Clast shape[3]**									
	Very angular (%)	Angular (%)	Sub-angular (%)	Sub-rounded (%)	Rounded (%)	Well rounded (%)	High (%)	Low (%)	Compact (%)	Compact-Platy (%)	Compact-Bladed (%)	Compact-Elongate (%)	Platy (%)	Bladed (%)	Elon-gate (%)	Very-Platy (%)	Very-Bladed (%)	Very-Elongate (%)
SD_A																		
G_{sup1}	18	32	43	6	1	0	18	82	3	4	3	2	8	12	11	15	31	11
G_{sup2}	26	48	19	7	0	0	24	76	3	0	6	5	6	20	8	12	34	6
SD_B																		
G_{sup3}	11	37	46	6	0	0	29	71	1	4	5	6	7	16	10	11	36	4
G_{sup4}	14	37	37	12	0	0	20	80	4	2	6	4	2	14	6	13	37	12
G_{sup5}	24	43	26	7	0	0	23	77	3	4	2	8	7	23	7	6	30	10
SD_C																		
G_{sun6}	12	45	28	15	0	0	20	80	0	0	1	0	7	13	5	28	40	6

1: Powers (1953)
2: Zingg (1935)
3: Snead and Folk (1958), Graham and Midgley (2000)

Supplementary Item 6. Roundness and Sphericity Index for individual grain size fractions of Gangotri medial moraine samples. A) coarse-medium gravel, B) fine gravel, C) coarse-medium sand, D) fine sand, E) silt-clay, F) sample summary (appears as Fig. 7).

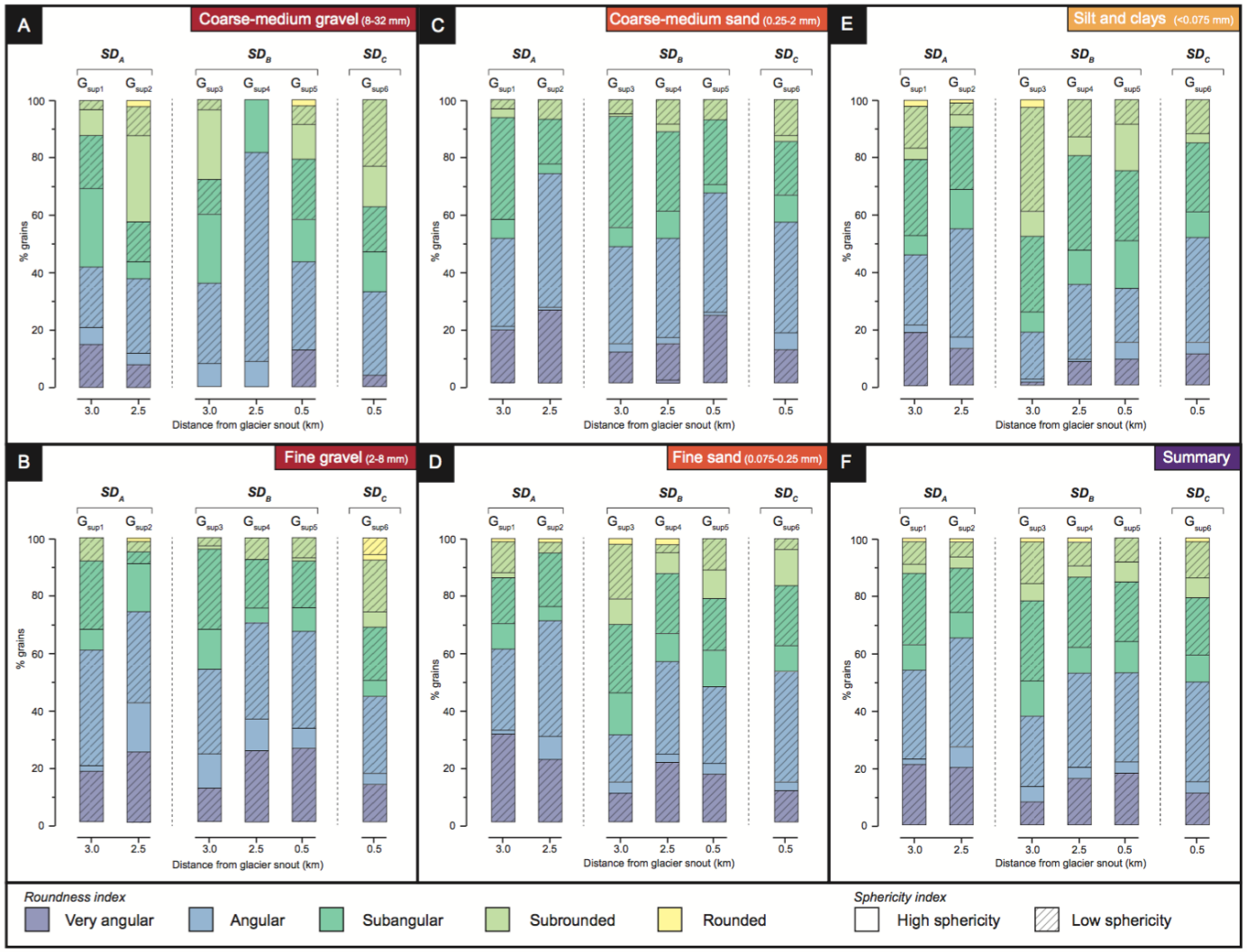

Supplementary Item 7. Clast shape of Gangotri medial moraine samples (ternary diagrams using methods of Graham and Midgley, 2000). upper) Clast shape categories defined by Snead and Folk (1958).

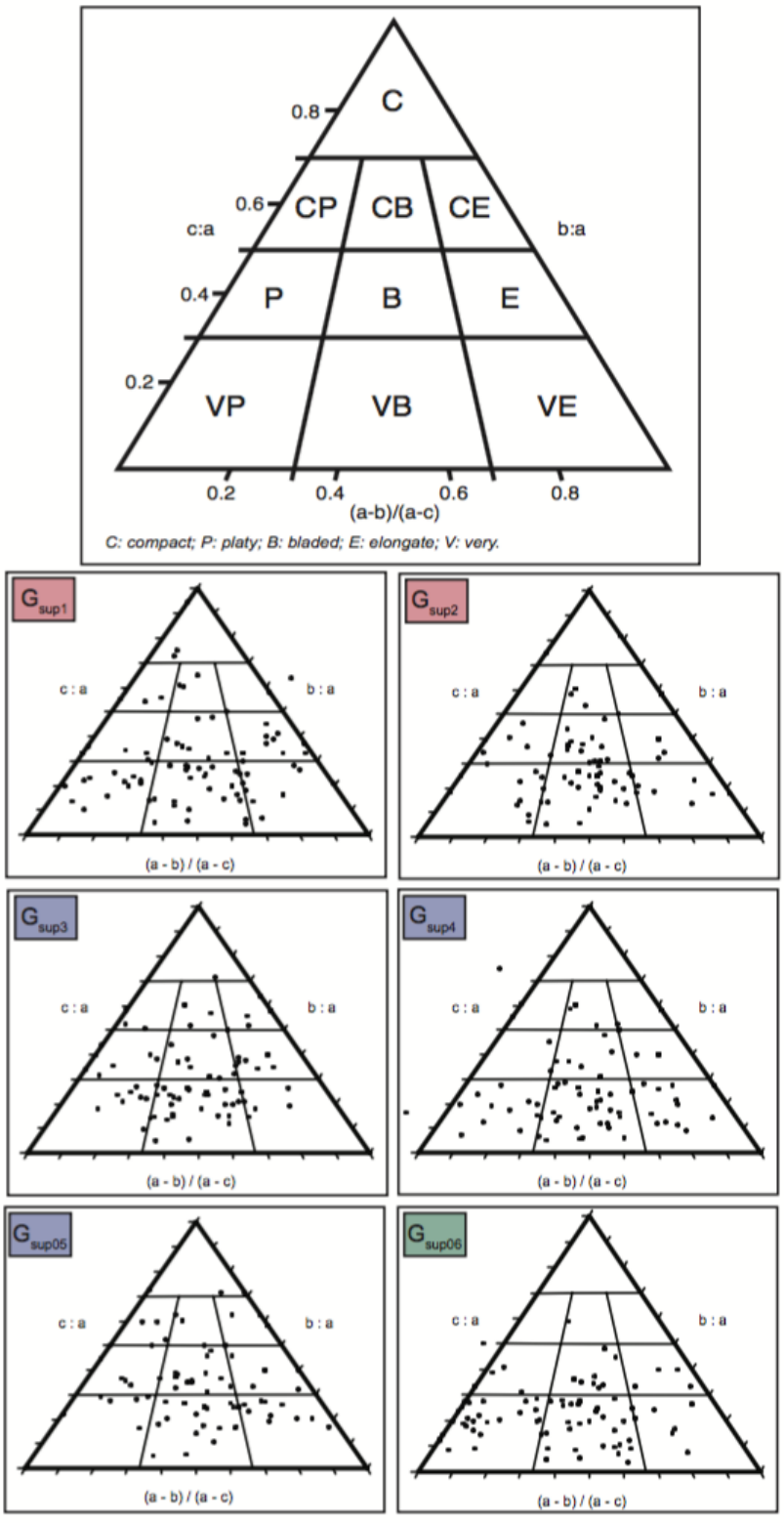

Supplementary Item 8. Percentage surface weathering for Gangotri medial moraine samples using the Sheridan and Marshall (1987) and the adapted Owen et al. (2003) visual estimation charts.

	Percentage surface weathering[1](%)								Mean surface weathering
Percentage classes:	30	40	50	60	70	80	90	100	(%)
SD_A									
G_{sup1}	6	11	20	14	11	12	15	11	66.4
G_{sup2}	0	2	10	20	17	19	18	14	70.2
SD_B									
G_{sup3}	2	3	18	7	15	28	15	12	75.1
G_{sup4}	2	8	17	10	15	26	14	8	73.4
G_{sup5}	2	1	8	13	13	25	22	16	77.7
SD_C									
G_{sup6}	0	3	6	9	24	32	21	5	75.9

1: Sheridan and Marshall (1987), Owen et al. (2003)

Supplementary Item 9. Plots of percentage distribution of surface weathering for Gangotri medial moraine samples.

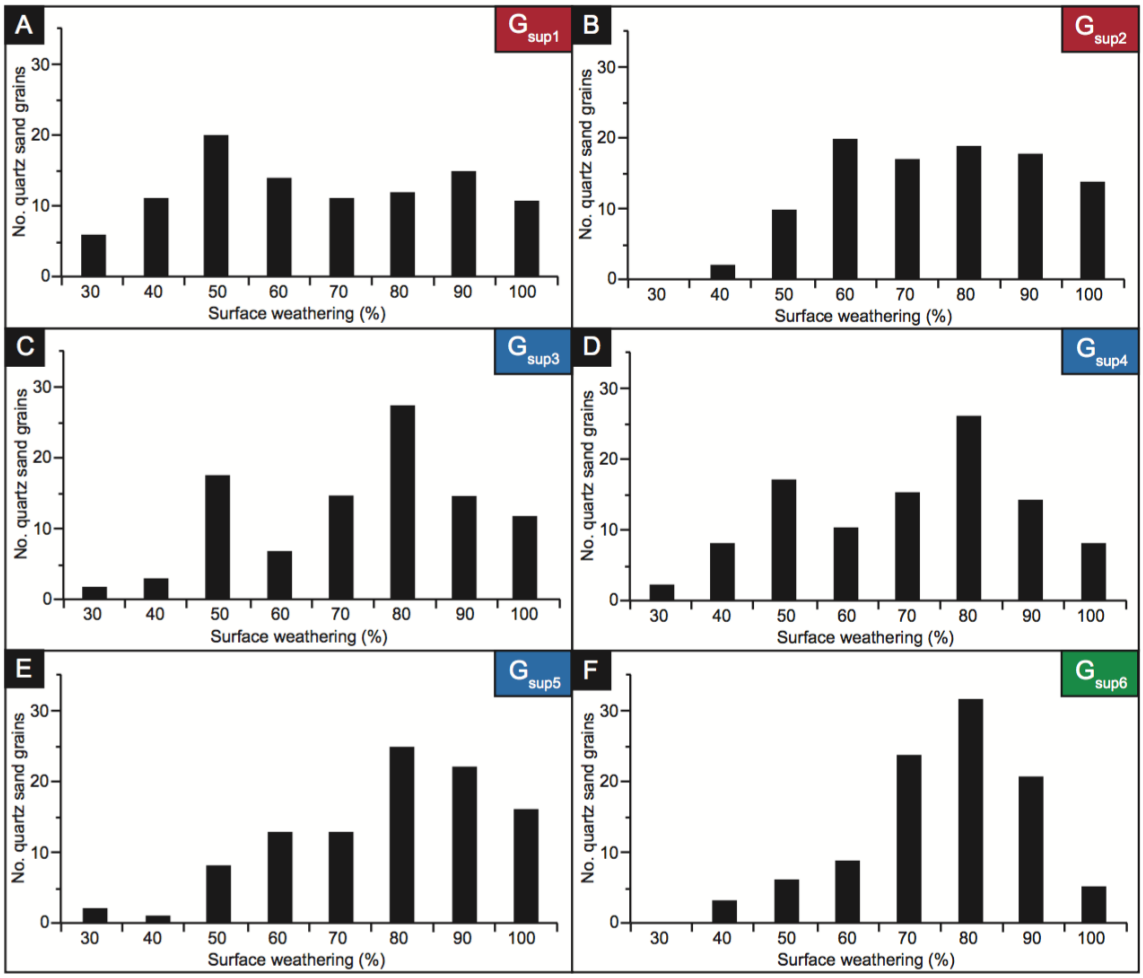

Supplementary Item 10. Diffraction patterns of the clay component of Gangotri medial moraine samples (CT: 1.0s, SS: 0.05°). A) G_{sup1}. B) G_{sup2}. C) G_{sup3}. D) G_{sup4}. E) G_{sup5}. F) G_{sup6}.

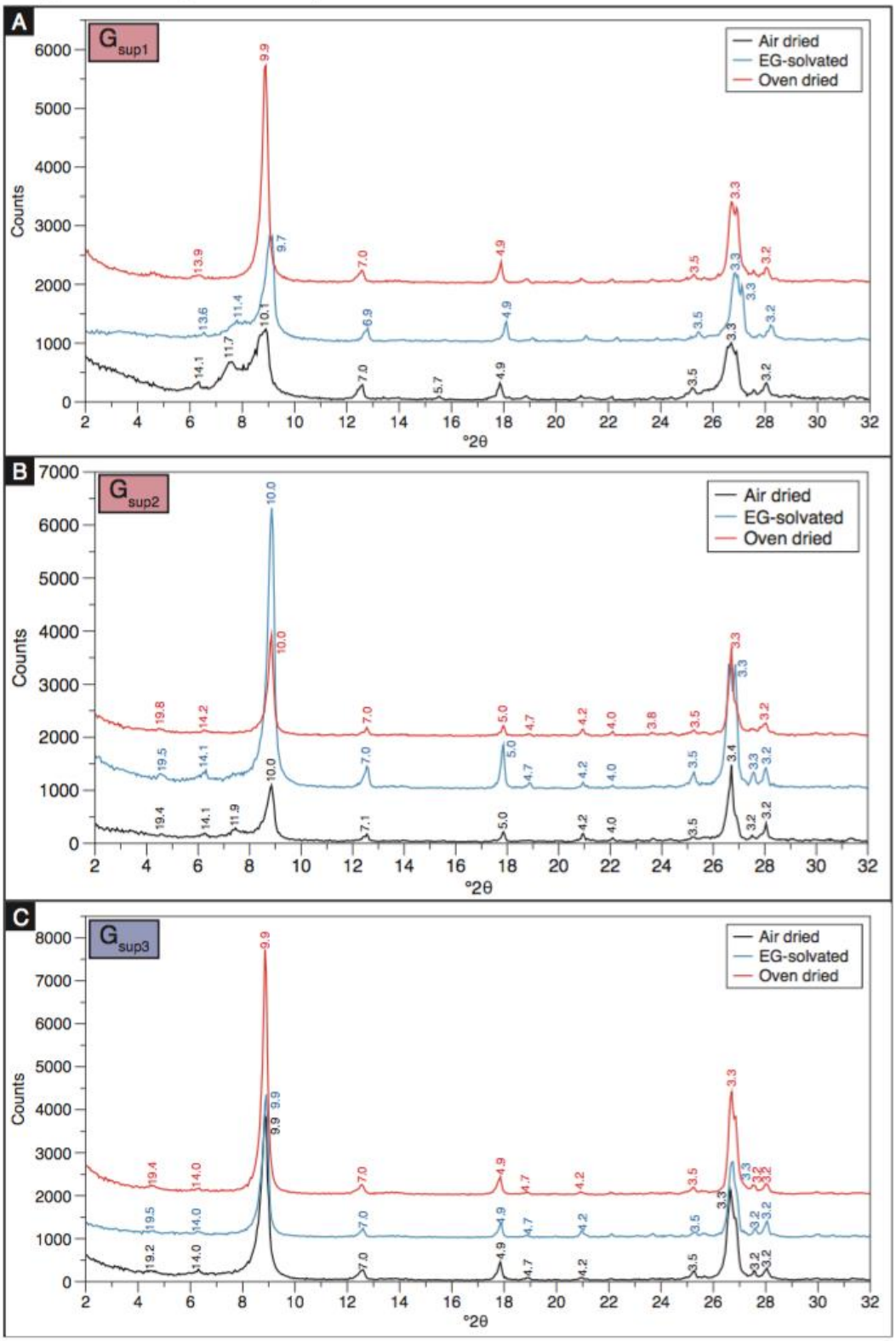

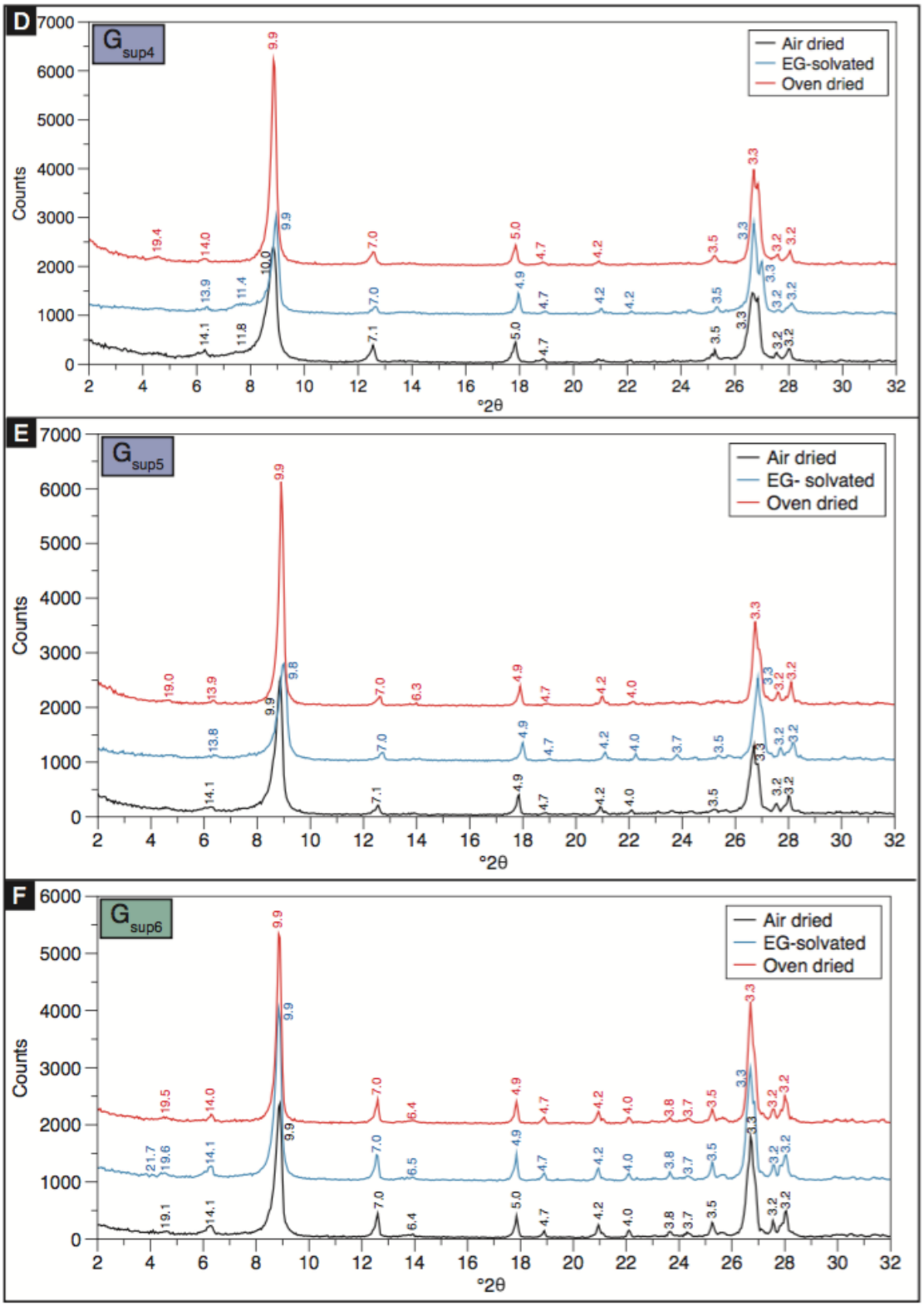
D
G sup4
Air dried
EG-solvated
Oven dried
Counts
°2θ
E
G sup5
Air dried
EG- solvated
Oven dried
Counts
°2θ
F
G sup6
Air dried
EG-solvated
Oven dried
Counts
°2θ

Supplementary Item 11. Elevation of landforms for the upper Bhagirathi catchment (≥3700 m asl). Landform elevation derived from highest point or apex. Circles denote individual landforms. Mean elevations (±StDev) represented by square points.

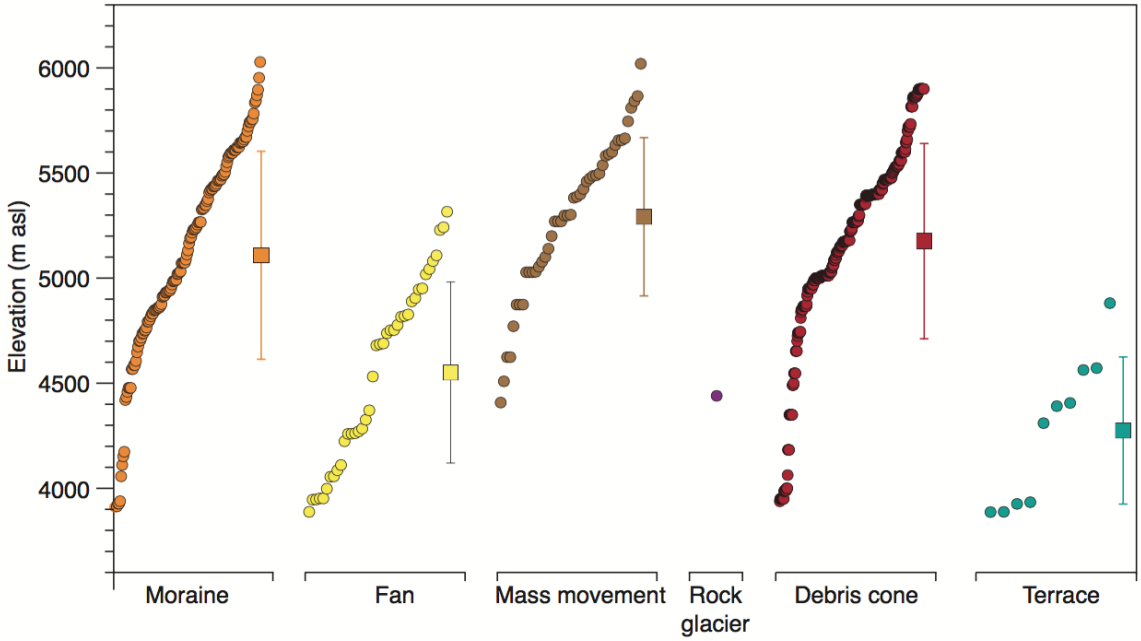

11.3. Supplementary Items 2 (Manuscript 2)

Supplementary Item 1. Catchment matrices defined for the 21 catchments detailed in this study.

Supplementary Item 1. Catchment matrices defined for the 21 catchments detailed in this study.

				CATCHMENT CHARACTERISTICS									GLACIER CHARACTERISTICS												LOCAL AND REGIONAL CLIMATE							GEOLOGICAL SETTING	
Samples	Catchment	^{10}Be conc.	^{10}Be conc. er.	Max. grain size	Catchment area	CA er.	Rockwall slope area	RSA er.	Catchment 3-km radius relief	CRR er.	Mean catchment elevation	MCE er.	Snowline elevation[1]	Mean catchment slope	MCS er.	Mean rockwall slope	MBS er.	Glacier area	GA er.	Mean glacier slope	MGS er.	Glacier aspect	Mean glacier velocity	MGV er.	Glacier class	Mean annual precipitation[2]	TRMM annual rainfall[2]	CRU. regional annual temp.[3]	Mean bedrock slope temp.[4]	MBST er.	Min. catchment temp.	Annual temp. range	Mean AFT age	AFT er.
		(10^3 at/g)	(10^3 at/g)	(mm)	(km^2)	(km^2)	(km^2)	(km^2)	(km)	(km)	(m asl)	(m asl)	(m asl)	(°)	(°)	(°)	(°)	(km^2)	(km^2)	(°)	(°)	(°)	(m/a)	(m/a)	-	(mm/a)	(mm/a)	(°C)	(°C)	(°C)	(°C)	(°C)	(Ma)	(Ma)
This study																																		
G_{Gop1}	Gopal	21	0.7	30	4.9	0.001	0.9	0.001	1	0.1	5559	173.4	5520	27.3	12.6	33.9	11.8	0.7	0.001	13.4	6.9	22.5	25	5	subpolar	87	<300	5.6	-10.6	2.5	-13	27.5	5.9	0.4
G_{Sto1}	Stok	6.1	0.7	30	4.1	0.001	0.8	0.001	0.7	0.1	5580	160.3	5540	26.6	12.4	30.8	11.8	1	0.001	14.4	6.7	45	25	5	subpolar	87	<300	5.6	-9.7	1.3	-11.6	27.5	5.9	0.4
G_{Amd1}	Amda	10.8	0.3	30	7	0.001	1.1	0.001	0.8	0.2	5620	185	5525	26.9	15.7	35.2	15.5	1.7	0.001	12.4	6.6	90	25	5	subpolar	87	<300	5.6	-9.8	2.5	-12.3	27.5	5.9	0.4
G_{Amd2}	Amda	9.6	0.3	30	7	0.001	1.1	0.001	0.8	0.2	5620	185	5525	26.9	15.7	35.2	15.5	1.7	0.001	12.4	6.6	90	25	5	subpolar	87	<300	5.6	-9.8	2.5	-12.3	27.5	5.9	0.4
G_{Kar1}	Karzok	213	3.5	30	3.9	0.001	0.7	0.001	0.9	0.1	5717.8	186.3	5530	25.9	12.2	26.3	12.4	0.3	0.001	18.8	10.9	360	25	5	subpolar	87	<300	5.6	-10.2	2.1	-12.3	27.5	39.8	0.3
G_{Kar2}	Karzok	213.5	3.2	30	3.9	0.001	0.7	0.001	0.9	0.1	5717.8	186.3	5530	25.9	12.2	26.3	12.4	0.3	0.001	18.8	10.9	360	25	5	subpolar	87	<300	5.6	-10.2	2.1	-12.3	27.5	39.8	0.3
G_{Kar3}	Karzok	260	12.5	30	3.9	0.001	0.7	0.001	0.9	0.1	5717.8	186.3	5530	25.9	12.2	26.3	12.4	0.3	0.001	18.8	10.9	360	25	5	subpolar	87	<300	5.6	-10.2	2.1	-12.3	27.5	39.8	0.3
G_{Men1}	Mentok	32.9	1.2	30	10.3	0.001	1.3	0.001	0.9	0.2	5707.4	168.9	5610	21.1	13.6	35.5	13	2.7	0.001	13.8	7.8	22.5	25	5	subpolar	87	<300	5.6	-11.6	2.1	-13.7	27.5	39.8	0.3
G_{Urg1}	Urgos	1.7	0.2	30	30.3	0.001	3.8	0.001	1.2	0.2	5047.6	377.1	4730	28.3	13.9	32.8	12.8	3.7	0.001	13.4	8.5	90	25	5	temperate	950	300-700	17.96	-6.9	7.4	-14.2	22	9.3	0.9
G_{Urg2}	Urgos	0.7	0.0005	30	30.3	0.001	3.8	0.001	1.2	0.2	5047.6	377.1	4730	28.3	13.9	32.8	12.8	3.7	0.001	13.4	8.5	90	25	5	temperate	950	300-700	17.96	-6.9	7.4	-14.2	22	9.3	0.9
G_{Pan1}	Panchi	19.4	4.5	30	20.5	0.001	5.6	0.001	1.3	0.3	4905.3	350.1	4560	29.5	14	34.8	12.1	4.5	0.001	14.7	8.7	360	25	5	temperate	950	300-700	17.96	-5.8	6.3	-12.1	22	9.3	0.9
G_{Shi1}	Shitidhar	3.2	0.4	30	22.2	0.001	4.3	0.001	1.8	0.5	4483.7	521.7	4050	39.1	14.5	42.8	12.7	1.5	0.001	18.7	7.3	22.5	25	5	temperate	950	300-700	17.96	-2	8.8	-10.7	18	2.3	0.3
G_{Bat1}	Batal	30.6	1	30	13.9	0.001	2.7	0.001	1.4	0.2	4981.4	401.7	4600	34.3	14.6	39.5	12.2	2.5	0.001	15.2	7.8	22.5	25	5	temperate	950	300-700	17.96	-5.8	6.3	-12.1	18	5.5	0.4
G_{Bat2}	Batal	3.5	0.3	30	13.9	0.001	2.7	0.001	1.4	0.2	4981.4	401.7	4600	34.3	14.6	39.5	12.2	2.5	0.001	15.2	7.8	22.5	25	5	temperate	950	300-700	17.96	-5.8	6.3	-12.1	18	5.5	0.4
G_{Chi1}	Chhota Shigri	3.2	0.3	30	44.9	0.001	3.2	0.001	1.3	0.3	5097.1	351.3	4905	29.4	15.8	36.5	14.8	13.3	0.001	16.2	9.2	360	27.6	4.3	temperate	950	300-700	17.96	-5.5	7.4	-12.8	18	3.8	0.3
G_{Chi2}	Chhota Shigri	4	0.3	30	44.9	0.001	3.2	0.001	1.3	0.3	5097.1	351.3	4905	29.4	15.8	36.5	14.8	13.3	0.001	16.2	9.2	360	27.6	4.3	temperate	950	300-700	17.96	-5.5	7.4	-12.8	18	3.8	0.3
G_{Chi3}	Chhota Shigri	4.2	1.3	30	44.9	0.001	3.2	0.001	1.3	0.3	5097.1	351.3	4905	29.4	15.8	36.5	14.8	13.3	0.001	16.2	9.2	360	27.6	4.3	temperate	950	300-700	17.96	-5.5	7.4	-12.8	18	3.8	0.3
G_{Chi4}	Chhota Shigri	1.1	0.004	30	44.9	0.001	3.2	0.001	1.3	0.3	5097.1	351.3	4905	29.4	15.8	36.5	14.8	13.3	0.001	16.2	9.2	360	27.6	4.3	temperate	950	300-700	17.96	-5.5	7.4	-12.8	18	3.8	0.3
G_{Chi5}	Chhota Shigri	1	0.05	30	44.9	0.001	3.2	0.001	1.3	0.3	5097.1	351.3	4905	29.4	15.8	36.5	14.8	13.3	0.001	16.2	9.2	360	27.6	4.3	temperate	950	300-700	17.96	-5.5	7.4	-12.8	18	3.8	0.3
G_{Ham1}	Hamtah	1.3	0.01	30	33.1	0.001	7.0	0.001	1.2	0.3	4774.4	404.9	4350	32.2	14.9	39.2	12.2	4.8	0.001	10.6	6	360	25	5	temperate	950	300-700	17.96	-5.8	7	-12.8	18	3.8	0.3
G_{Ham2}	Hamtah	2	0.2	30	33.1	0.001	7.0	0.001	1.2	0.3	4774.4	404.9	4350	32.2	14.9	39.2	12.2	4.8	0.001	10.6	6	360	25	5	temperate	950	300-700	17.96	-5.8	7	-12.8	18	3.8	0.3
G_{Ham3}	Hamtah	1.2	0.2	30	33.1	0.001	7.0	0.001	1.2	0.3	4774.4	404.9	4350	32.2	14.9	39.2	12.2	4.8	0.001	10.6	6	360	25	5	temperate	950	300-700	17.96	-5.8	7	-12.8	18	3.8	0.3
G_{Ham4}	Hamtah	0.8	0.1	30	33.1	0.001	7.0	0.001	1.2	0.3	4774.4	404.9	4350	32.2	14.9	39.2	12.2	4.8	0.001	10.6	6	360	25	5	temperate	950	300-700	17.96	-5.8	7	-12.8	18	3.8	0.3
G_{Bea1}	Beas_Kund	0.6	0.05	30	17.6	0.001	3.3	0.001	1.6	0.3	4168	318.2	3725	35.3	16.3	47.2	11.9	1	0.001	13.1	8.7	360	25	5	temperate	1020	>700	17.96	-5.8	9.1	-14.9	15	1.3	0.2
G_{Bea2}	Beas_Kund	0.8	0.1	30	17.6	0.001	3.3	0.001	1.6	0.3	4168	318.2	3725	35.3	16.3	47.2	11.9	1	0.001	13.1	8.7	360	25	5	temperate	1020	>700	17.96	-5.8	9.1	-14.9	15	1.3	0.2
G_{Bea3}	Beas_Kund	0.5	0.04	30	17.6	0.001	3.3	0.001	1.6	0.3	4168	318.2	3725	35.3	16.3	47.2	11.9	1	0.001	13.1	8.7	360	25	5	temperate	1020	>700	17.96	-5.8	9.1	-14.9	15	1.3	0.2
Orr et al. (*in review*)																																		
G_{Kir1}	Kirti	1.1	0.2	30	79.5	0.001	20.8	0.001	2.1	0.2	5385.1	547.9	5000	35.1	14.7	43.3	13.9	25.2	0.001	13.4	9.9	45	25	5	temperate	1650	>700	15.5	-9.3	8	-17.4	13.3	1.8	0.3
G_{Kir2}	Kirti	1.6	0.3	30	79.5	0.001	20.8	0.001	2.1	0.2	5385.1	547.9	5000	35.1	14.7	43.3	13.9	25.2	0.001	13.4	9.9	45	25	5	temperate	1650	>700	15.5	-9.3	8	-17.4	13.3	1.8	0.3
G_{Bha1}	Bhagirathi	2.7	0.3	30	772.7	0.001	16.0	0.001	1.7	0.4	5489.5	548	5160	36.5	15.2	43.3	13.9	409	0.001	11.5	10.1	330	48	4.8	temperate	1650	>700	15.5	-8.7	10.2	-18.9	13.3	1.8	0.3
G_{Bha2}	Bhagirathi	2.5	0.3	30	772.7	0.001	16.0	0.001	1.7	0.4	5489.5	548	5160	36.5	15.2	43.3	13.9	409	0.001	11.5	10.1	330	48	4.8	temperate	1650	>700	15.5	-8.7	10.2	-18.9	13.3	1.8	0.3
G_{Bha3}	Bhagirathi	2.6	0.3	30	772.7	0.001	16.0	0.001	1.7	0.4	5489.5	548	5160	36.5	15.2	43.3	13.9	409	0.001	11.5	10.1	330	48	4.8	temperate	1650	>700	15.5	-8.7	10.2	-18.9	13.3	1.8	0.3
G_{Bha4}	Bhagirathi	1.5	0.4	30	772.7	0.001	16.0	0.001	1.7	0.4	5489.5	548	5160	36.5	15.2	43.3	13.9	409	0.001	11.5	10.1	330	48	4.8	temperate	1650	>700	15.5	-8.7	10.2	-18.9	13.3	1.8	0.3
Schlerler and Egholm (2017)																																		
CS_1	Chhota Shigri	4.5	1.5	30	44.9	0.001	3.2	0.001	1.3	0.3	5097.1	351.3	4905	29.4	15.8	36.5	14.8	13.3	0.001	16.2	9.2	360	27.6	4.3	temperate	950	300-700	17.96	-5.5	7.4	-12.8	13.3	3.8	0.3
Seong et al. (2009)																																		
K2E-1	Baltoro C1	5.78	0.34	10	34.1	0.001	4.4	0.001	3	0.3	4939	704	5326	37.4	15	41.2	15.3	6.7	0.001	18	11.4	140	45	5	subpolar	150	<300	11.5	-7.8	11.5	-19.3	26.8	21.8	1.8
K2E-2	Baltoro C1	4.68	0.31	10	34.1	0.001	4.4	0.001	3	0.3	4939	704	5326	37.4	15	41.2	15.3	6.7	0.001	18	11.4	140	45	5	subpolar	150	<300	11.5	-7.8	11.5	-19.3	26.8	21.8	1.8
K2E-3	Baltoro C2	4.61	0.6	10	76.1	0.001	3.4	0.001	2.8	0.3	5101.8	635	5237	35.6	18	43.7	13.9	15.5	0.001	13.1	10.7	150	55	10	subpolar	150	<300	11.5	-9.6	10.4	-20	26.8	21.8	1.8
K2E-4	Baltoro C2	5.87	0.32	10	76.1	0.001	3.4	0.001	2.8	0.3	5101.8	635	5237	35.6	18	43.7	13.9	15.5	0.001	13.1	10.7	150	55	10	subpolar	150	<300	11.5	-9.6	10.4	-20	26.8	21.8	1.8
K2E-5	Baltoro C3	4.67	0.43	10	111.7	0.001	7.2	0.001	2.1	0.2	5237.5	564	5074	32.7	16	39.6	12.9	18.1	0.001	12.3	8.3	355	45	5	subpolar	150	<300	11.5	-9.6	11.1	-20.7	26.8	21.8	1.8
K2E-6	Baltoro C3	4.42	0.27	10	111.7	0.001	7.2	0.001	2.1	0.2	5237.5	564	5074	32.7	16	39.6	12.9	18.1	0.001	12.3	8.3	355	45	5	subpolar	150	<300	11.5	-9.6	11.1	-20.7	26.8	21.8	1.8
K2E-7	Baltoro C3	9.97	0.44	10	111.7	0.001	7.2	0.001	2.1	0.2	5237.5	564	5074	32.7	16	39.6	12.9	18.1	0.001	12.3	8.3	355	45	5	subpolar	150	<300	11.5	-9.6	11.1	-20.7	26.8	21.8	1.8
K2E-8	Baltoro C4	5.23	0.35	10	13.5	0.001	3.4	0.001	2.3	0.1	5031.6	583	4711	38.3	13	42.8	12.4	2.57	0.001	22.7	10.2	340	55	5	subpolar	150	<300	11.5	-3.6	5.2	-8.8	26.8	21.8	1.8
K2E-9	Baltoro C4	5.32	0.33	10	13.5	0.001	3.4	0.001	2.3	0.1	5031.6	583	4711	38.3	13	42.8	12.4	2.57	0.001	22.7	10.2	340	55	5	subpolar	150	<300	11.5	-3.6	5.2	-8.8	26.8	21.8	1.8
K2E-12	Baltoro C5	6.75	0.44	10	72.2	0.001	20.2	0.001	2.8	0.3	4988.4	409	4316	32.8	18	41.8	13.9	13.6	0.001	7.5	5.9	360	55	10	subpolar	150	<300	11.5	-12.4	14.6	-27	26.8	21.8	1.8
K2E-20	Baltoro C6	11.68	2.19	10	32.6	0.001	18.0	0.001	3.1	0.1	5747.6	673	4255	36.3	17	45.1	14.3	7.8	0.001	19.3	12.2	230	55	10	subpolar	150	<300	11.5	-14.8	12.2	-27	26.8	21.8	1.8
K2E-23	Baltoro C6	4.22	0.36	10	32.6	0.001	18.0	0.001	3.1	0.1	5747.6	673	4255	36.3	17	45.1	14.3	7.8	0.001	19.3	12.2	230	55	10	subpolar	150	<300	11.5	-14.8	12.2	-27	26.8	21.8	1.8
K2E-24	Baltoro C7	15.54	0.75	10	190.3	0.001	53.0	0.001	2.4	0.4	5856.2	643	5212	33.4	19	41	15.3	41.9	0.001	11.5	8.9	180	120	20	subpolar	150	<300	11.5	-19.4	15.3	-34.7	26.8	21.8	1.8
K2E-25	Baltoro C7	6.04	0.61	10	190.3	0.001	53.0	0.001	2.4	0.4	5856.2	643	5212	33.4	19	41	15.3	41.9	0.001	11.5	8.9	180	120	20	subpolar	150	<300	11.5	-19.4	15.3	-34.7	26.8	21.8	1.8

1: Mean of equilibrium line altitudes (ELA)/snowline elevation (SE) calculated using Area-altitude (AA), Area-accumulation ratio (AAR: 0.4,0.5,0.6) and Toe-headwall ratio (THAR: 0.4,0.5) methods from Benn et al. (2005) and Osmaston (2005).

2: Mean annual precipitation. Rainfall data from local weather stations. Leh Meteorological Station (34.18°N, 77.58°E, 3500 m asl; CRUTEM4 1876–1990, Jones et al., 2012; Osborn and Jones, 2014): Gopal, Stok, Amda, Karzok and Mentok. Chhota Shigri weather station (32.28°N, 77.53°E, 3900 m asl; 1980–2005; Wagnon et al., 2007; Azam et al., 2014): Urgos, Panchi, Shitidhar, Batal, Chhota and Hamtah. Bhutnar Observatory (1969–2012; 31.8°N, 77.1°E, 1130 m asl; Azam et al., 2014): Beas Kund

3: TRMM2B31 (1998–2009) annual rainfall data (Bookhagen and Burbank, 2010)

4:Temperature data from local weather stations. Leh Meteorological Station (34.18°N, 77.58°E, 3500 m asl; CRUTEM4 1876–1990, Jones et al., 2012; Osborn and Jones, 2014): Gopal, Stok, Amda, Karzok and Mentok. Chhota Shigri weather station (32.28°N, 77.53°E, 3900 m asl; 1980–2005; Wagnon et al., 2007; Azam et al., 2014): Urgos, Panchi, Shitidhar, Batal, Chhota, Hamtah and Beas Kund.

5: Temperatures estimated using local weather station data and an adiabatic lapse rate (ΔT/ΔZ) of 7°C/km Derbyshire et al., 1991; De Scally, 1997; Thayyen et al., 2005; Bashir and Rasul, 2010; Pratap et al., 2013; Katuel et al., 2013, 2015).

Supplementary Item 2. Analytical model variables to calculate the ^{10}Be inventory gained during transport of rock particles from bedrock slope to medial moraine.

Catchment	Horizontal distance[1] (m)	^{10}Be production rate[2] (at/g/a)	Slope[3]	Particle speed[4] (m/a)	Spall. air[5] (m)	Spall.ice[6] (m)	Particle depth[7] (m)	Mass balance gradient[8] (m/a/m)	Accummulated ^{10}Be[9] (at/g)
Gopal	250	105.6±13.7	0.24	25	1600	1.95	0	0.1	325.2
Stok	710	92.8±12.0	0.26	25	1600	1.95	0	0.1	275.7
Amda	930	90.5±11.7	0.22	25	1600	1.95	0	0.1	289.1
Karzok	130	99.3±12.9	0.36	25	1600	1.95	0	0.1	249.1
Mentok	410	103.4±13.4	0.25	25	1600	1.95	0	0.1	312.4
Urgos	1060	74.2±9.6	0.25	25	1600	1.95	0	0.1	224.5
Panchi	1840	74.4±9.6	0.27	25	1600	1.95	0	0.1	216.2
Shitidhar	770	55.5±7.2	0.40	25	1600	1.95	0	0.1	132.6.3
Batal	950	74.8±9.7	0.28	25	1600	1.95	0	0.1	205.7
Chhota Shigri	1330	80.3±10.4	0.30	27.6	1600	1.95	0	0.1	220.9
Hamtah	1720	65.6±8.5	0.19	25	1600	1.95	0	0.1	221.4
Beas Kund	540	53.7±6.9	0.24	25	1600	1.95	0	0.1	165.3

1: Mean horizontal distance from entry point at glacier head to ELA (measured from 20 profiles).
2: Catchment ^{10}Be production rate
3: Dimensionless slope of the glacier surface
4: Mean speed of rock particle on glacier surface
5: Spallation falloff scale in air
6: Spallation falloff scale in ice (0.65*3)
7: Initial depth of particle at entry point at glacier head
8: Accummulation of ^{10}Be between bedrock slope and medial moraine sampling location

Supplementary Item 3. *P* values between catchment matrices and geochemical data.

		SAMPLE CHARACTERISTICS		CATCHMENT CHARACTERISTICS								GLACIER CHARACTERISTICS				CLIMATIC CONDITIONS				GEO SET
	Class no.	^{10}Be sample conc.	Max. grain size	Catch. area	Source slope area	Peak elevation	Mean elev.	SL elev.	Catch. relief	Catch. slope	Source slope	Glacier area	Glacier aspect	Mean glacier slope	Glacier velocity	Total annual precip	Mean annual temp.	Min. catch. temp.	Mean slope temp.	Mean AFT age
NW Himalaya																				
^{10}Be conc.	(>10)	-	-	-	-	-	-	-	-	-	-	-	-	-	-	-	-	-	-	-
Max. grain size	(2)	6558.0	-	-	-	-	-	-	-	-	-	-	-	-	-	-	-	-	-	-
Catchment area	(>10)	47.5	0.4	-	-	-	-	-	-	-	-	-	-	-	-	-	-	-	-	-
Source slope area	(>10)	213.8	13.5	0.000003	-	-	-	-	-	-	-	-	-	-	-	-	-	-	-	-
Peak elevation	(>10)	1957.0	0.0001	0.001	0.0000005	-	-	-	-	-	-	-	-	-	-	-	-	-	-	-
Mean elevation	(>10)	0.004	1369.0	1412.0	279.3	2.2	-	-	-	-	-	-	-	-	-	-	-	-	-	-
Snowline altitude	(>10)	0.05	4704.0	4524.0	8460.0	3216.0	0.0001	-	-	-	-	-	-	-	-	-	-	-	-	-
Catchment relief	(>10)	2077.0	0.000000000005	19.0	38.3	0.04	9341.0	2950.0	-	-	-	-	-	-	-	-	-	-	-	-
Catchment slope	(>10)	91.7	0.5	1625.0	1427.0	1049.0	16.5	1.9	0.00004	-	-	-	-	-	-	-	-	-	-	-
Source slope	(>10)	0.6	12.7	854.3	802.8	1591.0	5.0	0.04	0.01	$1x10^{-7}$		-	-	-	-	-	-	-	-	-
Glacier area	(>10)	263.2	2.6	0.00002	3.6	2.4	6737.0	9651.0	3.6	725.7	110.7		-	-	-	-	-	-	-	-
Glacier aspect	(>10)	3867.0	9202.0	5100.0	9013.0	4601.0	932.5	408.2	9699.0	7567.0	7592.0	5130.0	-	-	-	-	-	-	-	-
Mean glacier slope	(>10)	385.5	5210.0	106.0	917.7	3382.0	3081.0	4648.0	3459.0	2301.0	4945.0	580.8	9063.0	-	-	-	-	-	-	-
Glacier velocity	(5)	5619.0	0.0001	0.0000004	0.00000000002	0.00000004	127.5	3768.0	0.03	121.4	215.4	$2x10^{-7}$	7239.0	6917.0	-	-	-	-	-	-
Total annual precip	(4)	0.1	0.1	1812.0	1658.0	0.9	0.002	0.03	173.1	7177.0	3876.0	2508.0	1398.0	2904.0	22.1	-	-	-	-	-
Mean annual temp.	(3)	0.001	781.6	8124.0	8502.0	448.1	0.0004	0.001	9431.0	237.6	118.3	7658.0	671.2	3403.0	2167.0	$2x10^{-12}$	-	-	-	-
Min. catch. temp.	(3)	8055.0	0.003	0.000004	0.00000002	0.0000000001	222.7	8746.0	0.01	606.3	141.0	$3x10^{-5}$	7306.0	613.5	$1x10^{-7}$	78.0	312.6	-	-	-
Mean slope temp.	(>10)	71.1	14.9	0.8	0.0003	0.0000006	0.0005	138.9	284.7	3874.0	8388.0	0.6	1815.0	1494.0	0.002	0.04	0.1	$1x10^{-7}$	-	-
Mean AFT age	(8)	0.001	13.9	3094.0	2889.0	21.2	0.3	4.2	627.9	3658.0	713.3	4106.0	4106.0	486.0	222.6	0.0001	0.0005	386.6	3.8	-
Regional analysis																				
Ladakh, Baltistan																				
^{10}Be conc.	-	-	0.4	2.9	380.0	100.0	10.1	30.0	1.8	0.5	0.001	0.2	311.3	311.5	90.0	-	-	135.2	700.0	-
Kullu, Lahul																				
^{10}Be conc.	-	-	-	430.9	320.0	600.0	70.0	74.0	832.7	799.0	495.1	419.5	200.0	86.9	791.6	-	-	4.1	470.0	-

Supplementary Item 4. Grain size distribution of supraglacial debris. A) Medial moraine sediment from this study B) Gangotri glacier sediment from Orr et al. (*in review*). C) Supraglacial debris from from Rakhiot, Chungphur and Glacier de Cheilon (Owen et al. 2003), Glacier de Tsidijore Nourve (Small 1983), Breidamerkurjokkull, Sore Buchananisen, and the Glacier d'Argentiere (Boulton 1978).

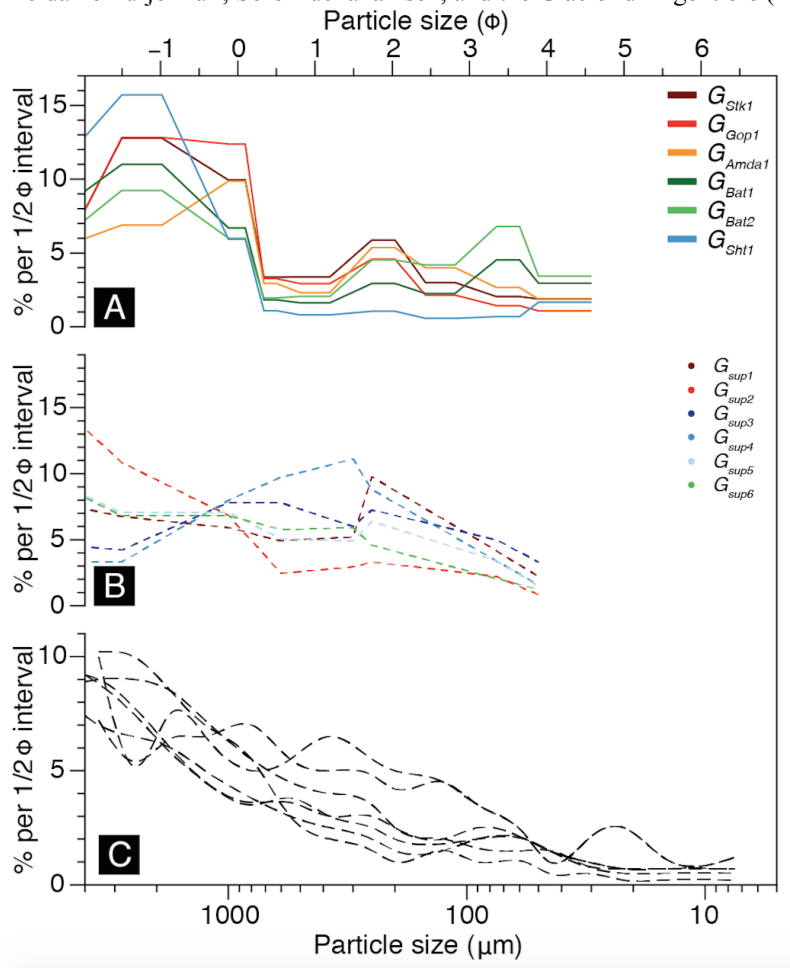

11.4. Supplementary 3 (Manuscript 3)

Supplementary Item 1. Images of sampled boulders from the Kullu, Chandra and Karzok fans

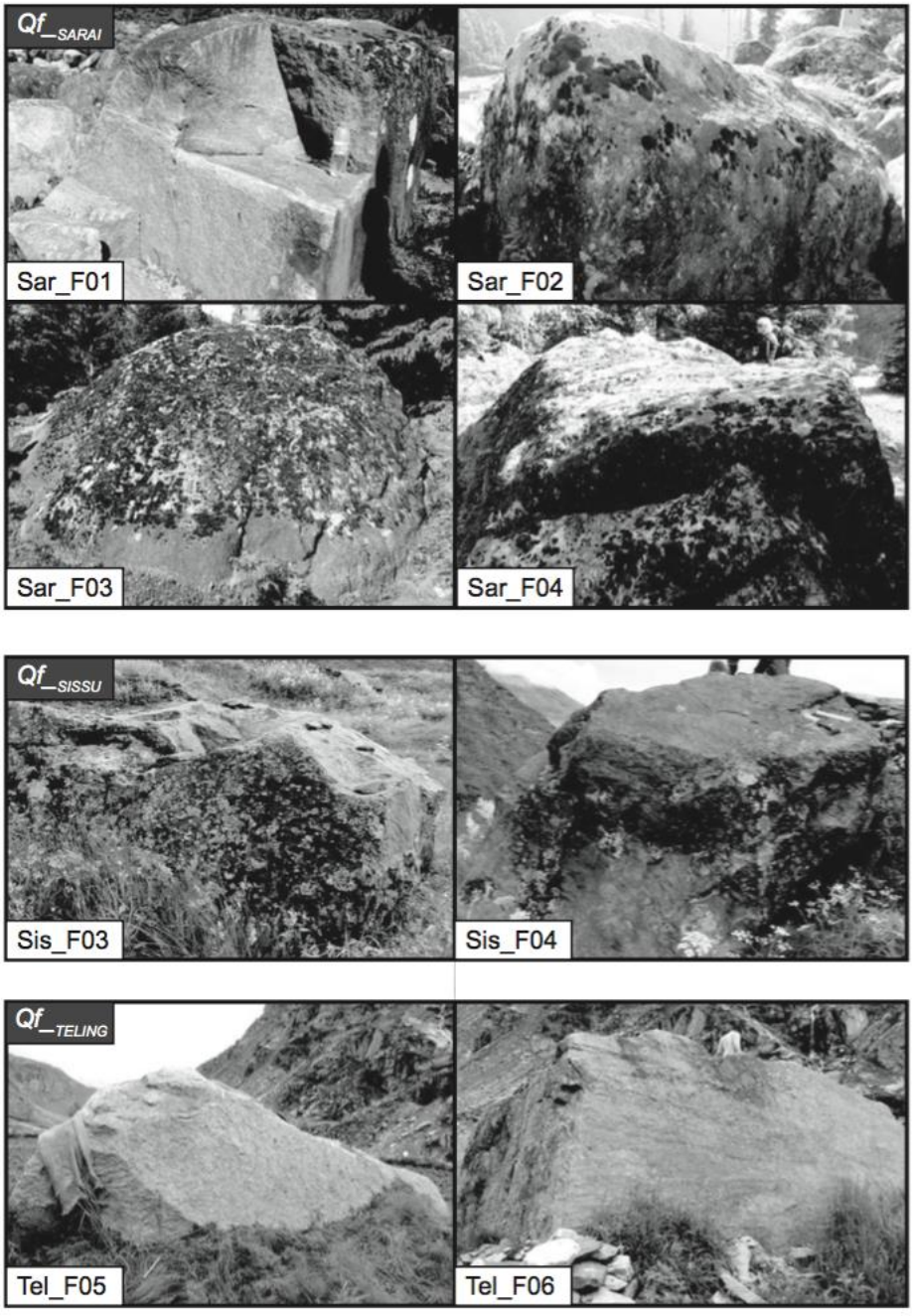

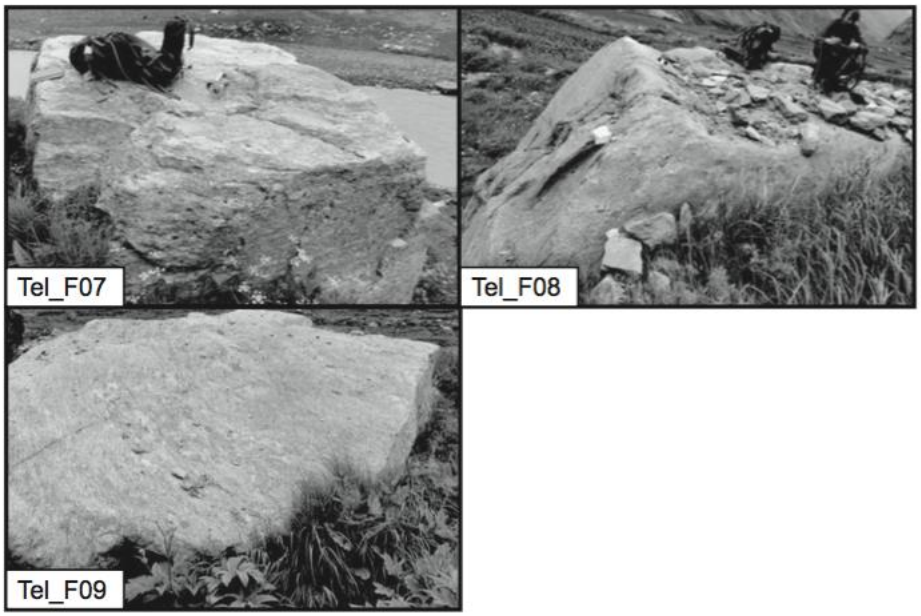
Tel_F07
Tel_F08
Tel_F09

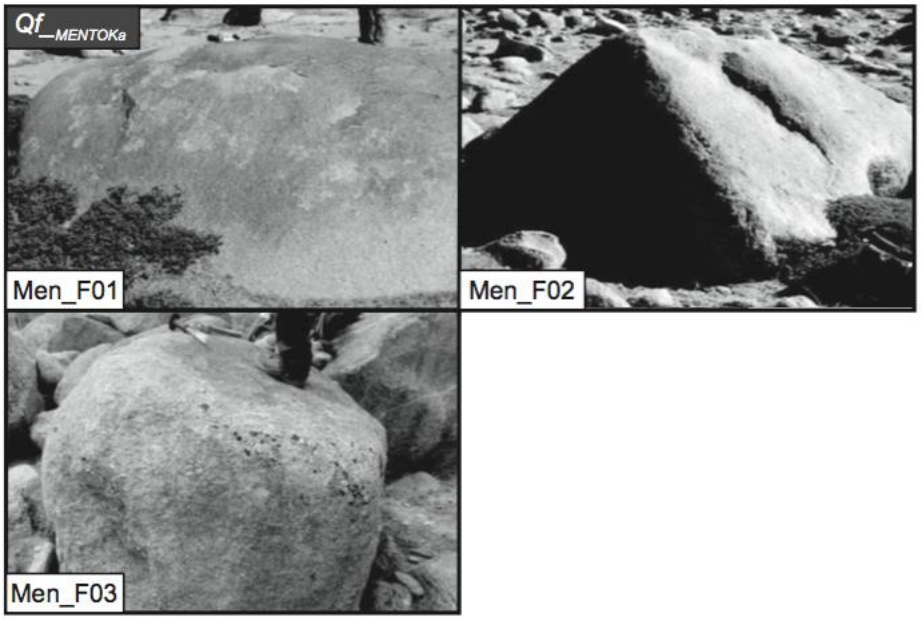
Qf—MENTOKa
Men_F01
Men_F02
Men_F03

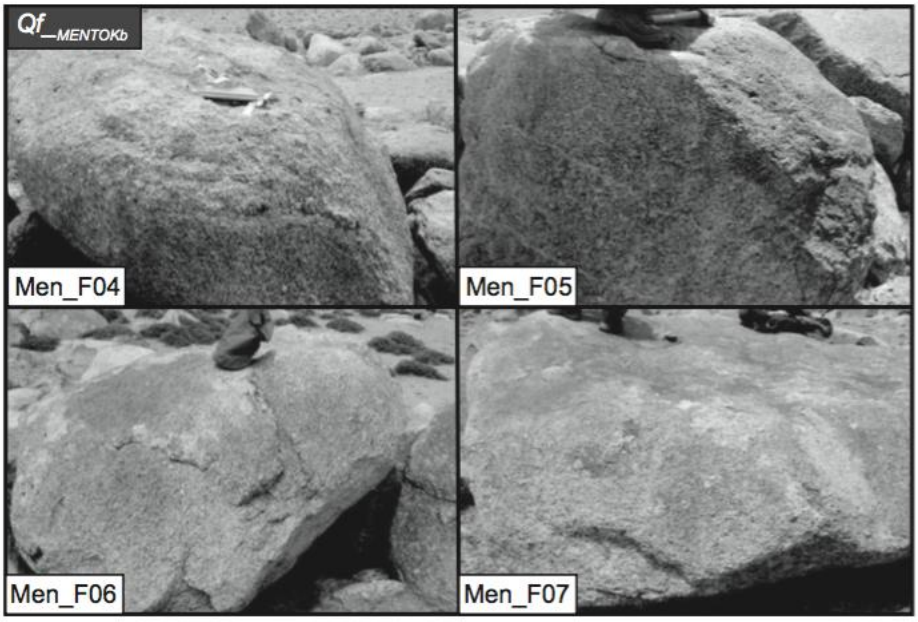
Qf_MENTOKb
Men_F04
Men_F05
Men_F06
Men_F07

Supplementary Item 2. Sample details with the initial and recalculated ^{10}Be ages (uncertainties expressed as 1σ)

Sample name	Fan	Location		Altitude	TSF*	^{10}Be	Int. exposure age†	LSD exposure age§	Internal error	External error
		Latitude (ºN)	Longitude (ºE)	(m asl)		(10^6 atoms/g)	(ka)	(ka)	(ka)	(ka)
R2	*Rilkot1*	30.31	80.21	3070	0.96	0.03±0.002	0.9±0.07	1.4	0.1	0.1
R3	*Rilkot1*	30.31	80.21	3196	0.96	0.02±0.002	0.5±0.06	0.9	0.1	0.1
R4	*Rilkot1*	30.31	80.21	3169	0.96	0.04±0.004	1.0±0.1	1.8	0.2	0.2
BH9	*Bhuj Kharak1*	30.96	78.94	3896	0.93	0.1±0.01	1.8±0.2	3.3	0.4	0.5
BH16	*Kedar Kharak1*	30.94	78.95	4314	0.97	0.4±0.01	6.6±0.2	9.8	0.2	0.6
BH21	*Rudugaira1*	31.00	78.92	3015	0.95	0.2±0.01	5.2±0.2	7.8	0.3	0.5
BH33	*Gaumukh1*	30.95	79.06	4140	0.97	0.2±0.001	3.7±0.2	5.5	0.2	0.3
B34	*Gaumukh1*	30.95	79.06	4145	0.97	0.1±0.01	1.9±0.1	3.1	0.2	0.3
BH38	*Gaumukh2*	30.95	79.06	3857	0.97	0.04±0.01	0.7±0.1	1.2	0.2	0.3
BH39	*Gaumukh2*	30.95	79.06	3863	0.97	0.05±0.01	0.9±0.1	1.5	0.3	0.3
KK97-36	*Tangtse1*	34.01	78.30	4350	0.98	2.0±0.1	32.0±3.0	32.2	1.9	2.6
KK97-37	*Tangtse1*	34.01	78.30	4350	0.98	2.4±0.2	37.5±4.1	38.6	2.6	3.2
KK97-38	*Tangtse1*	34.01	78.30	4350	0.98	1.1±0.1	16.4±2.1	19.0	1.5	1.7
KK97-39	*Tangtse1*	34.01	78.30	4350	0.98	1.3±0.1	19.7±2.0	21.7	1.3	1.6
KK97-40	*Tangtse1*	34.01	78.30	4350	0.98	1.3±0.1	20.5±2.1	21.7	1.3	1.6
KK98-9	*Tangtse1*	34.01	78.30	4350	0.98	1.1±0.1	17.3±1.7	19.0	1.5	1.7
KK98-10	*Tangtse1*	34.01	78.30	4350	0.98	1.1±0.2	16.8±2.9	19.0	2.9	3.0
KK98-11	*Tangtse1*	34.01	78.30	4350	0.98	1.0±0.1	16.3±2.1	17.5	1.6	1.8
KK98-12	*Tangtse1*	34.01	78.30	4350	0.98	1.2±0.1	18.5±1.9	20.4	1.3	1.6
KK98-13	*Tangtse1*	34.01	78.30	4350	0.98	2.9±0.2	45.9±4.2	45.1	3.7	4.7
KK98-1	*Tangtse2*	34.01	78.30	4350	0.98	0.1±0.04	2.3±0.6	2.1	0.9	0.9
KK98-3	*Tangtse2*	34.01	78.30	4350	0.98	0.2±0.03	3.3±0.6	4.2	0.6	0.6
KK98-4	*Tangtse2*	34.01	78.30	4350	0.98	0.5±0.05	7.1±1.0	9.4	1.0	1.1
KK98-5	*Tangtse2*	34.01	78.30	4350	0.98	0.1±0.01	1.8±0.3	2.1	0.2	0.3
KK98-6	*Tangtse2*	34.01	78.30	4350	0.98	0.4±0.04	5.6±0.8	7.5	0.7	0.8
KK98-7	*Tangtse2*	34.01	78.30	4350	0.98	0.3±0.1	4.8±1.0	5.9	1.6	1.7
KK98-8	*Tangtse2*	34.01	78.30	4350	0.98	0.8±0.1	12.7±1.3	14.3	1.5	1.7
KK98-14	*Tangtse2*	34.01	78.30	4350	0.98	0.1±0.01	1.7±0.3	2.1	0.2	0.3
KK98-15	*Tangtse2*	34.01	78.30	4350	0.98	0.1±0.01	1.3±0.2	2.1	0.2	0.3

*: Topographic Shielding Factor

†: Initial exposure ages: *Rilkot1, Gaumukh1-2* (Barnard et al., 2004b,a), *Tangtse1-2* (Brown et al., 2002,2003).

§: Production rate for the CREP calculator is 4.13±0.2 ^{10}Be atoms/grams SiO_2/year (Martin et al., 2016) with a ^{10}Be half-life of 1.36Ma. Minimum exposure age is calculated using the Balco et al. (2008) calibration dataset (^{10}Be decay constant of $5.1\pm0.3\times10^{-7}$) and Lifton et al. (2014) calculation scheme with the Lifton 2016 VDM geomagnetic database.

Supplementary Item 3. Sample details of monsoon western Himalayan ranges (MWHR) regional landform abandonment and incision events (uncertainties expressed as 1σ)

Landform No.	Sample Name	Latitude	Longitude	Elevation	Depth	TSF*	^{10}Be conc	Conc. Error	LSD exposure age†	External Error
		(ºN)	(ºE)	(m asl)	(cm)		(10^6 atoms/g)	(10^6 atoms/g)	(ka)	(ka)
REGIONAL AGGRADATION EVENTS										
Barnard et al. (2004b)										
Rilkot1	R2	30.3100	80.2100	3070	5	0.96	0.03	0.002	1.4	0.1
Rilkot1	R3	30.3100	80.2100	3196	5	0.96	0.02	0.002	0.9	0.1
Rilkot1	R4	30.3100	80.2100	3169	5	0.96	0.04	0.004	1.8	0.2
Barnard et al. (2004a)										
Bhuj Kharak1	BH9	30.9600	78.9400	3896	5	0.93	0.1	0.01	3.3	0.5
Kedar Kharak1	BH16	30.9400	78.9500	4314	5	0.97	0.4	0.01	9.8	0.6
Rudugaira1	BH21	31.0000	78.9200	3015	5	0.95	0.2	0.01	7.8	0.5
Gaumukh1	BH33	30.9500	79.0600	4140	5	0.97	0.2	0.001	5.5	0.3
Gaumukh1	B34	30.9500	79.0600	4145	5	0.97	0.1	0.01	3.1	0.3
Gaumukh2	BH38	30.9500	79.0600	3857	5	0.97	0.04	0.01	1.2	0.3
Gaumukh2	BH39	30.9500	79.0600	3863	5	0.97	0.05	0.01	1.5	0.3
Scherler et al. (2015)										
Pabbar	DS6-93	31.2262	77.8519	1679	5	0.9	0.016	0.00045	1.3	0.1
Tons	DS7-80	30.9185	77.8393	941	5	0.9	0.0083	0.00032	2.1	0.2
Tons	DS7-73C	30.7495	77.7048	845	5	0.9	0.023	0.00061	0.7	0.1
Yamuna	DS7-54B	30.8209	78.2281	1249	5	0.9	0.013	0.00036	1.4	0.1
Yamuna	DS6-17	30.7381	78.0793	1030	5	0.9	0.013	0.00048	1.1	0.1
Yamuna	DS6-15	30.7380	78.0791	1000	5	0.9	0.097	0.00027	1.5	0.1
Yamuna	DS7-60B	30.7244	78.0805	999	5	0.9	0.024	0.00064	0.6	0.0
REGIONAL INCISION EVENTS										
Adams et al. (2011)										
1	CV1	32.5490	77.6610	3568	5	0.92	0.47	0.73	1.1	0.2
1	CV2	32.5490	77.6610	3568	5	0.92	0.01	0.20	0.2	0.1
1	CV3	32.5490	77.6610	3568	5	0.92	0.07	0.33	1.7	0.2
2	KL1	32.5420	77.3680	3181	5	0.92	0.03	0.31	0.9	0.1
2	KL2	32.5400	77.3780	3189	5	0.92	0.19	0.61	5.4	0.5
2	KL3	32.5370	77.3810	3180	5	0.88	0.14	2.27	4.3	0.8
3	KO1	32.4170	77.4570	3108	5	0.93	0.04	0.60	1.0	0.2
3	KO2	32.4180	77.4480	3116	5	0.93	0.06	0.51	1.8	0.2
3	KO3	32.6700	77.4600	3122	5	0.93	0.12	0.55	3.6	0.4
3	ZK77	32.4180	77.2300	3135	5	0.91	0.11	1.45	3.5	0.5
4	KON2	32.6400	77.3480	3135	5	0.91	0.01	0.26	0.6	0.1
4	KON3	32.6410	77.3460	3129	5	0.91	0.02	0.32	0.7	0.1
5	PT1	32.4670	77.5480	3563	5	0.94	0.11	0.59	2.8	0.3
5	PT2	32.4580	77.5380	3599	5	0.89	0.03	0.32	1.0	0.1
5	PT3	32.4710	77.5450	3675	5	0.84	0.08	1.44	2.0	0.4

Barnard et al. (2004a)										
Gangotri	BH1d	31.0000	78.9300	3028	5	0.93	0.71	0.10	6.9	0.4
Gangotri	BH2	31.0000	78.9300	3015	5	0.93	0.11	0.004	7.3	0.5
Gangotri	BH3	31.0000	78.9300	3021	5	0.93	0.14	0.01	55.9	5.3
Rudugaira	BH24	31.0000	78.9200	3040	5	0.95	0.16	0.01	8.7	0.7
Barnard et al. (2004b)										
Rilkot	R5	30.3100	80.2000	3351	5	0.96	0.17	0.01	6.7	0.5
Rilkot	R6	30.3100	80.2000	3345	5	0.96	0.18	0.01	7.0	0.4
Rilkot	R7	30.3200	80.2100	3163	5	0.96	0.05	0.00	2.2	0.2
Rilkot	R8	30.3200	80.2100	3174	5	0.96	0.38	0.01	15.3	0.8
Rilkot	R9	30.3200	80.2100	3161	5	0.96	0.67	0.02	25.2	1.3
Rilkot	R10	30.3200	80.2100	3167	5	0.96	0.30	0.01	12.4	0.7
Rilkot	R11	30.3100	80.2100	3149	5	0.96	0.24	0.01	10.4	0.6
Rilkot	R12	30.3100	80.2100	3139	5	0.96	0.08	0.00	3.7	0.2
Rilkot	R13	30.3100	80.2100	3136	5	0.96	0.03	0.00	1.6	0.1
Rilkot	R14	30.3100	80.2100	3135	5	0.96	0.07	0.00	3.5	0.3
Rilkot	R15	30.3200	80.2100	3262	5	0.98	0.16	0.01	6.7	0.4
Rilkot	R18	30.3200	80.2100	3289	5	0.98	0.42	0.02	15.4	1.0
Bogdiar	R19	30.2100	80.2300	2315	5	0.77	0.08	0.00	7.3	0.5
Bogdiar	R20	30.2000	80.2300	2250	5	0.66	0.07	0.00	8.2	0.7
Lilam	R21	30.1200	80.2500	1412	5	0.93	0.05	0.00	7.1	0.5
Bookhagen et al. (2006)										
Chandra	BB1	31.3141	77.4165	1020	5	1	0.094	0.003	9.8	0.7
Chandra	BB2	31.3141	77.4165	1005	5	1	0.078	0.002	8.4	0.6
Chandra	BB3	31.3141	77.4165	1005	5	1	0.081	0.005	8.7	0.7
Chandra	BB4	31.3141	77.4165	1005	5	1	0.080	0.002	6.8	0.5
Chandra	BB5	31.3141	77.4165	1005	5	1	0.047	0.001	3.4	0.5
Chandra	BB8	31.3141	77.4165	965	5	1	0.059	0.003	3.0	0.3
Chandra	BB9	31.3141	77.4165	920	5	1	0.028	0.002	2.8	0.8
Chandra	BB10	31.3141	77.4165	892	5	1	0.023	0.002	6.7	0.5
Chandra	BB11	31.3141	77.4165	893	5	1	0.021	0.001	7.0	0.4
Dey et al. (2016)										
Kangra	T1	32.0680	76.3990	1125	5	0.9	0.411	0.015	42.2	5.6
Kangra	T2	32.1060	76.2620	1015	5	0.9	0.112	0.003	20.5	1.2
Kangra	T3	32.0580	76.2270	625	5	0.9	0.057	0.002	12.1	0.9
Kangra	T4	32.1170	76.2600	715	5	0.9	0.040	0.002	9.3	0.7
Kangra	T5	32.1830	76.2760	785	5	0.9	0.033	0.002	4.9	0.4
Kangra	T6	32.0920	76.3320	690	5	0.9	0.020	0.001	3.3	0.3
Kangra	T0	32.0910	76.2550	603	5	0.9	0.012	0.001	5.4	0.4
Dortch et al. (2011a)										
Chandra1	1	32.6760	77.2140	3471	5	0.92	1.84	0.14	55.9	5.3
Chandra2	2	32.5450	77.9720	2900	5	0.92	0.19	0.11	8.7	0.7
Chandra3	3	32.5260	76.9740	2908	5	0.94	1.53	0.19	62.5	7.7
Chandra4	4	32.5260	76.9700	2911	5	0.93	4.18	0.51	168.7	21.3
Chandra5	5	32.4170	77.2310	3132	5	0.92	0.59	0.03	22.0	1.3
Bhaga	6	32.4170	77.2300	3135	5	0.91	1.41	0.11	51.9	5.9

*: Topographic Shielding Factor

†: LSD age (internal/external errors quoted) is calculated using the Balco et al. (2008) calibration dataset (^{10}Be decay constant of 5.1±0.3x10-7), and Lifton et al. (2014) calculation scheme with the Lifton 2016 VDM geomagnetic database. Production rate for the CREP calculator is 4.13±0.2 ^{10}Be atoms/grams SiO_2/year (Martin et al., 2016) with a ^{10}Be half-life of 1.36Ma. Density of 2.7 g cm^3, AMS Standard of 07KNSTD.

Supplementary Item 4. Sample details of semi-arid western Himalayan ranges (SWHR) regional landform abandonment and incision events (uncertainties expressed as 1σ)

Landform No.	Sample Name	Latitude	Longitude	Elevation	Depth	TSF*	^{10}Be conc	Conc. Error	LSD exposure age†	External Error
		(ºN)	(ºE)	(m asl)	(cm)		(10^6 atoms/g)	(10^6 atoms/g)	(ka)	(ka)
REGIONAL AGGRADATION EVENTS										
Blöthe et al. (2014)										
Indus	Igor	34.1558	77.3633	3360	5	0.99	6.46	0.26	154.4	14.9
Zanskar	ZKR-TT-A	34.0970	77.2189	3340	5	0.97	5.00	0.10	121.9	10.9
Zanskar	ZKR-DD-Ter	34.1437	77.2993	3178	5	0.92	1.08	0.02	32.1	2.8
Zanskar	ZKR-DD	34.1437	77.2993	3178	5	0.92	1.02	0.02	30.4	2.7
Brown et al. (2002, 2003), Dortch et al. (2011b)										
Tangtse1	KK97-36	34.0060	78.2990	4350	5	0.98	2.00	0.10	32.2	2.6
Tangtse1	KK97-37	34.0060	78.2990	4350	5	0.98	2.40	0.20	38.6	3.2
Tangtse1	KK97-38	34.0060	78.2990	4350	5	0.98	1.10	0.10	19.0	1.7
Tangtse1	KK97-39	34.0060	78.2990	4350	5	0.98	1.30	0.10	21.7	1.6
Tangtse1	KK97-40	34.0060	78.2990	4350	5	0.98	1.30	0.10	21.7	1.6
Tangtse1	KK98-9	34.0060	78.2990	4350	5	0.98	1.10	0.10	19.0	1.7
Tangtse1	KK98-10	34.0060	78.2990	4350	5	0.98	1.10	0.20	19.0	3.0
Tangtse1	KK98-11	34.0060	78.2990	4350	5	0.98	1.00	0.10	17.5	1.8
Tangtse1	KK98-12	34.0060	78.2990	4350	5	0.98	1.20	0.10	20.4	1.6
Tangtse1	KK98-13	34.0060	78.2990	4350	5	0.98	2.90	0.20	45.1	4.7
Tangtse2	KK98-1	34.0060	78.2990	4350	5	0.98	0.10	0.04	2.1	0.9
Tangtse2	KK98-3	34.0060	78.2990	4350	5	0.98	0.20	0.03	4.2	0.6
Tangtse2	KK98-4	34.0060	78.2990	4350	5	0.98	0.50	0.05	9.4	1.1
Tangtse2	KK98-5	34.0060	78.2990	4350	5	0.98	0.10	0.01	2.1	0.3
Tangtse2	KK98-6	34.0060	78.2990	4350	5	0.98	0.40	0.04	7.5	0.8
Tangtse2	KK98-7	34.0060	78.2990	4350	5	0.98	0.30	0.10	5.9	1.7
Tangtse2	KK98-8	34.0060	78.2990	4350	5	0.98	0.80	0.10	14.3	1.7
Tangtse2	KK98-14	34.0060	78.2990	4350	5	0.98	0.10	0.01	2.1	0.3
Tangtse2	KK98-15	34.0060	78.2990	4350	5	0.98	0.10	0.01	2.1	0.3
REGIONAL INCISION EVENTS										
Dortch et al. (2011a)										
Stok	zk37	34.0030	77.5120	3923	5	0.92	17.60	0.44	400.7	25.1
Sacha	zk48	33.7870	77.8050	3479	5	0.91	23.30	0.66	790.2	43.4
Sacha	zk49	33.8110	77.8050	3495	5	0.92	20.10	0.45	631.6	42.6
Sacha	zk50	33.7360	77.7410	3490	5	0.94	15.00	0.37	442.8	30.1
Indus	I-66	34.1200	77.4320	3240	5	0.98	0.88	0.02	27.2	1.5
Indus	I-62	34.1210	77.4190	3235	5	0.98	1.17	0.02	36.5	2.0
Indus	I-63	34.1210	77.4190	3235	5	0.97	2.21	0.04	69.7	4.3
Indus	I-64	34.1240	77.4200	3120	5	0.95	0.37	0.05	14.2	1.8
Indus	I-67	34.0070	77.6890	3150	5	0.98	2.26	0.03	75.2	4.6
Indus	I-71	34.2630	77.0670	3010	5	0.96	0.31	0.01	12.4	0.8
Indus	I-72	34.2510	77.1050	3025	5	0.98	3.03	0.07	105.5	5.3
Indus	I-73	34.1660	77.3350	3097	5	0.96	0.26	0.01	10.3	0.6

Indus	I-76	34.1700	77.3320	3065	5	0.99	0.44	0.01	16.3	0.9
Indus	I-77	34.1690	77.3320	3055	5	0.98	0.30	0.01	11.5	0.6
Indus	I-78	34.1690	77.3320	3050	5	0.98	0.34	0.01	13.1	0.8
Ladakh	LDK-241	34.5170	77.4160	3783	5	1.00	3.18	0.05	69.1	4.2
Ladakh	LDK-240	34.5170	77.4160	3765	5	0.83	1.35	0.02	35.7	1.9
Ladakh	LDK-239	34.5170	77.4160	3741	5	0.56	0.17	0.01	7.8	0.5
Brown et al. (2002, 2003), Dortch et al. (2011b)										
Tangtse	Pang-8	34.0470	78.1540	3986	1	0.98	0.68	0.03	14.6	0.9
Tangtse	Pang-9	34.0470	78.1540	3983	5	0.98	0.72	0.04	15.8	1.0
Tangtse	Pang-10	34.0470	78.1540	3981	4	0.98	0.96	0.04	20.1	1.2
Tangtse	Pang-11	34.0470	78.1550	3982	5	0.98	0.63	0.02	14.0	0.8
Tangtse	Pang-12	34.0470	78.1540	3983	5	0.98	1.69	0.05	34.2	2.2
Tangtse	Pang-13	34.0470	78.1540	3978	5	0.98	2.44	0.09	48.6	4.3
Tangtse	Pang-14	34.0240	78.1950	4037	3	0.82	2.40	0.06	56.8	3.8
Tangtse	Pang-15A	34.0240	78.1970	4016	3	0.92	1.02	0.06	21.9	1.4
Tangtse	Pang-15B	34.0240	78.1970	4016	3	0.92	1.55	0.07	32.3	2.5
Tangtse	Pang-30	34.0090	78.3020	4164	2	0.98	2.31	0.06	40.4	1.8
Tangtse	Pang-31	34.0090	78.3020	4170	4	0.98	2.25	0.09	40.0	2.0
Tangtse	Pang-32	34.0090	78.3030	4167	5	0.98	2.48	0.06	43.7	2.8
Tangtse	Pang-33	34.0320	78.2090	4065	4	0.94	7.01	0.16	133.6	8.1
Tangtse	Pang-34	34.0330	78.2100	4028	3	0.93	0.61	0.03	13.8	0.9
Tangtse	KK97-24	34.0080	78.3110	4225	5	0.98	0.88	0.08	17.0	1.6
Tangtse	KK97-26	34.0080	78.3110	4225	5	0.98	1.36	0.13	24.3	2.3
Tangtse	KK97-27	34.0080	78.3110	4225	5	0.98	3.98	0.31	70.6	6.8
Tangtse	KK97-28	34.0080	78.3110	4225	5	0.98	0.73	0.08	14.3	1.5
Tangtse	KK97-29	34.0080	78.3110	4185	5	0.98	0.78	0.11	15.4	2.0
Tangtse	KK97-30	34.0080	78.3110	4185	5	0.98	0.73	0.08	14.5	1.5
Tangtse	KK97-33	34.0080	78.3110	4185	5	0.98	0.88	0.10	17.3	1.9
Tangtse	KK97-34	34.0080	78.3110	4185	5	0.98	0.63	0.05	12.9	1.2
Tangtse	KK97-35	34.0080	78.3110	4185	5	0.98	0.85	0.07	16.6	1.5
Tangtse	PK93-21	35.4800	75.4000	2235	1	0.98	1.30	0.14	31.9	2.5
Tangtse	PK93-22	35.4800	75.4000	2235	2	0.98	1.53	0.42	85.6	7.7
Tangtse	PK93-24	35.4800	75.3900	2198	1	0.98	1.45	0.09	37.7	4.5
Tangtse	PK93-25	35.5100	75.3500	2198	3	0.98	0.75	0.05	61.4	7.2
Tangtse	PK93-19	35.5100	75.3500	2082	3	0.98	1.17	0.04	115.0	12.0
Tangtse	PK93-30	35.6700	74.9200	1802	5	0.98	0.10	0.03	17.2	5.7
Tangtse	PK95-32	35.6700	74.9200	1822	1	0.98	0.10	0.03	3.4	0.9
Tangtse	PK95-36	35.6700	74.9200	1850	1	0.98	0.33	0.03	10.2	1.1
Tangtse	PK93-37	35.6700	74.9200	2138	5	0.98	0.01	0.00	0.9	0.2
Tangtse	PK93-38	35.6700	74.9200	1729	2	0.98	0.55	0.05	39.0	5.0
Tangtse	PK93-40	35.7100	74.7500	1883	1	0.98	0.09	0.02	3.0	0.6
Tangtse	PK95-21	35.6300	75.0600	1675	4	0.98	0.88	0.04	174.0	25.0
Tangtse	PK95-13	35.7800	74.6300	2009	3	0.98	0.13	0.01	10.8	1.3
Tangtse	PK95-13	35.7200	74.6500	1355	2	0.98	0.08	0.01	7.2	1.1
Tangtse	PK95-9	35.7200	74.6300	1311	2	0.98	0.10	0.01	9.6	1.1
Seong et al. (2007), Dortch et al. (2011b)										

Dassu	K2-21	35.7150	75.5220	2433	5	0.93	0.22	0.02	12.8	1.1
Chapok	K2-42	35.7320	75.6650	2671	5	0.98	0.04	0.01	2.0	0.4
Chapok	K2-43	35.7320	75.6650	2671	5	0.92	0.03	0.01	1.6	0.3
Pakora	K2-64	35.6910	75.7310	2855	5	0.82	0.03	0.01	1.6	0.3
Askole	K2-71	35.6710	75.8610	3010	5	0.76	0.31	0.01	14.8	0.8
Biafo	K2-100	35.6500	76.0330	3215	5	0.99	0.38	0.03	12.3	1.1
Phanmah	K2-101	35.6500	76.0330	3215	5	0.97	0.39	0.01	13.0	0.8

*: Topographic Shielding Factor

†: LSD age (internal/external errors quoted) is calculated using the Balco et al. (2008) calibration dataset (^{10}Be decay constant of 5.1±0.3x10-7), and Lifton et al. (2014) calculation scheme with the Lifton 2016 VDM geomagnetic database. Production rate for the CREP calculator is 4.13±0.2 ^{10}Be atoms/grams SiO_2/year (Martin et al., 2016) with a ^{10}Be half-life of 1.36Ma. Density of 2.7 g cm^3, AMS Standard of 07KNSTD.

Supplementary Item 5: Fan surface ^{10}Be ages from available calculation schemes

			Balco et al. (2008[1]) calibration dataset*†						Heyman (2014) calibration dataset					
Sample	Fan/ Moraine	^{10}Be concentration	Lal(1991)/ Stone(2000) time-dep	Lal(1991)/ Stone(2000) time-indep.	Lifton et al. (2005)	Lifton et al. (2014) LSD (Sf)	Lifton et al. (2014) LSD (Sa)	Desilets et al. (2003; 2006)	Dunai (2001)	Lal(1991)/ Stone(2000) time-dep.	Lal(1991)/ Stone(2000) time-indep.	Lifton et al. (2005)	Desilets et al. (2003; 2006)	Dunai (2001)
		(10^6 atoms/g)	(ka)	(ka)	(ka)	(ka)	(ka)	(ka)	(ka)	(ka)	(ka)	(ka)	(ka)	(ka)
Kullu valley														
Sol_F01	Qf_{SARAI}	0.1±0.02	6.6±1.1	6.6±1.1	7.8±1.4	7.95±0.4	7.9±0.4	7.7±1.4	8.0±1.5	6.6±1.0	6.7±1.0	7.6±1.2	7.4±1.2	7.8±1.2
Sol_F02	Qf_{SARAI}	0.06±0.02	3.4±1.0	3.3±0.9	4.0±1.2	3.6±0.4	3.5±0.4	4.0±1.2	4.2±1.3	3.4±1.0	3.3±0.9	3.9±1.1	3.8±1.1	4.0±1.2
Sol_F03	Qf_{SARAI}	0.06±0.008	3.3±0.5	3.1±0.5	3.8±0.7	3.9±0.5	3.9±0.5	3.7±0.7	3.9±0.7	3.3±0.5	3.1±0.4	3.7±0.5	3.6±0.5	3.8±0.6
Sol_F05	Qf_{SARAI}	0.04±0.003	2.3±0.3	2.1±0.2	2.7±0.4	3.0±0.2	2.0±0.2	2.7±0.4	2.8±0.4	2.3±0.2	2.2±0.2	2.6±0.3	2.6±0.3	2.7±0.3
Chandra valley														
Sis_F03	Qf_{SISSU}	0.06±0.007	2.6±0.4	2.4±0.3	2.9±0.5	2.1±0.2	2.1±0.2	2.9±0.5	3.1±0.5	2.6±0.3	2.4±0.3	2.9±0.4	2.8±0.4	3.0±0.4
Sis_F04	Qf_{SISSU}	0.3±0.02	10.8±1.3	10.8±1.2	11.7±1.6	8.5±0.7	8.4±0.9	11.7±1.6	12.1±1.6	10.8±0.9	11.0±1.0	11.4±1.1	11.4±1.1	11.8±1.2
Tel_F05	Qf_{TELING}	0.01±0.001	0.6±0.1	0.5±0.06	0.6±0.1	0.5±0.1	0.5±0.1	0.6±0.1	0.6±0.1	0.6±0.1	0.2±0.1	0.3±0.1	0.6±0.1	0.6±0.1
Tel_F06	Qf_{TELING}	0.02±0.003	0.8±0.08	0.7±0.1	0.9±0.2	0.7±0.1	0.7±0.1	0.9±0.2	0.9±0.2	0.8±0.1	0.7±0.1	0.9±0.1	0.8±0.1	0.9±0.1
Tel_F07	Qf_{TELING}	0.03±0.002	1.1±0.1	1.0±0.1	1.3±0.2	0.6±0.1	0.6±0.0	1.2±0.2	1.3±0.2	1.1±0.1	1.1±0.1	1.2±0.1	1.2±0.1	1.3±0.1
Tel_F08	Qf_{TELING}	0.3±0.04	10.4±1.0	10.4±1.8	11.3±2.1	9.0±1.5	8.9±1.5	11.3±2.2	11.7±2.2	10.4±1.7	10.6±1.7	11.0±1.8	11.0±1.9	11.4±1.9
Tel_F09	Qf_{TELING}	0.03±0.002	1.1±0.1	1.0±0.1	1.2±0.2	1.0±0.1	1.0±0.1	1.2±0.2	1.2±0.2	1.1±0.1	1.0±0.1	1.2±0.1	1.1±0.1	1.2±0.1
Karzok valley														
Men_F01	$Qf_{MENTOKa}$	8.2±0.2	108.6±10.7	126.3±11.6	95.4±11.3	54.8±13.3	53.6±3.9	98.8±12.4	95.7±11.7	109.3±6.3	129.1±8.0	93.6±6.6	96.5±7.5	93.6±7.0
Men_F02	$Qf_{MENTOKa}$	6.2±0.07	83.8±8.0	95.2±8.5	72.3±8.4	87.9±6.8	86.0±6.9	75.2±9.2	72.7±8.7	84.4±4.5	97.2±5.6	70.7±4.7	73.2±5.5	70.9±5.1
Men_F03	$Qf_{MENTOKa}$	4.5±0.05	62.2±5.9	70.3±6.2	53.5±6.2	61.8±5.9	60.1±5.1	56.0±6.8	54.0±6.4	62.6±3.3	71.7±4.1	52.1±3.5	54.2±4.0	52.4±3.7
Men_F04	$Qf_{MENTOKb}$	0.8±0.02	12.2±1.2	12.2±1.9	11.9±1.4	9.8±0.7	9.6±0.6	12.1±1.5	12.5±1.5	12.3±0.7	12.5±0.8	11.7±0.8	11.8±0.9	12.2±0.9
Men_F05	$Qf_{MENTOKb}$	3.3±0.07	63.5±6.1	71.8±6.4	54.7±6.4	41.5±4.2	40.5±3.2	57.3±7.1	55.2±6.6	63.9±3.6	73.3±4.4	53.3±3.7	55.5±4.2	53.6±4.0
Men_F06	$Qf_{MENTOKb}$	4.8±0.1	43.3±4.2	49.9±4.5	38.9±4.5	64.2±7.8	62.2±5.5	40.0±4.9	39.2±4.7	43.6±2.5	50.9±3.1	38.3±2.7	39.2±2.9	38.4±2.8
Men_F07	$Qf_{MENTOKb}$	4.1±0.07	55.1±5.3	62.7±5.5	47.0±5.4	54.4±4.5	53.2±3.7	49.0±6.0	47.4±5.6	55.5±3.0	64.0±3.7	46.1±3.1	47.6±3.6	46.2±3.3
Karzok valley moraine														
KO20	Kar_{M1}	9.8±0.2	120.9±11.7	142.3±12.8	104.3±12.2	98.7±8.3	96.2±8.1	108.2±13.4	104.3±12.6	121.7±6.7	145.4±8.6	102.4±7.0	105.7±8.0	102.2±7.5
KO21	Kar_{M1}	14.2±0.2	179.9±17.7	209.9±19.2	150.0±17.7	160.0±20.0	150.0±16.0	157.0±19.7	149.5±18.2	181.2±10.0	214.6±12.9	146.4±1.1	152.5±11.7	145.2±10.7
KO22	Kar_{M1}	7±0.2	88.9±8.7	100.8±9.1	75.8±8.9	42.3±4.9	41.1±3.6	79.0±9.8	76.1±9.2	89.5±5.1	103.0±6.3	74.3±5.2	76.8±5.9	74.3±5.5
KO23	Kar_{M1}	10.7±0.2	133.5±13.2	157.9±14.5	114.0±13.5	110.0±11.0	107.0±8.9	118.5±14.8	114.0±13.9	134.5±7.7	161.3±10.0	112.0±7.9	115.6±9.0	111.6±8.4

*: The Balco et al. (2008) global calibration production rate dataset was used due to the absence of a local calibration site for the Himalayan-Tibetan orogen. Production rate for the CRONUS calculator is 3.92±0.17 10Be atoms/grams SiO2/year (Brochers et al., 2016; Marrero et al., 2016)

†: Percentage difference between LSD derived ages and other schemes: 0−10 ka=0.1-20%; 10−40 ka=1.1−45%; 40-100 ka=0.2−42%; >100 ka= 0.1−52%.

References:

Balco, G., Stone, J., Lifton, N., Dunai, T., 2008. A complete and easily accessible means of calculating surface exposure ages or erosion rates from 10Be and 26Al measurements. Quaternary Geochronology 3, 174-195.

Desilets, D., Zreda, M., 2006. Elevation dependence of cosmogenic ^{36}Cl production in Hawaiian lava flows. Earth and Planetary Science Letters 246, 277–287.

Dunai, T.J., 2000. Scaling factors for production rates of in situ produced cosmogenic nuclides: a critical reevaluation. Earth and Planetary Science Letters 176, 157-169.

Heyman, J., 2014. Paleoglaciation of the Tibetan Plateau and surrounding mountains based on exposure ages and ELA depression estimates. Quaternary Science Reviews 91, 30-41.

Lal, D., 1991. Cosmic ray labelling of erosion surfaces: in situ nuclide production rates and erosion models. Earth and Planetary Science Letters 104, 429-439.

Lifton, N.A., Bieber, J.W., Clem, J.M., Duldig, M.L., Evenson, P., Humble, J.E., Pyle, R., 2005. Addressing solar modulation and long-term uncertainties in scaling secondary cosmic rays for in situ cosmogenic nuclide applications. Earth and Planetary Science Letters 239, 140– 161.

Lifton, N., Sato, T., Dunai, T., 2014. Scaling in situ cosmogenic nuclide production rates using analytical approximations to atmospheric cosmic-ray fluxes. Earth and Planetary Science Letters 386, 149-160.

Stone, J.O., 2000. Air pressure and cosmogenic isotope production. Journal of Geophysical Research 105, 23753–23759.

fin